NOVEL PROCESSING OF SOLID OXIDE FUEL CELL ANODES

By NOR BAHIYAH BABA

A thesis submitted in partial fulfilment of the requirements of Edinburgh Napier University for the award of Doctor of Philosophy

MARCH 2011

DECLARATION

This is to certify that the thesis comprises of only my original work towards the PhD except where indicated. This thesis contains no material which has been accepted for the award of any other degree or diploma in any University and is less than 80,000 words in length exclusive of tables, figures, bibliographies, appendices and footnotes. Based on the best of my knowledge, this thesis contains no material previously published or written by another person, except where due reference has been made.

Candidate*: NOR BAHIYAH BABA*
Date*:*

ABSTRACT

Solid oxide fuel cells (SOFCs) are of major interest in fuel cell development due to their high energy conversion efficiency, wide range of fuels and environmental friendliness. One important obstacle for their industrial development is their processing difficulties. These difficulties have recently been addressed by employing a novel technique namely electroless nickel - yttria-stabilised zirconia (YSZ) co-deposition which eliminates multi-layer processing and high temperature sintering.

The novel work carried out in this research programme investigates the effects of different processing parameters on the co-deposited anodes for SOFCs. In particular, YSZ particle size, electroless bath agitation method, electroless bath pH and substrate surface condition are investigated. These variables were investigated for their effect on (i) the ceramic to metal ratio – important in terms of matching the coefficient of thermal expansion of the anode and substrate, as well as providing electronic conductivity, and (ii) the porosity content in the deposited layers – required for fuel and exit gas penetration through the anode.

The experimental work was based on a full factorial Design of Experiment (DoE) approach and consisted of three phases – namely, designing, running and analysing. A 16 run 2^4 full factorial DoE with five replications was constructed with YSZ particle sizes of 2 and 10 µm; bath agitation of air bubbling and mechanical stirring; bath pH of 4.9 and 5.4; and substrate surface treatment of hydrofluoric acid etching and mechanical blasting. A total of 80 samples were analysed for nickel content by energy dispersive X-ray analysis and porosity content by Archimedes buoyancy measurement. The DoE was analysed by the ANOVA statistical tool in Minitab 15 software.

The co-deposition conditions that produced anodes with (i) the lowest volume percentage of nickel and (ii) the highest level of porosity were determined. Linear regression models for both nickel to YSZ content and porosity responses were built to estimate the correlation between experimental and predicted data. The coefficient of determination, R^2 for nickel to

YSZ content indicated a reasonable correlation between experimental and predicted values while the regression model for porosity response was less reliable.

One anode containing 50 vol.% nickel recorded an electronic conductivity at 400^{o}C in air that is comparable to the published data. Another series of tests at higher temperatures (up to 800^{o}C) in air and nitrogen resulted in encouraging electronic conductivities being recorded.

ACKNOWLEDGEMENTS

The author would like to express her gratitude towards her Director of Studies, Mr. Alan Davidson for his guidance, knowledge and support for the last four years. Also a token of appreciation to Prof. Tariq Muneer for his assistance and academic support that made it possible to submit the thesis within four years.

Special thanks to Dr. William Waugh for his industrial technical skills in EN plating and support for the work carried out in this report. The author would like to express her appreciation to Mr. Bill Brownlee, the ex-Materials laboratory technician and Dr. Neil Shearer for their valuable technical assistance and cooperation in completing the work.

A special appreciation to my husband, Abdul Rahman Abdullah and children, Imran Syafiq, Afifah Humaira, Ikhwan Syahmi and Ilham Danish for their constant support, patience and encouragement throughout the four years of study.

Finally, last but not least, a great acknowledgement is expressed to TATI University College (TATIUC) for the financial support.

TABLE OF CONTENTS

LIST OF FIGURES

LIST OF TABLES

LIST OF ABBREVIATIONS

Al	Aluminium
ANOVA	Analysis of variance
Ce	Cerium
CeSZ	Ceria-stabilised zirconia
CTE	Coefficient of thermal expansion
D.I.	Deionised
DoE	Design of experiment
EDXA	Energy dispersive X-ray analysis
EN	Electroless nickel
FEG	Field emission gun
GDC	Gadolinium-doped ceria
Ni	Nickel
O	Oxygen
OFAAT	One-factor-at-a-time
P	Phosphorus
rtp	Room temperature
SDC	Samaria-doped ceria
SEM	Scanning electron microscope
SOFC	Solid oxide fuel cell
SSZ	Scandia-stabilised zirconia
TPB	Triple phase boundary
Y	Yttrium
YDC	Yttrium-doped ceria
YSZ	Yttria-stabilised zirconia
Zr	Zirconium

1. INTRODUCTION

1.1 Background

Energy plays a crucial role in sustaining global development. The sources of energy have evolved generally from wood to coal, then to petroleum and currently towards renewable and green energy sources. In the 19th century the energy consumption rate increased exponentially spurred by the rapid increase in population (Smil 1997). The International Energy Agency (IEA) 2001 states that the distribution of the global energy consumption has been primarily led by oil (34.9%), followed by coal (23.4%) and gas (21.2%) then nuclear power (6.9%) and the remainder by renewable energy (13.6%) (IEA 2001).

In the 1970s the world energy crisis, especially in the US, as well as environmental issues, particularly - global warming brought on by the growth of carbon dioxide concentration in the atmosphere, combined to open windows to alternative energy sources such as renewable and nuclear power. Since energy can never be destroyed or created – it is conserved and can only be converted from one form to another (Cengel 2002) - the world is taking this opportunity to explore the advantages of using the abundance of earth's resources to supply useful energy power. Thus, since energy from natural sources can be converted from one type to another, the idea is to conserve the energy as efficiently as possible, consequently reducing cost and minimising environmental pollution.

Basically, energy can be categorised into renewable and non-renewable. Fig. 1 based on reviews Chang et al. (2003); Dincer (2000); Hubbard et al. (2003); Muller-Steinhagen and Nitsch (2005); Pitts (1994); and Rosa (2005) gives a general idea of the categories of energy and their sources based on reviews by. Non-renewable sources comprise fossil fuels and minerals, particularly radioactive ones, that are in limited supply. On the other hand, renewable sources are from natural resources that exist in abundance, such as sun, wind, water, and hydrogen gas. Recently, attention is increasingly focused on fuel cells using hydrogen as fuel.

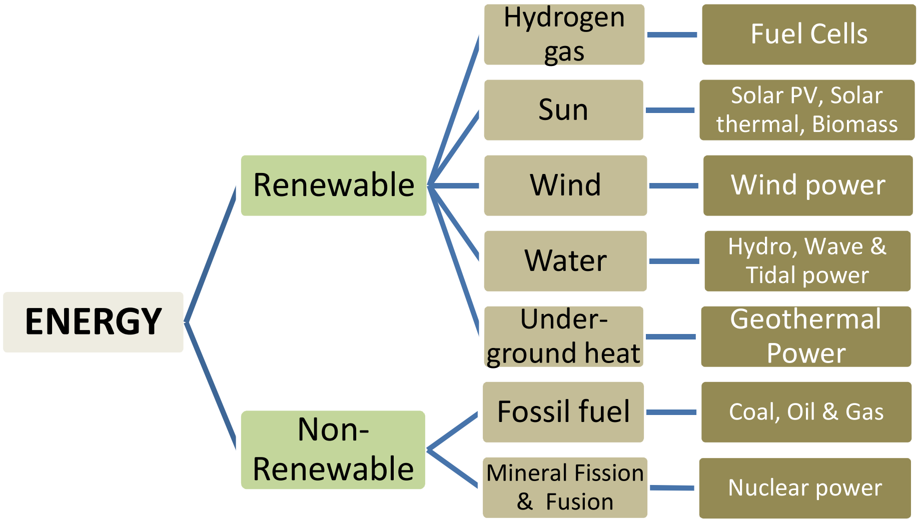

Fig. 1: Energy categories and their sources

1.2 Renewable Energy

Renewable energy has the great advantage of being totally environmentally friendly. Natural energy resources from the sun, water, wind, earth and gas are harnessed to produce alternative energy. The top five countries in renewable power capacity as of the end of 2008 are, in descending order, China, United State, Germany, Spain and India (REN21 2009). Fig. 2 illustrates the estimated world renewable electric power capacity as of end of 2008.

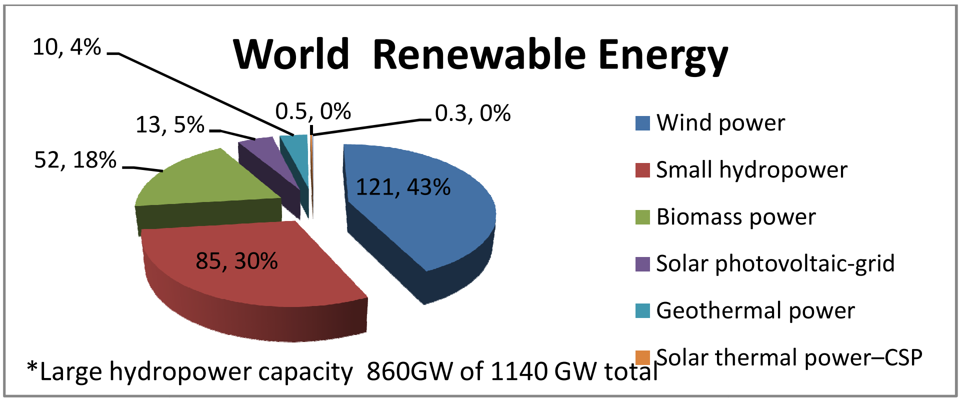

Fig. 2: World renewable electric power capacity in GW (estimated) end of 2008 (REN21 2009)

If both small and large hydropower were combined, hydropower - energy gained by movement of water is the major renewable energy source. Wind power derives from wind turbines started in Europe, especially in Holland. Next on the list is biomass power.

Biomass is the extraction of energy from plants such as palm oil and woods, contributes approximately 18% (exclusive of large hydropower) of the total world renewable energy capacity.

Solar power can be divided into photovoltaic (PV) power and solar thermal power. Solar PV power involves direct conversion of sunlight by a solid-state device whereas solar thermal power uses radiation of the sun to heat up water for hot water and heaters. The challenge for development and use of this energy technology is the cost. Geothermal power uses underground heat from magma as a heating source. This power source has been used for supplying heat in geothermally active countries such as New Zealand and Iceland.

There is one more highly potential renewable energy source that is yet to be discussed - the fuel cell. Fuel cell is like a battery but instead of storing electricity, it generates electricity. Fuel cell technology has been extensively studied due to its high efficiency and its production of virtually no pollution as it uses hydrogen as fuel and produces water as its waste product.

1.3 Hydrogen Economy

Recently the world has moved towards technology where hydrogen is used as an energy carrier. The combustion of hydrogen releases energy and electron as it combines with oxygen as in [equation 1.1] and this process is reversible. The production of water as its waste is cleaner and exerts less impact on the environment. Hydrogen economy has been proposed to reduce environmental damage that has been made by the combustion of hydrocarbon from fossil fuel and furthermore to reduce the dependencies on petroleum.

$$H_2(g) + \tfrac{1}{2}O_2(g) \leftrightarrow H_2O(l) \ \cdots \ E^{\vartheta} = -286kJ \quad (1.1)$$

Since hydrogen is denser and highly flammable in its natural gaseous form, transportation, distribution and storage of hydrogen presents safety issues (Ohadi and Qi 2007). However, hydrogen is a chemical fuel, similar in nature to petroleum, so it can be stored in a high pressure tank, transported by trucks, trains, planes, or ships or pumped through pipelines (Williams 1994).

Moreover, the present technology developed to accommodate oil and gas networks could be used to transport hydrogen gas. The combination of renewable technologies is also possible - for example, wind electricity for on-site electrolyser can be combined with solar power as an electrolyser for hydrogen generation (Mortimer 2008). The end use of hydrogen economy is the fuel cells as auxiliary, micro, transportation and stationary power sources in the future.

1.4 Fuel Cells

Fuel cells transfer chemical energy into electrical energy in the most efficient manner by electrochemical cells. The fundamental concept of fuel cells was discovered by Sir William Grove in 1839 by accident (Yamamoto 2000). The basic fuel cell block is built up by an electrolyte layer in contact with porous anode and cathode layers on each side. In 1950 the achievement of the alkaline fuel cell (AFC) of 5 kW led to the development of 12 kW AFC for NASA's space shuttle orbiter in the 1970s as a reliable power supply without any backup battery power.

The achievement of the fuel cell showed it has a great future. A comparison of various generation systems is tabulated in Table 1 (Kirubakaran et al. 2009). Fuel cells have power capacity ranging up to 2 MW, which is higher than those of photovoltaic and wind turbine systems. It may still not be at par with reciprocating engines but its efficiency is undoubtedly incomparable. The major drawback of fuel cell applications is the higher cost of installation, but they are less expensive to maintain.

Table 1: Comparison of different generation systems (Kirubakaran et al. 2009)

	Reciprocating engine: Diesel	Turbine generator	Photovoltaics	Wind turbine	Fuel cells
Capacity Range	500kW-5MW	500kW-25MW	1kW-1MW	10kW-1MW	200kW-2MW
Efficiency	35%	29-42%	6-19%	25%	40-60%
Capital Cost ($/kW)	200-350	450-870	6600	1000	1500-3000
Operating & Maintenance Cost ($/kW)	0.005-0.015	0.005-0.0065	0.001-0.004	0.01	0.0019-0.0153

Several types of fuel cell have recently been investigated: the alkaline fuel cell (AFC), proton exchange membrane commonly known as polymer electrolyte membrane fuel cell (PEMFC), direct methanol fuel cell (DMFC), molten carbonate fuel cell (MCFC), phosphoric acid fuel cell (PAFC) and solid oxide fuel cell (SOFC). The most reliable and aggressively investigated fuel cells are SOFC and PEMFC, which are more likely to be commercialised.

AFC is the first commercial fuel cell employed by NASA. AFC operates at low temperature (100^oC) with potassium hydroxide (KOH) as an electrolyte. When newly developed, it operated at 240^oC (EG&G Services et al. 2000). The operating temperature depends on the concentration of KOH – a high concentration (85 wt.%) operates at a high temperature ($\sim260^oC$) whereas a lower concentration (35-50wt.%) operates at a lower temperature ($>120^oC$). It transports negatively charged ions from cathode to anode and produces water as its waste. The disadvantage of the AFC is that it is very sensitive to both carbon monoxide and carbon dioxide.

PEMFC is an ion exchange membrane with solid polymer (fluorinated sulfonic acid or similar) as electrolyte, and it operates at a very low temperature of 100^oC. The electrolyte is an excellent proton conductor and electron insulator. It has higher power density and quick start up, and its low operating temperature makes it suitable for automotive, laptop computer, bicycle and mobile phone applications. The major disadvantage of PEMFC is lower operating efficiency and the high cost of the platinum used as a catalyst.

DMFC is a relatively new fuel cell. It operates at low temperature with polymer electrolyte, such as in liquid methanol (CH_3OH) in water to eliminate the requirement of external reformer. The disadvantage of DMFC is that the crossover of methanol from anode to cathode reduces system efficiency and electrochemical oxidation kinetics. It has many similarities to PEMFC.

MCFC operates at relatively high temperatures ranging between $600\text{-}700^0C$ with alkali carbonates retained in a lithium aluminium oxide ($LiAlO_2$) ceramic matrix electrolytes. At this high temperature the electrolyte turns to a molten salt that is highly conductive with carbonate ions as ionic conduction. The disadvantages of MCFC are its intolerance to sulphur and its slow start up.

PAFC operates at relatively low temperatures ranging from 150-220^{0}C with 100% phosphoric acid used as an electrolyte - minimising the water vapour pressure which helps the management of cell water. At lower temperature the phosphoric acid electrolyte is a poor ionic conductor, and platinum electrocatalyst becomes severely poisoned by carbon monoxide. The major disadvantage of PAFC is its increased cost from the application of platinum as a catalyst.

SOFC has become popular over the last few decades as it has shown a promising co-generation system efficiency of up to 70% where the heat produced is applied to another system producing more electricity, space heating and industrial processing. It is estimated that SOFCs are 5-10 years away from commercialisation (Li and Karimi 2007). SOFCs operate at high temperature ranging between 700-1000^{0}C with a solid ceramic electrolyte typically YSZ. The oxide ions are transported from cathode to anode, where they combine with hydrogen ions (H^+) to produce water and heat. The waste heat can be recycled for a cogeneration system. The disadvantages of SOFC are its slow start up, high cost and sulphur intolerance.

Recently, three types of fuel cells appear to be the most promising – SOFC, DMFC and PEMFC (Weins 1999-2010). SOFC is the most likely contender for both large and small electric power plants in the 1 kW and above size. DMFC is targeted to be the most promising as a battery replacement for portable applications such as cellular phones and laptop computers. Table 2 below compares all fuel cell types and their important features based on reviews conducted (EG&G Services et al. 2000; Haile 2003b, 2003a; Kirubakaran et al. 2009; Rosa 2005; Sammes 2006; Weins 1999-2010). Among the three most promising fuel cells, SOFC has the highest energy efficiency especially when cogeneration power is implemented besides multi-fuel capability. This is the main reason for the greater intensity of recent development in SOFC technology.

Table 2: Fuel cell types and their important features

Type of Fuel Cell	Operate T/ ^{0}C	Mobile ion	Electrolyte	Fuel	Max Power Output & Efficiency	Problem
AFC	100-260	OH^-	Liquid Alkaline - KOH	H_2	5-12 kW [a] 60-70%	Very sensitive to both CO and CO_2
PEMFC	80-100	$H(H_2O)_n^+$, H^+	Solid polymer-Sulfonated polymer (Nafion^{TM})	H_2, CH_3OH	250kW [b] 40-45%	Lower operating efficiency and high cost platinum as a catalyst
DMFC	100	$H(H_2O)_n^+$, H^+	Liquid alcohol-Methanol	H_2, CH_3OH	1W-1kW 25-40%	CH_3OH crossover reduces system efficiency and high cost platinum as catalyst
MCFC	600-700	CO_3^{2-}	Molten carbonate-Mixture of lithium and potassium carbonates	H_2, HC, CO	250kW-3MW 45% [c] 50-60%	Sulphur intolerant and slow start up
PAFC	160-220	H^+	Liquid Acid, H_3PO_4	H_2	200kW-1MW [d] 11MW 40%	High cost platinum as a catalyst.
SOFC	700-1000	O^{2-}	Ceramic Solid oxide – YSZ	H_2, HC, CO	25-100 kW [e], 2MW 50-60% ~70% (cogeneration)	Slow start up, high cost and sulphur intolerant.
a U.S. Apollo Space Programme (1960) b Ballard Generation Systems (Aug 1997) c Fuel Cell Energy (June 2000) d International Fuel Cell Corporation, IFC (Aug 2000) e Siemens Westinghouse Power Corporation/ National Fuel Cell Research Centre (2001)						

1.4.1 Solid Oxide Fuel Cells

SOFCs produce electrical power directly from a gaseous fuel by electrochemical reaction. The fuel cell by-products damage the environment only insignificantly. The fuel cell has a high energy conversion efficiency, bypassing chemical energy conversion (fuel) to mechanical or thermal energy like other power generation devices. SOFC is also known as ceramic fuel cell as its key characteristic is its ceramic electrolyte. What make for a unique and better performance is the application of ceramic as an electrolyte in the fuel cell, eliminating corrosion and electrolyte management system problems.

The ceramic material of the SOFC electrolyte under the solid oxide category only conducts electricity in the high temperature range between 600-1000^{o}C. At this high temperature the solid ceramic material allows the conduction of oxide ions through it. Due to this high temperature, SOFC materials are limited by the level of chemical stability in the reducing and oxidising environments, the level of chemical stability of contacting materials, conductivity and thermo-mechanical compatibility. Thus the present main technological challenge in the continued development of SOFC is the search for suitable materials and fabrication processes.

1.4.2 Future Needs in SOFC Development

Major technical difficulties in making SOFC commercially viable are the selection of materials and fuel cell manufacturing (Yamamoto 2000). The selection is limited in large part by the constraints imposed by the high SOFC working temperature of up to 1000^{o}C on the selection of materials as well as cell construction. The development of materials for SOFC components is based on (1) property compatibility between neighbouring components, (2) electronic and ionic conductivity of electrodes and electrolytes and (3) stability in reducing and oxidising environments. Although alternative materials for SOFC components have been studied and developed, in terms of fuel cell manufacturing, the main obstacle is the cost. Conventional ceramic fabrication methods are not very effective whereas modern and advanced methods are too costly. This is where the present research begins.

1.5 Research Aim

This research focuses on fabricating an SOFC anode where the electrochemical reaction of fuel takes place to produce electricity. The current fabrication processes require multi-layers and stages (therefore are time-consuming), followed by repeated sintering at high temperature (resulting in the high cost of heating). The goal is to fabricate the anode via a single process with no sintering, using EN co-deposition.

EN co-deposition has been used extensively in wear resistance and corrosion resistance applications. The application of this technique in fabricating an SOFC anode is still new, and the addition of ceramic YSZ to be deposited together onto the substrate makes it novel and it is called the EN co-deposition process. The advantages of this novel process include its simplicity as it is a single stage process, and since it does not require sintering or heating, it is more cost- and time- effective.

1.6 Research Objectives

The objectives of this research are:

1. To design the experiment and undertake tests to evaluate on a novel low-cost manufacturing process for SOFC anodes
2. To investigate and evaluate the critical variables that will affect the performance of the above process
3. To perform statistical analysis to relate the above variables
4. To perform optimisation condition suitable for low ceramic to metal ratios and acceptable porosity contents for SOFC anodes
5. To develop multiple linear regression models to inter-relate the DoE responses

1.7 Research Outline

The research was carried out in three phases. The first phase was a preliminary one-factor-at-a-time (OFAAT) experiment in determining the parameters and variables for the second phase work. The first phase consisted of 9 independent experiment parameters to measure the possible effect of each factor that might influence the EN co-deposition process.

The second phase, the body of the work, consisted of 2 levels factorial DoE. The data from the first phase were analysed and an experimental design was developed with a 2k full factorial of 4 factors in a 16-run experimental array; each run was replicated 5 times in random order. The responses of this second phase were the Ni to YSZ ratio and porosity percent. A linear regression model was developed for both responses. The models were used to predict the response and then compared with the experimental data.

The third phase was the DoE multiple response optimisation of conditions and anode performance of electrical conductivity in a simulated SOFC environment. All samples then underwent physical testing and characterisation using scanning electron microscopy (SEM) coupled with energy dispersive x-ray analysis (EDXA). The research work outline is shown schematically in Fig. 3.

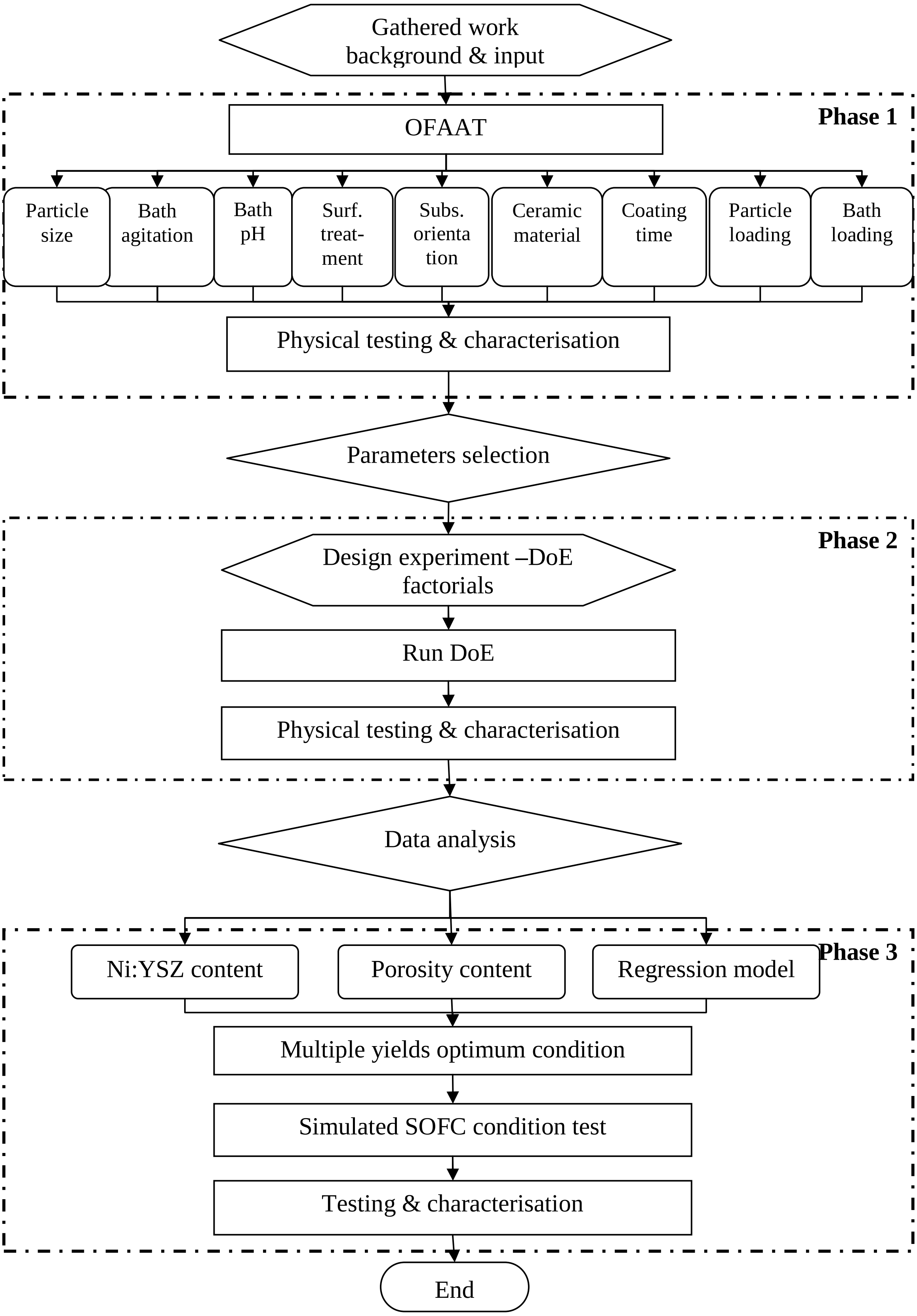

Fig. 3: Research workflow

2 LITERATURE REVIEW

2.1 Introduction

The possibility for SOFC technology only began with the Nernst's discovery of the solid-oxide electrolyte in 1899 (Minh and Takahashi 1995). Thirty-eight years later in 1937 the first SOFC was operated at 1000°C by Baur and Preis (Minh and Takahashi 1995). This first SOFC to be operated used ZrO_2-based ionic conductors with iron or carbon as anode and Fe_3O_4 as cathode. In early 1960, serious development of SOFC began along two fronts: the two - cell configuration and component materials.

Cell configuration development started with a flat-plate design followed by a segmented-cell-in-series design by Bell and Spigot (Minh and Takahashi 1995), which was then modified by a banded configuration. In 1980 seal less tubular SOFC was discovered, followed by monolithic SOFC two years later. Finally the flat-plate design evolved due to advances in ceramic forming and processing technologies. These flat-plate and tubular cell designs are found to be the best cell configuration today as shown in Fig. 4.

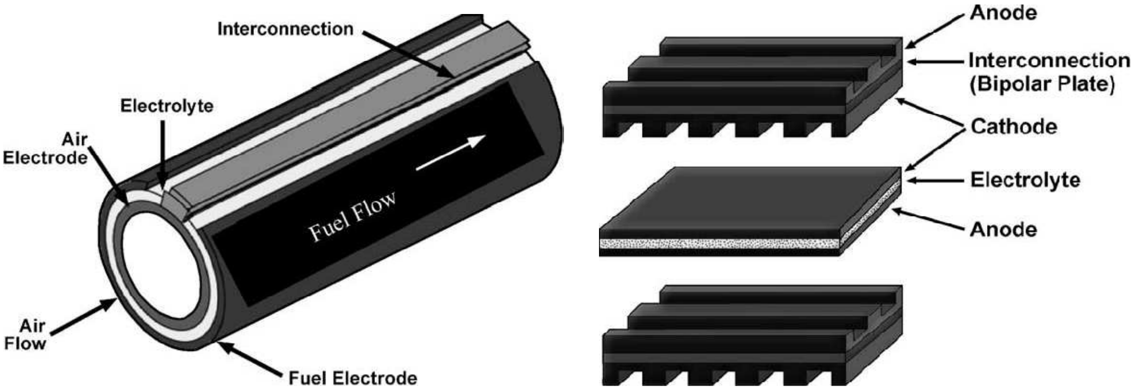

Fig. 4: SOFCs design, tubular (left) and planar (right) (Singhal 2002)

Cell design helps optimise surface contact between layers, thus increasing the output. The planar design has been found to be more capable of achieving very high power densities as well as affording possible significant cost reductions through a concept called 'mass customization' – multi-stack fuel cells as the planar design is simpler and easy to fabricate into multiple layers (Singhal 2002).

The development of SOFC component materials, on the other hand, began with the use of noble metals for electrodes and interconnects. Later, in the early 1970s Ni-YSZ was used as an anode, doped In_2O_3 as a cathode and $CoCr_2O_4$ as an interconnect. The interconnect materials were replaced by $LaCrO_3$ in 1980 and lastly by high-temperature alloys. For cathode materials, $LaMnO_3$ and $LaCoO_3$ have been found to be more reliable than the doped In_2O_3.

In general, the major challenges in determining SOFC performance and reliability are (1) materials degradation over long term operation and (2) total cell cost reduction, including cost of fabrication and materials (Williams et al. 2006). Ivers-Tiffee et.al (2001) found that the performance of the cells can only be improved by the selection of elevated materials for use. The next sub-section introduces SOFC working principles as well as its electrolytes, anodes and cathodes.

2.1.1 SOFC Working Principles

A fuel cell is basically a refuelable battery. It operates by electrochemical reaction that converts chemical energy directly to electrical energy. The electrochemical reactions are called reduction-oxidation (redox) reactions, where reduction is for capturing electrons and oxidation is for releasing electrons. A fuel cell is a stack of anode-electrolyte-cathode layers with interconnects and sealant. A schematic diagram of a SOFC with its major cell components – anode of porous composite, cathode of porous ceramic and dense solid oxide ceramic as an electrolyte is illustrated in Fig. 5.

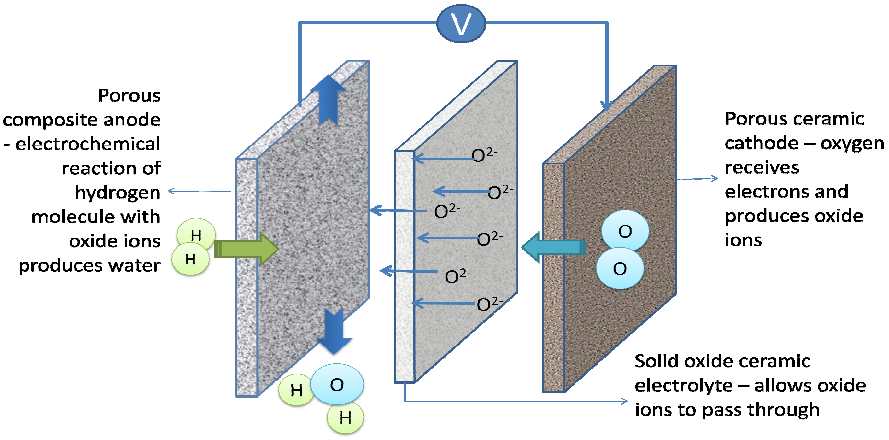

Fig. 5: Schematic diagram of a SOFC consisting of solid electrolyte and porous anode and cathode

At the cathode, the reduction of oxygen occurs when oxygen captures electrons, becoming oxide ions, as in [equation 2.1]. The dense solid electrolyte allows oxide ions to migrate from the cathode to the anode. The oxide ions then react with H_2 fuels at the anode and undergo an oxidation reaction, releasing electrons to the external circuit [equation 2.2], producing water as waste. This process is continuous as long as the fuel and oxygen are fed into the system. Electrons flowing through the outside circuit should be homogenised with the ionic charge through the electrolyte that produces the electrical power. The overall cell reaction is modelled in [equation 2.3].

$$Cathode\ reaction: \quad O_2 + 4e^- \rightarrow 2O^{2-} \quad \cdots (2.1)$$

$$Anode\ reaction: \quad 2H_2 + 2O^{2-} \rightarrow 2H_2O + 4e^- \quad \cdots (2.2)$$

$$Overall\ cell\ reaction: \quad H_2(g) + {}^{1}/_{2}\, O_2(g) \leftrightarrow H_2O(l) \quad \cdots (2.3)$$

2.1.2 SOFC Components

SOFC components can generally be divided into five main categories: interconnects, sealants, electrolytes, cathodes and anodes. The energy efficiency of an SOFC system is approximately 60% for a single cycle and up to 85% for the total system (Badwal and Foger 1996), achieved by optimising each cell components. Various companies have invested in developing SOFC components, as summarised by Tietz et al. (Table 3).

Table 3: Materials for SOFC components in electrolyte-supported planar cell design and corresponding fabrication (Tietz et al. 2002)

Company	Country	Component	Materials	Production Process	Thickness
Sulzer Hexis	CH	Electrolyte	YSZ	Tape casting	Ns
		Cathode	LSM	Screen printing	Ns
		Anode	Ni-YSZ	Screen printing	Ns
ECN/InDec	NL	Electrolyte	YSZ	Tape casting	Ns
		Cathode	LSM	Screen printing	50 µm (two layers)
		Anode	Ni-YSZ	Screen printing	Graded composite
Fraunhofer Ges., IKTS	D	Electrolyte	YSZ	Tape casting	150 µm
		Cathode	LSM	Screen printing	Ns, two layers
		Anode	Ni-YSZ	Screen printing	Ns

CFCL	AUS	Electrolyte	3YSZ, 8YSZ	Tape casting	100 μm
		Cathode	LSM	Screen printing	50-60 μm
		Anode	Ni-YSZ	Screen printing	50 μm
SOFCo	USA	Electrolyte	YSZ, $(Ce,Sm)O_2$	Tape casting	180 μm, 300 μm
		Cathode	$(LaSr)CoO_3$	Screen printing	Ns
		Anode	Ni-YSZ	Screen printing	Ns
Tokyo Gas	JP	Electrolyte	3YSZ	Tape casting	50-100 μm
		Cathode	LSM	Screen printing	150 μm
		Anode	Ni-(Ce,Y)SZ	Screen printing	30 μm
Mitsui Eng. & Shipbuilding	JP	Electrolyte	8YSZ	Tape casting	300 μm
		Cathode	$(La,Sr)(Mn,Cr)O_3$	Painting	150 μm
		Anode	Ni-YSZ	Painting	150 μm

Ns = not specified

The common material for SOFC components are 8YSZ for the electrolyte, Ni-YSZ for the anode and lanthanum strontium manganese (LSM) for the cathode. Electrolytes have been mostly produced by conventional ceramic processing tape casting whereas the anodes and cathodes are fabricated by screen printing. The average thickness ranges between 50-150 μm, with the exception of YSZ and $(Ce,Sm)O_2$ electrolytes by SOFCo which are 180 and 300 μm thick respectively. The last three companies in Table 3, SOFCo, Tokyo Gas and Mitsui Engineering & Shipbuilding, used different materials for electrolyte, anode and cathode.

The details of SOFC component materials and criteria will be further discussed in the next sub-sections.

2.1.2.1 Interconnects

SOFC interconnects connect the main SOFC components, namely anode and cathode, via an external circuit. Their primary function is to carry electrical current so must have good electrical conductivity. Additionally, they must be chemically and mechanically stable at high operating temperatures. Interconnects are also exposed to oxidation environment at one end, the anode, and a reducing environment at the other, the cathode. The material for interconnects must meet these criteria.

There are metallic and ceramic interconnects. Metals are very well-known for their good electrical conductivity, but they are very unstable in air which causes oxidation that reduces the conductivity of metallic interconnects at high temperatures. Common metallic interconnects are chromium-based alloys, ferritic stainless steels, austenitic stainless steel, Fe-Ni-Cr base alloys and Ni(-Fe)-Cr-based alloys (Fergus et al. 2009). Ceramic interconnects are usually made from semiconducting oxides that are compatible with other SOFC components. Semiconducting oxides are good at high temperatures but their low conductivity at lower temperature causes problems. Typical ceramic interconnects are pure $LaCrO_3$ (Sakai et al. 2004).

2.1.2.2 Sealants

SOFC sealants are used to ensure that the gases remain tight within the cell. Thermal stresses due to repeated heating and cooling are the main challenge in choosing sealants. The nature of the sealant is not an issue for the tubular design SOFCs, but it is a main concern in the planar design. Typical sealants are glass, glass-ceramic, ceramic-composite and compliant seals (Lessing 2007).

2.1.2.3 Electrolytes

The critical component of any fuel cell is the electrolyte. This is also true of SOFC, whose name is taken from the type of electrolyte materials used, solid oxide, usually a doped solid ceramic oxide, typically YSZ. This material has been used over the last two decades of fuel cell development (Haile 2003b). According to Minh and Takashi (2004) SOFC electrolytes should have (1) sufficient ionic conductivity in dual atmosphere, with the highest ionic conductivity possible and negligible electronic conductivity; (2) stability in dual atmosphere, both reducing and oxidising; (3) chemical compatibility with other cell components; (4) matching CTE to other cell components; and (5) dense ceramic (no open pore porosity) to prevent gas cross leakage.

The main criteria for suitable electrolytes are high conductivity for ions and negligible electron conductivity. The conductance of a ceramic electrolyte depends on (1) operating temperature, (2) thickness of electrolyte and (3) nature of electrolyte (Rosa 2005). Significant ionic conductivity of YSZ materials starts at 800^0C and thus it is possible to operate at this temperature with certain modifications or at higher temperatures, as shown in Fig. 6.

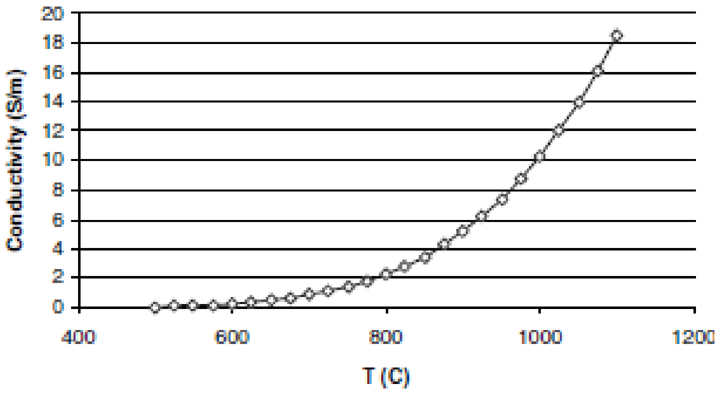

Fig. 6: Ionic conductivity of YSZ materials against temperature (Sammes 2006)

An electrolyte must be thin to achieve acceptable conductance. Ideally the electrolyte should be 5 µm thick, but current electrolytes have thicknesses between 50-75 µm (Williams et al. 2006). The thicknesses that are 10 times greater than ideal are due to the difficulty of maintaining gas impermeability at a very thin ceramic layer during fabrication. Furthermore, thin ceramic is very fragile and must be supported by either the anode or cathode.

The nature of the electrolyte depends totally on the internal properties of the materials. An intermediate temperature SOFC operating in the temperature range of 600-800^{o}C is possible using other ceramic materials such as samaria-doped ceria (SDC) or ceramic proton conductor ($BeCeO_3$). Any ceramic material chosen as an electrolyte must be chemically inert to the adjacent materials, i.e. the anode and the cathode, and meet all the criteria mention earlier.

2.1.2.4 Cathodes

According to Minh and Takashi (1995), a SOFC cathode should meet all the following criteria: (1) be chemically, morphologically and dimensionally stable in the oxidant environment; (2) have sufficient electronic conductivity to support electron flow; (3) be chemically compatible to other component materials and chemically stable at operating or higher temperatures with minimal diffusion or reaction; (4) matching CTE to avoid delamination or cracking; (5) have sufficient porosity (>50%) to allow gas transport to the reaction sites; and lastly (6) produce sufficient catalytic activity for the electrochemical reduction of the oxidant. General requirements such as high strength and toughness, fabricability and low cost should also be considered.

At the cathode, a reduction of oxygen to oxide ions occurs as in [equation 2.1]. Therefore the cathode material must be stable in an oxidant oxidising environment. As listed in Table 4 in previous sub-section, the most common cathode material is strontium-doped lanthanum manganate (Sr-$LaMnO_3$) or LSM. Other alternative materials are being investigated, such as $La_{1-x}Sr_xFeO_3$ (LSF) and $La_{1-x}Sr_xCo_yFeO_{3-\delta}$ (LCSF) (Sammes 2006). In the case of these materials, problems related to compatibility with neighbouring materials might arise.

2.1.2.5 Anodes

The anode is a positive electrode where hydrogen oxidation occurs to produce electrons, which then flow to the external circuit. Water is the waste product of the reaction when using hydrogen (H_2) fuel, as shown in [equation 2.2]. When carbon monoxide (CO) is used – [equation 2.4], carbon dioxide is the waste product, and similarly if methane (CH_4) is used as a fuel – [equation 2.5], both water and carbon dioxide together with electrons are produced. The SOFC has an advantage in that it allows for a wide range of fuels. In general, criteria for the anode are similar to those for the cathode, except that their environments are different as the anode exists in an oxidising environment.

$$Anode\ reaction: \quad 2H_2 + 2O^{2-} \rightarrow 2H_2O + 4e^- \quad \cdots\ (2.2)$$

$$Anode\ reaction\ (CO\ fuel): 2CO + 2O^{2-} \rightarrow 2CO_2 + 4e^- \quad \cdots\ (2.4)$$

$$Anode\ reaction\ (CH_4\ fuel): CH_4 + 4O^{2-} \rightarrow 2H_2O + CO_2 + 8e^- \quad \cdots\ (2.5)$$

As the main focus of this thesis is the fabrication of SOFC anode, the criteria and fabrication of this component will be discussed in detail in the next section.

2.2 Anode Criteria

Anode criteria must be identified and well understood. The fabricated anode should meet all the required criteria to perform efficiently as an SOFC anode. SOFC anodes should meet all the following criteria: (1) high electronic conductivity, (2) good catalytic activity, (3) adequate porosity content, and (4) matching CTE. Each of these criteria will be discussed further below, but first knowledge of anode materials is important to understand their behaviour and properties.

2.2.1 Materials

Materials for anodes have to be electrically conductive, have high electrocatalytic activity, match CTE with neighbouring components and be chemically stable in a reducing environment (Wincewicz and Cooper 2005). Anode materials are usually a combination of metal and ceramic (henceforth called cermet) where the metal part provides electrical conductivity and hydrogen oxidation catalytic property. The ceramic part, on the other hand, governs catalytic activity of the anode and provides ionic conductivity, inhibits Ni coarsening and also reduces the CTE of the cermet.

It has been shown that Ni is the best metallic element for an SOFC anode since Ni has acceptable electronic conductivity and is low in cost (Zhu and Deevi 2003). It is a good electrochemical catalyst for high electrochemical activity and is also good at catalysing the carbon-formation reaction (Gould 2005). Concentrations of Ni in an SOFC anode are between 40-60% which is above the percolation threshold (30% Ni) of the cermet anode (Pratihar et al. 2006). A problem arises at high temperature where Ni particles coarsen, causing a reduction in electrical conductivity by 33.3% from initial value (Simwonis et al. 2000).

A few attempts have been made to use metals as SOFC anode, among them are platinum, palladium, cobalt, copper, but none were found suitable and reliable for SOFC anode due to high cost, low melting temperature, toxicity and lower electronic conductivity (Gorte et al. 2002; Kikuchi et al. 2006; Ringuede et al. 2004). Noble metals are expensive, spurring the exploration of other possible metals or alloys for fabrication of the anode.

A number of studies have substituted Ni with copper (Cu) as Cu is more electrically conductive, less catalytic to carbon-forming and more sulphur tolerant (Boder and Dittmeyer 2006; Dongare et al. 2002; Gorte et al. 2004; Jung et al. 2006; Kim et al. 2006c; Senguttuvan et al. 2006; Xie et al. 2006). Unfortunately, the melting point of Cu is lower than that of Ni [Cu: 1083.4^{o}C, Ni: 1453^{o}C (Shackelford and Alexander 1992)] making it impossible to fabricate at YSZ processing temperature (Gorte et al. 2002).

Co-doping of two or more metallic elements has also been applied in several studies which have focused mainly on combinations of Ni and Cu with Co (Ringuede et al. 2004), Ti, Fe (Kikuchi et al. 2006), Rh, Pd, Pt (Gorte et al. 2004) or Fe and some of their oxides (Huang et al. 2007). These alternative metallic elements did improve the anode properties relating to electronic conductivity and fuel compatibility but failed to meet the other important anode criteria such as anode thermal and chemical stability, especially in the long term.

The best ceramic material for an SOFC anode has been found to be YSZ. It is the most commonly used SOFC electrolyte material and definitely has chemical compatibility with the adjacent component. YSZ is considered inactive, although it plays an important role in dictating the catalytic activity of the anode. Thus, the most popular and state of the art anode material is Ni-YSZ, which has been found to meet almost all anode requirements (Badwal 2001). Ni-YSZ has been used as a high temperature SOFC anode since 1964 (Steele 2000). Table 4 summarises properties of Ni-YSZ cermet in an anodic environment.

Table 4: Properties of Ni-YSZ cermet in anodic environment (Minh and Takahashi 1995)

Properties	Data
Melting point/ °C (Melting point of Ni)	1453
Density, g/cm^3 (30 vol.% Ni)	6.87
Conductivity at 1000°C, Ω^{-1}cm^{-1} (30 vol.% Ni, 30% porosity)	~500
Coefficient of thermal expansion, 10^{-6} K^{-1} (30 vol.% Ni, 30% porosity)	~12.5
Strength at 25°C, MPa (30 vol.% Ni, 30% porosity)	~100

Other studies have substituted YSZ with other materials which have high ionic conductivity on the ground that the materials used in the anode should suit the materials used in the electrolyte. Possible candidates are ceria-based ceramics such as scandia-stabilised zirconia (SSZ) (Huang et al. 2006a; Kishimoto et al. 2007), gadolinium doped ceria (GDC) (Guan et al. 2008; Wang et al. 2006b), samaria doped ceria (SDC) (Misono et al. 2006; Ohara et al. 2000; Suzuki et al. 2006; Yin et al. 2006), yttria doped ceria (YDC)

(Guan et al. 2008; Horita et al. 2004), ceria doped rare-earth (RDC) (Goodenough and Huang 2007) and the co-doped ceria (Martınez-Arias et al. 2005; Tsipis et al. 2005).

Besides ceria-based solid oxide, lanthanum-based perovskite-related ceramics (Delahaye et al. 2006) and others with brownmillerite, apatite, or pyrochlores (Mather et al. 2004; Sakai et al. 2006) and tungsten bronze structure (Sun and Stimming 2007) are also being studied. Ceria-based ceramic materials have mixed ionic conductivity which makes them suitable for anode but otherwise in electrolyte (Primdahl and Mogensen 2002; Sammes and Cai 1997). However, this material is not stable at low partial pressure and high temperature (Kharton et al. 2004).

Table 5 lists Ni-based anode materials being studied to-date. Information in this table is drawn mainly from Ivers-Tiffee et al. (2001) and Wincewicz and Cooper (2005).

Table 5: Advantages and disadvantages of currently investigated Ni-based anode

CERAMIC	CRITERIA	ANODE	ADVANTAGES	DISADVANTAGES
Zirconia-based	• More mechanically stable than ceria-based • High temperature application (700-1000°C) • Typical OCV ~1.1-1.2V	Ni-YSZ	Most common and state-of-the-art SOFC anode met most of anode criteria (Haile 2003b) Max. power density produced in single cell so far ~2 W/cm^2 at 800°C (Kim et al. 2006b)	Not suitable at lower temperature, formation of carbon when using HC (Holtappels et al. 2006; Sun and Stimming 2007), Ni coarsening (Drescher et al. 1998; Steele 2000) and thermal degradation (Mallon and Kendall 2005)
		Ni-ScSZ	Low overpotential and better stability compared to Ni-YSZ and better fuel flexibility with low carbon formation. (Huang et al. 2006a; Huang et al. 2007; Kishimoto et al. 2007; Ukai et al. 2001)	Expensive due to price and availability of scandium and phase transition and aging with time
Ceria-based	• Lower operating temperature (500-700°C) • Unstable at lower partial pressure. • Exhibit mixed ionic and electronic conductivity (Orera et al. 1994; Primdahl and Mogensen 2002) • Low OCV (~0.8-0.9 V)	Ni-GDC	Higher average ionic conductivity than YSZ, compatible to most cathode materials and suppressed carbon formation (Marina et al. 1999; Wang et al. 2006b) Max power density 1.43 Wcm^{-2} (with SNDC electrolyte at 650°C) (Ahn et al. 2010)	Less stability and high cost
		Ni-SDC	High ionic conductivity below 700°C, compatible with Ni and performance strongly dependent on microstructure (Lu et al. 2003) Max power density of 388 mWcm^{-2} (at 750°C) (Fang et al. 2004)	Not suitable at high temperature and require microstructure control (Ohara et al. 2000)

	• High fuel utilisation decreased the system efficiency	Ni-YDC	Least expensive and low carbon formation	Poor chemical stability than ceria
Fe-doped $CaTiO_3$	• Less catalytically active • Stability strongly dependent on partial pressure (Boder and Dittmeyer 2006)	Ni-FCT	Stable performance at more than 20 hours operation (Kikuchi et al. 2006)	Still unknown
Al_2O_3	• High catalytic activity towards methane that give long-term stability	Ni-Al_2O_3	Max power density of 0.07 Wcm^{-2} with 0.24 V activation polarisation and R_p 0.26 Ωcm^{-2} at 900°C at a current density of 1.2 Acm^{-2} compared to Ni-YSZ anode with max power density of 0.30 Wcm^{-2} at 900°C (Li et al. 2010)	Lower power density than the Ni-YSZ

2.2.2 Electrical Conductivity

Electrical conductivity of the SOFC anode is its critical criterion. It is usually determined by the metallic element in the cermet which most commonly is Ni. Metals usually have higher electronic conductivity compared to other types of material. Resistivity and conductivity are inversely proportional. Therefore, as the Ni content increases it is expected that the anode conductivity increases and the resistivity decreases, as illustrated in Fig. 7. Maximum possible anode conductivity is required to minimise ohmic losses due to ionic conductivity of the ceramic phase.

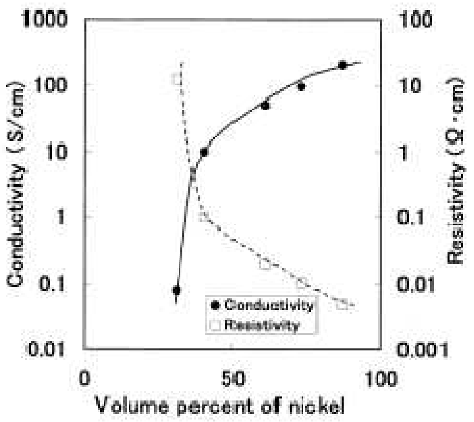

Fig. 7: Ni-YSZ volume ratio dependence of conductivity and anode resistance (Koide et al. 2000)

The percolation threshold of the anode is defined the minimum electronic conductivity that allows electricity flow. Theoretically, electrode performance reaches its effective conductivity when the composition of an electronically conducting network is close to the percolation threshold (Schneider et al. 2006). Zhu and Deevi (2003) report that most studies reviewed found that minimum Ni content is between 20-30 vol.%.

The minimum Ni content can be further reduced by improving the microstructure networking and the electrochemical reaction of hydrogen oxidation that are contributed by the ceramic phase. Recently, coating YSZ powder with Ni has proven to effectively enhance microstructural integration with adequate porosity and good three phase network. Such coating techniques are Pechini (Kim et al. 2006b), coat-mix (Simwonis et al. 1999), surface induced (Moon et al. 1999; Wang et al. 2004) and EN coating (Pratihar et al. 2004; Wen et al. 2000) which are then followed by solid state processing where the powder is compacted and sintered. Simwonis et. al (1999) compared the performance of an anode fabricated by coat-mix with those fabricated by the conventional ceramic method of tape casting, and found that anodes fabricated by coat-mix produced better microstructure, leading to higher conductivity.

The EN coated powders gave uniform distribution of Ni surrounding the YSZ particles as shown in Fig. 8. This morphology showed good metal-to-ceramic contact as well as a continuous metallic network that ensure good electrical conductivity. Pratihar et al. (2006) work producing anodes via EN coating has showed percolation thresholds with Ni content as low as 27.04 weight%. This is also supported by Jiang et al. (2005) and Lee et al. (2002) where they found that optimum electrical conductivity of anode can be achieved through its compositions and a good network of metallic elements.

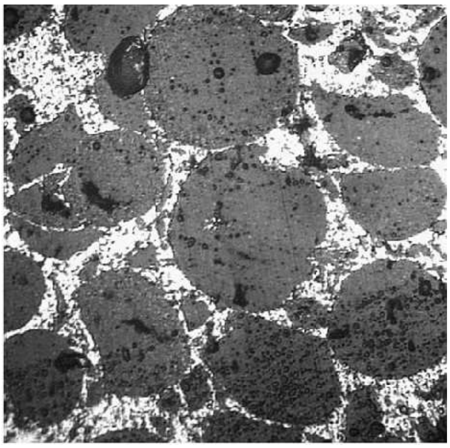

Fig. 8: Optical micrographs of Ni/YSZ cermet containing 20 vol.% Ni. Magnification 400× (Pratihar et al. 2004)

Yu et al. (2006) has shown that particle size of Ni and YSZ also play an important role in improving electrical conductivity of the anode while fine particles for both ceramic and metallic phases give better percolation and electrical conductivity as well as mechanical properties. Fine particles introduced smaller porosity directly enhancing the mechanical property of the anode, while coarse particles enhanced the contact and surface area for electrochemical reaction to take place (Wang et al. 2006c).

The combination of coarse and fine particles (bi-model) studied by Kim et al. (2006b) showed an enhancement of both chemical and electrical properties of the anode. Kim and co-authors successfully fabricated an Ni-YSZ anode having nano-size YSZ and NiO particles co-conjugated on the bigger diameter YSZ core particles, as illustrated in Fig.

9. This morphology is found to yield a homogeneous, durable and highly efficient electrode. The single cell run under 1.0 Acm^{-2} at 800°C for 550 h of operation has shown excellent durability with zero degradation with power densities of 1.5 Wcm^{-2}.

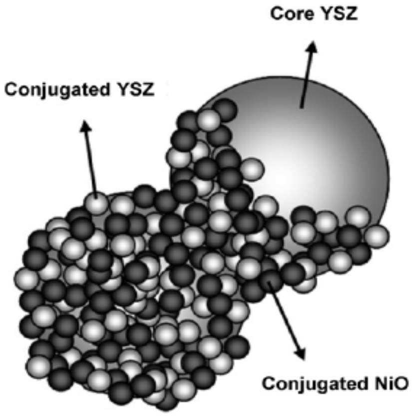

Fig. 9: Schematic diagram of the dual composite powder (Kim et al. 2006b)

A site where three phases (gas, metal and ceramic) meet and the electrochemical activity occurs is called a triple-phase boundary (TPB). Berkel et al. (1994) illustrated the effect of particle size on TPB length and anode performance (Fig. 10). A low YSZ/Ni particle size ratio was found to reduce TPB length with high voltage losses. On the other hand, a high YSZ/Ni particle size ratio increases TPB length and reduces voltage losses. The work of Berkel and colleagues described TPB length as directly proportional to the YSZ/Ni particle size ratio. The small particles tend to cluster around large particles. The fine Ni-particles give high surface area which then improves the metal-to-ceramic contacts, leading to higher electrical conductivity (Boer et al. 2000).

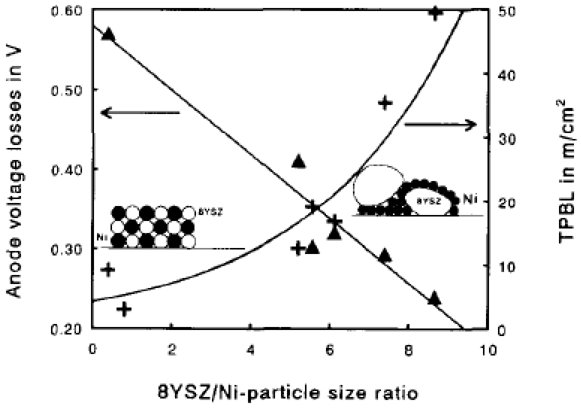

Fig. 10: Anode voltage losses and TPBL as a function of 8YSZ/Ni particle size ratio (Berkel et al. 1994)

The TPB of an anode can be improved by a good and precise fabrication method. The fabrication method determines good metal to ceramic interaction. The sintering and reduction process helps increase porosity, thus improving the three-dimensional network of metal-ceramic-pores that is called TPB. Pratihar et al. (2005) compared the variation in anode conductivity against temperature (Fig. 11) following various fabrication techniques, i.e. solid state, liquid disperse and EN coating. They found that the EN coating technique dramatically improved electrical conductivity as it results in better morphology and network formation than do other fabrication techniques.

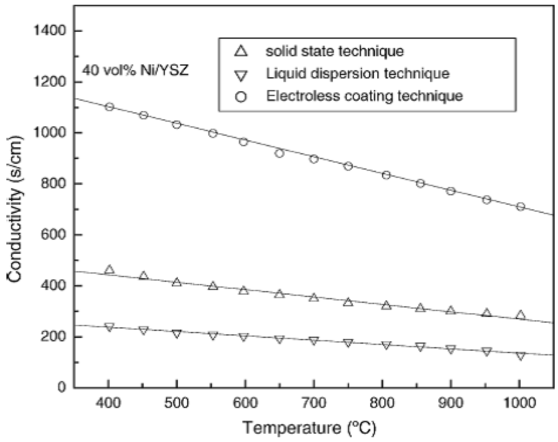

Fig. 11: Conductivity comparison of three different fabrication techniques (Pratihar et al. 2005)

In conclusion, a few factors have been found to maximise anode electronic conductivity: (1) composition of metal and ceramic, (2) particle sizes, and (3) morphology optimisation via method of fabrication. The next criterion for a good anode is the catalytic activity, elaborated in the next section.

2.2.3 Catalytic Activity

Catalytic activity of an anode is basically related to the electrochemical oxidation reaction of the fuel. Sufficient catalytic activity of electrochemical oxidation in the anode lowers polarisation. In order to improve the Ni-YSZ anode electrocatalytic activity, resistance of the cell - the root cause of reduced electrocatalytic activity - must be eliminated or at least minimised. The cell resistance derives from two sources of resistance: ohmic resistance (IR) and polarisation resistance (Jia et al. 2006; Pratihar et al. 2004). Ohmic resistance (IR) is usually taken to arise from electrode and the electrolyte, but the major source of IR is the electrolyte due to its ionic conduction as described by Virkar et al. (2000). The polarisation resistance of the anode is very sensitive to the contact area of Ni on the electrolyte material (Jia et al. 2007).

It has been argued that the electrochemical reaction actually occurs in the anode, either on the Ni or YSZ surface or at the interfacial layer between electrode and electrolyte. This is where the TPB comes into the picture as the site where the reaction occurs. Ioselevich et. al. (1999) gives clear illustration for the reaction mechanism movement as shown in Fig. 12. White circles resemble metallic phases, black circles resemble ceramic phases, empty spaces resemble pores and the shaded areas represent TPB. The reaction species i.e. the gas/ fuel, is supplied through the pores, as represented by the dotted lines. The charge transfer of the reaction species and the formation of H_2O are routed, as indicated by the solid lines, through the metallic and ceramic phases. These activities occur at the TPB, so increasing the TPB will increase catalytic activity. Furthermore, Bieberle and Gauckler (2000) found that the length of the reaction site or TPB is inversely proportional to the polarisation resistance.

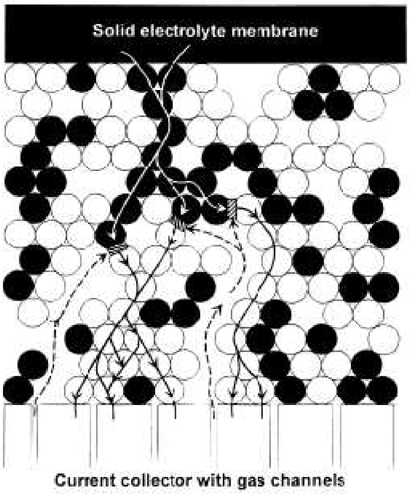

Fig. 12: Illustration of active site for electrochemical reaction (Ioselevich et al. 1999)

Other workers Abe et al. (2006); Holtappels et al. (2006); and Jiang and Badwal (1999) have noted that the reactions consist of four steps: (i) diffusion of reaction species, i.e. H_2 and H_2O in gas phase; (ii) dissociative adsorption of reaction gases at the solid surface, i.e. metal or oxide surfaces; (iii) surface diffusion of H_{ad}, O_{ad}, OH^-_{ad} on the anode surface or diffusion of H in the anode to the reaction site and (iv) charge transfer of reaction species and formation of H_2O at reaction sites. One of these reaction mechanisms could be rate-determining or limiting for anodic reaction.

Other than electrochemical reaction kinetics, another factor influencing cell resistance is the composition of the Ni-YSZ anode. A study by Koide et. al. (2000) showed that cell resistance (both ohmic and polarisation) at a constant current density of 0.3 Acm^{-2} at 1000^{o}C behaves differently as a factor of Ni composition. Fig. 13 (from Fergus et al. 2009) shows the maximum power output and cell resistance with varying levels of Ni. The maximum power output was found to be directly proportional to the Ni volume percent (Fig. 13a) whereas the ohmic resistance was inversely proportional to Ni content (Fig. 13b). Interestingly, polarisation resistance was found to be very sensitive to Ni content. Minimum polarisation was achieved at 40 vol.% Ni (Fig. 13b).

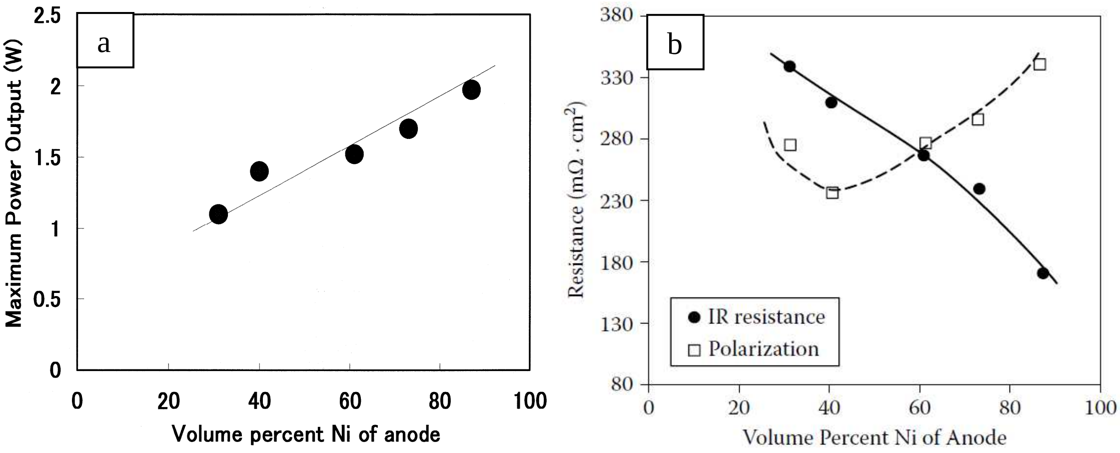

Fig. 13: Anode performance (a) maximum power output and (b) IR and polarisation resistance (Fergus et al. 2009)

2.2.4 Porosity Content

Adequate porosity content is also important as it helps managing fuel flow-in and reactant gaseous flow-out. Undesirable microstructural properties such as anisotropic packing and pore structure have been found to lower pore density and connectivity of metallic and pore phases, resulting in significantly reduced cell performance with the decreasing number of electrical conduction paths, effective gas diffusion paths and TPB length for anodic reaction (Fukui et al. 2003). Studies have shown that the acceptable degree of porosity in the anode is around 40 vol.% (Kim et al. 2006a). This upper limit of porosity is based on acceptable mechanical strength of the anode.

Increasing the length of the TPB by controlling the microstructure of the anode materials can increase the electrochemical reaction of the anode (Fukui et al. 2004; Virkar et al. 2000). Fig. 14 shows the differences in terms of porosity distribution in Ni-YSZ anodes fabricated by two different methods, liquid-dispersion and EN coating. The EN coating technique produced more porosity in the form of open pores than did the liquid-dispersion method leading to higher anode conductivity at 1000°C.

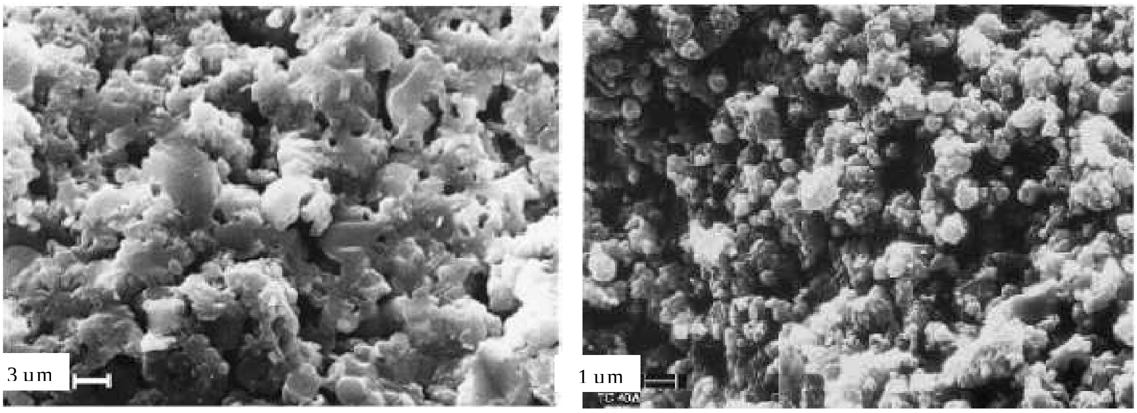

Fig. 14: SEM micrograph showing porosity in the anode fabricated by a) liquid-dispersion (b) electroless coating (Pratihar et al. 2005)

Porosity can also be enhanced by the addition of pore-former, sintering process (Clemmer and Corbin 2004) as well as reducing cyclic process (Fergus et al. 2009). The hydrogen reduction cycle during operation increases porosity volume in the anode but at the same time reduces fracture toughness due to low solid area (Radovic and Lara-Curzio 2004).

One study shows that the porosity of the anode increases with the increasing amount of coarse powders (Koide et al. 2000). The ideal combination is 20% fine and 80% coarse particles, as shown in Fig. 15, ending with approximately 40 vol.% porosity in Ni-YSZ cermet. A sufficient porosity level gives high electrical conductivity (>1400 Scm^{-1} at 800°C) with power output of 0.56 Wcm^{-2} due to effective percolation between Ni, YSZ and pores (Kim et al. 2006a).

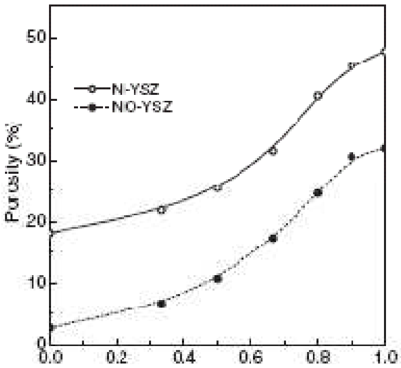

Fig. 15: Porosity as a function of coarse powder fraction (Koide et al. 2000)

2.2.5 Coefficient of Thermal Expansion

The ceramic phase in the anode depends on electrolyte materials because it provides chemical and thermal stability to the interface region. Thermal expansion of Ni-YSZ varies proportionally with the amount of Ni. The CTE of the anode should be made as close as possible to the CTE of the electrolyte. This can be achieved by reducing the Ni content in the anode as much as possible since the CTE of Ni (16.5 x $10^{-6}K^{-1}$) is higher than YSZ (10.7 x 10^{-6} K^{-1}) (Pratihar et al. 2004). Reduction of Ni content ensures matching CTEs between anode and electrolyte, thus avoiding delamination and cracking of the anode stack during fabrication or operation (Aruna et al. 1998).

A plot of the average CTEs of anode cermet for temperature ranges between room temperature and 1200^{o}C as a function of Ni volume percent is shown in Fig. 16 (Minh and Takahashi 1995). The plot shows that the addition of Ni to YSZ gives the cermet a higher CTE than that of the YSZ electrolyte, resulting in a significant degree of CTE mismatch, which can cause large stresses and cracking. Several studies have investigated methods for tolerating and minimising anode CTE mismatch by, for example, control of processing in order to reduce flaws in electrolyte fabrication or adding another constituent to reduce the anode CTE mismatch. The ceramic phase should be adjusted to best suit the metallic phase as well as to produce high ionic and electronic conductivity. Furthermore, maintaining matching CTE between the anode and the electrolyte is the key to achieving the optimum anode.

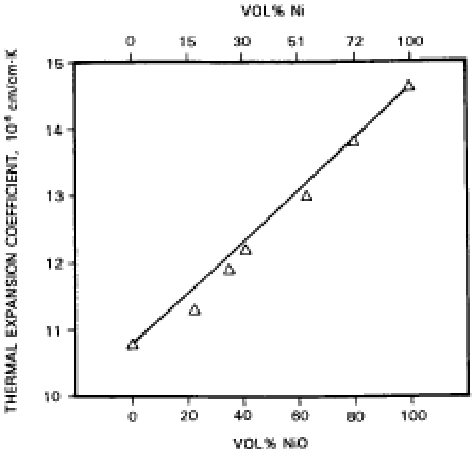

Fig. 16: Anode cermet CTE as a function of Ni content (Minh and Takahashi 1995)

In the following section, anode fabrication techniques will be elaborated further. This is the heart of this study as the production cost of anode is one of the major obstacles for SOFC applications in the industry (Yamamoto 2000).

2.3 Anode Fabrication

Fabrication of the anode depends, first of all, on the SOFC design, whether tubular or planar. Since the most popular and practical SOFC design is planar, investigation of the fabrication process has concentrated on planar SOFC anode. Planar SOFC comes in two types: anode-supported or electrolyte-supported. In order to reduce ohmic resistance the electrolyte has to be made as thin as possible - approximately less than 10 µm (Xin et al. 2006) or ultra-thin at less than 1 µm (Chen and Wei 2006) but an electrolyte that is too thin is not practical.

Most fabrication is based on electrolyte-supported processing where a layer of anode substrate is placed onto the electrolyte. The key factors in determining the best processing technique to be applied are anode performance and production cost. In general, anode substrate fabrication techniques can be divided into three major classes:

(1) Conventional ceramic processing techniques: tape casting (Basu et al. 2008; Misono et al. 2006; Qiao et al. 2007; Savignat and Chiron 2007; Simwonis et al. 1999), screen printing (Rotureau et al. 2005), slurry coating (Singhal 2000, Wang 2006a), solgel (Marinsek and Macek 2000; Suciu et al. 2008; Yin et al. 2006), tape calendaring (Han et al.

2008), electrophoretic deposition (EPD) (Besra and Liu 2007), and impregnation/ infiltration (Jiang 2006; Jin et al. 2010; Wang 2006b),

(2) Solid state processing techniques: conventional (Eguchi et al. 2000; Muller et al. 2002; Tucker et al. 2010), precipitation (Han et al. 2006; Wang et al. 2010), coat-mix (Simwonis et al. 1999), Pechini (Kim et al. 2006a), and EN coating (Pratihar et al. 2007),

(3) Direct deposition techniques: electrochemical vapour deposition (EVD) (Haldane and Etsell 2005), CVD (Liu et al. 2004), plasma spraying (Stöver et al. 2006; Benoved and Kesler 2009; Li et al. 2010), spray pyrolysis (Kawano et al. 2005; Liu et al. 2010; Suda et al. 2006), physical vapour deposition (PVD) (Wincewicz and Cooper 2005), and sputtering (Rezugina et al. 2010).

The stages of fabrication of the anode layer onto the electrolyte are given in Fig. 17.

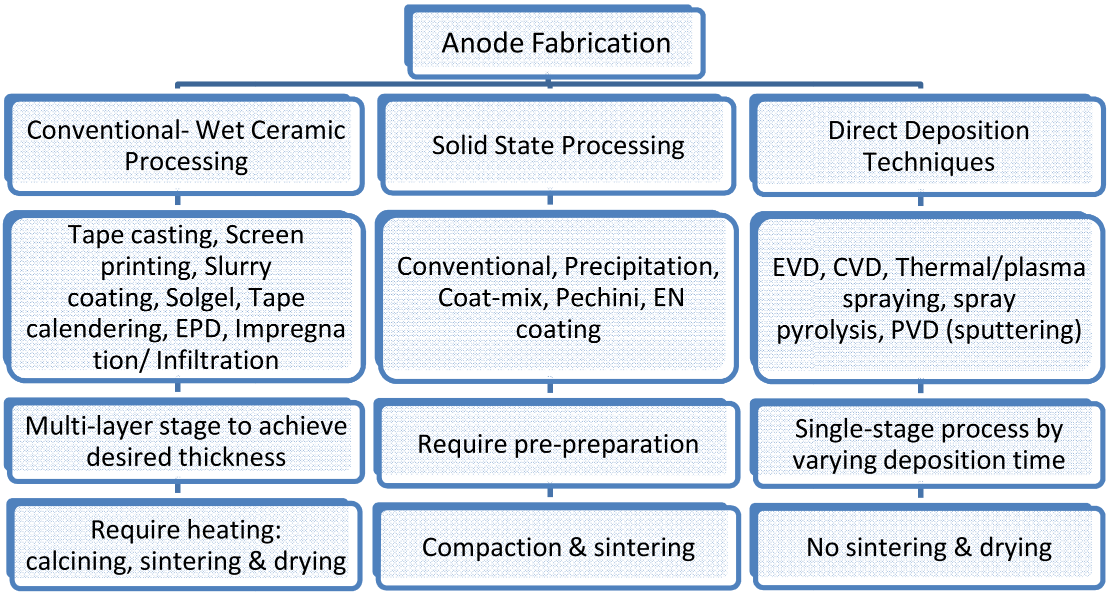

Fig. 17: Anode fabrication categories

2.3.1 Conventional Techniques

Since SOFC anodes are made of ceramic materials, one commonly used fabrication technique is conventional wet ceramic processing. Conventional anode fabrication techniques are relatively reliable for production of reasonable SOFC anode performance. A variety of ceramic conventional processes have been investigated, but the most popular are tape casting, screen printing, painting and slurry coating, sol-gel and EPD.

2.3.1.1 Tape casting

Tape casting is the most common processing method for fabrication of SOFC anode-supported electrolyte. The process involves dispensing a slurry of the desired powder composition from a slurry vessel onto a moving carrier film, as illustrated in Fig. 18. The slurry passes under the doctor blade to form a flattened layer of green (unfired) ceramic tape. The slurry comprises of dispersant in a suitable solvent with organic additives such as binder, plasticiser and homogeniser. Slurry thickness can be controlled through the doctor blade and viscosity adjustment. Organic pore formers (pyrolyzable particles), which will burn-out during firing, are added to increase anode porosity.

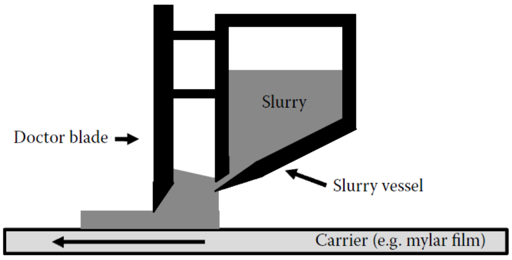

Fig. 18: Schematic diagram of tape casting process for producing a ceramic green film (Savignat and Chiron 2007)

Multilayered plates can be produced by casting multiple layer tapes, which are then laminated together and co-fired to yield the finished product. Multiple green tape casting layers of various thicknesses were successfully produced by Moon et al. (2008), then co-fired to improve cell electrochemical performance and long-term stability. The application of hot pressing lamination on a green tape casting was found to give a gas-tight electrolyte and good overall cell performance without cracking (Song et al. 2008).

For the fabrication of planar SOFC anodes, tape casting is the most popular method. A recent study has shown that gradient anode porosity was successfully achieved by tape casting and that the power density in the unit cell increases with porosity concentration distribution from 76 mWcm^{-2} to 101 mWcm^{-2} at 600^{o}C in humidified hydrogen (An et al. 2010). A new approach for tape casting has recently been investigated where the Ni-YSZ anode and YSZ electrolyte layer were successfully simultaneously tape casted and co-fired without crack, warping or delamination, giving a high power density of 1085 mWcm^{-2} at 850^{o}C (Le et al. 2010).

2.3.1.2 Screen printing

Screen printing is widely used in commercial production of planar SOFC, especially of the electrolyte. It is a simple method. The screen printing machine is an apparatus enabling printing on ceramic material, including low temperature co-fired ceramic material. The prepared slurry is poured onto the screen of a setup machine (Fig. 19) and a print head pressure is applied to flatten and remove excess slurry.

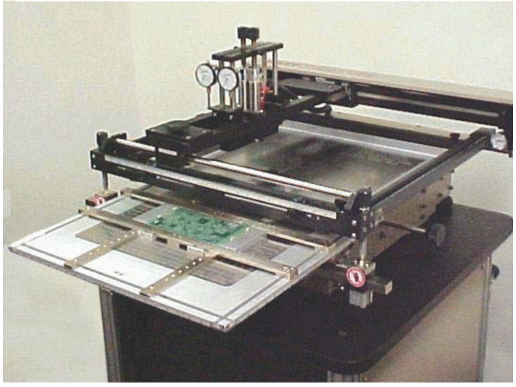

Fig. 19: Screen printing press

A very precise final product is possible as the machine includes predetermined patterns and a movable fixture to adjust separation distance between the fixture support plate and the print head during the screen-printing operation. After flattening and removal of excess slurry, the product is sintered at approximately 1400°C for the electrolyte and 900-1200°C for the cathodes. Rotureau et al. (2005) found that an Ni-YSZ anode and an LSM cathode that had been screen printed onto YSZ electrolyte to form a single-chamber fuel cell (SCFC) had a power density of 1.2 mWcm^{-2} at 800°C in methane.

2.3.1.3 Painting & slurry coating

Painting is a simple technique in which a slurry of the powder to be deposited is applied by brushing onto support layers. The problems with painting are the method’s low production consistency, the difficulty in scaling up for mass production and it is not being readily reproducible. Slurry coating is sometimes used to deposit the anode layer on the electrolyte (Singhal 2000). Slurry spin coating has been shown to give more uniform thickness through controlled spinning speed (Chen et al. 2006; Wang et al. 2006a).

2.3.1.4 Sol-gel

Sol-gel is a polymerisation process of a solid body from a metal compound solution, a process that is sometimes referred to as the liquid precursor method. In the sol–gel process, a solution of metal compounds or a suspension of very fine particles in a liquid (referred to as a *sol*) is converted into a highly viscous mass (the *gel*). The two types of sol–gel processes are distinguished by their use of a sol or a solution. A sol (suspension of fine particulates) produces particulate gel which upon drying produces dried gel and a dense product after firing. A solution of polymer, typically a solution of metal-organic compounds (such as metal alkoxides), produces a chain of polymeric gel, which turns into dried gel upon drying and a dense product after firing.

Basically the process for both sol and solution type sol-gel can be simplified into 3 major stages as illustrated in Fig. 20. This solution sol–gel process is receiving considerable research interest; however, the sol–gel process based on the gelling of suspensions sees more widespread industrial application.

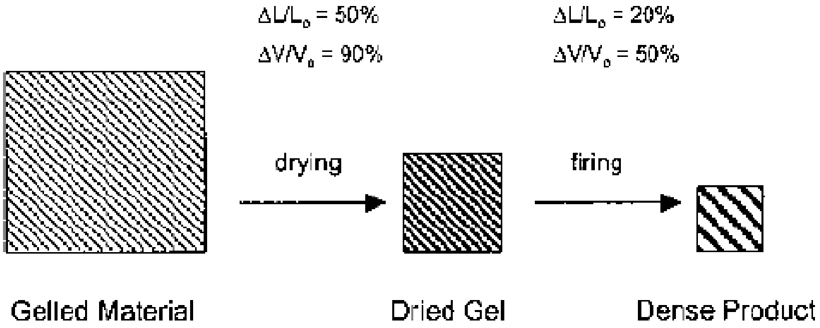

Fig. 20: Three major sol-gel stages and the significant shrinkage upon drying and heating (Rahaman 2003)

The application of a sol-gel process in fabricating an NiO-SDC anode of 35 µm was successfully achieved, giving a long-term stability over 7 days (Yin et al. 2006). Also, other studies have varied sol-gel solution composition (Huang et al. 2006b), pre-cursor compositions and YSZ-NiO proportions (Marinsek and Macek 2000; Suciu et al. 2008). The studies found that these factors altered product morphology, increasing electrical conductivity at Ni volume above 35% and particle sizes to near-optimal SOFC anode production and continuous phases.

2.3.1.5 Tape calendaring

Tape calendaring is a process involving tape forming of electrolyte and support electrodes. First the powders and organic binders of electrolyte and electrodes are mixed together in a high-intensity mixer to form plastic masses. Then these electrolyte and electrode plastic masses are rolled into tape as illustrated in Fig. 21. These two tapes are then rolled together to form a bilayer and then rolled again with another electrode to form anode-electrolyte-cathode layers. The product is cut, then fired to give the final deposited electrode application. A study by Han et al. (2008) on a tape calendaring-produced anode of thickness range 0.8-1.0 mm co-fired at 1300-1350^{o}C finally yielded a 15-20 µm active functional layer with maximum power density of 0.95 Wcm^{-2} at 800^{o}C.

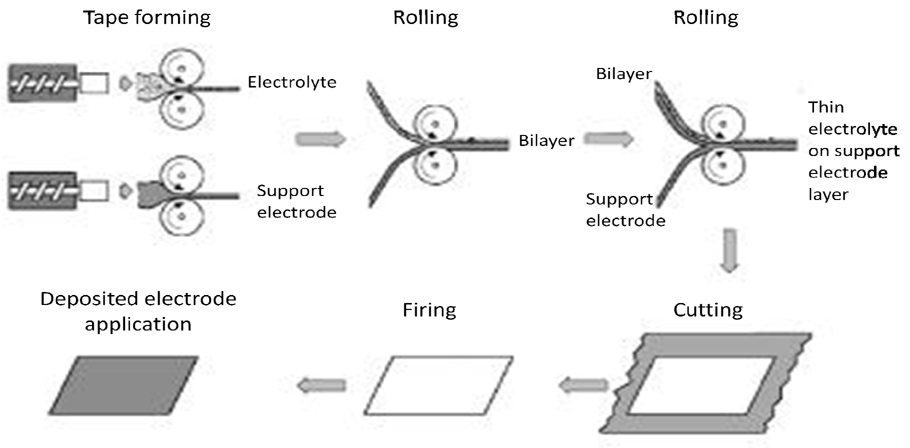

Fig. 21: Tape calendaring process in fabrication of planar SOFC (Minh et al. 1999)

2.3.1.6 Electrophoretic deposition

Electrophoretic deposition (EPD) is a colloidal processing technique that offers potential reliability in producing ceramic films and components through control of the initial suspension and its evolution during shaping. The foundation of EPD theory is the movement of clay particles in water due to electrical field induction. EPD uses direct current (DC) to deposit thin layers of particle where the charged powder particles are dispersed or suspended in a liquid medium, then attracted and deposited onto a conductive substrate of opposite charge (Fig. 22).

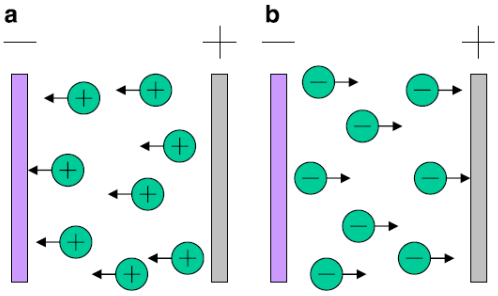

Fig. 22: Schematic diagram of EPD (a) cathodic, (b) anodic (Besra and Liu 2007)

The process has advantages of a short formation time, its need for only a simple apparatus, little restriction on the shape of substrate, its ability to orient anisotropic powders allowing texturing of materials, and its having no requirement for binder burnout as the green coating contains few or no organics. Though the process is simple, easy to use and cost-effective, it requires thoughtful choice of solvent media. This ensures an appreciable magnitude of surface charge developed on the suspended powder surface to stabilise the suspension as well as promoting high electrophoretic mobility (Besra and Liu 2007).

2.3.1.7 Sintering

Tape casting, screen printing, painting and slurry coating, sol-gel and EPD are deposited in green (unconsolidated) form using slurries of various viscosities with a suspension liquid as the carrier. Therefore a sintering (firing) process is required to densify the layers to achieve good bonding and contact between the particles. The firing temperature must be high enough to fully densify the green body—typically 1400^{o}C for most electrolytes. At such high temperatures inter-reactions between some electrolyte-cathode pairs are likely to occur, so the firing steps are often done in two separate sintering steps: (1) a high-temperature step to co-sinter the anode and electrolyte together, and (2) a lower-temperature step to consolidate the cathode (Wincewicz and Cooper 2005).

2.3.1.8 Impregnation/ Infiltration

Impregnation or infiltration is a process to form an electrode via a series of stages as illustrated in Fig. 23. A porous pre-form electrode is obtained by sintering at a temperature that achieves good contact between the porous electrode and the adjacent electrolyte. Then the porous pre-form is infiltrated or impregnated with either nano-particle slurry or precursor solution. The body is then fired again at a low temperature, and sometimes this stage is repeated many times to obtain sufficient electrode reaction sites.

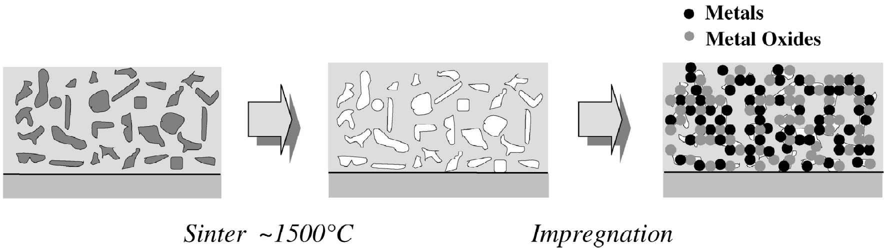

Fig. 23: Illustration of impregnation stages (Gorte et al. 2002)

Some anodes are fabricated by impregnation or infiltration methods. An Ni-YSZ anode infiltrated by the optimal 1/14 wt.% SZY was found to improve the electrochemical properties of the anode (Jin et al. 2010). Another study on GDC-impregnated Ni anode was found very stable in weakly humidified environment (~3%H_2O) at 800^oC (Wang et al. 2006b).

2.3.2 Solid State Processing

Solid state processing is a fabrication of a composite anode in its solid state. The fabrication of Ni-YSZ anode is done by a pre-preparation process, either conventional precipitation, or coating of powders. The conventional pre-prep process includes the stage of ball milling the powders to ensure good mixing. Then the mixed product is uniaxially pressed and sintered at 1100-1300^oC. The precipitation process, the most common of which is the glycine-nitrate process (GNP), crystallises powders from a suspension. The powders are then dried, compacted and sintered. The process of coating of powders could be done by EN coating of the YSZ powders with Ni. Then the powders are dried and compacted to produce the green pellet and then sintered.

In a recent study using new anode materials, Ni–LnO_x (Ln = La, Ce, Pr, Nd, Sm, Eu, and Gd) cermet anodes fabricated by GNP were found to give better porosity with peak density of 730 $mWcm^{-2}$ and total interfacial polarization resistance down to 0.12 Ωcm^2 (He et al. 2010). The studies modifying the precipitation method such as coat-mix (Simwonis et al. 1999) and Pechini (Kim et al. 2006a) found that these methods gave improved anode microstructure with adequate porosity, electronic conductivity and good durability.

A composite of Ni-YSZ at 50-50 vol.% fabricated via solid state precipitation was manipulated to give thread-like Ni particle microstructure. This gave percolation with porosity greater than 65% and a mechanically stable composite with structural density greater than 80% (Gonzalo-Juan et al. 2010). Another study by (Pratihar et al. 2005) compared anodes fabricated via conventional solid state, liquid dispersion and EN coating and found that the anode fabricated with EN coating showed improved 3-D networking of the Ni ring, improving anode electronic conductivity.

2.3.3 Direct Deposition Techniques

Multi-stage wet-ceramic processing followed by sintering at high temperature causes tremendous degradation in terms of unwanted layer inter-reactions, microstructural coarsening, and possible oxidation of a metal support layer for metallic interconnect-supported cells. Direct deposition techniques that do not require a high-temperature consolidation step after deposition of the layers open-up other processing alternatives. Several direct deposition techniques i.e. EVD, CVD, PVD and plasma spraying that have been developed for SOFC fabrication will be discussed below.

2.3.3.1 Electrochemical vapour deposition

Electrochemical vapour deposition (EVD) is a process where mixed chlorides of the specific metals involved react in the gaseous state with water vapour, resulting in deposition on the support tube/air electrode substrate. The thickness of the impervious thin oxide layer deposited ranges between 20 and 50 microns. This process occurs in an internal heater, such as a heat pipe, that is placed within the support tube/cathode substrate and induces a uniform temperature profile to give precise and uniform oxide deposition. Since the process is only suitable for tube substrate, it is currently utilized to produce the electrolyte on cathode-supported tubular cells. This technique is particularly adapted for large-scale, commercial fabrication of SOFCs.

EVD is sometimes used to deposited anode layers onto cathode-electrolyte bilayer tubes as the anode cannot be fired at a very high temperature to fully densify the electrolyte (Fergus et al. 2009). In one study, a metal anode was fabricated using polarised electrochemical vapour deposition (PEVD) which resulted in a densification of the metallic electrode during deposition (Haldane and Etsell 2005). This densification problem can be controlled by lowering the deposition temperature.

2.3.2.2 Chemical vapour deposition

Chemical vapour deposition (CVD) is a well-established technique that can be used to deposit all classes of materials, including metals, ceramics, and semiconductors. The process involves transportation of reactive molecules in the gas phase to a surface where they chemically react and form a solid film. CVD can cover a wide range of coating dimensions and thicknesses, making it amenable to mass production.

CVD has a number of process variables that must be manipulated to produce a deposit with the desired properties, including such factors as (1) flow rate of the reactant gases, (2) nature and flow rate of any carrier gases, (3) pressure in the reaction vessel, and (4) temperature of the substrate. Of these four factors, substrate temperature is the most critical since it influences the deposition rate and is the main factor controlling the structure of the deposit, i.e. high temperatures give crystalline deposits while low temperatures result in amorphous deposits, while moderate temperatures produce polycrystalline deposits.

CVD is especially targeted for fabricating thin electrolyte films, but an SOFC anode has been successfully fabricated by combustion chemical vapour deposition (CCVD). Porosity-graded LSM-GDC/ LSM-LSC-GDC/ LSC-GDC cathode and NiO-GDC anodes were deposited onto YSZ electrolyte via CCVD, giving a reasonable maximum power density of 0.48 Wcm^{-2} at 800^oC (Liu et al. 2004).

2.3.2.3 Plasma spraying

The plasma spraying process gives a very precise and excellent finish in terms of rapid deposition rate, continuous morphology, ability to control compositions, direct deposition without sintering and low metal interconnect oxidation during cell fabrication. Based on these excellent qualities, this technique is ready for mass production and adaptable to fully automated manufacturing. Unfortunately, the process is high in cost.

The plasma spraying process involves feeding a powder that is suspended in either a gas carrier or liquid such as water or ethanol, or the feeding of solution precursors, into a plasma jet. There are two types of plasma jet feedstock, - radial and axial injection as shown in a schematic diagram in Fig. 24. The high temperatures that reach up to 10,000 K melt the particles and the molten droplets are propelled toward a substrate where they solidify rapidly to form a coating.

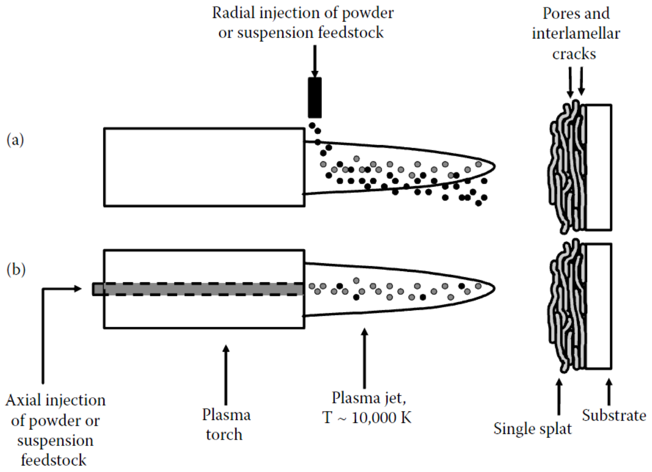

Fig. 24: Schematic diagram of plasma spray (a) radial injection (b) axial injection (Fergus et al. 2009)

In recent times, plasma spraying technology has been commonly used in fabricating SOFC anodes. The Ni-YSZ anode and YSZ electrolyte of a functional graded PEN (positive-electrolyte-negative) planar SOFC were fabricated via atmospheric plasma spraying (APS) and the LSCF cathode by solgel, resulting in improved electrochemical cell performance (Wei-sheng et al. 2009).

2.3.2.4 Spray pyrolysis

Spray pyrolysis is a process of depositing SOFC components in three consecutive stages. This process uses a carrier gas delivery system, an ultrasonic atomiser, furnaces and spraying nozzle as shown in Fig. 25. The precursor solution is filled into an ultrasonic atomizer where the atomised droplets are transported via carrier gas through the furnaces. They are then pressurised through the spraying nozzle and deposited on the substrate.

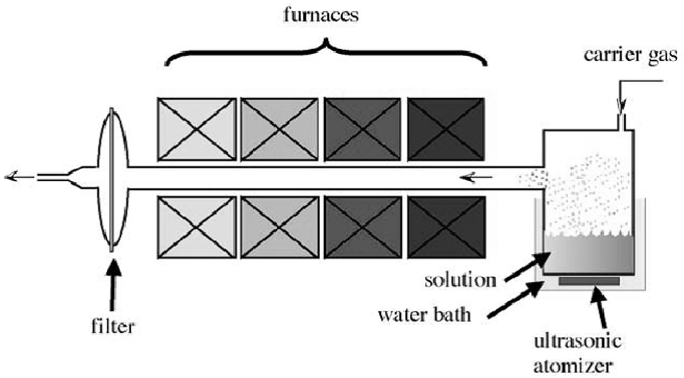

Fig. 25: Schematic diagram of spray pyrolysis system (Suda et al. 2006)

Ultrasonic spray pyrolysis has been investigated for its ability to control the Ni-CGO anode microstructure. It was found that the deposition temperature and precursor solution concentration are the most critical parameters that influence anode morphology, optimally yielding homogeneous elemental distribution, porosity content of 21-52% and particle size between 2- 17 µm (Liu et al. 2010). Another study by Suda et al. (2006) found that an Ni-SDC anode fabricated via spray pyrolysis produced spherical NiO-SDC composite particles of 0.6-0.7 µm giving a higher SOFC cell performance than the mixing method.

2.3.2.5 Physical Vapour Deposition

Physical vapour deposition (PVD) can be categorised as pulsed-laser deposition (PLD), sputtering and molecular beam epitaxy (MBE). PLD is more common in fabricating electrolytes and cathode layers. Sputtering has commonly been used to fabricate electrolytes but some studies have shown successful anode and cathode fabrication using RF sputtering (Rezugina et al. 2010; Yoo 2006).

2.3.2.6 Sputtering

The sputtering process is held in a vacuum chamber and a pump for supplying an ionisable gas into the vacuum chamber. There are two types of sputtering techniques: RF and DC sputtering. The difference between the two is the source of the power supply. In the case of thin-film deposition, the sputtering technique is combined with photolithography where the etched area is protected from ion bombardment during sputter operation. The sputtering technique is much more versatile than other deposition techniques as it allows excellent control of composition and morphology, and requires relatively low temperatures, helping to prevent the unwanted reactivity observed at higher temperatures. However, the major limitations are equipment costs and slow deposition rates (~5 μm/h) (Holtappels et al. 2005).

2.3.4 Summary of Anode Fabrication

The three categories of fabrication methods discussed above are used for anode fabrications. The summary of studies done on anode fabrications by conventional ceramics, solid state and direct deposition are listed in Table 6. The most common anode material used is NiO-YSZ followed by Ni-SDC, Ni-GDC and Ni-ScSZ, and the recent investigated anode material is Ni-Al_2O_3. The conventional techniques give a maximum P_{max} of 1.2 Wcm^{-2} at 800^oC. The solid state techniques having a maximum P_{max} of 2.005 Wcm^{-2} at 800^oC whereas the direct deposition techniques maximum P_{max} is 0.57 Wcm^{-2} at 1000^oC. On average the maximum power output obtained in most cells is about 0.5 Wcm^{-2} with an anode thickness as thin as 15 μm and as thick as 3 mm.

Table 6: Summary of anode fabrication over the last 10 years

	FABRICATION	ANODE MATERIALS	ANODE THICKNESS	PERFORMANCE	REFERENCES
Conventional Ceramics	Tape Casting	Ni-YSZ	27 mm	48 vol.% porosity	Simwonis et al. (1999)
		Ni-YSZ	20 µm active site 45 µm active site	P_{max} 0.73 Wcm^{-2} @ 700°C P_{max} 0.20 Wcm^{-2} @ 700°C	Moon et al. (2008)
		Ni-YSZ	570 µm	P_{max} 0.17, 0.23 Wcm^{-2} @ 750°C	Song et al. (2008)
		Ni-SDC	ns	P_{max} 460, 750, 910 mWcm^{-2} @ 550, 600, 650°C	Misono et al. (2006)
		Ni-GDC	ns	P_{max} 909, 623, 335 and 168 mWcm^{-2} @ 650, 600, 550 and 500°C	Fu et al. (2010)
		Ni-YSZ	1500 µm	101 mWcm^{-2} @ 600°C with 35% porosity	An et al. (2010)
		Ni-YSZ	1.5 mm	P_{max} 661, 856, 1085 mWcm^{-2} at 0.7V and 750, 800 and 850°C	Le et al. (2010)
	Screen Printing	Ni-TZ3Y	ns	P_{max} 350 mAcm^{-2} with OCV 90mV @ 800°C	Jiang et al. (2000)
		NiO-YSZ	1.5 mm	P_{max} 1.2 Wcm^{-2} @ 800C	Basu et al. (2008)
		Ni-YSZ	>10µm	Porosity 26%, CTE min 12.3X10^{-6}K^{-1}	Muller et al. (2002)
		Ni-YSZ	ns	P_{max} 1.2 mWcm^{-2} for SCFC @ 800°C	Rotureau et al. (2005)
	Sol-gel - Gel-casting	Ni-8YSZ (sintered @ 1300°C)	ns	σ= 7.0 Scm^{-1}	Huang et al. (2006b)
		NiO-SDC (sintered @ 1350°C)	ns	P_{max} 491 mWcm^{-2} @ 600°C	Yin et al. (2006)
	Tape calendering	NiO-YSZ	15-20 µm	P_{max} 0.28, 0.51. 0.95 Wcm^{-2} @ 700, 750, 800°C	Han et al. (2008)
	EPD	Ni-YSZ (60:40 wt%)	ns	P_{max} 150, 300, 450 mWcm^{-2} @ 700, 750, 800°C	Besra and Liu (2007)
		Ni-coated Pt	ns	P_{max} 200 mWcm^{-2} @ 700°C	

	Impregnation/ Infiltration	NiO-YSZ	ns	P_{max} 434 mWcm^{-2} @ 800°C	Besra et al. (2006)
		Ni-CeO$_2$/YSZ	ns	P_{max} 230, 420, 530 @1173 K for 25wt%Ni, 5wt%CeO2-25wt%Ni/YSZ, 10wt%CeO2-25wt%Ni/YSZ respectively	Qiao et al. (2007)
		NiO-ScSZ impregnated with Ni catalyst	ns	119 mW cm^{-2} @ 750°C	Zhang et al. (2010)
Solid state	Precipitation	YSZ-Cu alloy	ns	P_{max} 275 mAcm^{-2} operated for 110h at 700-800°C	Tucker et al. (2010)
	Precipitation calcined @400	NiO-YSZ (electrolyte by slurry coating)	0.6-0.7 mm	P_{max} 658 mWcm^{2} @ 650°C	Chen et al. (2006)
	Precipitation GNP	NiO-YSZ (electrolyte by slurry coating)	ns	P_{max} 900, 1567, 2005 mWcm^{-2} 700, 750, 800°C	Wang et al. (2006a)
	Precipitation coat-mix	Ni-YSZ	2.7 mm	43 vol% porosity – high gas permeability	Simwonis et al. (1999)
	Precipitation with surface modification	NiO-YSZ	2-3 mm	σ = 430 Scm^{-1} @ 800-1000°C 33% porosity	Han et al. (2006)
	Conventional Liquid dispersion EN coating	NiO-YSZ	2 mm (green)	σ= 400 Scm^{-1} @ 700°C σ=200 Scm^{-1} @ 700°C σ=900 Scm^{-1} @ 700°C	Pratihar et al.(2005)
	Co-precipitation	Ni-YSZ	ns	P_{max} 315 mWcm^{-2} @ 800°C	Bao et al. (2005)
		Ni-SDC	ns	30-40% porosity P_{max} 209, 306 and 388 mWcm^{-2} @ 650, 700 and 750°C	Fang et al. (2004)

	Coating precipitation	Ni-YSZ	ns	σ=900 Scm^{-1} between 600-800°C 30% porosity sintered @ 1350°C.	Wang et al. (2004)
	Pechini Process	NiO-YSZ	0.5 mm (green) 1.2 mm (green)	P_{max} 388 mWcm^{-2} @750°C P_{max} 0.56 Wcm^{-2} @ 800°C	Kim et al. (2006a)
Direct deposition	CVD - Combustion CVD (CCVD)	NiO-GDC	ns	P_{max} 0.48 Wcm^{-2}, R_p 0.11 Ωcm^2 @ 800°C	Liu et al. (2004)
	Plasma spraying	Cu-SDC	ns	Anode R_p 4.78Ωcm^2 @ 712°C P_{max} 0.3, 0.57 Wcm^{-2} at 900, 1000°C	Benoved and Kesler (2009)
		NiO-YSZ	1.5 mm	P_{max} 500 mWcm^{-2}	Stöver et al. (2006)
	Atmospheric plasma spraying	M-YSZ, M=Ni,Cu,Co,Cu-Co & Ni-Cu-Co-YSZ (1:1:1:2 ratio)	ns	M-YSZ (monometallic) and trimetallic Ni-Cu-Co-YSZ has the best microstructure and porosity level with stability @ 800°C.	Benyoucef et al. (2009)
	Oxygen-acetylene flame-spraying	NiO-YSZ Ni-Al_2O_3	50 μm	P_{max} 0.30 Wcm^{-2} with 0.1 V activation polarisation and Rp 1.6 @ 900°C P_{max} 0.07 Wcm^{-2} with 0.24 V activation polarisation and R_p 0.26 Ωcm-2 @ 900°C	Li et al. (2010)
	Spray pyrolysis	Ni-CGO	ns	21-52% porosity	Liu et al. (2010)
		NiO-SDC	ns	P_{max} 248 mWcm^{-2} at 0.3 Acm^{-2} @ 750°C	Kawano et al. (2005)
		NiO-SDC	ns	453 mWcm^{-2} at 1.0 Acm^{-2} at 700°C	Suda et al. (2006)

ns = not specified

2.4 EN Deposition

EN deposition has been used extensively in industries since the early 1980s. The technique was first developed by Brenner & Riddell (Baudrand 1978). EN techniques have been used in many precision engineering applications in, for example, the aerospace, electronics, petroleum, automotives industries but the primary interest in this technique is related to wear and corrosion resistance (Feldstein 1990).

Increasing demand in this field is due to its outstanding characteristics such as superior corrosion and wear resistance as well as mechanical and physical properties, good solderability, wide range of thicknesses, excellent uniformity, and surface lubricity (Baudrand 1978). Besides good EN deposition characteristics, this process can be applied on the surfaces of almost all materials, such as plastics (Guo et al. 2005), ceramics (Alirezaei et al. 2004), alloys (Szczygiel et al. 2008) and powders (Pratihar et al. 2004; Wen et al. 2000). Basically EN depositions can be divided into 3 main categories (Fig. 26).

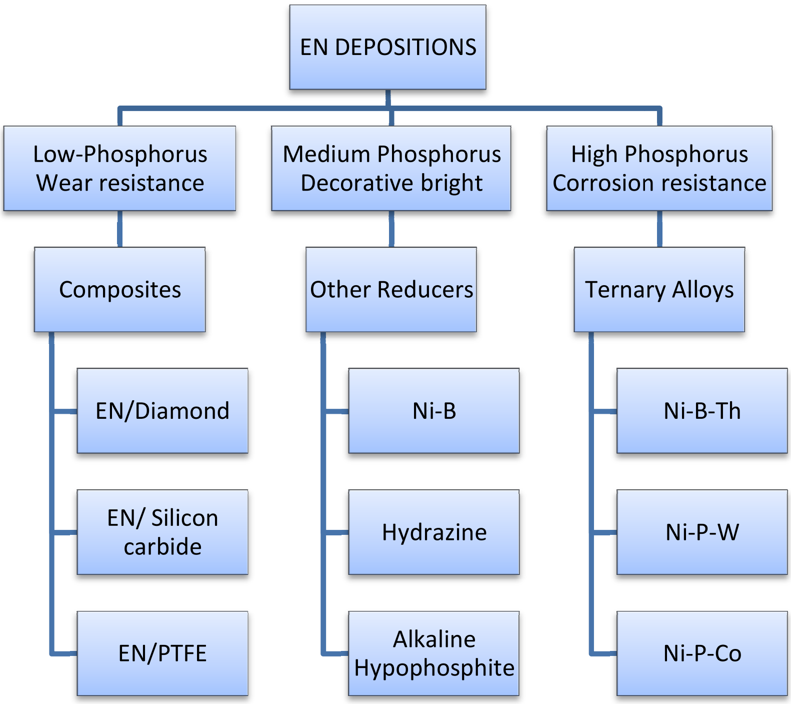

Fig. 26: Categories of EN deposition and their sub-divisions

2.4.1 EN Process

Since EN depositions are deposited by the controlled chemical reduction of Ni ions onto a catalytic surface, the characteristics of EN depositions are strongly dependent on the composition of the EN bath. The main ingredients for an EN solution are a Ni source, a reducing agent, complexing agents, buffering agents, accelerators and an inhibitor. Their typical chemicals and functions are tabulated in Table 7 which was compiled from reviews by Agarwala and Agarwala (2003), Baudrand (1994) and Taheri (2002).

Table 7: EN bath composition, commercial chemicals and their functions or criteria

Composition	Chemical	Functions/ Criteria
Ni sources	Nickel sulphate	Supply Ni ions for EN deposition
Reducing agents		Supply electrons for the reduction of Ni
	Sodium hyphophosphite	Most common reducing agent operates at pH 4.4-5.5 Advantages: lower cost, greater ease of control, better corrosion resistance
	Aminoborane	Limited to compounds: (1) N-dimenthylamine borane (DMAB) – readily soluble aqueous system (2) H-diethylamine borane (DEAB) – must be mixed with short chain aliphatic before it can dissolve in aqueous system Typically operated at pH6-9 and temperature between 50-80°C can be used as low as 30°C
	Sodium borohydride	Most powerful reducing agent – hydrolysis of borohydride ions is very fast and operate at pH12-14, temperature between 90-95°C
	Hydrazine	Not very popular due to bath unstability, difficult to control, brittle and results in highly stressed deposits Operate at pH 11-12, temperature between 90-95°C
Complexing agents	Citric acid or glycolic acid	Control free Ni available for the reaction thus avoiding spontaneous decomposition of EN solutions and controlling the reaction to occur only on the catalytic surface
Inhibitors	Three types: (1) Sulphur compounds: thiourea (2) oxyanions:	Stabilisers that helps control reduction Without inhibitor the EN solutions will decompose unexpectedly initiated by colloidal/ solid particles in the solution, i.e. dusts or blasting media. Inhibitors

	molybdates or iodates (3) heavy metals: Pb, Sn, Bi, or Cd	absorbed on any colloidal or particle impurities Indication of EN solution decomposition are increasing hydrogen evolution and fine black appearance precipitates
Buffering agents	Acetate, propionate, succinate salts	Resist pH changes caused by the hydrogen generated during deposition
Accelerators	Most common: Succinic acid Others: Carbonic acids/ soluble fluorides	Helps increase the speed of reaction due to the addition of complexing agent Loosen the bond between hydrogen and P atoms in hyphophosphite molecules
Energy	Heating	To set the optimum condition for the reaction to occur
Reaction byproducts	Orthophosphite	HPO_3^{2-} ions accumulate as Ni is reduced As concentration of HPO_3^{2-} increases, deposition rate reduces, P content in deposits increases Uncontrolled HPO_3^{2-} concentration caused (1) nickel phosphite precipitation to give rough surface and spontaneous decomposition, (2) HPO_3^{2-} co-deposition causes highly stressed, porous deposit
	Borates	BO_2^- accumulates as borohydride or boric acid and reduces deposition rate without decomposition
	Hydrogen ions	H+ produced by reduction reaction causing pH to decrease

EN bath could be either alkali or acidic, depending on the EN solution used (Henry 1984). It has been found that acid solutions are better as they give higher plating rate and better stability with ease of control and better corrosion resistance (Baudrand 1994). The details of commercial hypophosphite-reduced EN solutions are listed in Appendix A, while details of aminoborane- and borohydride-reduced EN solutions appear in Appendix B. The chemical reactions of hypophosphite-reduced EN during the process are modelled in equations below:

$$(H_2PO_2)^- + H_2O \rightarrow H^+ + (HPO_3)^{2-} + 2H_{abs} \quad \cdots \ (2.6)$$

$$Ni^{2+} + 2H_{abs} \rightarrow Ni + 2H^+ \quad \cdots \ (2.7)$$

$$(H_2PO_2)^- + H_{abs} \rightarrow H_2O + OH^- + P \quad \cdots \ (2.8)$$

$$(H_2PO_2)^- + H_2O \rightarrow H^+ + (HPO_3)^{2-} + H_2 \quad \cdots \ (2.9)$$

All substrates are subjected to sensitisation prior to EN deposition. This process ensures a catalytic surface and the presence of sufficient energy, hypophosphite ions $(H_2PO_2)^-$. In [equation 2.6] the hypophosphite comes from sodium hypophosphite which is oxidised to orthophosphate $(HPO_3)^{2-}$. Some of the hydrogen evolved in the process [equation 2.6] is adsorbed onto the catalytic surface and reduces Ni ions near the surface [equation 2.7]. The adsorbed active hydrogen also reduces a small amount of hypophosphite, producing water, P and hydroxyl ions [equation 2.8]. Some hypophosphite in the solution is catalytically oxidised to orthophosphite and hydrogen gas evolved [equation 2.9], causing low efficiency of the EN solution.

2.4.2 EN Process Parameters

In addition to bath composition, EN deposition is controlled by several factors such as bath composition, bath temperature, bath pH and soaking time (Dugasz and Szasz 1993).

2.4.2.1 Bath temperature

Temperature is the most important factor determining the amount of energy present for the EN deposition process. The processing temperature should be approximately 70-94^{0}C but it varies according to the EN solution used (Shearer and Davidson 2005). The effects of temperature of acidic hypophosphite-reduced EN solution on deposition rate are given in Fig. 27. The rate of deposition increases rapidly with temperature, and optimum temperature ensures good and economical deposition.

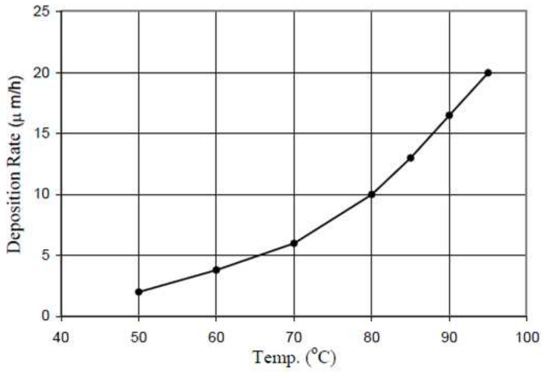

Fig. 27: Effect of temperature on deposition rate for acidic hypophosphite-reduced EN solution (Parkinson 1997)

2.4.2.2 *Bath pH*

Bath pH, whether alkali or acidic, is strongly dependent on the bath composition (Appendix A and B). The bath pH varies between 8-11.5 for the alkali bath (Jappes et al. 2005) and 4-5.5 for the acidic bath (Liu et al. 2006). Most hypophosphite reduce EN solutions at pH 4-5.5 (Appendix A), and the optimum pH is between 5-6.5 (Keping et al. 1996). The bath pH determines P content in the EN deposits as well as the deposition rate, as shown in Fig. 28. Increasing bath pH reduces the P content by weight (Henry 1984; Honma and Kanemitsu 1987), but a complementary observation has been made that bath pH increases with the rate of deposition (Fig. 28).

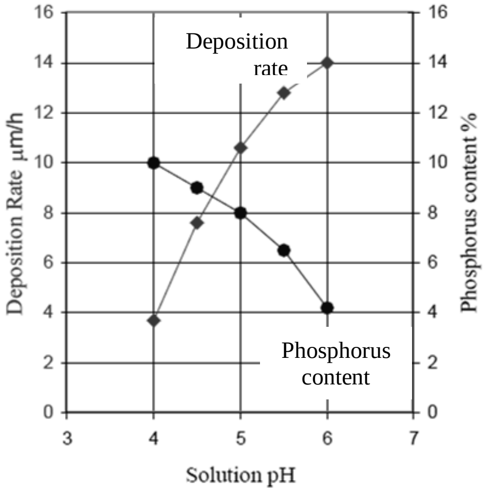

Fig. 28: Effect of pH change on deposition rate and P content (Baudrand 1994)

2.4.2.3 *Bath loading*

Bath loading is a term used to define the ratio of deposition surface to the bath volume. A commercial bath operates in a bath loading range of 0.1 to 1.0 dm^2/l depending on the EN bath solution used (Reidel 1997). Lower bath loading gives better deposition rate in the same temperature range as shown in Fig. 29a. A similar trend was found by Grunwald (1983) (Fig. 29b), where lower bath loading was found to give a better deposition rate against time.

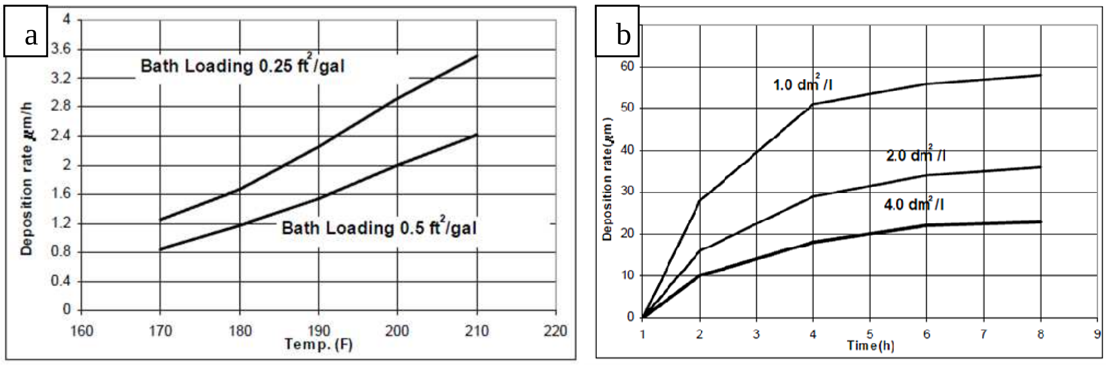

Fig. 29: Effect of bath loading on deposition rate against (a) temperature and (b) time (Grunwald 1983)

2.4.2.4 Bath agitation

Bath agitation has been applied in EN deposition to improve deposition rate and deposition surface. Conventional modes of agitation such as air pressure, inert gas pumping, magnetic stirring, rotating fan and modern ultrasonic agitation were found to effectively improve the deposition and reaction rate. The work by Sevugan et. al. (1993) used agitation mainly to improve reaction rate and reduce absorbed hydrogen or oxygen, but agitation was found to have indirectly improved deposition rate as well. Absorbed gases near the surface can lead to pitting or holes, but agitation helps remove or relieve them. Bath agitation is mainly required to ensure adequate particle suspension throughout the EN deposition process.

2.4.2.5 Substrate surface treatment

Substrate surface treatment is a treatment either mechanical or chemical, to make substrate surfaces either rougher or smoother. Mechanical treatment could be by brushing or sanding or blasting with high pressure air or particles; whereas chemical treatment is performed by etching in various acid solutions depending on the substrate to be treated. A study by Teixeira and Santini (2005) of surface treatment on a polymeric substrate resulted in rougher polymeric surface which improved deposition uniformity and adherence.

2.4.3 EN Deposit Properties

The properties of the EN deposits depend on a couple of criteria: microstructure which is strongly dependent on the P content and porosity content. The physical and mechanical properties of the EN deposits are strongly influenced by these two criteria.

2.4.3.1 Microstructure

The composition of EN deposit using hypophosphate-reduced solutions is typically 92% Ni and 8% P (Parkinson 1997), although P content may reach up to 12% (Baudrand 1994). P content in EN deposits can be categorised into 3 levels: low (2-5%), medium (6-9%) and high (10-13%) (Jackson et al. 1990). EN deposit microstructures are strongly based on the level of P content. Crystallinity is only found in EN deposits with low P content between 1-3% (Keping et al. 1996) and the intermediate levels show a mixture of the two phases. The formation of the amorphous phase is also promoted by the EN stabiliser and bath temperatures higher than 87°C (Jappes et al. 2005).

The microstructures of these three P content level-defined EN deposit categories can be altered by heat treatment. Heat treatment improves hardness of EN deposits with the precipitation of Ni_3P acting as precipitation hardening (Keong et al. 2003), as shown in the phase diagram in Fig. 30, where (a) shows the equilibrium state for solidified Ni-P alloy after melting or EN deposition after heat treatment and (b) shows the non-equilibrium state for as-deposited EN deposition.

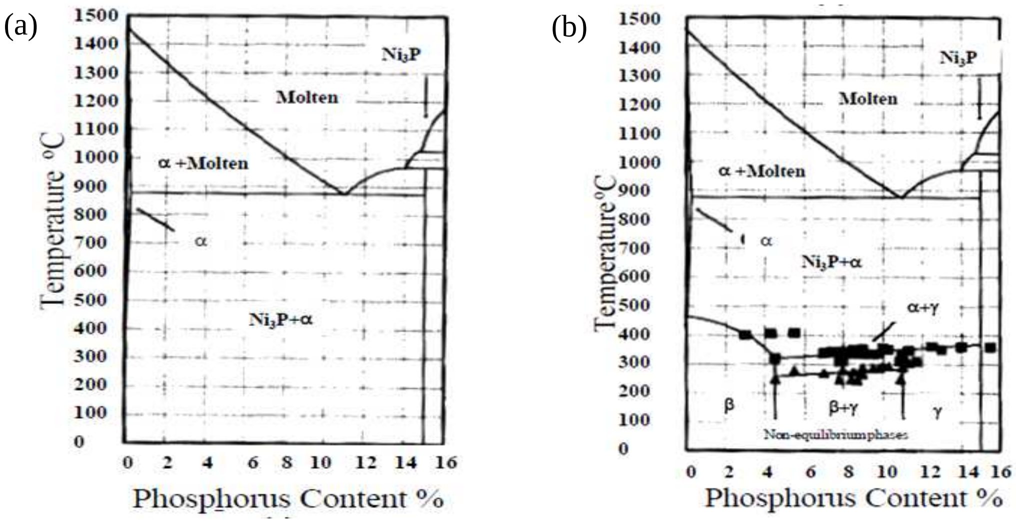

Fig. 30: Ni-P phase diagram (a) equilibrium state (b) non-equilibrium state (Duncan 1996)

The prediction of the microstructure of the as-deposited EN using phase diagram (a) is not accurate as described in detail by D. Baudrand (2005; 2006). In the non-equilibrium graph (b), β (P < 4%) is crystalline phase and γ (P > 10%) is fully amorphous phase. Thus heating the EN deposit to 320°C will transform all the amorphous phase to Ni_3P crystalline phase. Heating EN deposit to a temperature of 400-850°C for 10-15 minutes resulted in removal of P from the deposit surface (Baudrand 2006) and heating at 1107-1517°C (1380-1790 K) showed partial evaporation of Ni_3P that proceed by the reaction in [equation 2.10] (Viksman and Gordienko 1992).

$$Ni_3P\ (c) \rightarrow 3Ni\ (c) + {}^{1}\!/_{2}\, P_2\ (g) \qquad \cdots \ (2.10)$$

2.4.3.2 Porosity

In most EN deposition studies porosity has been considered as a defect in the deposition. Increased porosity has been found to cause a rough surface as well as to reduce its mechanical strength. The porosity of EN coated surfaces is higher, especially when the thickness of the deposition is less than 10 µm and almost dense microstructure can be obtained above 25 µm as shown in Fig. 31.

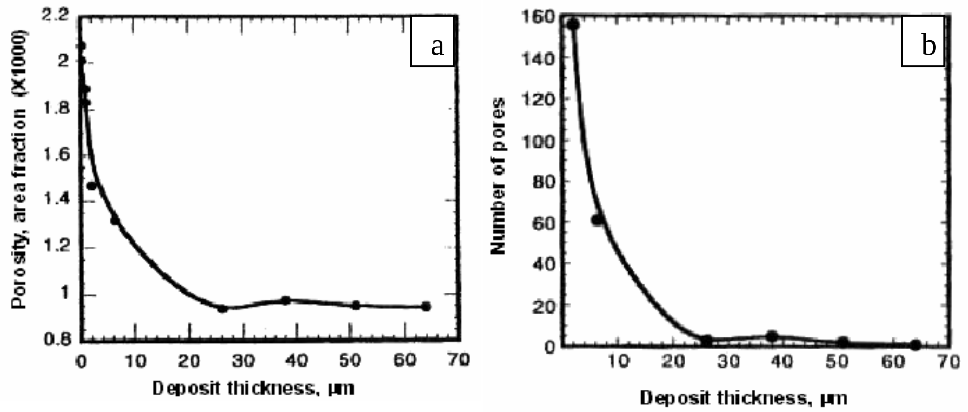

Fig. 31: Porosity against deposit thickness (a) porosity area fraction (b) number of pores (Das and Chin 1959)

Leisner and Benzon (1997) showed that the open pores on EN coated surfaces participated in a galvanic reaction in which the deposition surface is the cathode and the small pore area acts as the anode. As a result of the severe galvanic corrosion, the uncoated area of the pore corrodes drastically. The P content also influenced the EN deposits' porosity level; deposits with high P content are denser and those with low P content are more porous. Impurities and organic contamination in the EN bath, such as degreasing solvents, oil residues, mould releases and foreign inorganic ions such as heavy metals with improper balance and control, will cause deposit roughness, porosity and poor adhesions (Henry 1984).

The study of Vaghefi et al. (2003) on EN composite of Ni-B_4C found that as deposition thickness increases from 10-35 µm, the amount of particles in the deposition increases three times and the smoothness of the deposition decreases (Fig. 32).

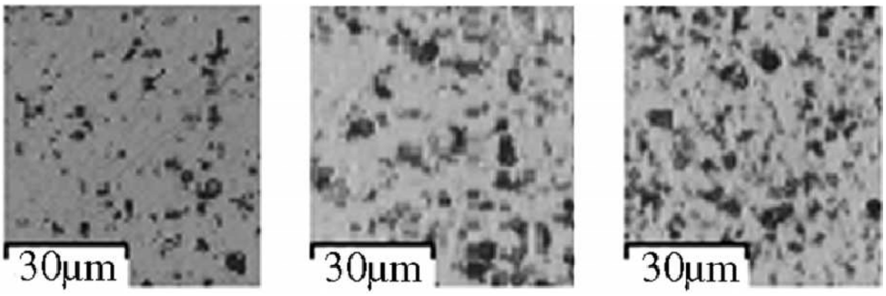

Fig. 32: The effect of deposition thickness on surface topography (a) 10 µm (b) 25 µm (c) 35 µm (Vaghefi et al. 2003)

2.4.3.3 *Physical and mechanical properties*

It was shown that the properties of EN deposition are very much dependent on the P content in the deposits, which may vary between 3% and 12% (Parkinson 1997). For comparison, the physical and mechanical properties of pure Ni are tabulated in Appendix C. Fig. 33a, 33b and 33c show the variation of melting point, density and CTE, respectively, with P content in EN deposition. All three properties of the EN deposits are not as high as those of pure Ni and all are inversely proportional with P content.

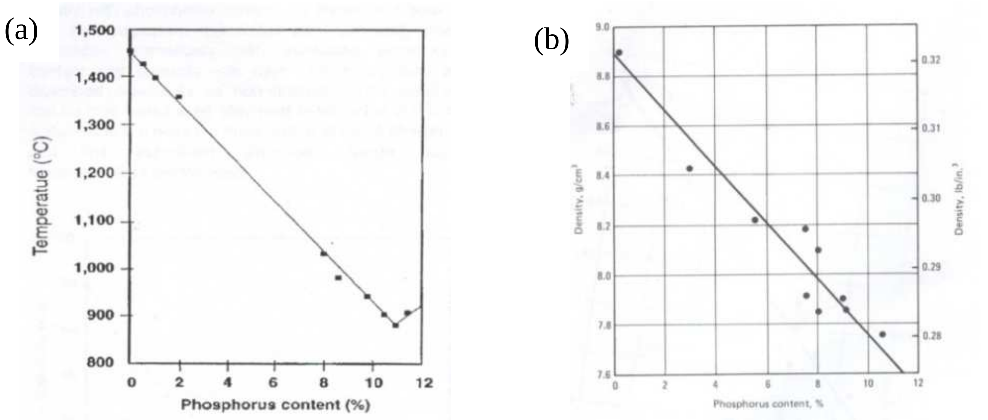

(c)

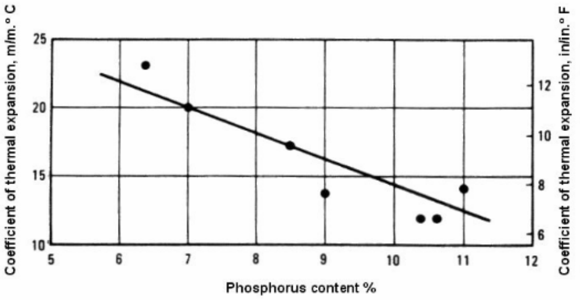

Fig. 33: Effect of P content on (a) melting point (Parkinson 1997) and (b) density (c) CTE (Baudrand 1994)

Electrical resistivity varies proportionally with P content, as described in Fig. 34 (Parkinson 1997). Heat treating reduces deposit resistivity where EN microstructure transformation occurs at 320^{o}C (amorphous to crystalline), giving better electrical conductivity. Since SOFC works at high temperature (700-1000^{o}C), the high resistivity can be overcome. However, the possibility of grain coarsening at high temperature is inevitable, as found by Staia et al. (1997); when heat treatment of the deposition at 400^{o}C caused extended cracking.

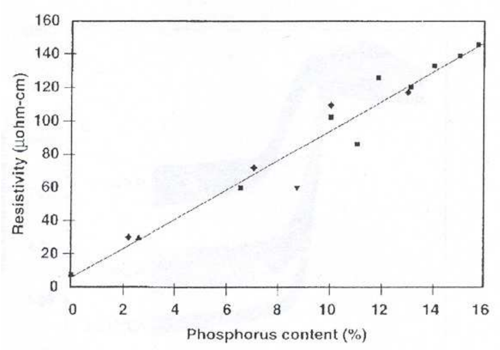

Fig. 34: Effect of electrical resistivity on EN deposition (Parkinson 1997)

2.4.4 EN Composites

The deposition of EN co-depositions is also termed as EN co-deposition. The co-deposition of fine particle in-situ in an electroless metal-matrix is very attractive as it saves energy and time. Conventional fabrications for particulate composites are limited to solid state powder processing and thermal spraying techniques. Typical co-deposition consists of particulates in the size range of 0.1-10 µm with loading of up to 40 vol.% of the total matrix (Feldstein 1990).

Extensive research has been carried out in recent years on EN co-deposition varying the particulate materials and sizes (micro or nano). Various studies have sought to optimise some properties of conventional EN (Ni-P) depositions, including incorporation of various particles, as listed in Table 8.

Table 8: Types, names and formulas of the particles used in EN co-deposition

Types	Particle	Molecular formula	References
Inert/ hard materials	Diamond	C	Hung et al. (2008); Matsubara et al. (2007); Sheela and Pushpavanam (2002)
	Silicon nitride	Si_3N_4	Balaraju and Rajam (2008); Dai et al. (2009); Das et al. (2007)
	Silicon carbide	SiC	Berkh et al. (1996); Kalantary et al. 1993; Lin et al. (2006)
	Silicon oxide	SiO	Dong et al. (2009)
	Boron carbide	B_4C	Vaghefi et al. (2003)
	Alumina	Al_2O_3	Balaraju et al. (2006a); Hazan et al. (2008a; 2008b)
	Ceria	CeO_2	Necula et al. (2007)
	Yttria	Y_2O_3	McCormack et al. (2003)
	Zirconia	ZrO_2	Shibli et al. (2006)
	Iron oxide	Fe_30_4	Zuleta (2009)
Others	Polytetrafluoroethylene	PTFE	Ger and Hwang (2002)
	Titanium oxide	TiO_2	Balaraju et al. (2006b)
Multiple	Silicon carbide- Alumina	$SiC-Al_20_3$	Li et al. (2005a); Li et al. (2005b); Li et al. (2006)
	Silicon carbide-Graphite	SiC-G	Wu et al. (2006)
	Silicon carbide- PTFE	SiC-PTFE	Huang et al. (2003)
	Zirconia-Alumina-Zirconium aluminide	$ZrO_2-Al_2O_3-Al_3Zr$	Sharma et al. (2005)

The properties and affecting factors of conventional EN deposition might or might not be applicable to EN composites. A study showed that the structural characteristics and phase transformation of EN composite incorporating Si_3N_4, CeO_2 and TiO_2 remained unchanged as from those of the conventional Ni-P deposition. In general, various factors have been shown to affect the deposition of EN composites, including (1) particle catalytic inertness, (2) particle charge, (3) EN bath composition, (4) bath reactivity, (5) particle compatibility with the matrix, (6) plating rate, and (7) particle size distribution (Feldstein 1990). Several factors that contribute to an increase in particle loading in the matrix are discussed below.

2.4.4.1 Particle stability

Particle stability in this case could be the charge stability of the particles in the solutions. Particle stability determines the particle dispersion in the solution and particles' tendency for agglomeration or sendimentation. Necula et al. (2007) found that particles are having good dispersion stability in deionised water but not so in the EN solution. Studies on alumina (Hazan et al. 2008b, 2008a), boron carbide (Vaghefi et al. 2003) and ceria (Necula et al. 2007) particles showed that the dispersion stability strongly depends on pH and the low stability caused a short sedimentation time. Studies by Hazan et al. (2008b; 2008a) on dispersion stability in Ni-P-Al_2O_3 EN system incorporating comb-polyelectrolyte showed high particle concentrations of up to 50 vol.% particle incorporation.

Periene et al. (1994) concluded that volume percent of co-deposition particles is dependent on powder conductivities and hydrophobic/ hydrophilic properties. Another study done on co-depositing boron carbide (B_4C) with particle sizes ranging from 5 to 11 µm in hypophosphite-reduced EN solution gave a maximum of 33 vol.% B_4C when the B_4C particles were wetted with surfactant before being added into the bath (Vaghefi et al. 2003). The surfactant is a blend of surface active agent which contains both hydrophilic and hydrophobic groups which helps increase deposition, even at 8 gl^{-1} particle loading. The application of surfactant in the deposition of PTFE on low carbon steel substrate showed strong adsorption (Ger and Hwang 2002).

2.4.4.2 Particle shape and size

Shape and size of the particles play an important role as they influence the deposition surface area and energy. It was found that spherical particles with smaller particle size (average 1 µm boron particles and 3.4 µm alumina particles) gave high particle concentration in the matrix (Apachitei et al. 1998). Study done Balaraju et al. (2006a) varying alumina powder sizes of 50 nm, 0.3 µm and 1.0 µm showed that the highest particle incorporation occurred at 1.0 µm particle size.

2.4.4.3 Particle loading

Particle loading is the amount of powder particles in a litre solution. Co-depositing very fine polycrystalline diamond ranging between 8 and 12 µm with varying concentrations from 2-10 g/l onto aluminium substrate at 70-90^{o}C for an hour yielded as high as 18.40 vol.% diamond powder in the deposit (Sheela and Pushpavanam 2002). The particle incorporation in a Ni-P-ZrO_2 EN system was found to be directly proportional to increase particle loading up to 9 g/l as well as the deposition rate (Shibli et al. 2006). In Ni-P-B_4C EN system, particle composition in the matrix increased from 12 to 33 vol.% as the particle loading increased from 1 to 8 g/l (Vaghefi et al. 2003). It was found that a particle loading more of than 15 g/l SiC in hypophosphite-reduced solution caused extensive bath foaming which reduced the plating rate (Kalantary et al. 1993).

2.4.4.4 Bath conditions

The addition of silicon carbide (SiC) powders with particle size ranging from 4-7 µm in varying EN solution conditions (composition, pH, temperature and time) showed an increase in SiC loading in the deposition but a reduction of the deposition rate and deposition weight (Kalantary et al. 1993). Another study showed that co-deposition of SiC (1-5 µm) in sodium hypophosphite-reduced EN solution at pH 4.5-5.5, 80-90^{o}C with air agitation resulted in 25-30 vol.% SiC in the deposition (Li 1997). Aggressive agitation might cause substrate or deposition abrasion by other factors such as particle hardness, particle shape and size, particle loading and bath movement (Kalantary et al. 1993).

2.4.4.5 Substrate orientation

Substrate orientation is defined as the position of the substrate in the EN bath during the EN deposition. The variations of substrate position have shown to give an effect on the EN deposition. In a study by Sheela & Pushpavanam (2002) on diamond EN co-deposition in hypophosphite-reduced solution showed that a vertical substrate position gave less than 20% particle incorporation compared to the horizontal position. Another study on Ni-P-SiC using hypophosphite-reduced solution with a particle loading of 25 g/l showed that the substrate held tangentially gave the highest particle composition in the matrix and a vertical position leading to uniform particle incorporation and adherence provided, that uniform agitation was used (Kalantary et al. 1993).

2.6 Design of Experiments

Design of Experiments (DoE) is of high interest in engineering to get robust and reproducible results with a minimum number of experiments (Woll and Burkhard 2005). DoE was founded by Sir Ronald A. Fisher in the 1920s in Rothamsted, England (Kuehl 2000). The goal of DoE is to eliminate bias through collection of observations to gain maximum information in the most efficient manner. DoE for engineering can be divided into three major categories: Taguchi; Response Surface Methodology (RSM); Factorials. Each method has its own strengths and limitations.

2.6.1 Taguchi

The Taguchi method started in the early 1980s. The Japanese engineer Genichi Taguchi published a quality improvement methodology which involved the use of designed multifactor experiments. The design also known as robust design, focuses on the robustness of a product which performs consistently on target and is not sensitive to changes in factors that are difficult or impossible to control. The Taguchi philosophy involves the concept of ‘loss to society’ (typically modelled as a quadratic function of deviation from target) instead of the ‘binary’ view of product quality which stems from the use of specification limits in the factorial design. Taguchi design is arranged in orthogonal arrays with the simplest as L_4 equivalent to 2^3 factorial arrays.

2.6.2 Response Surface Methodology

RSM is a combination of mathematical and statistical techniques based on a mathematical model. RSM was developed by Box and Wilson in 1951 (Montgomery 2009). The techniques used to analyse an interest response are influenced by several variables and the objective is to optimise this response. The technique basically comprises (1) a procedure to move into the optimum region, (2) behaviour of the optimum region, (3) estimation of optimum condition, and (4) verification.

2.6.3 Factorials

Factorials design is the basis of DoE. Factorials design is the most efficient way to study the effects of two or more factors. For example, 2-levels is simplified as 2^k or three levels as 3^k. Factorial design investigates all possible combinations of factor levels for each complete trial or replication of experiment. This is because the factors arranged in a factorial design are crossed by the Yates algorithm (Bisgaard 1998). A 2^k factorial design is used to study the effects of k factors with two levels for each factor. The k represents a multiple-factor design with a variation of treatment designs where a set of treatments (*factors*) are tested over one or more sets of treatments (*levels*). In practice the higher-order interactions are usually not significant, thus most design are limited to 2-3 levels.

Factorial designs can be categorised as balanced and random designs. Balanced design uses the same number of samples for each factor-level combination. Random design can be divided into with or without blocking. Random design with blocking is also known as fractional factorials. Random design without blocking is categorised as full factorials. Appendix D tabulates the 2-factorial experimental design with number of run, blocks, and factors, indicating whether they are full or fractional factorial (Bisgaard 1998). The 2^k design is widely used in factor screening experiments at the early stages of experimental work when there are many factors to investigate.

DoE is the arrangement of samples used to control variation error. Multiple-factor design in an experiment allows for treatments of more than one factor, allowing for the possibility that one factor influences another – a possibility that cannot be evaluated with a one-factor-at-a-time (OFAAT) experiment. The major disadvantages of OFAAT are: they require more experimental runs than DoE; they are incapable of detecting the factor interaction; and they cannot detect the specific level of each factor that will optimise a response variable. In order to design an experiment, all three fundamental components described by Fisher should apply: blocking (local control), replication and randomisation.

2.6.3.1 Blocking

Blocking is a local control to reduce experimental variation error. The experimental error is defined as a variation among identically and independently treated samples, due possibly to natural variation, measurement, inability to exactly repeat the experiment, treatment-sample interaction and other extraneous factors. Blocking is grouping the samples such that the variability of samples within the group is less than that among all samples prior to grouping. Major criteria for blocking are proximity, physical characteristics, time and management of task in the experiment. Blocking can be divided into complete blocking or incomplete blocking. Complete blocking is used when precision is the major concern whereas incomplete blocking is applied to reduce block size. Reducing block size will minimise error variance.

2.6.3.2 Replication

Replication is an independent repetition of experiment as a means to estimate experimental error variance. It proves that the results are reproducible at least for the particular experimental setup. It provides assurance against results due to unforeseen accidents; the means to estimate experimental error. Replication has two important properties that are (1) to obtain an estimate of experimental error and (2) to obtain a more precise estimate of the factor-interaction effect. Sufficient replicates provide precision in the inferences concerning the effects of factors and their interactions.

The terms ‘replication’ and ‘repetition’ are not technically the same. Repetition is repetition of testing or measurement done on the same sample or same set of experimental conditions whereas replication means repeating an experiment separately producing another sample. Replication reflects sources of variance between runs and within runs.

2.6.3.3 Randomisation

Randomisation is an arrangement of experimental procedures to reduce the effect of experimental bias. For example, the experiment might be affected by such factors as operator errors, time, humidity, ambient temperature, and power surges. Randomisation of the experiment provides a valid estimation of experimental error variance by averaging out the effects of noise factors. Practising randomisation in DoE is to eliminate those biases in comparison of treatments that arise through systematic assignment of treatments to samples. It evaluates the statistic for all possible arrangements of treatments on the samples. A well designed experiment determines the results. The results need to be analysed to extract important information which will lead to the answer for the problem.

2.6.4 Model building

Model building is developing an equation for predicting response values for different combinations of the process parameters at their best levels. Franceschini and Macchietto (2008) have reviewed a model-based experiment design technique for increasing parameter precision especially in chemical and biological processes, which has become increasingly important recently. Roy et al. (2008) also reviewed the application of DoE in optimisation that results in the development of a surrogate model in various engineering application.

A predicting responses value equation is derived from the important effects that have been identified. The relationship between a response and a set of parameters which affect the response can be built by a regression model approach. A regression model for factors at 2-levels is usually of the form:

$$\hat{y} = \beta_0 + \beta_1 x_1 + \beta_2 x_2 + \cdots + \beta_{12} x_{12} + \beta_{13} x_{13} + \cdots + \varepsilon \qquad (2.13)$$

where β_1, β_2... are the regression coefficients and β_0 is the average response in a factorial experiment. The term ε is the random error component. β_{12}, β_{13}... correspond to the interactions between the process parameters x_1 and x_2. This was applied in a parametric optimisation and prediction of electroless Ni-B deposition (Oraon 2007) and also in model building for fuel cell component characterisation (Wahdame et al. 2009). Similarly, two studies done using Taguchi DoE successfully developed a mathematical model to predict the DoE responses (Azmir and Ahsan 2008; Azmir et al. 2009).

3 RESEARCH METHODOLOGY

This chapter elaborates on the chemical preparation for the EN co-deposition, substrate preparation, types of ceramic powder used, EN co-deposition variables, OFAAT methodology, DoE process and methodology, model building for predicting the response function and finally the testing methodology.

3.1 Chemical Preparation

3.1.1 Cuprolite

Cuprolite supplied by Alfachimici is an alkaline cleaner conditioner for the direct-plating process. It consists of a mixture of two types of liquid, Cuprolite X 96 DP A and B, in a ratio of 10 to 1 (see Appendix E). 250 ml of Cuprolite X 96 DP A was pipetted into a clean 5 l beaker, and then 25 ml of Cuprolite X 96 DP B were added. Deionised (D.I) water was added to the mixture to make it up to 5 l volume and stirred thoroughly. All work was done in a fume cupboard. A fresh Cuprolite X-96 DP solution was made up to 5 litres for each batch and kept in a Winchester bottle.

3.1.2 Pre-catalyst

UNIPHASE PHP pre-catalyst supplied by Alfachimici is a colloidal catalyst composed of mainly palladium and tin. The pre-catalyst helps prevent water drag-in pollution in the subsequent catalyst bath, thus avoiding catalytic colloidal stability problems. The pre-catalyst is made by mixing UNIPHASE PHP salts A with acid and D.I. water (see data sheet Appendix F). Fresh pre-catalyst was made by filling a clean 5 l beaker up to three-quarters full with D.I water. Then 1000 g of salt A was added and mixed thoroughly till it dissolved. The solution was filtered to remove any undissolved salts. 100 ml of 37% hydrochloric acid was pipetted into the solution, which was then well-mixed while adding D.I water up to 5 l volume.

3.1.3 Catalyst

UNIPHASE PHP catalyst supplied by Alfachimici consists of UNIPHASE PHP salts A and UNIPHASE PHP solution B (see Appendix G). A clean 5 l beaker was filled with D.I water to three-quarters full and 1000 g of salt A was dissolved in it. The solution was filtered to eliminate any suspended particles. 100 ml of 37% hydrochloric acid was added and mixed well prior to addition of 100 ml of UNIPHASE PHP B and D.I to reach the final volume of 5 l. All work was done in a fume cupboard. When the prepared solution was ready for use, it was kept in a Winchester bottle to avoid excessive chemical degradation due to UV light. Deterioration of the catalyst's dark brown colour indicated degradation of the catalyst and thus the need for a new fresh solution to be prepared.

3.1.4 Niplast

NIPLAST AT 78 supplied by Alfachimici is an excellent activator and its use is a fundamental step for direct EN plating. It preserves EN stability and is stable over time. The details of NIPLAST AT 78 can be found in Appendix H. A fresh 5 l Niplast solution was prepared by mixing 500 ml of NIPLAST AT 78 with D.I water to volume in a clean 5 l beaker and kept in a Winchester bottle.

3.1.5 EN Solution

EN SLOTONIP 1850 supplied by Schloetter is a hypophosphite-reduced EN solution with a medium phosphorus range that is easy to operate and is suitable for high speed EN bath. It consists of three main components: SLOTONIP 1851 Starter, SLOTONIP 1852 Ni solution and SLOTONIP 1853 Replenisher (see Appendix I). A fresh EN solution was prepared in a clean 5 l beaker by filling the beaker half full with D.I water before adding 750 ml of SLOTONIP 1851 starter. The solution was then mixed well. Next, 30 ml of SLOTONIP 1853 replenisher was added to the solution and mixed. Then, D.I water was added to 5 l volume. The bath pH was adjusted to the manufacturer standard pH4.9 by adding either 50% ammonium hydroxide or 10% sulphuric acid. The prepared EN solution was kept in a Winchester bottle to slow down chemical degradation.

3.2 Substrate Preparation

A substrate is the surface where EN deposition grows. The substrate used in this work was a solid and fully dense alumina tile supplied by Coors Ceramics U.K. with manufacturer dimensions of 50 mm x 50 mm x 1 mm (Fig. 35). An alumina substrate was used instead of YSZ as alumina is cheaper, easier to handle and similar to YSZ where alumina obtain good EN adhesion (Honma and Kanemitsu 1987). An EDXA spectrum (Fig. 36) shows an alumina substrate containing Al and O as the main components with traces of P, C, and Na.

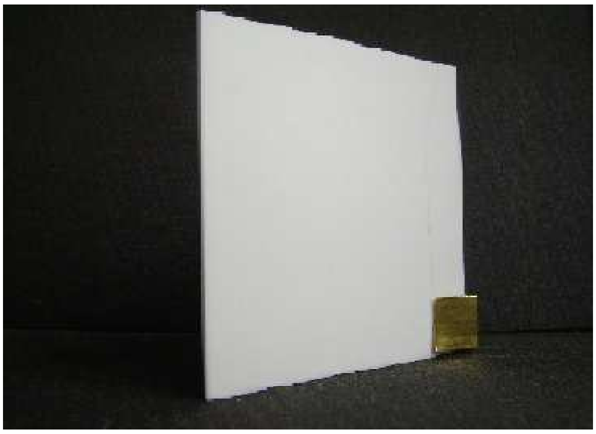

Fig. 35: Alumina substrate for EN co-deposition

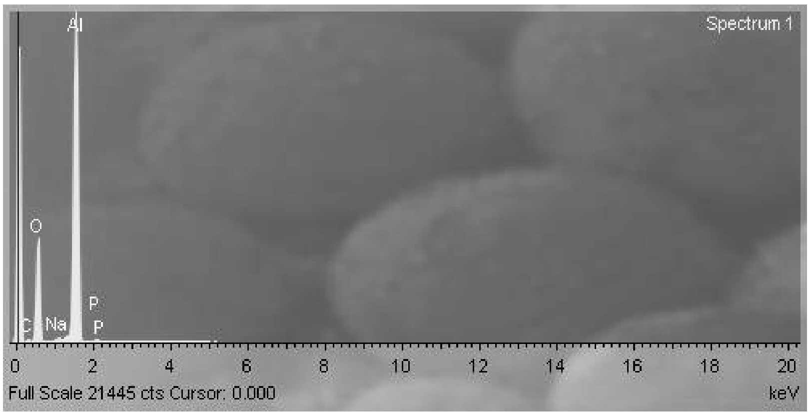

Fig. 36: Alumina substrate EDXA spectrum

3.2.1 Substrate Cutting

An alumina tile with manufacturer standard dimensions of 50 mm by 50 mm was cut into 25 mm by 25 mm tiles for DoE experiments. A single tile can easily be cut using a hand-held diamond scoring pen. The alumina tile surface was first scored with the pen. Then with a support directly under the score, pressure was applied to either side of the cut till the tile snapped along the score. Snapping pressure must be constant along the scored line to ensure a smooth cut.

Multiple tiles were cut using a ceramic cutting machine (Struers Accutom-5) with a diamond blade. A stack of 4 to 5 alumina tiles were clamped snugly but not too tightly as too much pressure increases the risk of ceramic tile breakage during cutting. The machine was set to a position at the centre with alumina tiles rotating counter to the direction of the wheel in such a way as to cut both sides of the alumina tile upon spinning. Water-based coolant was used to avoid cutter blade over-heating. The machine is fully automated and accurate setting according to the manual is important for a good and accurate cutting dimensions.

3.2.2 Substrate Etching

Surfaces of the substrates were treated by etching as required by for OFAAT or DoE substrates. The substrates were placed in a stainless steel basket with the surface to be treated facing upwards. A mixture of 1 part hydrofluoric (HF) acid (20ml/l) and 5 parts ammonium fluoride (NH_4F) (2g/l) made up the HF etching solution. The basket was immersed in the solution for 5 minutes at room temperature. Substrates were then washed and rinsed with D.I. water and air dried.

3.2.3 Substrate Blasting

Another substrate surface treatment used was mechanical blasting. The substrates were affixed onto a flat plate and introduced into a blasting chamber where brown alumina sands under high pressure blasted the alumina substrate for 1-2 minutes. Substrates were then washed and rinsed with D.I. water and air dried.

3.2.4 Substrate Cleaning

Some substrates that had been subjected to blasting were contaminated with dirt and required ultrasonic cleaning. Substrates were submerged individually in beakers filled with acetone. The beakers were then arranged in an ultrasonic bath in such a way to avoid toppling. Ultrasonic cleaning was done for 30 minutes at room temperature. Then substrates were rinsed with D.I. water and hot air dried.

3.3 Ceramic Powders

3.3.1 Yttria Stabilised Zirconia

Yttria stabilised zirconia (YSZ) is a ceramic phase that is commonly used in fabrication of SOFC anodes and electrolytes. It is very well-known that ceramics in general have high hardness, good scratch and corrosion resistance, and very good thermal resistance, but they are also characterised by low toughness and high brittleness. Normally the addition of ceramic particles in composites increases the composite's mechanical properties in term of its hardness, corrosion resistance and thermal resistance, but in this research the addition of ceramic particles was chosen for the purpose of improvement of the catalytic activity in a SOFC anode as well as to reduce CTE difference between the anodes and the electrolytes.

YSZ is composed of yttrium, oxygen and zirconium. The properties and stability of YSZ depend highly on the yttria (Y_2O_3) composition, whether 8, 9 or 10 mol% (Kharton et al. 2004). The main criterion for choice of YSZ is its high ionic conductivity, which is achieved by its cubic fluorite structure, typical of classical oxygen ion-conducting oxide materials. Zirconia has three stable polymorphs: monoclinic (below 1167^{o}C), tetragonal (between 1167 – 2367^{o}C) and cubic (2367^{o}C to melting point at 2677^{o}C).

The Zr^{4+} cations are too small to sustain fluorite cubic structure, therefore they require doping to stabilise them. Besides dopant concentration, operating temperature also influences the ionic conductivity of this material. Dopant concentration of 3 mol% Y gives a tetragonal YSZ, known as TZP. It has been reported that maximum ionic conductivity occurred at 8 mol% Y content (Kilner and Steele 1981). The ionic conductivity of this

8YSZ can be enhanced by judicious choice of heat treatments (Mori et al. 2002). Besides its good ionic conductivity, stabilised Zr has higher strength and toughness than Ce-based ceramics, with a bend strength of 143 MPa at room temperature compared to that of 400 MPa for fully stabilised Zr (Sammes et al. 1996).

Before introduction of the substrate, 50 g/l of YSZ powder was added to the EN solution and set in suspension by appropriate agitation. The YSZ powders used were commercial 8 mol% YSZ (Unitec Ceramics - UCM) with two different nominal particle sizes, 2 µm and 10 µm. Detail specifications are given in Appendix J and K respectively. An SEM micrograph of uncoated 2 µm nominal size 8YSZ powder under 3k magnification appears as Fig. 37. These powders were not subjected to pre-treatment or a sensitising process prior to deposition as the alumina substrate was. Such treatments would promote Ni deposition on the powders and thus increase the amount of Ni in the EN co-deposition. The result would then work contra to the objective of this research which is to reduce the Ni to YSZ ratio in the deposition.

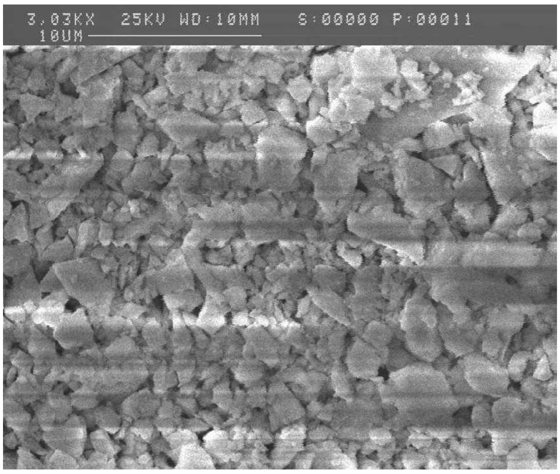

Fig. 37: SEM micrograph of uncoated 2 µm nominal size 8YSZ powders under 3k magnification

3.3.2 Ceria Stabilised Zirconia

Another ceramic powder used was ceria stabilised zirconia (CeSZ). Based on literature studies, Ce-based ceramics are a good alternative material for SOFC electrolytes at lower temperature (500-750^{o}C). It gives better performance in moist environments, good mechanical properties, lower price and wider range of solubility (Sukuma and Shimada 1985; Wang et al. 1992). Thus, Ni-CeSZ is a potential SOFC anode material. The addition of Ce between 10-16 mol% (Attaoui et al. 2007) to Zr stabilises the high temperature phases and gives a stable tetragonal phase with reasonable sinterability and high ionic conductivity. At low partial pressure of oxygen ($P_{O_2} < 10^{-23}$), ceria is developing electronic conductivity where Ce^{4+} ion is reduced to Ce^{3+} which gives mixed conductivity (Orera et al. 1994). The mixed conductivity is an advantage in SOFC anode applications but not in the electrolyte as good electrolyte should be fully ionic conducting.

Similar procedure was carried out for Ni-CeSZ co-deposition where a 50 g/l powder was added into the bath to allow in-situ co-deposition. The commercial 14 mol% CeSZ by UCM with nominal size of 2 µm was used – details of composition and particle size distribution is given in Appendix M.

3.4 EN Co-deposition

The idea of this process is to deposit Ni and ceramic powders *in-situ* on to the ceramic substrate. Prior to EN co-deposition, the substrate has to be sensitised as a requirement to make the substrate more reactive for Ni deposition. The sensitisation process consists of four stages – cleaning by Cuprolite, surface catalysing by Pre-catalyst and Catalyst then followed by surface activation by Niplast. It was found that during the sensitising process the critical stage is determined by surface adsorption of metallic palladium (Pd^0) on the ceramic substrate instantaneously in the redox sensitisation bath as in [equation 3.1] (Mukhopadhyay et al. 2008).

$$SnCl_2 + PdCl_2 \rightarrow SnCl_4 + Pd^0 \quad \cdots \quad (3.1)$$

The trade name and composition of sensitising agents are listed in Table 9. Each stage required different working temperatures but similar soaking times of 15 minutes. Preferentially, EN co-deposition process is done immediately after sensitising to avoid catalytic degradation on the substrate surface. EN solution is green in colour which shows the presence of Ni ions. The reducing agent is sodium hypophosphate with acidic bath medium. Working temperature condition is controlled at 89^0C and should be kept as close as possible with variation allowance of $\pm 2^0$C.

Table 9: Chemical for sensitising and EN deposition process (Schloetter 2006)

Trade name	Composition	Time	Temperature
Cuprolite X96DP	50 ml/l Cuprolite X96 DP A 5 ml/l Cuprolite X96 DP B D.I water to volume	15 min	60°C
UNIPHASE PHP Pre-catalyst	200 g/l Uniphase PHP A salt 20 ml/l 37%Hydrocloric Acid RP D.I water to volume	15 min	20°C
UNIPHASE PHP Catalyst	200 g/l Uniphase PHP A Salt 20 ml/l 37%Hydrocloric Acid RP 20 ml/l Uniphase PHP B D.I water to volume	15 min	30-35°C
NIPLAST AT 78	100 ml/l Niplast AT 78 D.I water to volume	15 min	35-40°C
EN SLOTONIP 1850	5.0-6.4 g/l Ni 25-34 g/l Sodium hypophosphite	30 min	89°C

The duration of deposition was kept at 30 min unless stated otherwise as referred to the previous study by Chen and Chen (1997). Other bath compositions such as sodium hypophosphite, nickel sulphate concentration were kept constant as per the manufacturers data sheet in each experiment. During deposition, the bath composition, concentration and volume were reduced throughout the deposition time. Therefore the addition of Ni solution was required to keep the volume constant throughout the plating.

Every individual substrate was weighed and their dimensions were recorded prior to sensitising and deposition. After the 4-stage sensitising process, the substrate was covered with thin aluminium tape on one side to ensure only one-sided deposition – that represents the SOFC anode. The substrate was kept suspended in the bath by a very fine aluminium wire that was suspended on a retort hand. It was very difficult to keep the substrate positioned in the centre of the bath throughout the deposition.

A ceramic powder of 50g/l was added into the bath along with the substrate. Appropriate bath agitation methods, i.e. stirring or bubbling were used to keep the ceramic powders suspended in the bath. The suspended particles near the surface will be co-deposited onto the substrate surface. The overall EN co-deposition process is simplified in the schematic diagram (Fig. 38). It is important to keep all utensils used in the process as clean as possible to avoid chemical contamination. The equipment was rinsed with D.I. water after tap water to reduce any possibility of pH change.

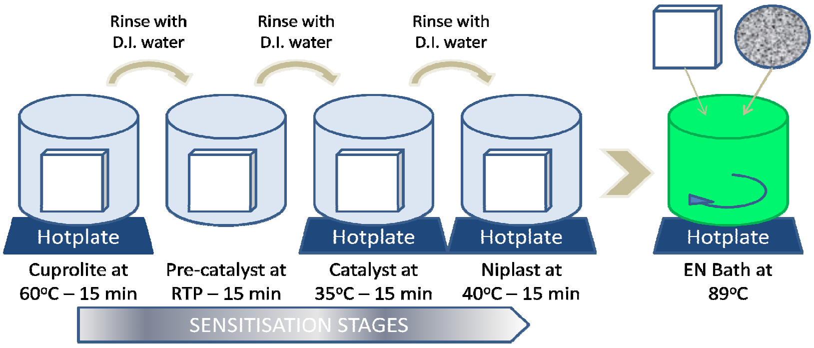

Fig. 38: Schematic diagram of the sensitising and EN co-deposition

3.4.1 Bath pH

Bath pH changes the effect of the deposition rate – a higher bath pH gives higher deposition rates and vice-versa for a low bath pH. The EN solution used was an acidic hypophosphite-reduced to a pH window between pH 3-6 (Appendix A). In order to maintain the bath pH, Ni solution was added as and when required. The bath pH was monitored with a Hanna digital pH meter (HI8014).

3.4.2 Bath Temperature

The process was done in a small, controlled, closed environment – the temperature was kept constant at 89 ± 2^0C during the deposition. This can be done by controlling the air ventilation in the fume cupboard. The agitation keeps the ceramic particles suspended in the bath and also helps in removing excess heat in the bath. The temperature was closely monitored using a digital thermometer (Testo 925). The effect of EN bath evaporation was significant after 10-15 minutes of deposition which then requires the addition of Ni solution to maintain the bath volume, Ni ions concentration and bath temperature. In order to avoid an uncontrolled temperature drop, the volume of Ni solution being added was controlled.

3.4.3 Bath Agitation

Good bath agitation in conventional Ni-P EN deposition helps remove entrapped hydrogen gas on the substrate surface as well as improve the reaction rate. In EN co-deposition, the agitation is crucial to keep all powder particles in suspension for co-deposition. In this research there were two types of bath agitation that will be investigated: air bubbling and mechanical stirring.

Air bubbling agitation was done by flowing a constant air pressure using a small 4W power air pump at the bottom of the bath. There is no air pressure control but it is important to keep the air flow at the centre bottom of the bath to ensure uniform bath agitation. Mechanical stirring is simply using a Jenway hotplate magnetic stirrer. The stirring has to be controlled as not to cause a high vortex in the bath. The evaporation should also contribute to this phenomenon where the constant stirring rate becomes too high as the bath volume reduces. High vortex caused hollow area in the centre of the bath which limits the deposition area, i.e. not all substrate area is submerged.

3.5 One-Factor-At-A-Time

There are many factors that might affect the EN co-deposition. The kinetics of conventional Ni-P deposition is still not fully understood and this makes the EN co-deposition even more challenging. The addition of ceramic powders might upset the optimum EN conventional bath condition. Thus experiments called one-factor-at-a-time (OFAAT) were required to determine which factors really have an effect on this system. The possible factors were gathered from previous studies in conventional EN Ni-P and EN co-deposition.

The nine OFAAT parameters are as listed in Table 10. The standard EN bath properties and processes are: standard manufacturer pH 4.9 and temperature 89^{o}C; 30 minutes deposition time; 8YSZ ceramic powders; 2 µm nominal particle size; particle loading of 50 g/l; bath loading of 0.5 dm^{2}/l; stirring agitation; vertical placement and substrate surface as received. Factor varies accordingly but the rest were kept constant as the standard.

Table 10: Summaries of OFAAT parameters, variables and their justification

No	Parameters	Variables	Justification
1	Particle size of ceramic powders	2 µm 10 µm	Studies done so far show varying particle size ranges between 50 nm-12 µm. Nano-particles (sub-micron) leading to low co-deposition but all the studies carried out at varying particle loading and bath conditions. Both 2 µm and 10 µm are fall within the range.
2	Types of ceramic powders	8 mol% YSZ 14 mol% CeSZ	This factor has never been studied directly before. There are reports discussing the stability of the particles – the charges of the particles in EN solution – hydrophilic or hydrophobic, van der walls, hydrogen forces might also contribute.
3	Types of agitation methods	Air bubbling Mechanical stirring	The agitation is affecting EN deposition especially in increasing the particle concentration in the matrix. Many studies report various agitations effect and in this research these two factors were used.
4	Substrate surface conditioning	HF etching Mechanical blasting	Effect of substrate surface condition was reported affecting the porosity content in the deposit. As SOFC anode, porosity content up to 40% is required therefore it is worth noting the effect of these factors.
5	Bath pH	3.4 – 5.4	Bath pH has been widely discussed either in conventional EN deposition or EN co-deposition. The range is within the acidic hypophosphite-reduced solution windows.
6	Bath loading	0.21-1.25 dm^3/l	Bath loading has been reported to have strong effect on conventional EN deposition. The bath volume was varied between 50-300 ml
7	Deposition time	30 – 120 min	Deposition time is definitely proportional to the deposition thickness but the quality of deposition and co-deposition properties and deposition rate related in EN composites deposition is worth studying
8	Surface orientation	Vertical Horizontal	There were studies reporting the effect of varying surface orientation (vertical, tangential or

			horizontal) in EN Ni-P-SiC system at 25 g/l.
9	Particle loading	12.5 - 100 g/l	Particle loading in EN composite influencing the particle concentration in the matrix. A study described particle loading greater than 15 g/l can generate high foam and caused low deposition rate.

3.6 Design of Experiment

Design of experiment (DoE) is a tool used to obtain accurate results within limited time and cost. The main criterion for using factorials against the others is that it does not compare results directly against a control or standard data but it evaluates all effects and interactions by evaluating their significant statistical differences among them. Factorials are widely used as it offers many options: general, full and fraction. The fraction factorials are very similar to Taguchi. A well-planned design leads to a good outcome(s) conclusions.

There are four basic steps in establishing a good design of experiment: planning phase; designing phase; conducting phase and analysing phase. All these phases will be discussed and elaborated in great details in the next sub-sections.

3.6.1 Planning Phase

Planning phase is the core of DoE as it determines the success of the overall target outcome and would not mislead the objective. In this stage, the problem statement of the overall experimentation is clearly stated and understood. Once the objective and target are determined, the selection of parameters, responses, variables, levels and interactions can be sort out and identified.

3.6.1.1 Problem definition

The manufacturing process should not hinder the basic requirement of the SOFC anode. The main requirements for the SOFC anode are good electronic conductivity which is provided by the metallic Ni. Ceramic YSZ phase help reduces CTE difference between the anode and the electrolyte with acceptable composition of 50 vol.% YSZ; and lastly the importance of continuous porosity for fuel and product gases flow in and out of the anode which is ideally up to 40%.

Expected problems gathered from the literature were the composition of incorporated particles as low as 12 vol.% in various EN composite systems. To date, the EN deposition engineering applications require a dense and uniform deposition, thus porosity is considered as a major defect. However, some literature showed that porosity decreases as the deposition thickness increases. Porous deposition was obtained at thicknesses below 10 µm whereas dense deposition was obtained at thicknesses above 25 µm (Das and Chin 1959). This indicates porosity is possible in the EN deposition. Thus, the current problems in EN co-deposition process are: low ceramic composition and low porosity level.

Understanding these requirements and challenges, the responses of the DoE were determined: (1) to decrease Ni content to as low as 30 vol.% and (2) to increase porosity level up to 40 vol.%. The measurement of ceramic composition is obtained by EDXA in term of Ni in wt.%. Therefore the quality characteristic for Ni content is the *lower the better* as the main objective is to increase the amount of YSZ ceramic in the composite. The second quality characteristic for porosity content is the *higher the better*.

3.6.1.2 Possible Factors

There are many factors that might affect the EN co-deposition process. In the conventional EN deposition literatures, possible factors are bath temperature, pH, loading, agitation and substrate surface condition. On the other hand, in the EN co-deposition possible factors are particle stability, shape & size, loading; bath condition and substrate orientation. Fig. 39 shows a ‘cause and effect’ diagram related to the EN co-deposition for the SOFC anode. The diagram simplified the possible causes into 4 categories that affect the responses. Human factors such as accuracy in chemical handling and equipment cleanliness are almost inevitable but it can be reduced. Machine parallax is also a contributing factor but can be overcome by calibration.

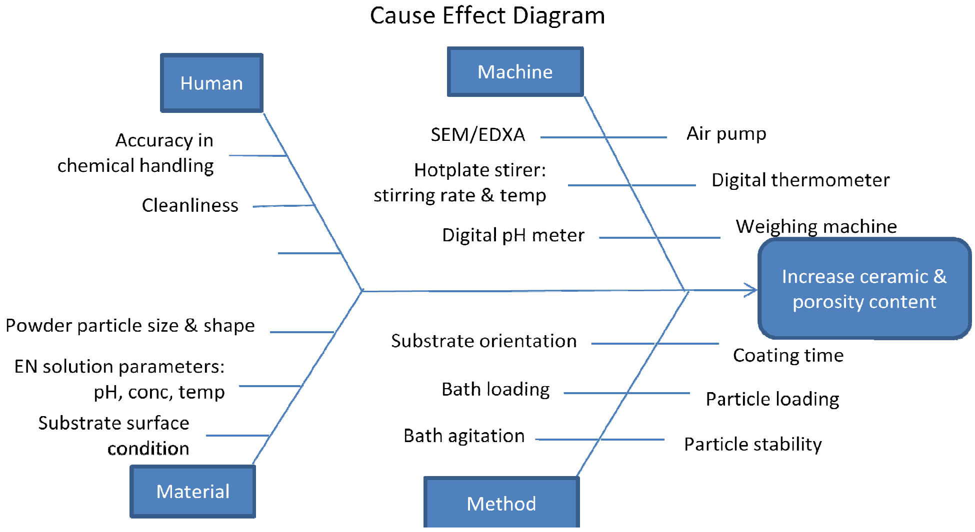

Fig. 39: Cause and effect diagram of EN co-deposition for SOFC anode

Fig. 39 lists all the possible causes that might affect the yield of responses but not all possible causes are worth investigating. Therefore few OFAAT experiments were carried out as described in the previous section and the results will be used in the next stage to classify and narrow down the choices.

3.6.1.3 Classification of process variables

The OFAAT experiments are representing the design factors that are 'allowed-to-vary', Z. Four factors out of nine are worth investigating after taking into consideration of the DoE scopes; resources and time limitations. The other design factors will be 'held-constant', M. Noise is the nuisance factor, X, which can be classified as controllable or uncontrollable. Noise might be contributed from human and machine parameters but they will not be included in this DoE as it will incur a high cost of chemical consumption and machine calibration. All classified factors as M, X and Z are the contributing factors that affect the response, Y. Fig. 40 simplified the classified factors and their factors affecting the response. Based on this narrow selection of experimental parameters, the level will be identified in the next sub-section.

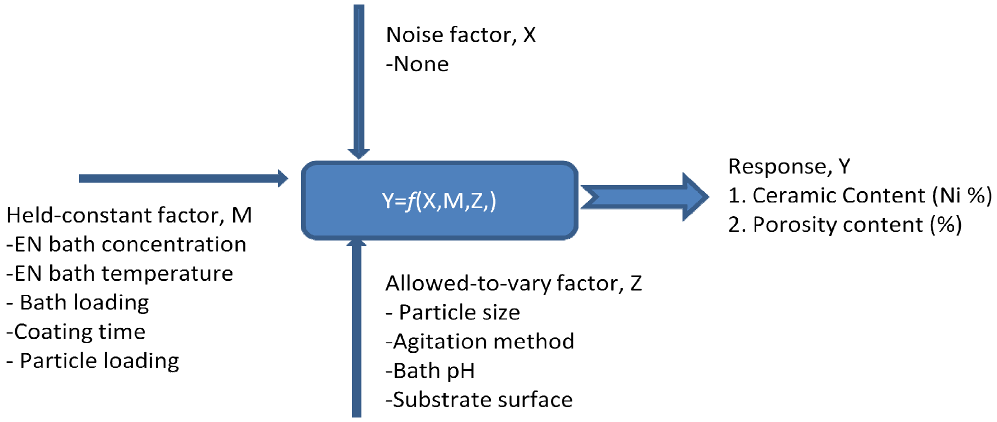

Fig. 40: Classified factors and their parameters

3.6.1.4 Determining the DoE process variables

Based on the OFAAT experiments, the experimental parameters to provide a low Ni to ceramic ratio as well as a high porosity level, were determined as ceramic particle size, agitation method, bath pH and substrate surface condition. The substrate orientation was kept in the vertical position as it showed low Ni content for both types of agitation. Besides that, this position is easier to handle and keep still. As for ceramic materials, YSZ was selected because (i) it is the most common ceramic used in SOFCs and (ii) two variations in particle size were available while the ceria was only available in 2 µm particle size. The deposition time was kept constant at 60 minutes as it was found that beyond this time, there was no gain in deposition rate. A similar trend was observed in particle loading in that there was no effect on Ni content at particle loadings greater than 25 g/l so 50 g/l was chosen as an average. The bath loading of 0.63 dm^2/l was selected as this provided the lowest Ni content deposit.

The particle sizes for 8YSZ (UCM) available were 2 and 10 µm thus they were set to be the low and high level respectively. Bath agitation that was used was mechanical stirring and air bubbling was introduced via a small power air pump. The bath pH was varied between the standard manufacturer level of 4.9 and an upper value for EN coating of 5.4. Higher pH levels are known to increase the deposition rate and this might increase the incorporation of ceramic particle in the coating. Substrate surface treatments of chemical and mechanical roughening were chosen. These two treatments are commonly used and available at Aerospace Machining Technology (AMT) in Edinburgh.

As the objective of the experiment is to obtain optimum process condition, i.e. increase ceramic and porosity content, the suitable experimental design is either process characterisation or factor screening category. Montgomery (2009) explained that for this experimental design category, it is best to keep the number of factor levels low. In general, two factor levels with high and low level will work very well. Table 11 shows the parameters and factor level of DoE that have been determined by few important stages.

Table 11: DoE parameters and factor levels

Parameters	Symbols	Level	
		Low (-)	High (+)
Particle size	A	2 μm	10 μm
Agitation	B	Air Bubbling	Mechanical Stirring
Bath pH	C	4.9	5.4
Surface Treatment	D	HF Etching	Mechanical Blasting

3.6.2 Designing Phase

The next step after determining the parameters and factor levels of the DoE are to consider the sample size (number of replicates), select a suitable run order and determine whether blocking or randomisation restriction is required. A critical decision in design problem is to determine the number of replicates to run.

The number of corner points is the number of run in one replicate which is 16 and effect is the minimum difference between two levels that is 20 vol.%. The power values are usually between 0.8-1.0 where minimum β risk of 0.20 is usually acceptable and standard deviation of 20. Fig. 41 illustrates the assumption of effect and standard deviation taking into consideration of Ni-content response.

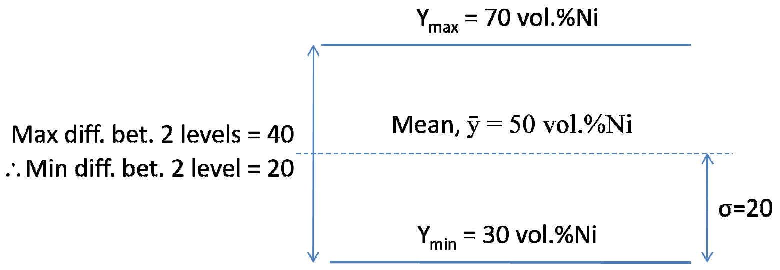

Fig. 41: Illustration of the assumption of effect and standard deviation

The power curve for 2-level factorial design obtained from Minitab 15 is given in Fig. 42a whereas its outcome is shown in Fig. 42b. Power analysis is its ability to detect an effect. The acceptable power is above 80% or β risk of 0.2 and below. Fig. 42a illustrate the effect is within the acceptable power range - above 0.8. This indicates three replications are an adequate sample size to identify any effect and ensure normally distributed data (Fig. 42b). As the variability of a sample mean decreases as the sample size increases and the shape exhibits normal distribution, five replications of experiment were therefore deemed to be a reasonable sample size and would improve the accuracy of the analysis. Clearly, further replications would continue to enhance accuracy, but a greater number of replications considered to be unrealistic in terms of time and cost.

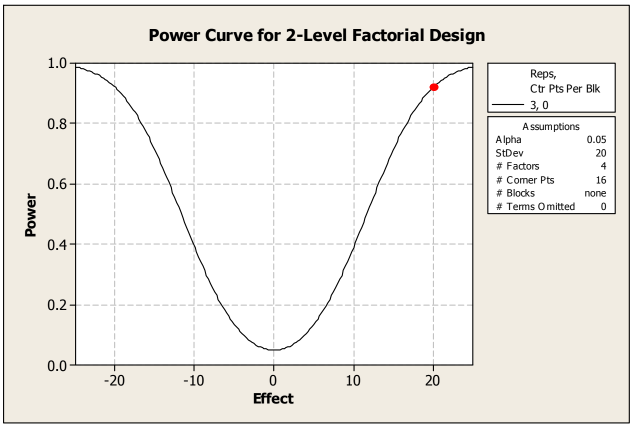

a.

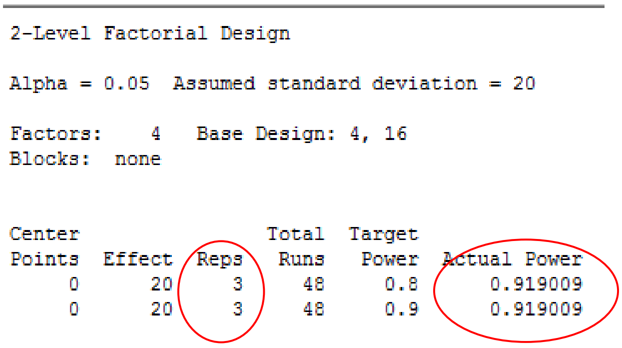

```
2-Level Factorial Design

Alpha = 0.05  Assumed standard deviation = 20

Factors:     4   Base Design: 4, 16
Blocks:   none


Center                   Total  Target
Points  Effect  Reps     Runs   Power  Actual Power
     0      20     3       48     0.8      0.919009
     0      20     3       48     0.9      0.919009
```

b.

Fig. 42: Power and sample size: (a) power curve (b) number of replicate with its power

In sub-section 3.6.1.3, it was decided that no noise factor should be included and all known enemies are kept constant, thus the experiment design will not include blocking. This then lead to a full-factorial design experiment. As there are 4 factors and two levels, the full factorials give 16 run experiments. All these 16 run experiments will be carried out in random order to avoid any effect of surrounding temperatures, humidity, time that can affect the properties/ weight of the ceramic particle/ substrate, bath evaporation rate and others.

The current research will use a sixteen run array full factorial where there are four factors and two levels of variables. Below is the list of factors and variables selected for the research. It is in Yates standard order (Bisgaard 1998) and tabulated in Table 12. There are sixteen experiments and each experiment will be repeated five times in random order. The acceptance criteria are within 95% confidence.

Table 12: DoE for EN co-deposition

STD. ORDER	PARAMETERS				REPEAT	RESPONSES	
	A	*B*	*C*	*D*		Ni Contents	Porosity Contents
1	–	–	–	–	5	The lower the better characteristics. Targeted value as low as 30 vol.%	The higher the better characteristics. Targeted value up to 40%
2	+	–	–	–	5		
3	–	+	–	–	5		
4	+	+	–	–	5		
5	+	–	+	–	5		
6	+	–	+	–	5		
7	–	+	+	–	5		
8	+	+	+	–	5		
9	–	–	–	+	5		
10	+	–	–	+	5		
11	–	+	–	+	5		
12	+	+	–	+	5		
13	–	–	+	+	5		
14	+	–	+	+	5		
15	–	+	+	+	5		
16	+	+	+	+	5		

3.6.3 Conducting Phase

There were 16 run experiments with five replications each leading to a total of 80 experiments. All the 80 experiments were conducted in a random order. The deposition time of 30 minutes in the OFAAT experiments had showed inconsistency and inadequate deposition thickness. As a result of this, the deposition time was increased to 60 minutes. The alumina substrates dimension used are 25 x 25 x 1 mm and this is being compensated by the bath volume which gives an acceptable bath loading of 0.63 dm^2/l where the bath volume was 100 ml.

3.6.4 Analysing Phase

The DoE results have to be statistically analysed to obtain results and conclusions that are objective rather than judgemental in nature. Statistical methods ensure efficiency of experiment and strengthen the conclusions obtained. Basic statistical tools to analyse DoE use analysis of variance (ANOVA) in Minitab 15.

Analysis of the DoE factorial results involves sorting the important effects from the unimportant ones after obtaining all the main effects and interaction effects. The 16-run full factorials gives 15 effects and is calculated as illustrated in Appendix M. This analytical method depends on the number of replications. No replication test means no estimate of experimental error. Effects that are near or close to zero are usually due to experimental error or noise. The higher-order effects are usually non-significant and the two-factor interaction effects are usually the most important ones in the experiment. In the multi-factorial design, main effects and interaction can be simplified using a graph called effect plots. A main effect plot is obtained by plotting the average response against the levels factors. Interaction effect can be plotted against another interested factor.

In general there are two ways DoE can be analysed: hypothesis testing and confidence interval procedures for comparing means of two treatments (Montgomery 2009). The most common procedure for analysis is by hypothesis testing. Hypothesis testing or confirmatory data analysis is a test of significance, a method of making statistical decisions using experimental data. In most cases, these decisions are determined by the null hypothesis, H_0, which simply indicates that the first and second samples do not vary significantly. The critical region of a hypothesis test is the set of all outcomes having a significant difference causing the null hypothesis to be rejected in favour of the alternative hypothesis, H_1.

A null hypothesis experiment is known to be non-robust to non-normality. If a null hypothesis of constant means is rejected, the next step is to determine which means differ significantly from one another (Rosenkrantz 1997). The probability value of the F-test, P-value, can be used in hypothesis testing. The P-value is said to be the smallest level of significance that would lead to rejection of the null hypothesis. This is due to the limit set by the level of significance, the α-value, which normally is 0.05. This is the analysis carried out by the Minitab 15 software that interprets the data variance from the normal. Higher variance indicates significance effect.

The analysed experimental data is used to construct and evaluate models. This could be done by understanding and obtaining the basic features of the numerical data description. There are four objectives of DoE data analysis that are to determine (1) the design parameters and process variables that affect the means process performance (2) the design parameters and process variables that influence performance variability (3) the design parameter levels that yield optimum performance, and (4) whether further improvement is possible (Anthony 2003).

The ANOVA results are summarised in ANOVA tables containing source of variation, degree of freedom (*df*), sum of squares (*SS*), mean squares (*MS*), F-ratio (a ratio of mean squares) and P-value (probability more than F-value). An ANOVA table for a single-factor is simplified in Table 13. For a DoE with replication *r* for each of the *d*-cells of the design, the degrees of freedom is *rd-1* (Upton and Cook 1966).

Table 13: ANOVA table of single factor, fixed effect model (Montgomery 2009)

Source of variance	*SS*	*df*	*MS*	*F*	*P>F*
Between treatments	$SS_t = n\sum_{i=1}^{a}(\bar{y}_{i.} - \bar{y}_{..})^2$	$a-1$	MS_t	$F = \frac{MS_t}{MS_E}$	
Error (within treatments)	$SS_E = SS_T - SS_t$	$N-a$	MS_E		
Total	$SS_T = \sum_{i=1}^{a}\sum_{j=1}^{n}(y_{ij} - \bar{y}_{..})^2$	$N-1$			

3.6.4.1 *Analytical tools of DoE*

The analytical tools discussed here are based on Minitab software. There are seven analytical tools which help interpret the DoE analysis as listed in Table 14.

Table 14: Minitab DoE analytical tools

Tools	Significant	Interpretation
Main effects plot	Mean response values at each level of design factors	▪ Depending the target objective- higher the better or lower the better. ▪ The effect can be mathematically calculated as follows: $$E_f = \bar{F}_{(+1)} - \bar{F}_{(-1)}$$ Where $\bar{F}_{(+1)}$ is average response at high level and $\bar{F}_{(-1)}$ is average response at low level ▪ The sign of a main effect is the direction of the effect ▪ The magnitude is the strength of the effect
Interactions plot	The mean response of two factors at all possible combinations of their settings	▪ Parallel lines indicates no interaction between the two factors ▪ Non-parallel lines indicates presence of interaction between the factors
Cube plots	Display average response values at all combinations of process	▪ Use to determine the best and the worst combination of factor levels for achieving the desired optimum response
Pareto plot of factor effects	Display absolute values of effect and draw a reference line on the chart	▪ Use to determine the factor and interaction effects which are most important to the process or design optimisation ▪ Any effect pass the reference line is potentially important
Normal probability plot of factor effects	A plot of main and interaction effects or factors against cumulative probability (%)	▪ Inactive main and interaction effects tend to fall along a straight and the active main and interaction effect tend to appear further away from the normal (straight line) ▪ The α-value is set at 0.05
Normal probability plot of residuals	A plot that evaluates the normality of a data set	▪ Moderate departure from normality does not necessarily imply a serious violation of the assumptions ▪ Gross deviations from normality are potentially

		serious and require further analysis ▪ Residual fall approximately along a straight line indicate the normally distributed residual ▪ Otherwise, not normally distributed residuals indicate that the data do not come from a normal population thus require variance-stabilising transformation on the data
Response surface plots	Contour and surface plot that show 2-D or 3-D view of the results	▪ Helps to understand the nature of the relationship between the two or more factors

3.6.4.2 Minitab software

Minitab is one of the most common and widely used statistical software to analyse DoE in industry. Minitab 15 contains three basic windows: session, worksheet and project manager. Each window contains important information. The worksheet is where all the work is being done in the window. The session window records all the instructions or commands and activities in the worksheet. The project window keeps the overall project tree and manages the whole project in the worksheet.

DoE design in Minitab is created by leaving the cursor at the first row and column in the worksheet window. The steps to construct DoE full factorial in Minitab is illustrated in Fig. 43. The response column either the Ni content or porosity content were keyed-in, then proceeds with the DoE analysis.

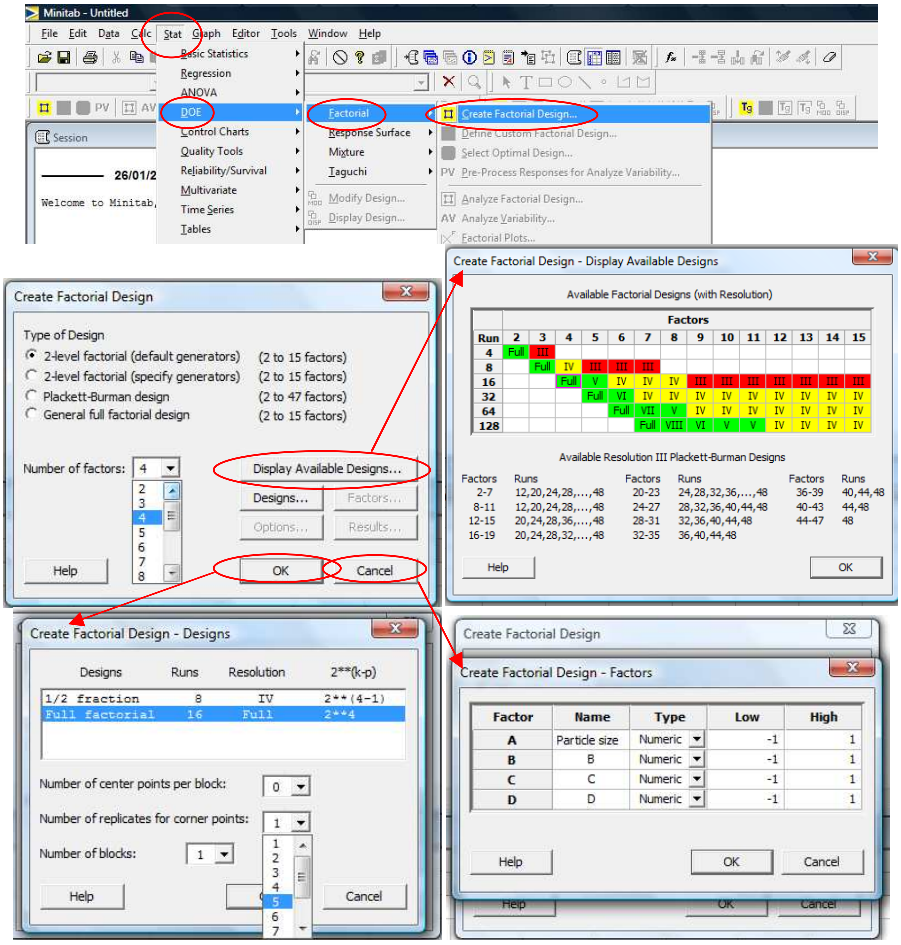

Create Factorial Design

Type of Design

● 2-level factorial (default generators) (2 to 15 factors)
○ 2-level factorial (specify generators) (2 to 15 factors)
○ Plackett-Burman design (2 to 47 factors)
○ General full factorial design (2 to 15 factors)

Number of factors: 4

Create Factorial Design - Display Available Designs

Available Factorial Designs (with Resolution)

	Factors													
Run	2	3	4	5	6	7	8	9	10	11	12	13	14	15
4	Full	III												
8		Full	IV	III	III	III								
16			Full	V	IV	IV	IV	III	III	III	III	III	III	III
32				Full	VI	IV	IV	IV	IV	IV	IV	IV	IV	IV
64					Full	VII	V	IV	IV	IV	IV	IV	IV	IV
128						Full	VIII	VI	V	V	IV	IV	IV	IV

Available Resolution III Plackett-Burman Designs

Factors	Runs	Factors	Runs	Factors	Runs
2-7	12,20,24,28,...,48	20-23	24,28,32,36,...,48	36-39	40,44,48
8-11	12,20,24,28,...,48	24-27	28,32,36,40,44,48	40-43	44,48
12-15	20,24,28,36,...,48	28-31	32,36,40,44,48	44-47	48
16-19	20,24,28,32,...,48	32-35	36,40,44,48		

Create Factorial Design - Designs

```
Designs              Runs   Resolution   2**(k-p)
1/2 fraction         8      IV           2**(4-1)
Full factorial       16     Full         2**4
```

Number of center points per block: 0

Number of replicates for corner points: 1

Number of blocks: 1

Create Factorial Design - Factors

Factor	Name	Type	Low	High
A	Particle size	Numeric	-1	1
B	B	Numeric	-1	1
C	C	Numeric	-1	1
D	D	Numeric	-1	1

Fig. 43: Creating DoE in Minitab 15 worksheet step (a)-(e)

3.6.4.3 Response optimiser

Response optimiser is a menu in Minitab 15 that helps evaluate multiple response optimisation simultaneously. It provides a scientific and logical approach to balance the competing needs. It also provides a more accurate model of the real world for those cases where more than one response must be considered. Both responses were keyed-in in the same worksheet in order for them to be analysed simultaneously as shown in Fig. 44. ‘Importance’ and ‘Weight’ determines the responses importance and their weight; in this case both responses are equally important.

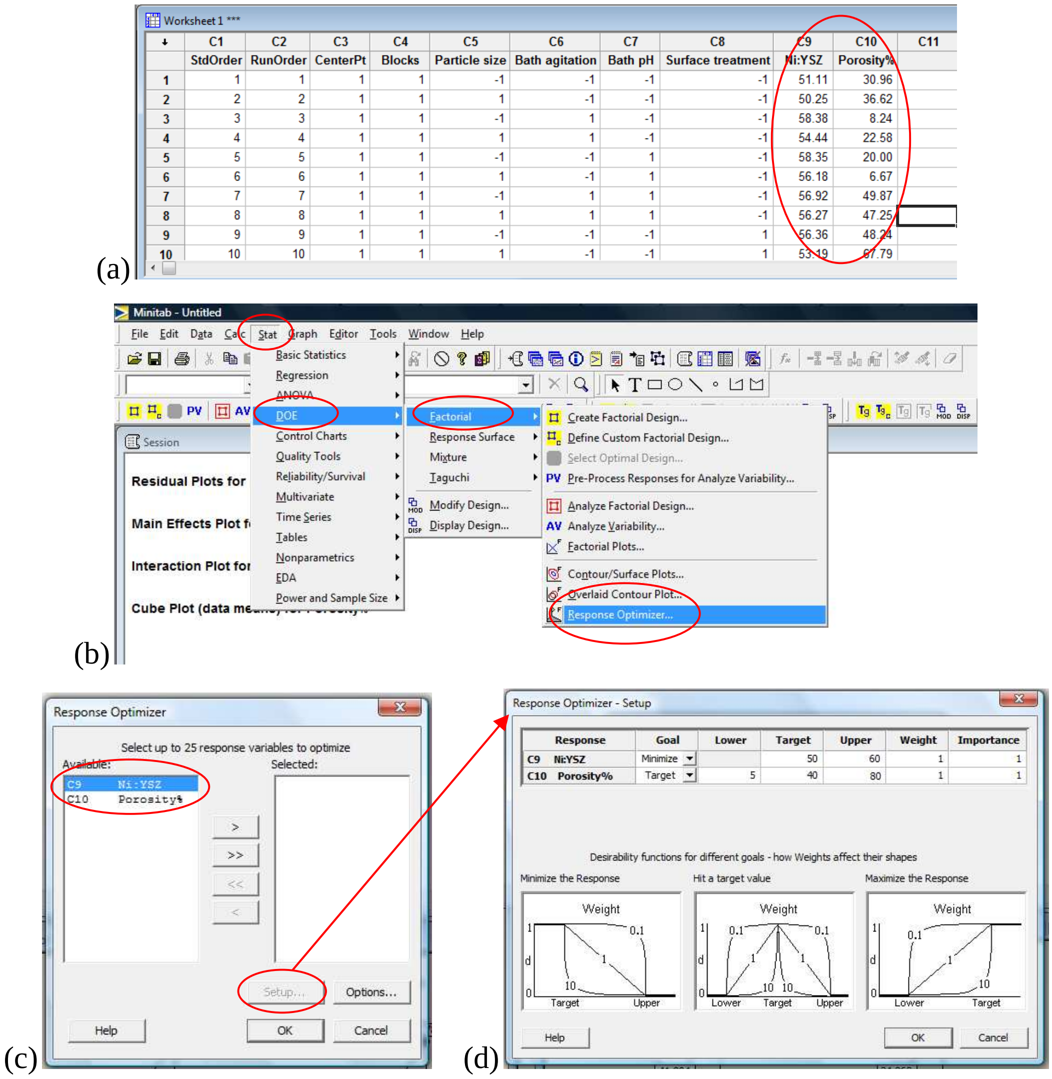

Worksheet 1 ***

↓	C1	C2	C3	C4	C5	C6	C7	C8	C9	C10	C11
	StdOrder	RunOrder	CenterPt	Blocks	Particle size	Bath agitation	Bath pH	Surface treatment	Ni:YSZ	Porosity%	
1	1	1	1	1	-1	-1	-1	-1	51.11	30.96	
2	2	2	1	1	1	-1	-1	-1	50.25	36.62	
3	3	3	1	1	-1	1	-1	-1	58.38	8.24	
4	4	4	1	1	1	1	-1	-1	54.44	22.58	
5	5	5	1	1	-1	-1	1	-1	58.35	20.00	
6	6	6	1	1	1	-1	1	-1	56.18	6.67	
7	7	7	1	1	-1	1	1	-1	56.92	49.87	
8	8	8	1	1	1	1	1	-1	56.27	47.25	
9	9	9	1	1	-1	-1	-1	1	56.36	48.24	
10	10	10	1	1	1	-1	-1	1	53.19	67.79	

Response	Goal	Lower	Target	Upper	Weight	Importance
C9 Ni:YSZ	Minimize		50	60	1	1
C10 Porosity%	Target	5	40	80	1	1

Fig. 44: Response optimiser menu and setup (a) worksheet window (b) Minitab menu (c) Response optimiser window and (d) response optimiser setup

The results were displayed in an optimisation plot where it optimises the overall desirability and also the individual desirability of each response. The 'Multiple response optimisation' is best coupled with the 'Overlaid contour plot'. This helps in finding the region of the optimum response. The results of response optimiser give predicted optimum conditions for both low Ni content and high porosity content response. Usually a set of confirmation test should be developed and this consists of another set of fractional factorial DoE.

3.7 Model Building for Predicting Response Function

The model building is used to predict the response function at various operating conditions of the process. The model is developed using a multiple regression model approach as in [equation 3.2] (Montgomery and Peck 1992).

$$\hat{y} = \beta_0 + \beta_1 x_1 + \beta_2 x_2 + \ \ldots + \beta_k x_k + \varepsilon \ \cdots \quad (3.2)$$

where β_1, β_2 ... are the linear function of the unknown parameters regression coefficients and β_0 is the intercept of the regression plane and the average response in a factorial design. The k represents k number of regressor variables that relate to the response y. The term ε is the random order component which is approximately normally and independently distributed with a zero mean and constant variance σ^2.

The response value obtained in [equation 3.2], ŷ is Ni content in vol.% and porosity content in %. Two forms of the linear regression model were employed in the analysis. The first used coded parameters assigned as -1 and +1 together with numerical parameters. The coded parameters were applied to those factors that were not numerically justified – these were (i) bath agitation and (ii) substrate surface treatment. In order to make the model more generally applicable, a second approach was adopted whereby the non-numerical factors were replaced by representative data value namely (i) the actual deposition rate resulting from the type of agitation in µm/min and (ii) the average surface roughness resulting from the substrate treatment in µm as tabulated in Table 16.

3.8 Testing Methods

3.8.1 SEM/EDXA

SEM is an abbreviation for Scanning Electron Microscope that produces images by detecting incident electrons from sample's surface. SEM can magnify up to 300 000 times the size of object studied with an advantage of 3-D images. SEM can be divided into five major components: (1) electron gun which provides the high speed electrons from a tungsten filament in a vacuum chamber; (2) lenses made of magnets that focus and control the direction of electron beams; (3) sample chamber where the sample is placed and it is vibration free with movable and rotatable device; (4) detector is to detect and collect various types of electron beams that are x-ray, backscattered and secondary electrons; and (5) vacuum chamber is to provide a vacuum medium for the electron beam to accelerate efficiently. The SEM features are schematically illustrated in Fig. 45.

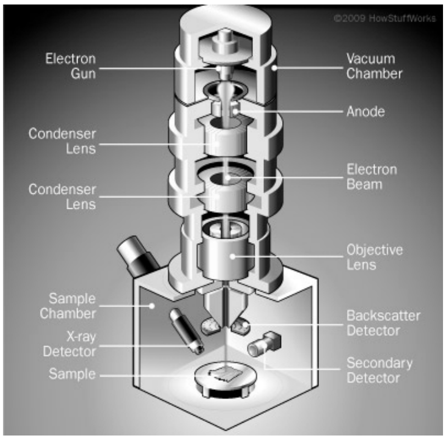

Fig. 45: Schematic diagram of SEM components (Source: HowStuffWorks website 2010)

There are few types of incident electrons in SEM including secondary electrons, characteristic x-rays, and back scattered electrons. The SEM is capable of producing high-resolution images of a sample surface using secondary electron imaging which has a great depth of field and the wide range of magnifications. The common setting of SEM is 24 mm working distance and 25 kV acceleration voltage unless stated otherwise to ensure optimum condition for EDXA. Magnification at 1000 or 2000 and resolution are varied according to the requirement (3.9-6.0). The EDX expose time was kept constant at 300s and expose area was kept close to the whole screen.

SEM enables surface morphology and chemical microanalysis in conjunction with EDXA. EDXA stands for Energy dispersive X-ray Analysis where an x-ray emitted during electron beam targeted to the sample surfaces is detected and collected for elemental composition characterisation. The electron beam bombardment knock-out the electron near the surface and resulting electron vacancy is filled by higher energy electron level. This energy is between 10-20 eV, depending on the materials and emits x-rays to balance the energy difference between the two electron states as illustrated in Fig. 46.

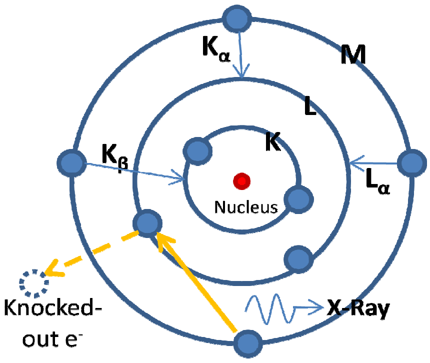

Fig. 46: Electron energy level and emitted energy

EDXA allows element characterisation as well as its distribution that give sample's chemical stoichiometry. EDXA is useful when used to characterise loose grains or unpolished materials and very effective with electron imaging methods. EDX collaborated with INCA software extends its ability for quantitative analysis, qualitative analysis, elemental mapping, and line profile analysis. Both SEM and EDX equipment will be used intensively in this research.

3.8.2 Optical Microscope

Optical microscope is used for general analysis of the specimen surface morphology or specimen cross-section. A Leitz Aristomet optical microscope has six variation of objective lenses range from 2 to 100 magnifications. The objective magnification does not represent the real image magnification because the eye-piece has 10 time magnification. Images size can be measured using a graticule with scale division designed to the standard magnifications customary in metallography. Table 15 below shows the relationship between objective magnification, true magnification and graticule division.

Table 15: Optical microscope specifications

Objective Magnification	Objective Colour	True Magnification	One division of graticule /mm
2	-	20	0.0625
5	Red	50	0.02
10	Yellow	100	0.01
20	Green	200	0.005
50	Blue	500	0.002
100	White	1000	0.001

Another important factor taken into consideration in determining good images is the incident light. This can be determined by using either brightfield or darkfield mode. In this research, only brightfield mode was used. In brightfield mode, diaphragm module is useful to perform interference contrast. The contrast such as polarisation and oblique light enhance certain feature of the captured image. Oblique illumination was largely used in this research to achieve the effect of relief-like and unprepared surfaces. The samples for optical microscopy require grinding and polishing to give flat and mirror finish surface.

3.8.2.1 Grinding

Grinding process removes the deep scratch on the specimen surface. Grinding paper with the range of 200-800 grit SiC is used and the grinding starts on the rough SiC paper. This can be done on a static planar bench or rotating wheel under adequate running water. After all the deep scratches were removed, the specimen is brought to a polishing wheel.

3.8.2.2 Polishing

Polishing is a step to remove all the fine scratches to a mirror finish. There are few types of polishing cloth of 1-6 microns and lubricant available depending on the materials to be polished. For a composite of Ni-YSZ, ceramic polishing cloth was used starting with 6 micron cloth and finally to 1 micron giving a smooth mirror finish with minimal fine scratches.

3.8.3 Image Pro-plus Software

The software comes with Leitz Aristomet optical microscope and it will be used to determine the amount of porosity in the deposition. Image Pro-Plus Version 5.1 requires an image data in standard image file format to process them. SEM micrograph can also be analysed by this software. The software works by differentiating between dark and bright area. The image can be enhanced by using powerful colour and contrast filter including Fast Fourier Transforms (FFT), morphology, field flattening, background subtraction and other spatial and geometric operations. Trace and count functions are used to calculate objects by manual or automatic operation. It measures objects attributes such as area, angle, perimeter, diameter, roundness and aspect ratio. The parameters will be adjusted according to research requirement.

3.8.4 Talysurf Profilometer

The talysurf profilometer is a general-purpose instrument used to measure surface profiles and surface roughness. Taylor-Hobson is the leading company in surface topography measurement either by contact and non-contact talysurf profilometer. Contact measurement is the traditional method first introduced by Taylor Hobson in 1941 using a diamond stylus traversed across the component to detect variations in the texture of the surface (AMETEK 2007). This derives direct representation to the surface measurement. This machine is used to measure the surface profile in term of surface roughness, R_a. It is done by comparing R_a of an untreated surface with Ra of the treated surface to determine the degree of surface profile alteration. Table 16 lists the surface roughness for 16 samples of Run 1 DoE.

Table 16: Surface roughness before and after treatment for Run 1 DoE samples

Mechanical blasting (R_a/ µm)		HF etching (R_a/ µm)	
Before Treatment	After treatment	Before Treatment	After treatment
0.60	1.23	0.71	0.71
0.56	1.48	0.71	0.67
0.66	1.28	0.57	0.58
0.52	1.01	0.61	0.64
0.63	1.34	0.69	0.61
0.69	1.51	0.63	0.74
0.76	1.65	0.66	0.67
0.64	1.67	0.65	0.68
Ave: 0.63	Ave: 1.40	Ave: 0.65	Ave: 0.66

Mechanical blasting showed great degree of substrate surface alteration compared to HF etching. The average surface alterations are 0.77 µm for the mechanical blasting and 0.01 µm for the HF etching.

3.8.5 Porosity Measurement

Archimedes specific density can be used to measure the porosity fraction in a material. The basic Archimedes principle states that the amount of displaced water volume is equal to the immersed object volume. The determination of the solid substance density can be done by buoyancy or displacement methods. Then, porosity fraction, f_p can be calculated by determining the difference between unity and the fraction of bulk and true density as described in [equation 3.3] (Kingery et al. 1976).

$$f_p = \frac{\rho_t - \rho_b}{\rho_t} = 1 - \frac{\rho_b}{\rho_t} \quad \cdots \quad (3.3) \quad \rho_b \equiv Bulk\ density, \rho_t \equiv True\ density$$

The bulk density is the quotient of mass over the total volume of a body [equation 3.4]. It is the overall density including the space in a body. The bulk density was not measured but calculated instead. Complications arise in measuring the bulk density as the deposition thickness is very low range between 3-20 µm. Thus the bulk density was measured based on the deposition thickness, *t*.

$$\rho_b = \frac{m_a}{At} \qquad \cdots \quad (3.4) \quad m_a \equiv mass\ of\ body\ in\ air, A \equiv area\ of\ sample$$

The true density on the other hand is the total solid density. The true density is measured via Archimedes buoyancy method. Fig. 47 (Sartorius 1991) illustrates the Archimedes density buoyancy methods. The density of a solid body is defined as a product of fluid density and fraction of solid mass over fluid mass [equation 3.5]. The apparent weight of a body in a liquid – weight reduced by buoyancy force is measured, m_l. The mass of fluid is defined in [equation 3.6]. The calculation of density is used in combination with the weight in air as in [equation 3.7]. The density of water at room temperature is assumed to be unity.

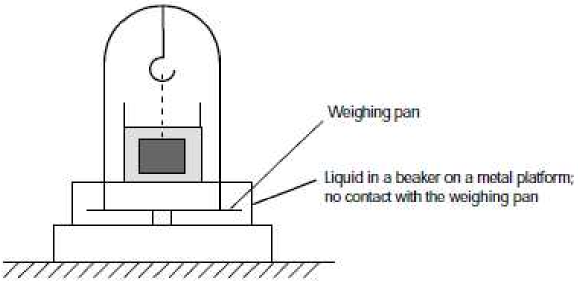

Fig. 47: Schematic diagram of Archimedes density buoyancy measurement (Sartorius 1991)

$$\rho_s = \rho_{fl} \frac{m_s}{m_{fl}} \qquad \cdots (3.5)$$

$where\ \rho_{fl} \equiv density\ of\ fluid,$

$m_s \equiv mass\ of\ solid = weight\ of\ a\ body\ in\ air = m_a$

$$m_{fl} \equiv Mass\ of\ fluid = m_a - m_l \quad \cdots (3.6)$$

$where\ m_l = weight\ of\ a\ body\ in\ liquid$

Substituting [equation 3.6] in [equation 3.5], the density of a solid is defined as

$$\rho_s = \rho_{fl} \frac{m_a}{m_a - m_l} \quad \cdots (3.7)$$

The electrolyte material for SOFC (YSZ) is solid and dense - contain no pores. The alumina tile substituting the YSZ in this research is assumed to be fully dense thus the calculation of pores of deposition will not be affected by the substrate.

3.8.6 Electrical Performance

3.8.6.1 Anode electrical performance test

The anode fabricated via EN co-deposition was tested in term of its electrical resistivity and conductivity performance. Usually for general purpose resistance measurement, 2-point electrical probe is used. The drawback of this system is the voltage drop measured over the total resistance of the sample, lead and contact. Therefore for relatively low measure resistance where the resistance of contact and lead are relatively high, the 4-point electrical probe is used to yield more accurate results. The resistance of Ni-YSZ anode was measured using 4-point electrical probe as illustrate in Fig. 48.

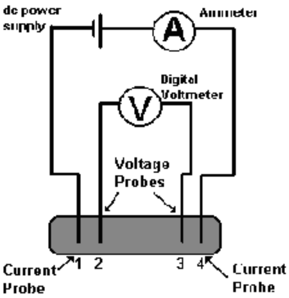

Fig. 48: Schematic set-up of the four point electrical probe

Theory of 4-point measurement is described based on Fig. 48. A power supply provides a constant current flow between probe 1 and 4. The current output can be obtained by an ammeter. The second set of probe (probe 2 and 3) is used for sensing and since negligible current flows in these probes – only voltage drop – thus accurate resistance is measured. A resistance of the sample between probes 2 and 3 is the ratio of the voltage registering on the digital voltmeter to the value of the output current of the power supply.

The resistivity or sheet resistivity, ρ (Ωcm) can be expressed as in equation 3.9 (Chan and Freidberg 2002) below.

$$\rho = \frac{\pi t}{\ln 2}\left(\frac{V}{I}\right) = \left[\frac{\pi}{ln2}\left(\frac{V}{I}\right)\right]t = R_s t \qquad \cdots (3.9)$$

Where V is the voltage drop in mV, I is the current flow in mA, t is thickness of the deposition in cm and R_s is the sheet resistance in **Ω**. The conductivity (Scm^{-1}) of the sample is just an inverse of resistivity and can be simplified in equation 3.10.

$$\sigma = {}^{1}/_{\rho} \qquad \cdots (3.10)$$

A simple 4-point measurement at room temperature was done at 1 mA, 50 mA and 90 mA at two different points as a trial test.

3.8.6.2 Anode performance in simulated SOFC condition

The electrical performance of the Ni-YSZ anode fabricated by EN co-deposition was tested in simulated SOFC condition. In real practice SOFC is operated at 800^{o}C where it is heated up slowly to avoid drastic temperature change to the ceramic electrolyte. SOFC used hydrogen gas as a fuel and nitrogen is used when it is not operating or during heating or cooling. The simulated SOFC condition was created in a furnace, heating the anode in air environment up to 420^{o}C and another set of test up to 800^{o}C. Then another set of test where the nitrogen gas was purged into the furnace. The anode sample was heated at 20^{o}C/min up to 600^{o}C. A 4-point electrical probe was used to measure the sheet resistance and thus the resistivity and conductivity of the anode at every 5-15^{o}C increment under 50 mA current.

4. RESULTS & DISCUSSION

This section is divided into three sub-sections that represent the three phases of the work. The first phase is the experiments carried out to determine the variables and factors for the work in Phase 2. These experiments are called one-factor-at-a-time (OFAAT) where a factor was varied at one time and the others were kept constant. In Phase 2, the factors and variables determined in Phase 1 are used in designing a 2^k full factorial Design of Experiments (DoE). This then allows the determination of the optimum conditions for EN co-deposition in producing low Ni to YSZ ratio and high porosity content. The final phase is to predict the optimum combination of DoE responses and determination of anode performance under SOFC simulated operating condition.

4.1 One-Factor-At-A-Time

Several single factor experiments were carried out to investigate the effect of EN process parameters on the Ni to YSZ ratio and porosity content. According to the literature, conventional (metallic) EN deposition is very much affected by bath temperature (Parkinson 1997), bath pH (Jappes et al. 2005; Keping et al. 1996; Liu et al. 2006), bath agitation (Sevugan et al. 1993), bath loading (Reidel 1997) and substrate surface condition (Teixeira and Santini 2005). Composite EN deposition is influenced by the particle stability (Necula et al. 2007; Vaghefi et al. 2003), particle shape and size (Apachitei et al. 1998; Balaraju et al. 2006b), particle loading (Kalantary et al. 1993; Sheela and Pushpavanam 2002; Shibli et al. 2006; Vaghefi et al. 2003), bath condition (Kalantary et al. 1993; Li 1997) and substrate orientation (Kalantary et al. 1993; Sheela and Pushpavanam 2002).

The studies above were carried out using different variables, settings and materials. Phase 1 allowed the determination of several EN parameters based on available resources and constraints. The uniform and dense EN deposition is ideal in most engineering applications (Baudrand 1978).

4.1.1 Initial Co-depositions

The EN co-deposition was carried out on an alumina substrate that was initially subjected to a sensitising pre-treatment process prior to deposition. EN co-deposition can be carried out on almost all types of material surfaces as long as the suitable sensitising process is applied. At this stage, the most critical sensitising step is the catalysing stage where the palladium activates the surface after cleaning. The EN Ni-YSZ co-deposition was then examined to ensure that both materials had been co-deposited. This was confirmed using energy dispersive x-ray analysis (EDXA) where a typical spectrum is shown in Fig. 49.

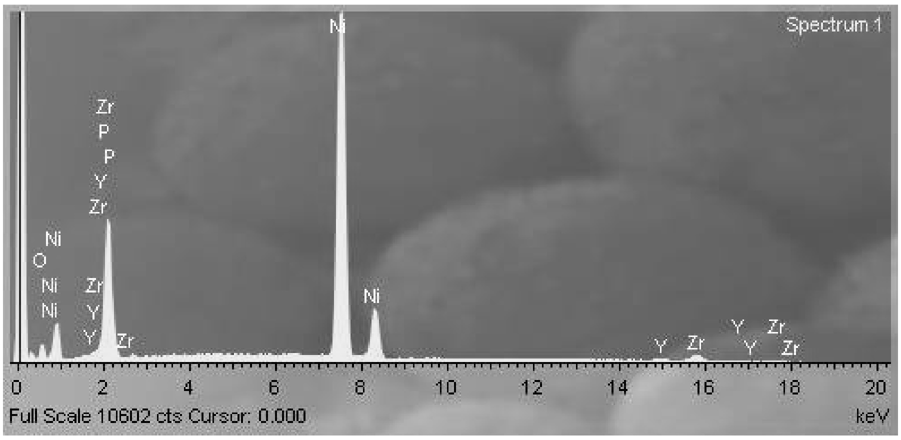

Fig. 49: EDXA spectrum of EN Ni-YSZ co-deposition

The spectrum shows the expected peaks of Ni, Zr, Y and O but also the presence of phosphorus (P) in the deposition. This can be explained as P is one of the major elements in the EN hypophosphite-base bath solution. The mechanism of the Ni-P deposition reaction in hypophosphite-based bath is not yet completely understood but it can be illustrated in a schematic diagram of the chemical reaction involved as shown Fig. 50 below. At the first stage, water reacts with hypophosphite ions to release hydrogen ions and adsorb hydrogen atom [H_{abs}] on the ceramic substrate. These active [H_{abs}] then reduce the Ni ions near the surface and release hydrogen ions. In step 3 the reaction between the hypophosphite ions and adsorbed H atom at the substrate surface results in a reduced P atom, water molecule and hydroxide ion. Thus phosphorus is expected to be present in the EN deposition. Some of the hypophosphite ions react with water to gives hydrogen gases.

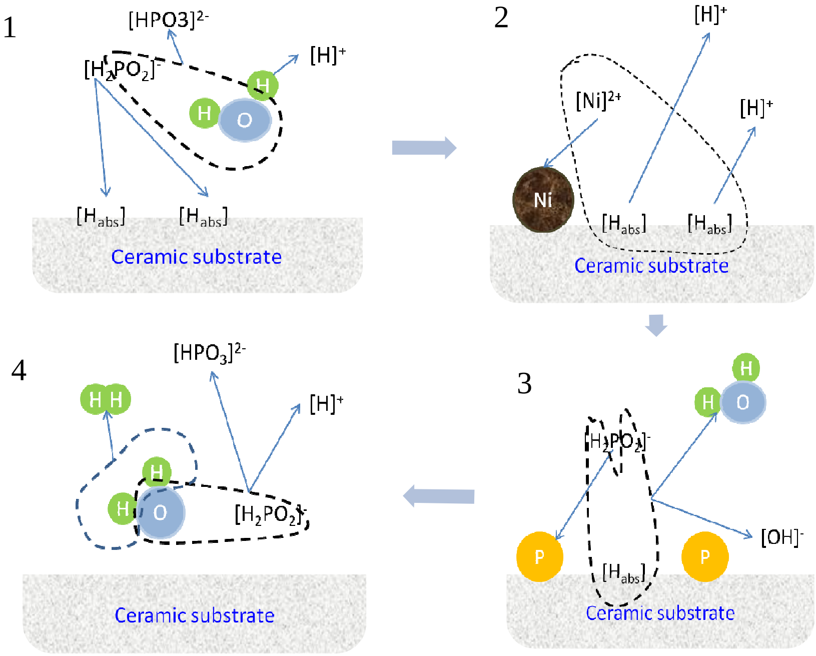

Fig. 50: Schematic diagram of EN deposition mechanism

The mechanism in Fig. 50 is solely on the Ni-P deposition and is not involved in Ni-P-YSZ co-deposition. In step 2, all Ni ions near activated/ sensitised alumina substrate are reduced autocatalytically. Entrapped YSZ particles near the surface are co-deposited with the Ni as illustrated in Fig. 51.

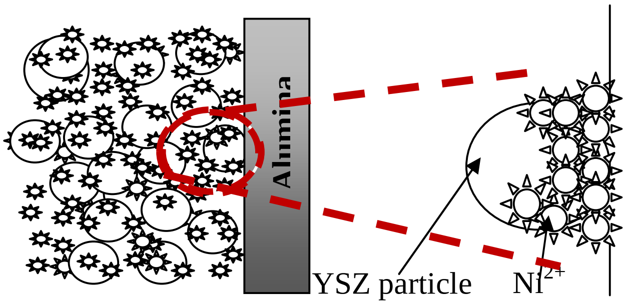

Fig. 51: Schematic diagram illustrating EN co-deposition

Ni ions near the surface are reduced to Ni atoms at a very fast rate continuously and trapped nearby YSZ particles. Although, in term of size, YSZ particles are much larger than the ions which are in a few nanometres scale, it is postulated that, like a fishing net, the ions drag the ceramic particles onto the surface and co-deposit. This was proven by the EDXA spectrum in Fig. 49 where all major elements of Ni, Zr, Y with primary Kα and Lα peaks were present.

A theoretical study on the EN co-deposition of spheroidal diamond particles and Ni-P showed independence of phase composition on the deposition rate. This indicates that the particle embedding mechanism was merely a mechanical embedding model and the reducible ions adsorbed by the ceramic surface play critical roles (Bozzini et al. 1997). In addition, the ceramic particle size and shape do influence the amount of ceramic powders co-deposited in the matrix (Apachitei et al. 1998; Balaraju et al. 2006a).

An optical micrograph cross-section of the deposited layer approximately 13 μm in thickness is shown in Fig. 52. The deposition thickness is consistently uniform with the bright yellow area being the metallic Ni while the dark parts are ceramic YSZ particles embedded in the Ni matrix phase. This porosity allows fuel and reactant gas to flow in and out of the anode. The thickness of the deposition is proportional to the deposition time - longer time develops thicker deposition.

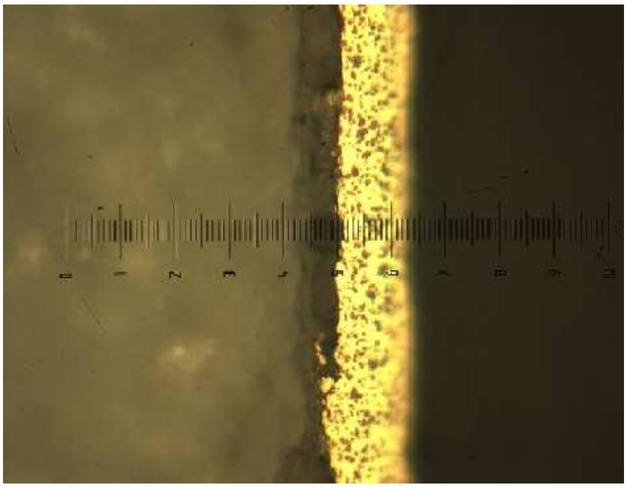

Fig. 52: Brightfield optical micrograph under 1000x, 2.0 oblique function – each division represent 1 μm.

Single-side deposition is achieved by masking one side with an aluminium tape. Taping the substrate before the sensitising process caused contamination to the surface to be coated. This is because the aluminium tape reacted with the sensitising chemical and resulted in uncoated surface area especially at the substrate edges (Fig. 53). Thus surface masking was only carried out after substrate sensitising process but before EN deposition.

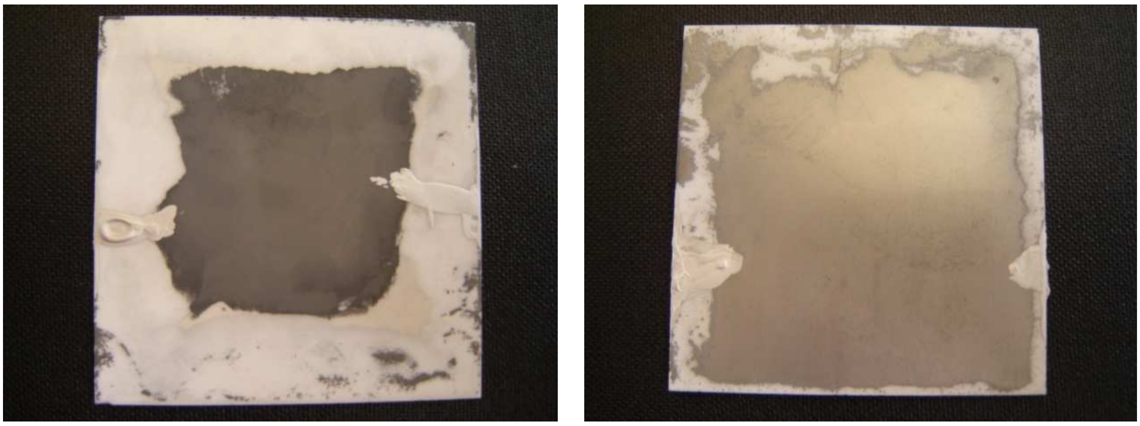

Fig. 53: Non-uniform deposition of Ni due to surface contamination

4.1.2 Particle Size

The particle size and shape were found to be an influential factor in EN co-deposition. This is because they influence the deposition surface area. Smaller particles provide greater surface area. Higher surface area indicates hydrophilic particles and thus provide complete wetting. Some studies have been carried out on various types of ceramic particles but none on YSZ.

The YSZ particles used in this research were commercial UCM 8%YSZ with varying nominal particle size of 2 µm and 10 µm and a combination of the two sizes. The co-deposition of varying particle sizes were successfully coated by EN co-deposition where all other the parameters were kept constant. The elemental composition of EN co-deposition for 2, 10 and mixture of the two in weight (wt.%) and volume percent (vol.%) are given in Table 17.

Table 17: Elemental composition in EN co-deposition varying particle sizes

Elements	2 µm		10 µm		Mixed	
	Wt.%	Vol.%	Wt.%	Vol.%	Wt.%	Vol.%
Ni	73.08	48.32	71.99	49.23	86.22	67.96
Zr	16.63	15.05	18.87	17.66	7.95	8.58
Y	0.98	1.29	1.17	1.59	0.63	0.99
O	5.90	24.31	5.26	22.41	2.29	11.25
P	3.41	11.04	2.72	9.11	2.91	11.23

The results were obtained using EDXA by INCA software in wt.%. As most literatures refer to Ni content in vol.% rather than in wt.%, both wt.% and vol.% are given as reference. Knowing the density of each element, the wt.% was converted to vol.%. The physical data for the respective elements is given in Appendix N.

As mentioned in the literature, Ni content in an anode should be between 20-30 vol.% (Zhu and Deevi 2003). The results obtained showing Ni content ranging from 48-68 vol.%. Comparing all the three particle size variations, it can be concluded that changing the particle size from 2 to 10 µm slightly increase Ni content in vol.%. The mixed particle size showed the highest Ni content as illustrate in Fig. 54 below. The deposition thickness decreases with increasing particle size and the mixed particle size was the lowest.

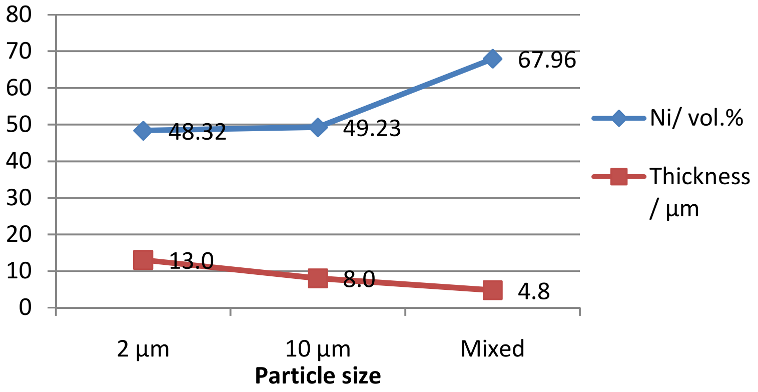

Fig. 54: Ni content and deposition thickness vary with particle size

Fig. 55 shows an SEM micrograph of 2 µm 8YSZ particles along with the EDX spectrum for the white and grey area. The white area as in spectrum 1 shows a higher Zr peak than Ni confirming that those white areas are YSZ particles. On the other hand, spectrum 3 for the grey area shows higher Ni peaks of both Kα (7.460 and 7.477 keV) and Lα (0.849 keV) energy levels confirming that the grey area is the Ni matrix. Comparing the white areas to the scale, it represents the 2 µm particle.

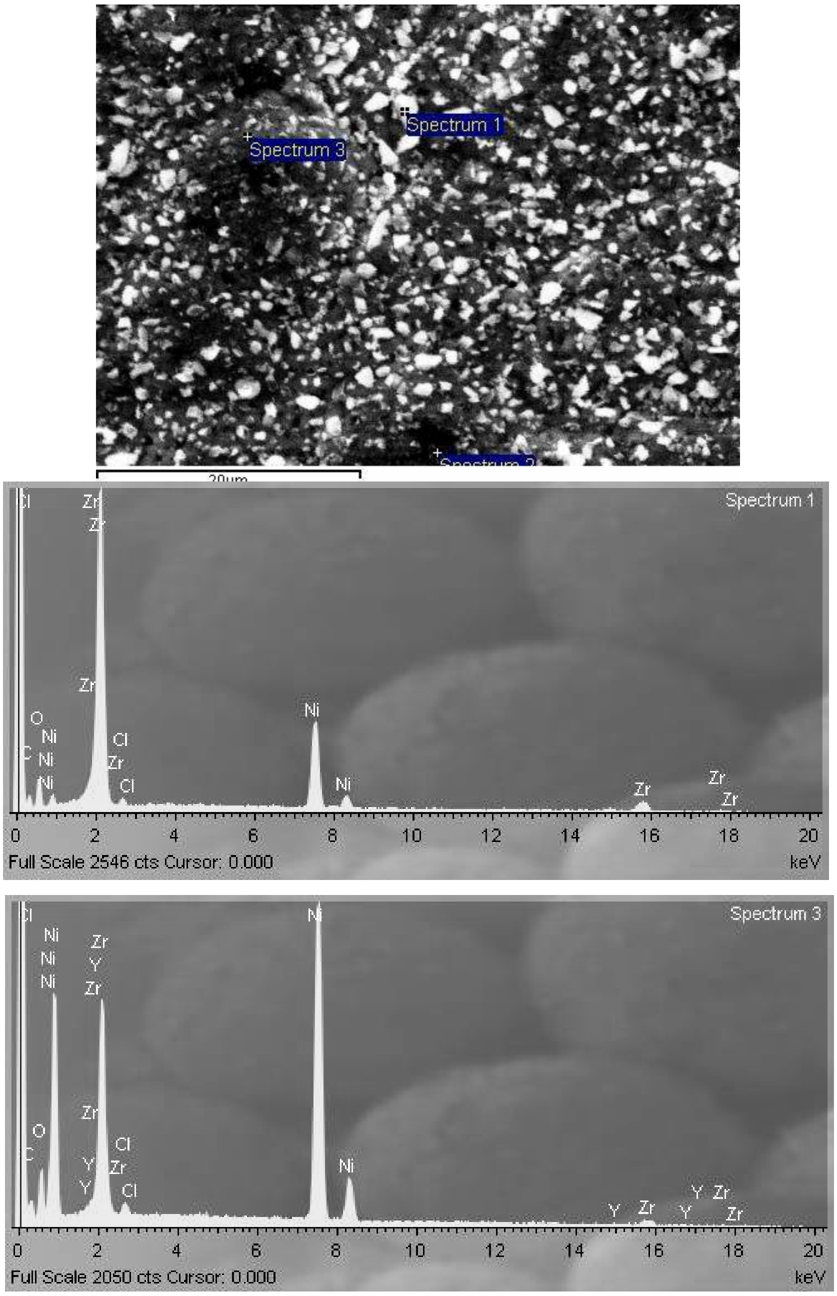

Fig. 55: SEM micrograph of 2 µm 8YSZ and EDXA spectrum on white and dark areas

Higher resolution SEM micrographs of 2 and 10 µm particles size EN co-deposition were captured by FEG SEM machine as shown in Fig. 56. The morphology of the two show more highly populated white YSZ particles in the 10 µm EN co-deposition (Fig. 56b) compared with the 2µm (Fig. 56a). This is confirmed by the EDXA data in Table 17 where the 10 µm was slightly higher in vol.%.

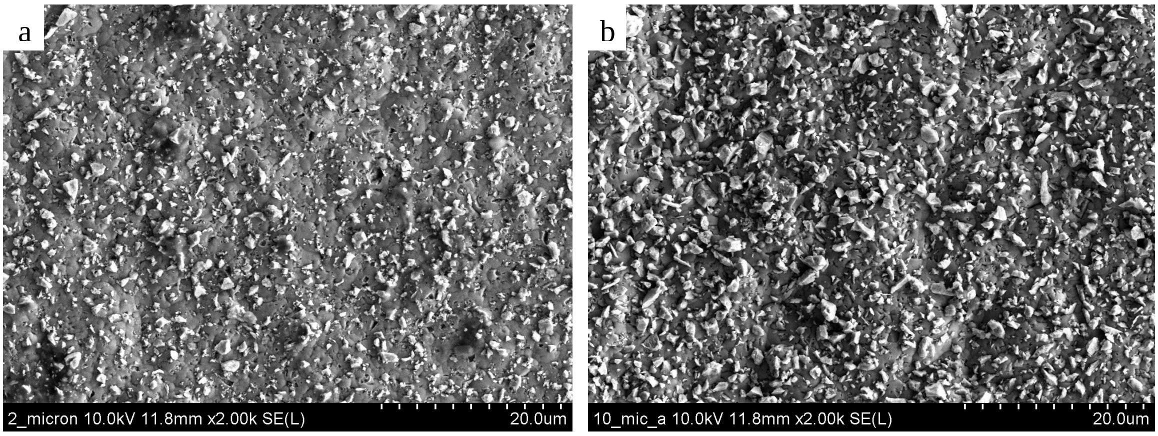

Fig. 56: Comparison of surface morphology of 8%YSZ (a) 2 µm and (b) 10 µm

The study done by Balaraju et al. (2006) showed that the larger particle size (among 50 nm, 0.3 µm and 1.0 µm) gave the highest particle incorporation in the matrix. Based on this study, it can be concluded that the larger particle size resulted in higher particle concentration in the EN composite. In terms of surface area, larger particle size provides less surface area and thus less contact required for co-deposition.

The particle size diameters were measured in both the 8%YSZ 2 µm and 10 µm EN co-depositions to confirm the particle size deposited and are shown in Fig. 57. Comparing the two micrographs in general, Fig. 57b confirmed a larger particle size compared to Fig. 57a. The SEM micrograph at the higher magnification (10kx) shows a diameter of 1.41 µm in the 2µm EN co-deposition was measured (Fig. 58a). On the other hand, Fig. 57b represents the 10 µm EN co-deposition showed a maximum particle size of 2.66 µm was measured. These low sizes are probably due to the 'iceberg' effect.

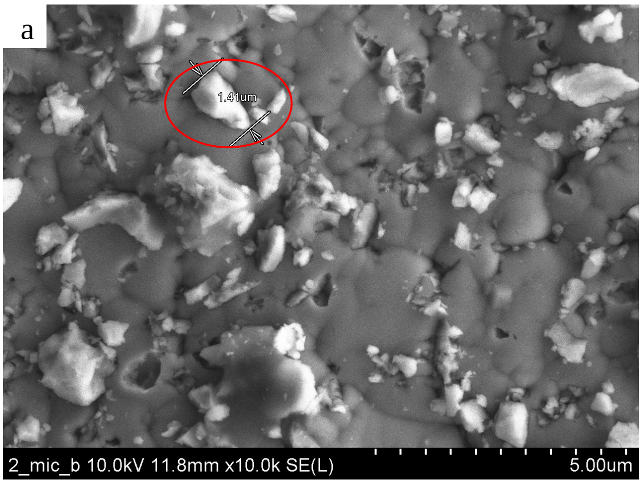

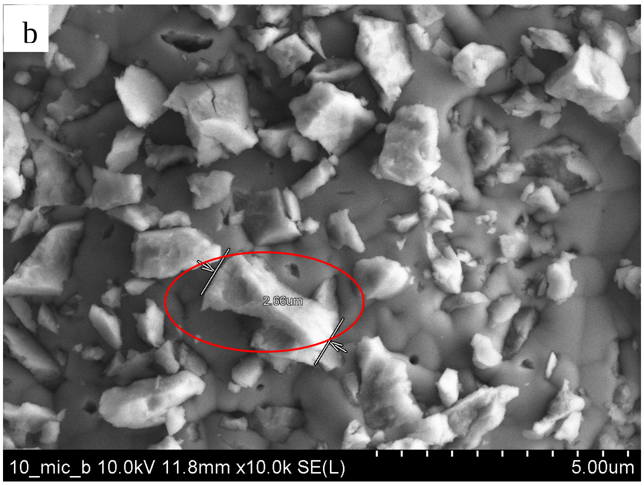

Fig. 57: Particle size measurement in SEM micrograph of 8%YSZ (a) 2 µm and (b) 10 µm

The SEM micrograph in Fig. 58 shows the mixed small and large particle sizes together by a ratio of 50:50. It is obvious that the morphology of the mixed particles is rougher than the 2 µm particle size micrograph as shown in Fig. 55. There are obvious surface pores in the micrograph that are represented by the dark area. This might be due to the deposition of smaller and larger particles where the smaller particles tend to cluster around larger particles and caused uneven surface deposition which created more pores (Berkel et al. 1994). This is encouraging in terms of porosity content but in terms of Ni content as listed in Table 17, the mixed particle sizes show a higher Ni content deposition than either of the single-size deposits.

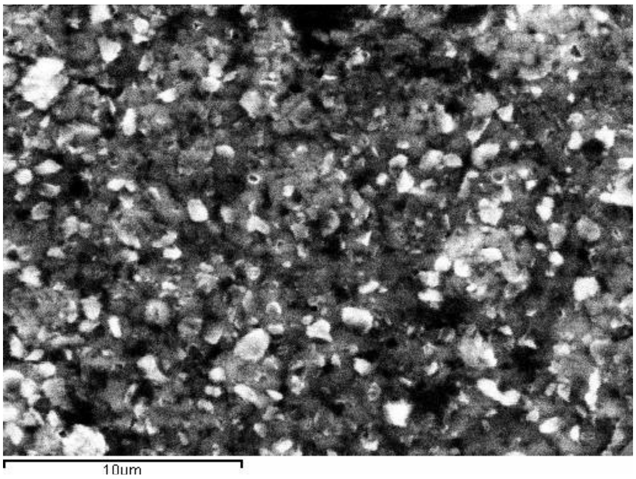

Fig. 58: Mixed particle size powder

An SEM elemental mapping was carried out on the surface of both 2 and 10 µm EN co-depositions. The Ni elemental mapping of 2 and 10 µm are shown in Fig. 59a and 59b respectively. The distribution of Ni elemental mapping in both EN co-depositions is uniform with no sign of particle agglomeration in either co-deposition. This is very promising for the application of SOFC anodes as it provides good network for electronic conduction and thus lowers the percolation threshold of the anode (Pratihar et al. 2006; Simwonis et al. 1999).

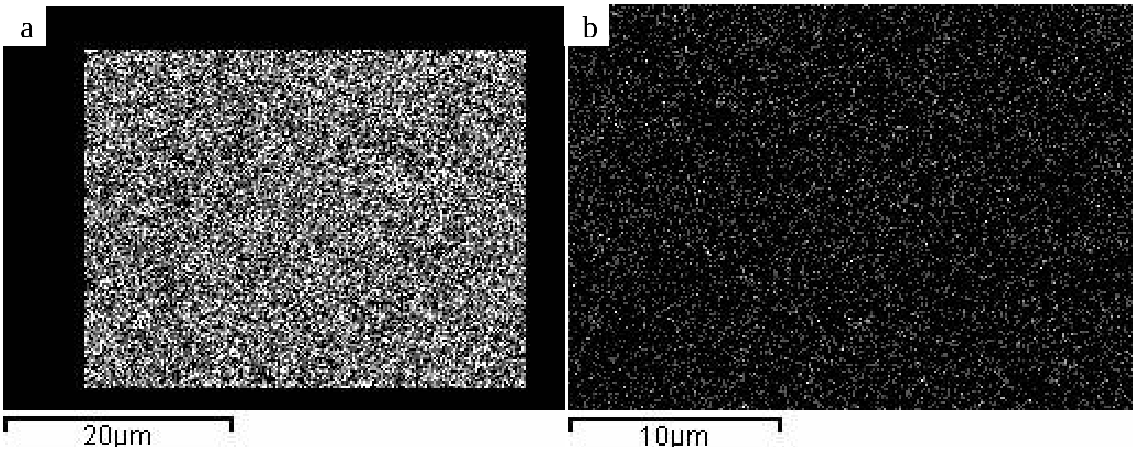

Fig. 59: Elemental mapping of Ni distribution in (a) 2 µm (b) 10 µm EN co-deposition

4.1.3 Bath Agitation

Agitation helps improve the deposition of suspended particles in an EN co-deposition process (Sevugan et al. 1993). There are two type of agitation investigated in this research; mechanical stirring and air bubbling. The purpose of varying the bath agitation is to increase the amount of YSZ in the coating. Theoretically, agitation keeps the particles in suspension and the suspended particles near the substrate will have a greater chance to be co-deposited in the EN composite coating. Table 18 lists all the major elemental compositions for EN composite coating for the two bath agitations at 250 and 500 ml bath volumes and similar particle loadings of 50 g/l.

Table 18: Major elements composition in wt.% and vol.% for stirrer and bubbler agitation

Agitation	Mechanical Stirrer				Air bubbler			
Bath Volume	250 ml		500 ml		250 ml		500 ml	
Elements	Wt.%	Vol.%	Wt.%	Vol.%	Wt.%	Vol.%	Wt.%	Vol.%
Ni	79.95	65.79	73.08	48.32	76.91	61.62	75.32	51.03
Zr	11.55	13.01	16.63	15.05	13.78	15.11	14.69	13.62
Y	1.08	1.77	0.98	1.29	0.60	0.96	1.01	1.36
O	3.79	19.43	5.90	24.31	4.47	22.31	4.65	19.63
P	3.64	14.66	3.41	11.04	4.23	16.59	4.33	14.36

The lowest Ni content was obtained in the higher bath volume for both methods of agitation as illustrated in Fig. 60. In the current work, the minimum amounts of Ni in the deposition is 48 vol.% by mechanical stirring and 51 vol.% by air bubbling. Though this value is still higher than the commercial SOFC anode value, 50 vol.% is considered an acceptable Ni content in SOFC anodes (Fergus et al. 2009). In the 250 ml bath volume, the opposite behaviour was observed with air bubbling giving a lower Ni content than mechanical stirring.

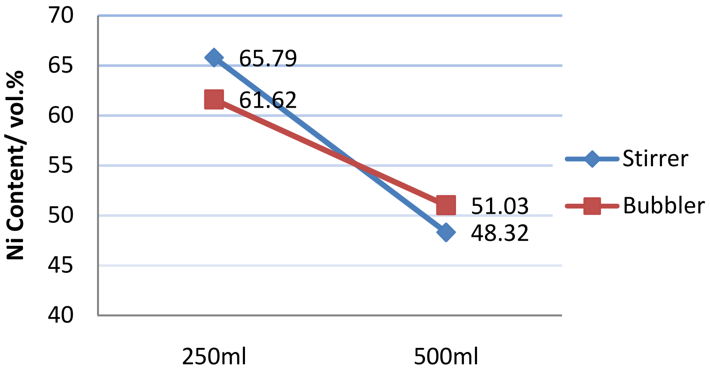

Fig. 60: Ni content at 250 and 500 ml bath volume for stirrer and bubbler agitation

EDXA smart mapping of samples from both agitation methods are shown in Fig. 61. Ni elemental mapping revealed uniform distribution in both mechanical stirring (Fig. 61a) as well as in air bubbling (Fig. 61b). Uniform distribution of Ni and YSZ is important in SOFC anodes as it gives good electronic conductivity and uniform CTE within the anode reducing the possibility of anode cracking. This shows that both mechanical stirring and air bubbling agitation methods are suitable in EN co-deposition for SOFC anode fabrication.

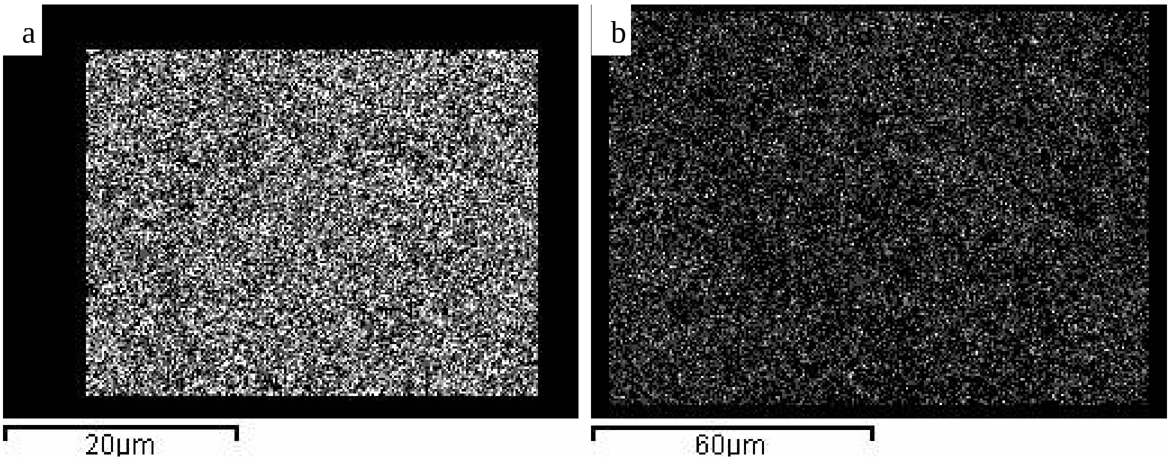

Fig. 61: Smart mapping of Ni distribution of (a) mechanical stirrer (b) air bubbler

The SEM micrographs in Fig. 62a and 62b show the surface morphologies of EN co-depositions using mechanical stirring and air bubbling. Basically there is not much difference between the two but as the scale of the two SEM micrographs are slightly different, the air bubbling looks finer and more populated with ceramic particles. What is important is that there is no particle agglomeration or cracking within the deposition.

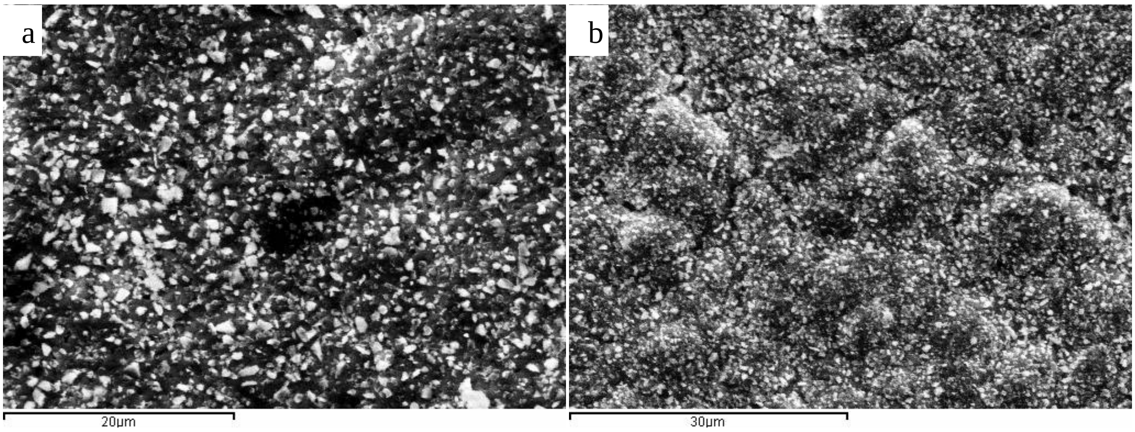

Fig. 62: SEM micrograph of EN co-deposition by (a) mechanical stirring (b) air bubbling

4.1.4 Bath pH

Altering the pH of the EN solution has been discussed in the literature review – for example where it influences the deposition rate and the P content (Baudrand 1994). The common pH range for an EN hypophosphite-based bath is between 4 and 6 (Appendix A). In this research, a pH range of between 3.4 and 5.4 has been selected to observe its effect on deposition performance. The pH values of 3.4, 4.4, 4.9 and 5.4 represent the pH values for well-below normal, just-below normal, normal (or standard) and above normal values respectively.

The bath agitation method used was mechanical stirring in a volume of 250 ml and using vertical substrate placement. Levels of deposition thickness varied between 4 and 13 µm with the thinnest deposition, 4.38 µm belonging to the sample of pH 5.4 and the thickest deposition, 12.6 µm was for the sample in pH of 4.9 i.e. the standard pH bath. Note that this latter result might have been due to 'plating out' during deposition as a result of the chemical reaction becoming too vigorous and flowing out of the beaker. When this happened, the heat was turned off to reduce the reaction and therefore the temperature was not at its optimum throughout the experiment.

Overall, the Ni content varied between 48 and 58 vol.%. All the major elemental composition in both wt.% and vol.% for the four selected bath pH are tabulated in Table 19 below.

Table 19: Major elemental composition at pH range 3.4-5.4

	pH 3.4		**pH 4.4**		**pH 4.9**		**pH 5.4**	
Element	Wt.%	Vol.%	Wt.%	Vol.%	Wt.%	Vol.%	Wt.%	Vol.%
Ni	75.26	48.14	78.97	56.78	79.95	57.38	78.31	56.71
Zr	12.98	11.36	10.64	10.47	11.55	11.34	12.70	12.59
Y	0.57	0.73	3.48	4.98	1.08	1.54	2.51	3.61
O	4.95	19.73	3.60	16.13	3.79	16.95	4.26	19.22
P	6.40	20.04	3.31	11.65	3.64	12.79	2.22	7.87

The trend of Ni content against bath pH is given in Fig. 63. From this figure, the Ni content was increasing rapidly as the pH increases from pH3.4 to pH4.4 but then remains almost constant. Even though the pH of 3.4 is out of common EN bath range, it showed the lowest Ni content but bath pH values of between 4.4 and 5.4 showed a consistency of elemental analysis results.

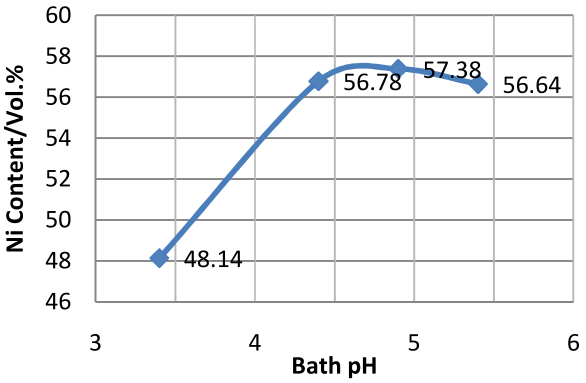

Fig. 63: Relationship of Ni content against bath pH

The relationship between plating thickness and the rate of deposition equation is discussed in the literature (Sevugan et al. 1993). Equation 4.1 simplifies the relationship to give the deposition rate being directly proportional to the co-deposition thickness. Thus the rate of deposition can be calculated from the deposition thickness.

$$Rate\ of\ deposition, r = \frac{w\ x\ 10^4}{ad} = \frac{V}{a} = t \qquad \cdots\ (4.1)$$

$\therefore r\ \propto t \qquad \cdots\ where \quad w = weight\ of deposit\ in\ g$

$a = area\ in\ cm^2$

$d = density\ in\ g.cc$

$t = thickness\ in\ cm$

The literature discusses how the deposition rate and P content are inversely proportional to each other upon increasing the EN bath pH (Baudrand 1994). This is illustrated in Fig. 64. The P content decreases from 20 to 7.9 vol.% with increasing bath pH. This trend is similar to the work carried out by other researchers previously (Henry 1984; Honma and Kanemitsu 1987).

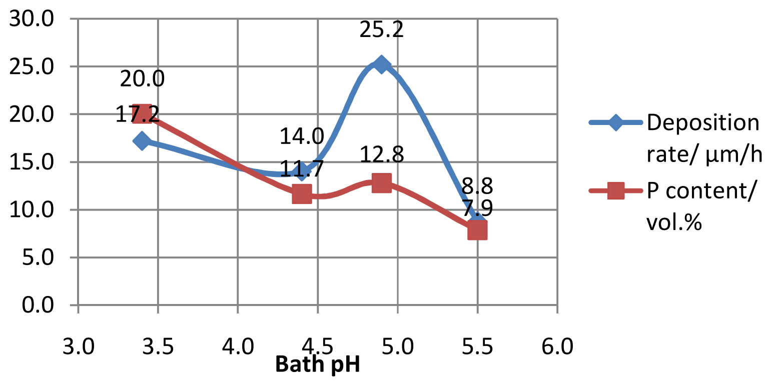

Fig. 64: Effect of bath pH on deposition rate and P content

The deposition rate found in this current research is not as described in the literature. The deposition rate increased with bath pH up to 4.9 but then fell sharply to 8.8 µm/h at pH of 5.4. The discrepancy between these results and those of Baudrand (1994) might be due to a 'plating out' incident at a pH of 5.4 in which a very vigorous reaction caused solution overflow and with the heat supply being removed, the resulting low temperature might have caused the low deposition rate.

EN deposition is very well-known for its uniform and dense deposition. The main benefit to fuel cell electrodes of changing the pH is to increase the amount of pores in the deposition. Baudrand (1994) mentioned that by altering the pH, the rate of deposition is increased. Theoretically, increasing the rate of deposition causes the particles to deposit in a rapid random order where the particles do not have enough time to settle uniformly thus creating more pores or holes. Table 20 lists the Archimedes porosity measurement for each sample at different bath pH levels.

Table 20: Archimedes porosity fraction at varying pH

Bath pH	t/ µm	m_a	m_l	ρ_b	ρ_t	Porosity/ %
pH3.4	8.6	0.1720	0.1548	3.20	10.00	68.0
pH4.4	7.0	0.1168	0.1000	2.67	6.95	61.6
pH4.9	12.6	0.2612	0.2196	3.32	6.28	47.2
pH5.4	4.4	0.0392	0.0276	1.43	3.38	57.8

The measured porosity ranges between 47-68% with the highest value obtained at a pH of 3.4. The value of porosity measured using Archimedes density was found to be too high. Therefore, further investigation on the pH 5.4 sample was run using a FEG SEM and the images are shown in Fig. 65. The images show the surface morphology at various magnifications (a) 6k, (b) 10k and (c) 20k. Clearly the images confirmed the existence of various pore spots in Fig. 65a and at higher magnification (Fig. 65c) the pores seemed to be open or connected.

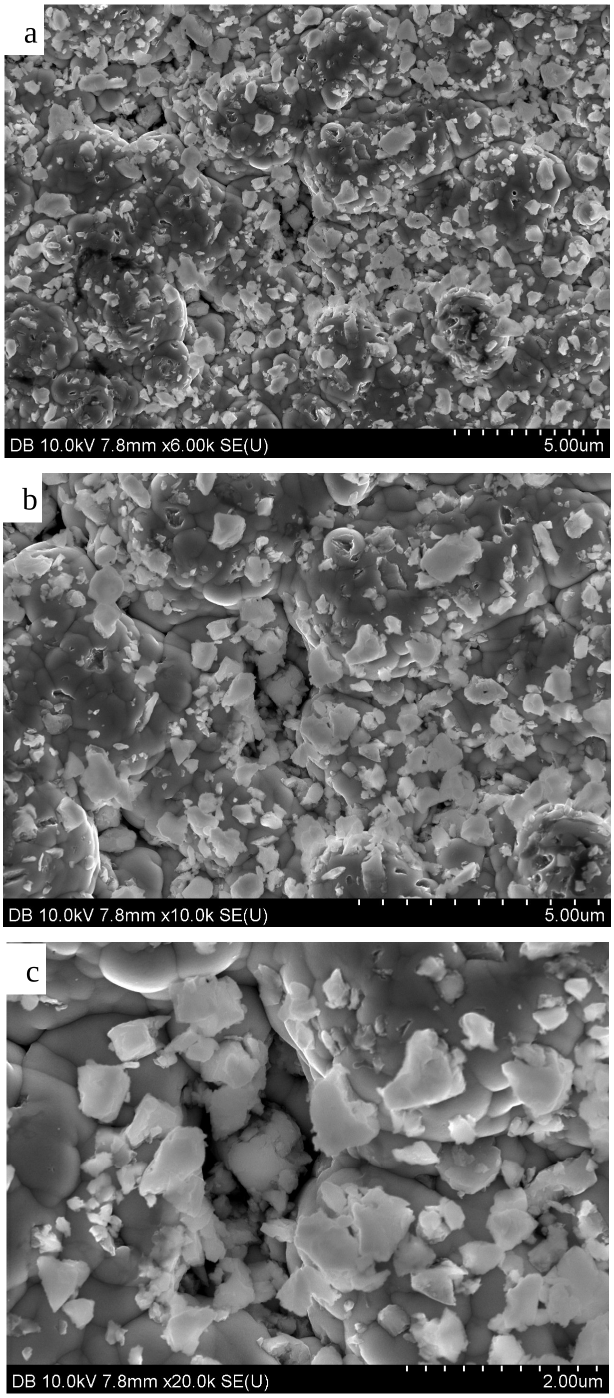

Fig. 65: EN Ni- 8YSZ (2 µm) and bath pH5.4 at varying magnification (a) 6k (b) 10k and (c) 20k

The porosity percentage gained by Archimedes method is disappointingly high when compared to the FEG SEM – it seems not proportional. One possible cause might be due to the very thin layer of deposition up to few microns to tens microns. Porosity measurement using Image Pro-Plus software was conducted. An SEM image of an EN co-deposition (8YSZ, 2 µm in bath pH5.4) is shown in Fig. 66a. This image was then analysed using colour contrast for porosity measurement. The red coloured area was the amount of porosity in the deposition (Fig. 66b). It can be estimated that the coloured porosity area is approximately 20%.

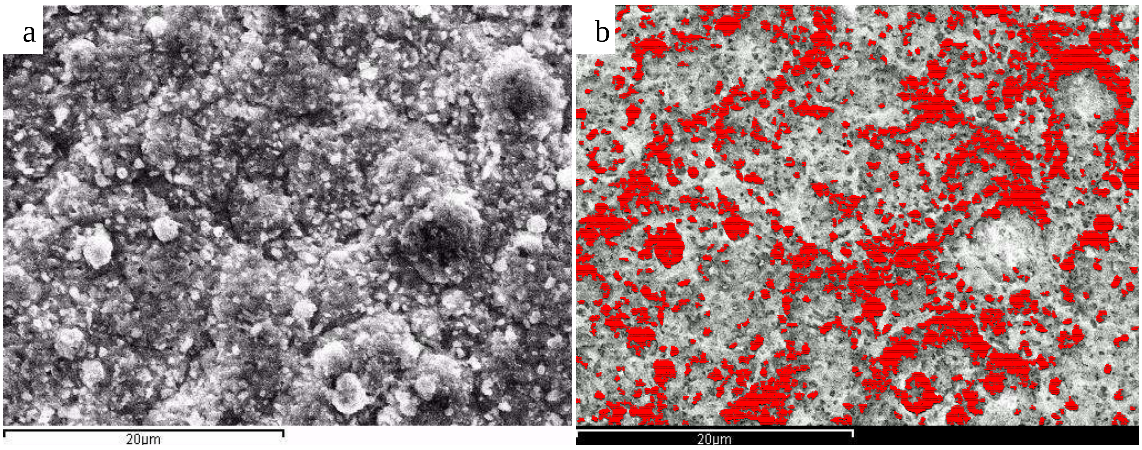

Fig. 66: Image Pro-Plus porosity measurement; (a) SEM image (b) porosity area mapping

4.1.5 Substrate Surface Treatment

A study of the condition of the substrate surface was carried out on an acrylonitrile-butadiene-styrene (ABS) substrate by etching treatment. The ABS substrate surface was etched by sulphuric acid in order to improve the surface bonding between the polymer and metallic coating (Teixeira and Santini 2005). In this research, the surface of a ceramic alumina substrate has been altered by two means, i.e. mechanical and chemical treatment.

Mechanical treatment was carried out by blasting with a strong air flow containing brown alumina particulates for 1-2 minutes while the chemical treatment involved etching the alumina tiles in a 5% hydrofluoric acid (HF) for 5 minutes. Both these treatments promote variations in surface roughness and were compared with each other and with an untreated sample. Fig. 67 shows the optical images of alumina tiles of (a) as-received, (b) after mechanical blasting and (c) after chemical etching respectively.

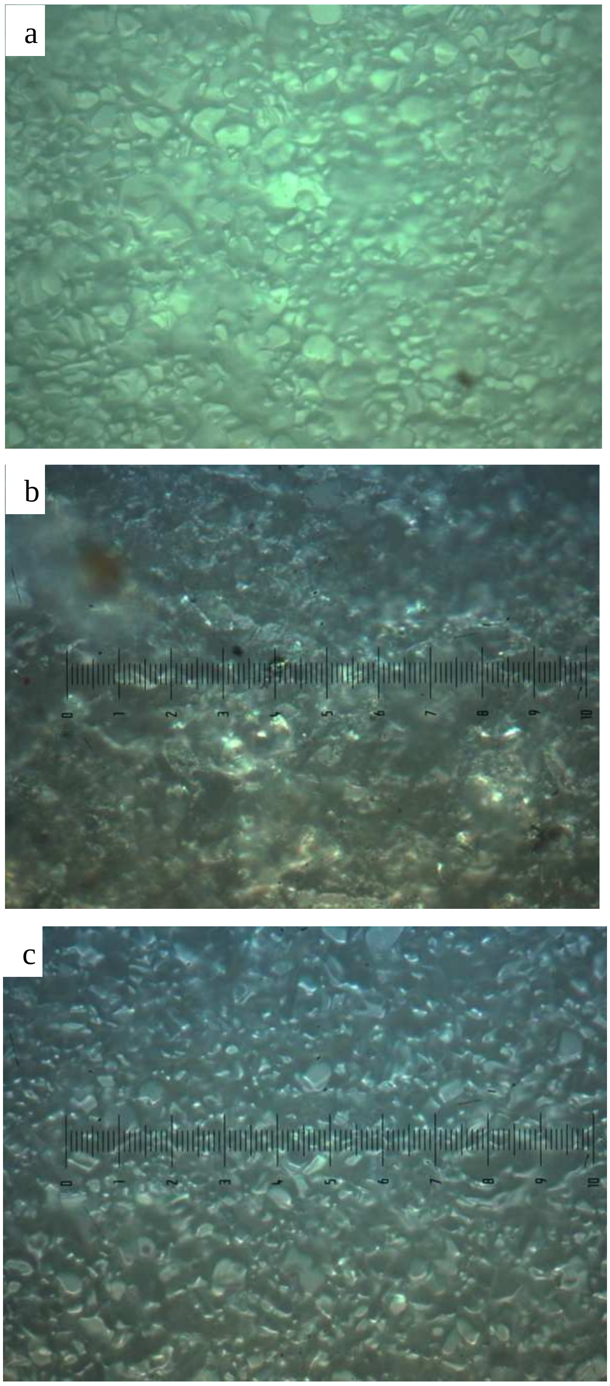

Fig. 67: Alumina surface under optical microscope at 1000x Brightfield Oblique function 3.0 (a) as-received (untreated) (b) mechanical blasting (c) chemical etching

The surface of as-received alumina shows a relatively even surface as there were only a few unfocused spots in the image (Fig. 67a). However, after being subjected to mechanical blasting, the surface was rougher with valleys of unfocused areas. In addition, there was no evidence of alumina grain as seen in Fig. 67a and 67c. In addition, the image was darker than the other two which might be due to dirt contamination from the brown alumina blasting.

On the other hand, chemical etching of the alumina showed enhancement of the alumina grain boundaries with an even surface. The HF attacked the grain boundaries and resulted in the image as in Fig. 67c. These three surface profiles were confirmed by talysurf profilometer results of surface roughness, R_a in µm as tabulated in Table 21.

Table 21: Summarise surface roughness of treated alumina

Samples	*As-received*		*Mechanical Blasting*		*Chemical Etching*	
R_a/ µm	0.71	0.69	1.04	1.02	0.64	0.56

The data from Table 21 confirms that mechanical treatment by abrasive blasting gives significantly higher surface roughness compared to untreated and chemically etched alumina. Even though the surface roughness for chemical etching seemed to be less than as-received, the enhancement of the grain boundaries may provides good ceramic - metal surface bonding in terms of micro scales. The optical micrographs in Fig. 68 show the difference in deposition surface microstructure on mechanically and chemically treated alumina. The obvious difference is that the amount of ‘black dots’ in the mechanically treated substrate deposition is higher than in the chemically treated sample.

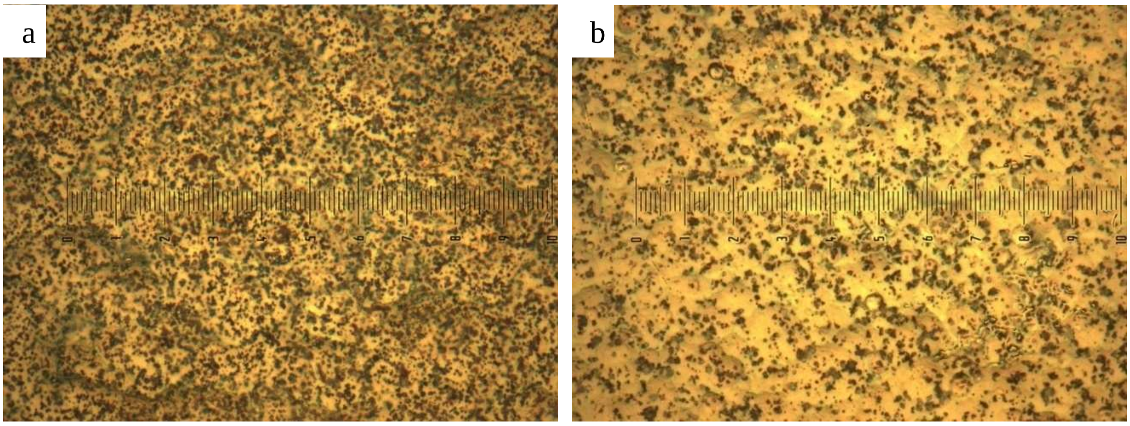

Fig. 68: EN co-deposited on (a) mechanical treated alumina (b) chemical treated alumina under optical microscope at 1000x Brightfield - oblique 2.5

The elemental composition in both wt.% and vol.% is tabulated in Table 22 for all substrate surface conditions. Generally, the mechanically blasted substrate showed a higher Ni content but this is not borne out by the number of 'black dots' in the optical micrographs. Therefore the initial assumption that the 'black dots' were representing the YSZ particles is not valid.

Table 22: Element composition in weight and volume percent

Element	As-received		Mechanical Blasting		Chemical Etching	
	Wt./ %	Vol.%	Wt./ %	Vol.%	Wt./ %	Vol.%
Ni	73.08	48.32	89.97	72.54	86.43	67.10
Zr	16.63	15.05	4.87	5.36	7.28	7.74
Y	0.98	1.29	0.10	0.16	0.83	1.28
O	5.90	24.31	1.82	9.14	3.02	14.61
P	3.41	11.04	3.24	12.79	2.44	9.27

The Ni content composition in vol.%, deposition thickness in µm and surface roughness in µin is summarised in the graphs shown in Fig. 69. It reveals the as-received having the lowest Ni content and the highest thickness deposition. Comparing blasting and etching, both Ni content and deposition thickness did not vary significantly. The trend between Ni content and the surface roughness indicates that the surface condition influences the amount of particles embedded in the composites.

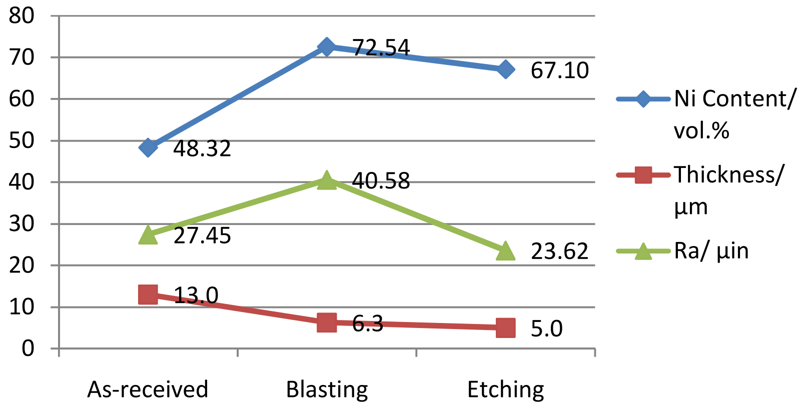

Fig. 69: Relationship of Ni content, deposition thickness and surface roughness against substrate surface condition

SEM micrographs of both surface treated depositions are compared in Fig. 70. The mechanically-treated surface is found to contain more surface porosity represented by the black spots or areas. In Fig. 70b, the etching surface morphology was shown smoother and denser with no black spots or area. Based on these two SEM micrographs, the rougher surface area has more porosity as expected. In order to clarify this, further examination was carried out on the samples under FEG SEM in order to capture better quality and higher magnification images.

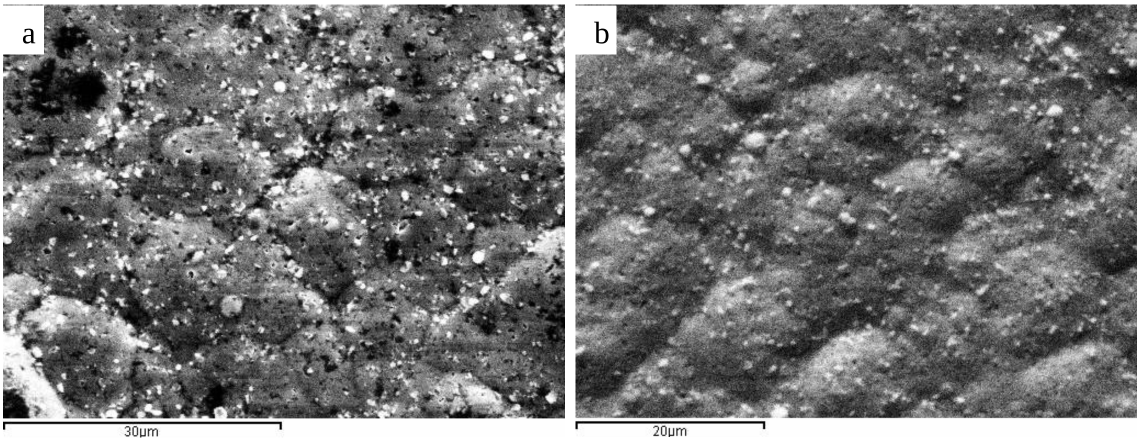

Fig. 70: SEM micrograph at 2000x magnification of (a) mechanical blasting and (b) chemical etching deposition

The images of FEG SEM at various magnifications from 1-20k are shown in Fig. 71. The images compare mechanical blasting (all images on the left represented by a, c and e) and chemical etching (all images vertically on the right represented by b, d and f). At the 1000x magnification, Fig. 71a (mechanical) indicated more highly populated black areas compared to Fig. 71b (etched). The chemically etched surface morphology is flatter.

At 5000x magnification, the difference is more obvious and it is confirmed that the black areas or spots were the pores. At even higher magnification (20,000x), the mechanically blasted deposition (Fig. 71e) exhibits many open or connected pores which are highlighted with white circles compared to the chemically etched deposition (Fig. 71f).

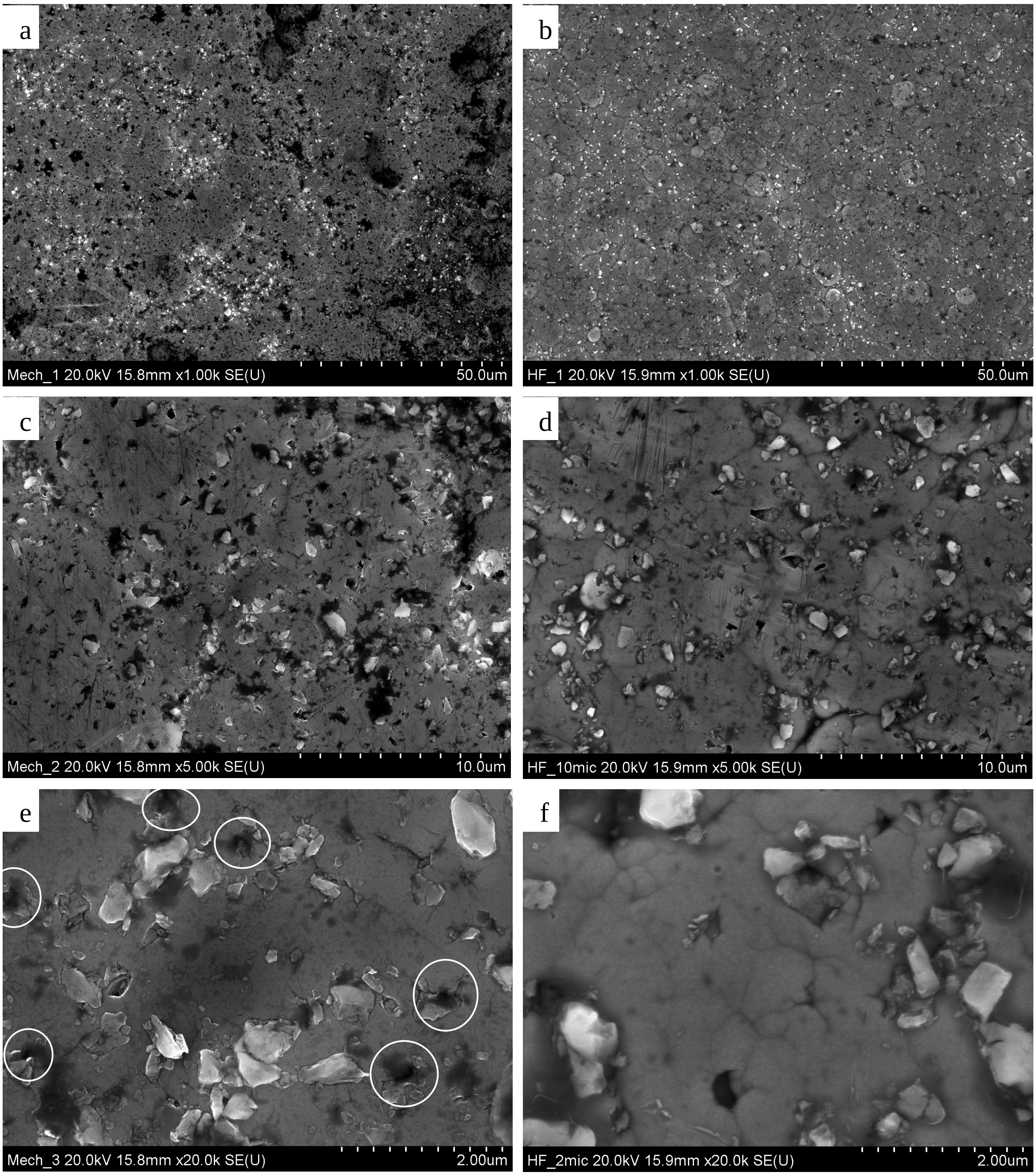

Fig. 71: SEM micrographs at 1k, 5k and 20k magnification. Mechanical treated surface deposition (left: a, c, e) and chemical treated surface deposition (right: b, d, f).

4.1.6 Substrate Orientation

A study by Kalantary et al. (1993) highlighted the importance of the orientation of substrate angle during deposition in influencing particles deposition. The target of varying the substrate orientation in this research is to get the highest amount of particle deposited within the deposition. All previous experiments were based on the alumina substrate being held vertically in the EN bath. Now, the position of the substrate in EN bath was made to be either horizontal or vertical. The Ni coated side was faced downwards. The major elemental compositions of EN co-depositions at these two substrate orientations are tabulated in Table 23 below.

Table 23: Elemental composition in vol.% for varying substrate orientations and bath agitations

Orientation	Vertical		Horizontal	
Element	Stirring	Bubbling	Stirring	Bubbling
Ni	48.32	51.03	55.35	50.31
Zr	15.05	13.62	12.41	14.03
Y	1.29	1.36	2.21	0.56
O	24.31	19.63	20.55	20.45
P	11.04	14.36	9.49	14.65

One of the main SOFC anode requirements is that the Ni content should be as low as 30-40 vol.%. Variation of Ni content in vol.% against substrate orientation and agitation method is illustrated in Fig. 72, which shows that the lowest Ni content was obtained with 48 vol.%. This was due to a combination of vertical orientation and mechanical stirring. For horizontal orientation, air bubbling gave the lowest Ni content (highest ceramic deposition) – perhaps due to the upward rising of bubbles on to the horizontal substrate.

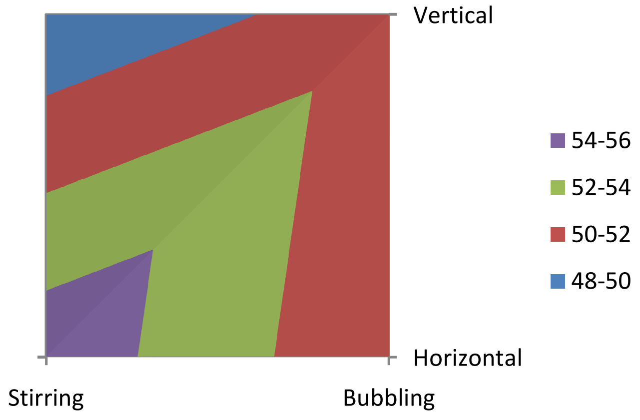

Fig. 72: Ni content in vol.% for varying substrate orientations and bath agitation

The relationship of deposition thickness against substrate orientation at varying bath agitation is given in Fig. 73. Again, the vertical substrate orientation has more significant effect on deposition thickness compared to the horizontal. Varying bath agitation methods showed an opposite trend as the substrate orientation varied from vertical to horizontal. In conclusion, stirring has greater effect than the bubbling. Typical anode thickness for flat-plate electrolyte supported SOFC ranges between 25-100 µm (Minh and Takashi 1995). The maximum thickness (13 µm) obtained in 30 minutes deposition was half of the typical commercial anode and this can be optimised by increasing the deposition time or carrying out a multi-layer deposition.

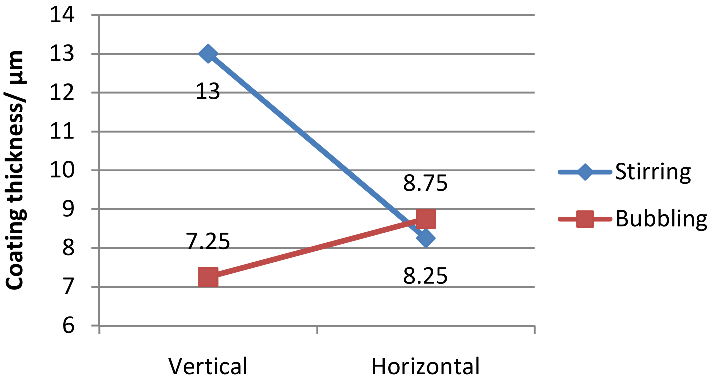

Fig. 73: Deposition thickness against substrate orientation

4.1.7 Ceramic Materials

As stated in the literature section, ceria is an alternative ceramic phase in the anode material since it has mixed conducting (electronic and ionic) property but it is not stable at higher temperatures (above 800°C) and low partial pressures ($P_{O2}<10^{-23}$) (Orera et al. 1994). The most common and promising ceria-based anode is nickel-gadolinium doped ceria (Ni-GDC) but ceria stabilised zirconia (CeSZ) is a new material in this application and worth investigating. Therefore a comparison of Ni-8YSZ and Ni-13CeSZ was analysed and compared in this work. As Ni-YSZ was successfully manufactured via EN co-deposition, the same applies to Ni-CeSZ and was verified by EDXA spectrum in Fig. 74.

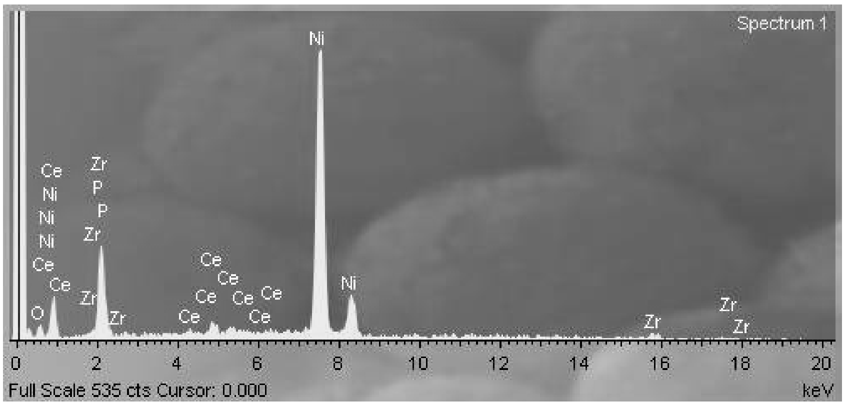

Fig. 74: EDXA spectrum for Ni-CeSZ EN deposition

All major elements, Ni, Zr and Ce peaks were in the spectrum. All major elemental composition in wt.% and vol.% are tabulated in Table 24. The difference of Ni content in wt.% was not significant to be considered as a major issue.

Table 24: Elemental composition of Ni-CeSZ EN deposition in vol.%

	Mechanical Stirring		Air Bubbling	
Element	Wt.%	Vol.%	Wt.%	Vol.%
Ni	75.64	54.14	76.11	50.86
Zr	14.49	14.20	11.75	10.75
Ce	2.46	2.32	2.35	2.07
O	3.53	15.74	4.81	20.03
P	3.88	13.60	4.98	16.29

An elemental mapping of Ni and Ce is given in Fig. 75a and 75b respectively. The distribution of Ni is found to be uniform with no sign of agglomeration. As Ce composition is less than Ni, the distribution was not as populous but generally it is populated evenly across the area. Even though prior to deposition Ce powders tend to agglomerate and required soft crushing before pouring into the EN bath, the mapping shows no sign of agglomeration of Ce powders.

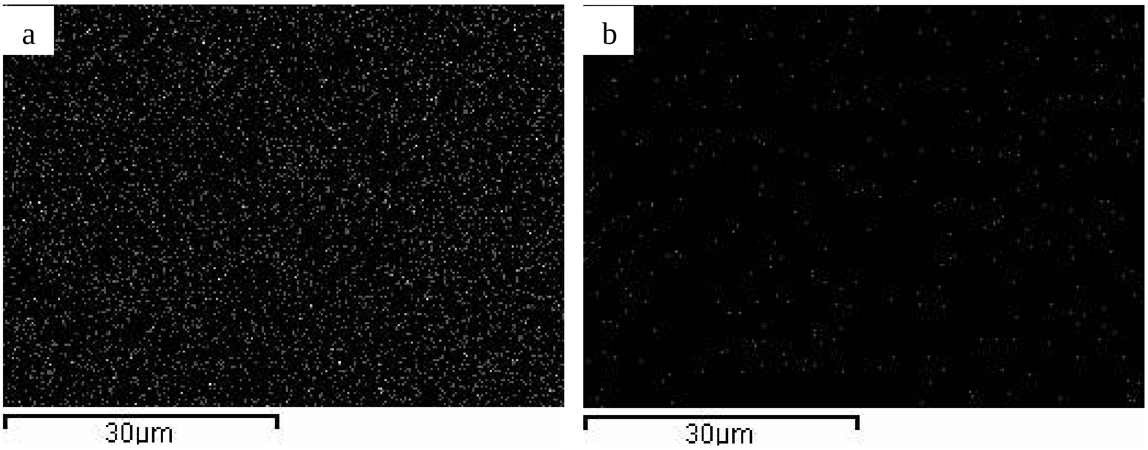

Fig. 75: Smart mapping of (a) Ni (b) Ce distribution

EN co-deposition of both Ni-CeSZ and Ni-YSZ have Ni content in the range of between 48 to 62 vol.% which were obtained by mechanical stirring and air bubbling agitation. Fig. 76 summarises the 3-D relationship of Ni content against EN co-depositions and bath agitation methods. It is concluded that for Ni-CeSZ, the lowest Ni content was obtained with air bubbling whereas for Ni-YSZ, the lowest Ni content was obtained with mechanical stirring. Comparing the two EN co-depositions, Ni-YSZ gave the better anode composite in terms of having the lowest Ni content.

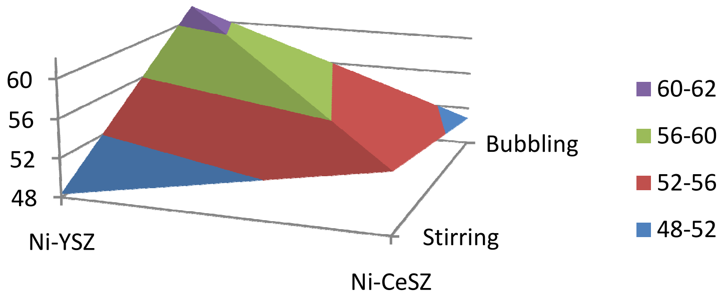

Fig. 76: Ni content against EN composites and bath agitation

4.1.8 Deposition Time

In theory, deposition thickness should be directly proportional to the deposition time. There is also a study that showing that porosity decreases as deposition thickness increases (Das and Chin 1959). As one of the objectives of this research is to increase the amount of porosity in the composite, this theory is investigated in the EN Ni-YSZ system.

Previously all the depositions were carried out over a period of 30 minutes. Now the deposition times were varied between 30 and 120 minutes to observe Ni content as well as porosity fraction. The alumina substrates used were 25 by 25 by 1 mm dimension for this work.

The trend showed a rapid decrease in Ni content between 30 and 60 minutes deposition time then gradually increasing between 60 and 120 minutes. The results are summarised in Fig. 77. The lowest Ni content was obtained at a 60 minutes deposition time with 54.74 vol.%. The highest Ni value was 61 vol.% obtained in 30 minutes deposition time. Even though there are many other factors that might influence the performance of EN deposition, based on this observation, it can be concluded that the optimum deposition time for low Ni content is 60 minutes.

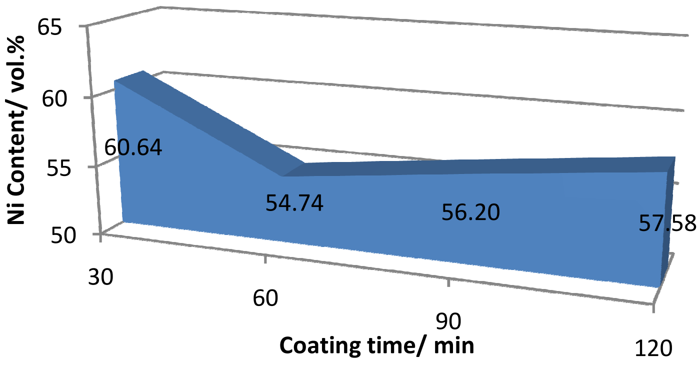

Fig. 77: Ni content against deposition time relationship

Porosity levels at different deposition times were measured using the Archimedes buoyancy method and is illustrated in Fig. 78. In general, the trend is linear with a negative slope indicating that porosity was inversely proportional to deposition time. There is an outlier at 90 minutes deposition time that gives the highest porosity fraction with 61.4%. Overall, the inverse proportion of porosity fraction against deposition time is encouraging as it follows the theory. Increasing deposition time should increase deposition thickness and reduce amount of porosity in the deposition (Das and Chin 1959).

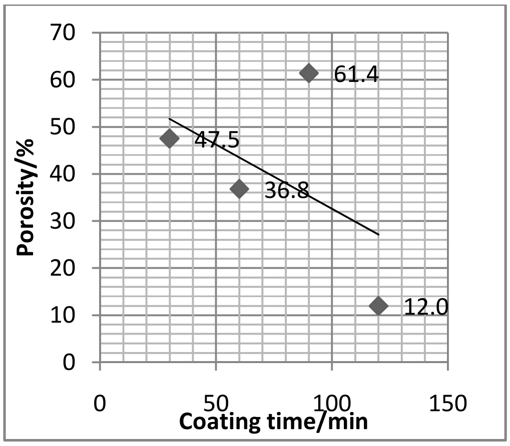

Fig. 78: Porosity fraction against deposition time

4.1.9 Particle Loading

Increasing the amount of particles in the EN bath hopefully will increase the possibility of particles being embedded in the EN co-deposition. The amount of particle added in a specific bath volume is termed as ‘Particle loading’. Previous studies carried out on any other inert particles showed that deposition of particles in the composite was directly proportional to the particle loading (Shibli et al. 2006; Vaghefi et al. 2003).

This work consists of varying the particle loading between 12.5 and 100 g/l. The Ni content was again obtained via EDXA and the relationship between Ni content and particle loading is given in Fig. 79. The Ni content decreased rapidly from 57 vol.% to 34 vol.% for particle loadings of 12.5 g/l and 25 g/l respectively. This indicated that in the co-deposition, increasing particle loading increases particle incorporation in the deposition from 43 vol.% to 66 vol.% as Ni content is inversely proportional to the particles content. It then appeared that increasing particle loading to greater than 25 g/l did not give any significant increase in particle deposition in the composite.

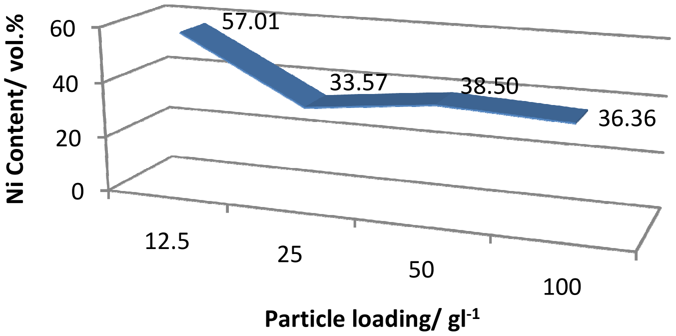

Fig. 79: Ni content against particle loading

The study by Kalantary et al. (1993) reported that a loading of more than 15 g/l in a Ni-SiC system caused extensive foam that reduced the plating rate. Another study by Vaghefi, Saatchi et al. (2003) reported that a maximum of 10 g/l gives a maximum of 33 vol.% particles content. From this current work, it can be concluded that particle loading is directly proportional to particle content up to 25 g/l. The particle loading over 25 g/l gives a plateau in Ni content. The particle content obtained at 25 g/l particle loading is 66 vol.% and is equivalent to 3 times more than reported in the previous studies at 8 g/l particle loading (Vaghefi et al. 2003).

4.1.10 Bath Loading

The bath loading is the ratio of deposition surface to the bath volume. According to the Schloetter (2006) manual sheet, the minimum bath loading is 0.25 dm^2/l and the ideal is 1.2 dm^2/l. As the deposition surface was 25 by 25 mm, the bath volume should be at least 50 ml which gives a 1.25 dm^2/l bath loading which just exceeds the ideal recommended bath loading. The bath volume was changed from 50 ml to 300ml. Therefore the bath loading varied between 1.25 dm^2/l and 0.21 dm^2/l i.e. it fell between just above the ideal and just below the minimum bath loading.

A scatter plot of Ni content obtained by EDXA against bath loading is given in Fig. 80. It shows a polynomial trendline with the highest Ni content observed at bath loading lower than minimum recommended bath loading. The lowest Ni content was obtained at a bath loading of 0.63 dm^2/l where the bath volume was 100 ml. Exponential increases in Ni content were observed above and below the bath loadings of 0.63 dm^2/l.

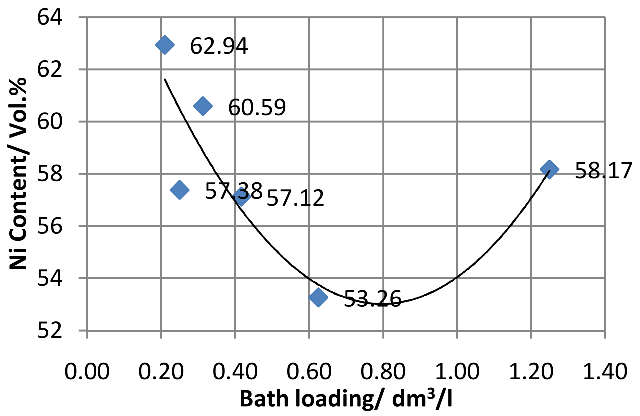

Fig. 80: Ni content against bath loading

Similar to the Ni content trend, the deposition thickness of the composite also shows a polynomial trend. Fig. 81 shows the relationship of deposition thickness to bath loading. In general, the deposition thickness reduces with increasing bath loading. The lowest thickness was obtained at bath loading of 0.63 dm^2/l, i.e. where the lowest Ni content was obtained as discussed previously.

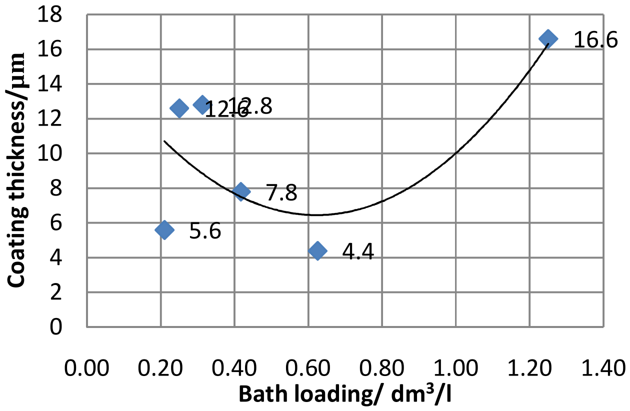

Fig. 81: Relationship between deposition thickness and bath loading

4.1.11 OFAAT Conclusions

EN co-deposition has been successfully achieved with acceptable deposition thickness and promising YSZ to Ni ratio content for SOFC anode application. The 9 EN factors are: ceramic particle sizes, bath agitation methods, bath pH, substrate surface treatment, substrate orientation, ceramic materials, deposition time, particle loading and bath loading were investigated independently.

The measured elemental composition of EDXA represents the Ni content in the EN co-deposition or the Ni to YSZ ratio. Ni content of all the samples in 9 OFAATs obtained ranged between 33 and 73 vol.%. The deposition thickness varied from as low as 4.4 µm to 20.8 µm in a standard of 30 minutes deposition time. This is comparable to the average EN deposition thickness by other studies which was 20 µm in an hour. The measured porosity fraction in 2 out of 9 OFAATs and porosity fractions obtained ranged between 57 and 68%. The summary of all OFAAT experiments are tabulated in Table 25.

Table 25: Summary of all 9 OFAAT experiments

	Parameters	Variables	Observations		
			Ni/ vol.%	Thickness/ µm	Porosity / %
1	Particle size	2 µm	48.32	13.0	
		10 µm	49.23	8.0	
		Mixed	67.96	4.8	
2	Bath agitation	Stirring 250ml	65.79	12.6	
		Stirring 500 ml	48.32	13.0	
		Bubbling 250 ml	61.62	7.3	
		Bubbling 500 ml	51.03	13.8	
3	Bath pH	pH3.4	48.14	8.6	68.0
		pH4.4	56.78	7.0	61.6
		pH4.9	57.38	12.6	47.2
		pH5.4	56.71	4.4	57.8
4	Substrate surface treatment	As-received	48.32	13.0	
		Mechanical blasting	72.54	6.3	
		Chemical etching	67.10	5.0	
5	Substrate orientation	Vertical bubbling	48.32	12.6	
		Vertical stirring	51.03	7.3	
		Horizontal stirring	55.35	8.3	
		Horizontal bubbling	50.31	8.8	
6	Ceramic materials	YSZ stirring	48.32	13.0	
		YSZ bubbling	61.62	7.3	
		CeSZ stirring	54.14	6.9	
		CeSZ bubbling	50.86	10.1	
7	Deposition time	30 min	60.64	12.2	47.5
		60 min	54.74	6.2	36.8
		90 min	56.20	14.2	61.4
		120 min	57.58	11.2	12.0

8	*Particle loading	12.5 g/l	57.01	20.8
		25 g/l	33.57	16.0
		50 g/l	38.50	7.0
		100 g/l	36.36	20.0
9	Bath loading	1.25 dm^2/l	58.17	16.6
		0.63 dm^2/l	53.26	4.4
		0.42 dm^2/l	57.12	7.8
		0.31 dm^2/l	60.59	12.8
		0.25 dm^2/l	57.38	12.6
		0.21 dm^2/l	62.94	5.6

*These values were determined using the HITACHI FEG SEM

The 9 OFAAT parameters were found to have an effect on the YSZ to Ni ratio, coating thickness and also porosity. A successful Ni-YSZ composite coating of 13 µm thick was confirmed by the existence of major elemental peaks of Ni, Zr, Y and P. The lowest Ni content was obtained for the samples tested for different particle loadings. However, due to the Cambridge SEM being under repair, the Ni content in the anodes of samples for 'particle loading' in point 8 (Table 25) above were measured using a FEG SEM with fully quantitative EDXA software. In order to determine the difference between the two analysers, five other samples were analysed later on both machines and the results are presented in Table 26.

Table 26: Comparison of elemental analysis composition on both SEM machines

Elements	Cambridge SEM/ vol.%					FEG SEM/ vol.%				
	#6	#7	#12	#46	#47	#6	#7	#12	#46	#47
Ni	61.38	52.31	57.60	61.28	52.66	36.70	38.34	33.31	39.58	37.16
Zr	8.71	15.78	12.76	10.78	15.72	10.42	14.30	10.46	10.46	13.23
Y	0.64	1.92	2.06	0.636	2.16	0.00	0.00	0.00	0.00	0.00
O	14.82	20.60	17.42	15.02	19.61	29.21	25.51	35.05	25.85	22.87
P	14.45	9.39	10.16	12.28	9.86	23.67	21.84	21.18	24.11	26.74

The results showed that the Ni content obtained using the Cambridge SEM was higher than those obtained using the FEG SEM. The elemental analysis in the FEG SEM was carried out after analyser calibration using a cobalt standard and the following conditions: 25 keV, x2000 magnification and exposure time for 50 seconds. Despite these differences in the elemental analysis of the two machines, it is emphasised all except four of the samples analysed were carried out on the same SEM and so any analyser errors would be similar for all these samples.

As mentioned earlier, the targets of the work are to get low Ni and high porosity content in the deposition. Particle size and bath agitation parameters were shown to be important and this finding was confirmed by many literature sources. In bath pH OFAAT, it was proven that this affected the porosity content. Based on materials and equipment availability together with the outcomes of the OFAAT, the following 4 parameters were selected for the Phase 2 DoE work. Particle sizes of 2 and 10 µm, with mechanical stirring and air bubbling agitation, bath pH 4.9 and 5.4, and substrate surface treatment of mechanical blasting and chemical etching were chosen.

The other five parameters were kept constant. Vertical substrate orientation is preferred to horizontal as it gave the lowest Ni content. 8YSZ ceramic particle is readily available in both 2 and 10 µm particle size. A deposition time of 60 minutes was found to be reasonable, to conduct the next 80 run experiments. In addition, 60 minutes deposition time resulted in the lowest Ni content and gave approximately 40% porosity fraction. Particle loading was maintained at 50 g/l. Bath loading for deposition surface area of 25 by 25 mm was decided to be 0.63 dm^2/l.

The second phase of the work consists of DoE of four parameters; particles size, bath agitation, bath pH and substrate surface treatment at two levels. The levels are the variables selected for each parameter. A full 2^4 factorials were constructed and the details were discussed in the methodology section.

4.2 Design of Experiments

This part is the second phase of the overall work. It consists of the experimental work based on factorials DoE approach – a full factorial design of 16 runs with 4 parameters at low and high levels and was replicated five times. A total of 80 samples were collected and analysed. It is predicted that particle size and bath agitation parameters will boost the amount of YSZ in the composite while bath pH and surface treatment parameters will induce more porosity in the composite. These 4 parameters are combined and arranged in standard Yates order. Particle size of the powders of 2 and 10 µm; bath agitation in stirring and bubbling; bath pH of 4.9 and 5.4; and substrate surface treatment of mechanical blasting and chemical etching.

DoE factorial analysis does not compare results against a control or standard but evaluates all the parameters and their interactions between the levels. It determines if there is a statistically significant difference among them. This study evaluates four effects at high and low levels on the Ni to YSZ ratio and porosity content. The desired responses of the DoE are low Ni to YSZ ratio and high porosity content. The experiment responses are in Ni content and porosity fraction where the ideal response should have the lower-the-better and higher- the-better characteristics respectively.

The effects of the parameters were analysed using Minitab 15 through analysis of variance (ANOVA). There are a number of available statistical software widely used in industry as well as in academic such as Design-Expert, JMP and Minitab (Montgomery 2009). Minitab is a very well known software to investigate DoE especially in industry. It is a tool that is very user friendly and easy to interpret. The tools provided by the software helps simplify the understanding of the analysis.

4.2.1 Ni to YSZ Ratio

One of the DoE responses is to minimise Ni to YSZ ratio. The design parameters are more conveniently labelled as A for particle size; B for bath agitation; C for bath pH and D for substrate surface treatment. The variables of high and low level are coded as +1 and -1 respectively. The Ni content (Ni to YSZ ratio) response of 5 replicates of the 16 DoE experiments arranged in Yates standard order and run in random are given in Table 27. Each replication was duplicated three times and averaged to give the replicated value. The last two columns contain sample mean, $\bar{y}$, and sample variance, $s^{2,}$ of the ‘Ni Content’ response on the five replicates in vol.%.

Table 27: Ni content response in vol.%

Std Order	A	B	C	D	Ni Content/ vol.%					$\bar{y}$	s^2
					R1	R2	R3	R4	R5		
1	-1	-1	-1	-1	51.11	55.21	53.55	56.85	55.21	54.39	1.94
2	+1	-1	-1	-1	50.25	54.55	49.55	53.51	54.64	52.50	2.17
3	-1	+1	-1	-1	58.38	58.76	50.11	58.02	56.24	56.30	3.22
4	+1	+1	-1	-1	54.44	43.94	53.27	44.47	53.33	49.89	4.67
5	-1	-1	+1	-1	58.35	57.55	55.37	57.96	60.61	57.97	1.68
6	+1	-1	+1	-1	56.18	52.76	48.86	52.78	51.19	52.35	2.39
7	-1	+1	+1	-1	56.92	57.46	54.22	56.36	58.50	56.69	1.42
8	+1	+1	+1	-1	56.27	58.57	55.39	53.07	55.15	55.69	1.78
9	-1	-1	-1	+1	56.36	56.16	56.82	48.94	57.16	55.09	3.09
10	+1	-1	-1	+1	53.19	51.02	47.62	53.21	56.03	52.21	2.80
11	-1	+1	-1	+1	58.55	58.85	51.04	57.57	56.08	56.42	2.86
12	+1	+1	-1	+1	55.29	54.46	50.50	54.16	54.41	53.76	1.68
13	-1	-1	+1	+1	58.15	56.69	54.89	57.70	57.60	57.01	1.16
14	+1	-1	+1	+1	53.27	48.46	53.45	50.57	51.61	51.47	1.85
15	-1	+1	+1	+1	58.47	49.88	58.75	57.05	55.84	56.00	3.23
16	+1	+1	+1	+1	57.00	52.81	53.76	53.36	53.62	54.11	1.48

The standard deviation, s^2 shows the variability or dispersion of Ni content in each experiment run. It indicates that all 16 runs do not vary very much from the mean. The normality of the data was represented by residual plots as in Fig. 82. Residual plots are the plots of residuals in time order of data collection to detect the correlation between the residuals. The plots consist of normal probability, histogram, versus fits and versus order.

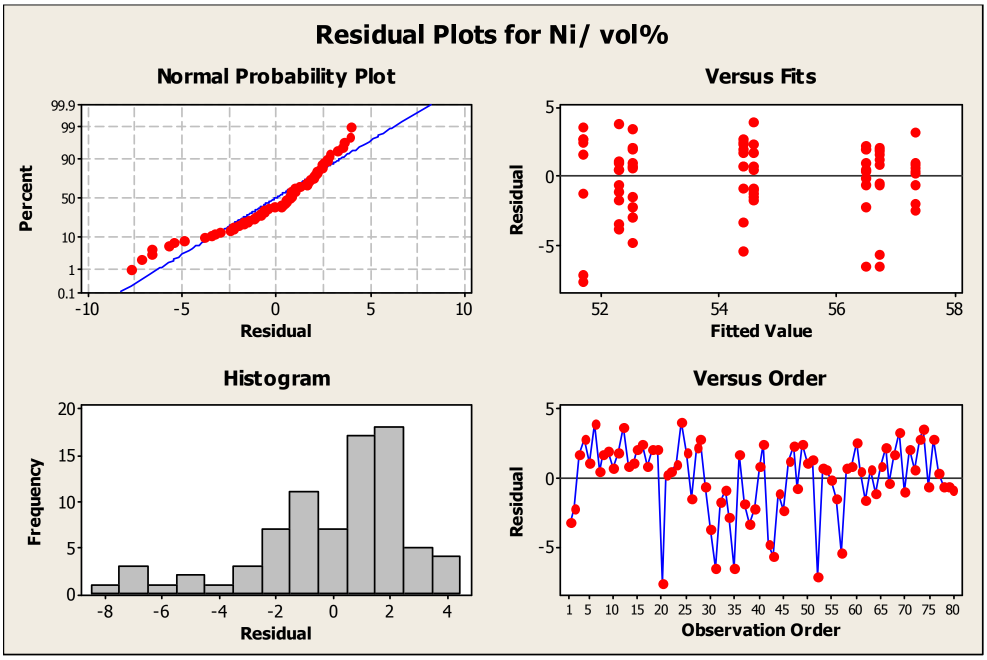

Fig. 82: Residual plots of the reduce model for Ni content response

Normal probability plot of residuals with a blue straight line gives an impression that the error distribution is approximately normal. The tendency of the normal probability plot to bend slightly downwards and upwards is acceptable and anticipated in the normal distribution. There is no apparent outlier in the plot. This is confirmed by the histogram of the residual where the errors were normally distributed with a bell-curve shape slightly skewed towards larger values (skewed to the right).

The residual versus fitted value plot verifying whether or not the experimental model and the assumption are satisfied. The residual plot against fitted value in Fig. 82 shows balanced fixed effect models (equal sample size in all treatments) indicating the assumption of homogeneity of variance was satisfied. The variance is constant throughout the fitted ranges in a constant band.

The residual versus order plot is used to check the drift of the variance during the experimental process. The error variation for all the 80 samples are balanced and randomly distributed around zero with residuals leaning towards negative as in the histogram. This confirmed that there is no drift in the process. All in all, the data is normal and normally distributed.

Analysing the DoE results involves separating the important effects from the less important ones after obtaining all the interaction effects. This can be achieved by setting the required significant level (α-value) usually to a 0.05 level of significance – commonly known as P-value approach. The P-value is the cut-off probability value of the highest level of significance that can be accepted. The details of estimated effects and coefficients for all four main parameters, six 2-way interactions, four 3-way interactions and one 4-way interactions are given in Table 28. The term 'Coef' is the standard coefficient, 'SE Coef' is the standard error of coefficient and 'T' is the T-test output.

Table 28: Estimated effects and coefficient for Ni content

Term	Effect	Coef	SE Coef	T	P
Constant		54.491	0.3126	174.34	0.000
A	-3.483	-1.742	0.3126	-5.57	0.000
B	0.734	0.367	0.3126	1.17	0.244
C	1.341	0.671	0.3126	2.15	0.036
D	0.036	0.018	0.3126	0.06	0.954
A*B	0.494	0.247	0.3126	0.79	0.432
A*C	-0.027	-0.013	0.3126	-0.04	0.966
A*D	0.246	0.123	0.3126	0.39	0.696
B*C	0.188	0.094	0.3126	0.30	0.765
B*D	0.393	0.196	0.3126	0.63	0.532
C*D	-1.065	-0.533	0.3126	-1.70	0.093
A*B*C	1.571	0.785	0.3126	2.51	0.015
A*B*D	0.472	0.236	0.3126	0.76	0.453
A*C*D	-0.447	-0.224	0.3126	-0.72	0.477
B*C*D	-0.501	-0.250	0.3126	-0.80	0.426
A*C*B*D	-0.714	-0.357	0.3126	-1.14	0.258
S = 2.79557	PRESS = 781.521				
R-Sq = 44.13	R-Sq (pred) = 12.70%		R-Sq (adj) = 31.03%		

The 'P' column represents the P-value. Any P-value less than 0.05 indicates the effect is significant. Referring to Table 27, main parameter A and C are significant and 3-way interaction of ABC is significant. The 'Effect' column represents the relative strength of the effects. The value is relatively proportional to the effect i.e. the higher the value, the greater the effect on the response. This again showed the highest effect is A followed by C and then the 3-way interaction ABC.

Filtering out the insignificant effects, ANOVA reduces the full model which includes the two main effects and one three-way interaction. The reduce model ANOVA table (Table 29) shows P-values of both main effects and 3-way interactions less than 0.05 indicating well-fitted model. The main effects selected here are particle size, bath agitation and bath pH as the 3-way interaction involving these three parameters.

Table 29: ANOVA of the reduce model for Ni content

Effect	Sum of Square	DF	Mean Square	F	P
Main effects	289.381	3	96.460	13.00	0.000
3-way interactions	49.329	1	49.329	6.65	0.012
Residual error	556.468	75	7.420		
Total	895.179	79			

4.2.1.1 Main effects

There are four main effects that were analysed by the DoE namely particle size (A), bath agitation (B), bath pH (C) and substrate surface treatment (D). The Pareto chart (Fig. 83) set a reference line of 1.998 and any effects that extend past this reference line are considered potentially important. Effect A was found to be extremely important with the highest effect of 5.6 followed by the 3-way interactions of ABC and effect C which barely past the reference line. There were two effects that are closest to zero and they are D, the substrate surface treatment effect and AC, the interaction of particle size and bath pH. This will be further discussed with reference to the effect and the interaction plots.

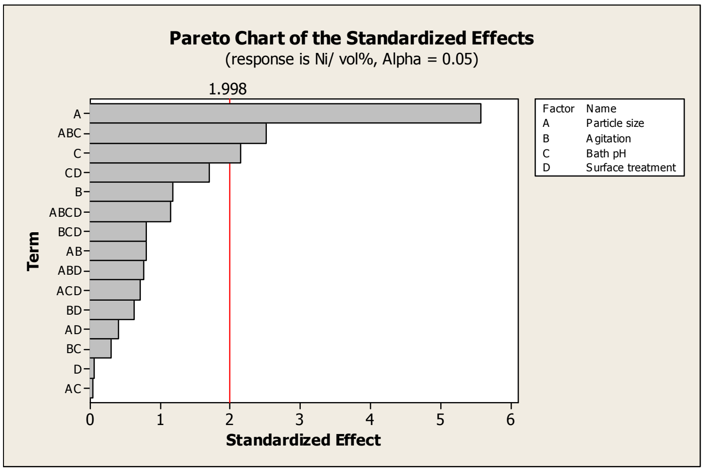

Fig. 83: Pareto chart of the standardized effects for Ni content response

The main effect plot of all the four main effects namely particle size (A), agitation (B), bath pH (C) and substrate surface treatment (D) is illustrated in Fig. 84. The main effect plot is a plot of the mean Ni content in vol.% at each level of a design parameter. The bigger the difference between the high and low levels, the higher is the effect. Referring to Fig. 84, it is clearly indicated that the most significant factor is A with 3.483 strength effects followed by C (1.341), then B (0.734) and lastly D (0.036). The effect of parameter D is almost zero, since there is almost no difference between the high and low level.

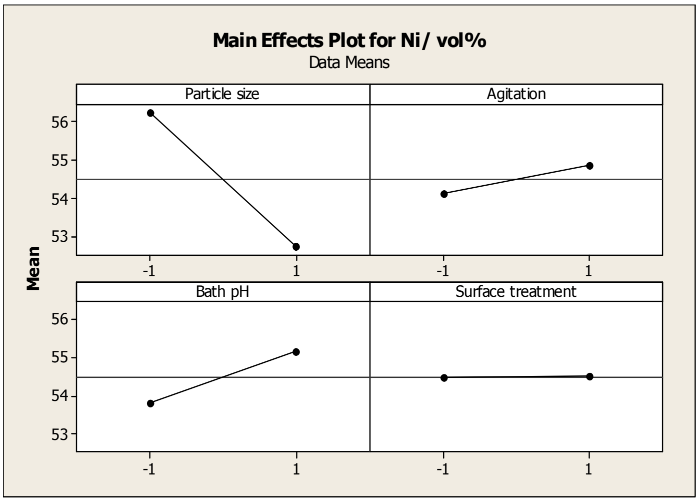

Fig. 84: The main effect plots for Ni content response

Generally, by referring to the main effect plot above, particle size at high level, bath agitation at low level and bath pH at low level give the lower Ni content. This concluded that the main effects that influence the EN co-deposition process for lower Ni to YSZ deposition are particle size and bath pH. Generally, particle size (A) effect at high level (10 µm) and bath pH (C) at low level (pH 4.9) gives lower Ni to YSZ ratio. The interaction between factors will be discussed in the next sub-section.

4.2.1.2 Interaction effects

The interaction effects consist of all possible interactions in 2-way, 3-way or 4-way. The particle size (A) and bath pH (C) are the significant main effects. The interaction between these two main parameters was important to analyse. The interaction plot in Fig. 85 illustrates the interaction between these two factors. The parallel lines indicated that there is no interaction between parameter A and C. Even though they both have a high variance between the two levels, they are both independent from each other. This means varying the bath from pH 4.9 to pH 5.4 does not affect the amount of Ni deposition both for low and level particle size.

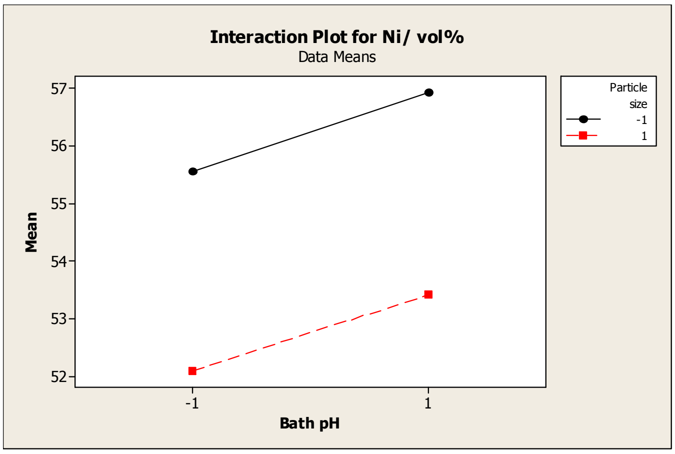

Fig. 85: Interaction plot for Ni content response between particle size and bath pH

Based on the Minitab analysis on Table 26 and Pareto chart, the most significant interaction is the 3-way interactions between factors A, B and C. A contour plot shows variation of A with C where B is kept constant for air bubbling (-1) (Fig. 86a) and mechanical stirring (+1) (Fig. 86b). Under air bubbling, the high level particle size (+1) shows lower Ni content with no effect in varying bath pH from pH4.9 to pH5.4 as shown in Fig. 86a.

The amount of Ni content increases as pH increases towards pH5.4 and particle size reduces to 2 µm. This indicates greater influent in pH change as the particle size decreasing to the low level of 2 µm (-1). The opposite trend was observed under mechanical stirring agitation as shown in Fig. 86b. At the low level particle size (-1), changing the bath pH has insignificant affect on Ni to YSZ ratio. Ni content gradually decreases as the particle size increases towards the high level (+1) and the bath pH decreases to the low level (-1).

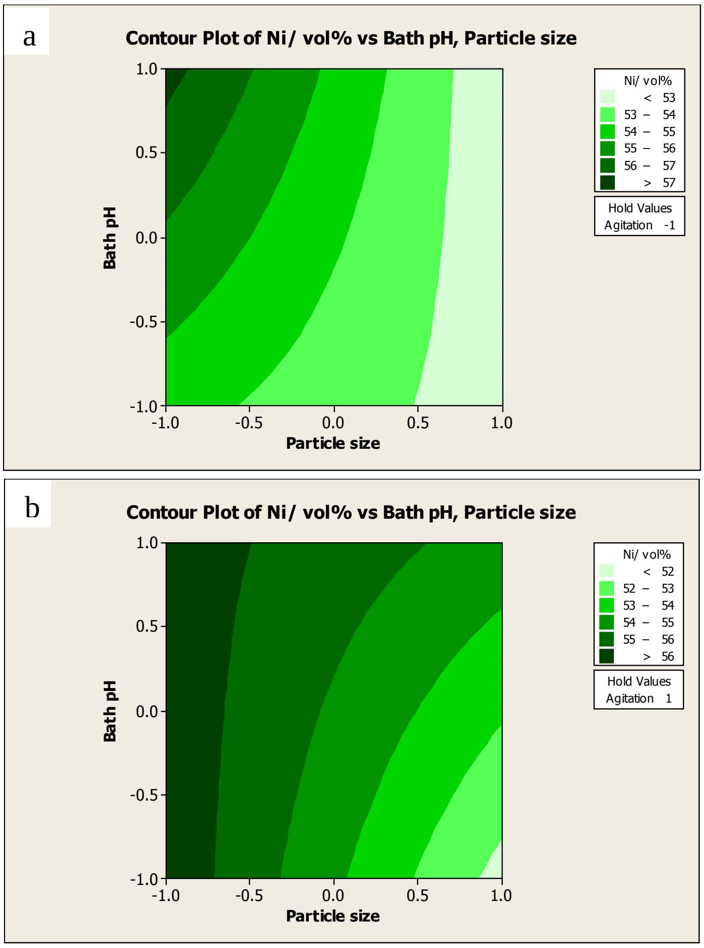

Fig. 86: Contour plots for Ni content, pH and particle size at (a) low level – air bubbling and (b) high level – mechanical stirring agitation

Therefore, the best deposition parameter combination for the 3-way interaction based on this observation are high level particle size of 10 um, low level bath pH of 4.9 and high level agitation of mechanical stirring (A+1B+1C-1).

4.2.1.3 Optimum condition for Ni to YSZ ratio

The significant main effects are the particle size (A) and bath pH (C) and the significant interaction effect is the 3-way ABC interaction. The best optimum condition to achieve low Ni to YSZ ratio can be justified by considering all significant factors combination of A, B and C as in Table 30. The lowest Ni content was obtained at combination of A+1B+1C-1 with 51.83 vol.%. This means the optimum condition for low Ni to YSZ ratio can be achieved with particle size of 10 µm under mechanical stirring bath agitation at bath pH of pH4.9. The substrate surface treatment either by chemical etching or mechanical blasting has little influence to the process parameter.

Table 30: Ni content values of all low and high combination for ABC

DoE Parameters			Mean Ni Content in vol.% of ABC
A	B	C	
+	+	+	55.40
+	+	–	51.83
+	–	+	51.91
+	–	–	52.36
–	+	+	56.35
–	+	–	56.36
–	–	+	57.46
–	–	–	54.74

Thus to achieve low Ni to ceramic ratio, the conditions are (1) large particle size of 10 µm, (2) mechanical stirring agitation and (3) bath pH of 4.9. Larger particle size was found easier to be co-deposited in EN deposition rather than smaller particle size. This was supported by Balaraju et al (2006) on alumina powder sizes of 50 nm, 0.3 µm and 1.0 µm that resulted in the highest particle incorporation at 1.0 µm particle size. A study done by Vaghefi et al. (2003) showed 33 vol.% of B_4C particle with particle size ranges 5-11 µm which indicates that larger particle sizes give higher particle incorporation in the EN composite.

In terms of bath agitation, it is crucial to keep the particles in suspension throughout the deposition (Sevugan et al 1993). Mechanical stirring showed higher incorporation of particles in this research compared to air bubbling. It should be noted that this is in contradiction to the finding by Vaghefi (1997) in electroless nickel-phosphorus-molybdenum disulfide which showed that air purging was better than magnetic stirring. However, the particles used in this research were ceramic YSZ which, in terms of inertness, wettability and particle stability to the substrate (Necula et al. 2007, Apachitei et al. 1998) are different to the study by Vaghefi. As for the bath pH, it is shown that a higher bath pH caused a higher deposition rate in conventional EN deposition (Baudrand 1994).

Thus at a higher deposition rate, it is possible that less ceramic particles were able to be dragged along in the EN co-deposition. This resulted in the observation that the incorporation of ceramic particle is higher at lower pH of 4.9 than at 5.4.

The typical SEM micrograph for most DoE samples is as shown in Fig. 87. The ceramic YSZ phase was uniformly distributed. There were some SEM micrographs that show agglomerations or unevenly distributed ceramic YSZ phase. The sample of Expt.6, Rep.1 (2 µm particle size, air bubbling, pH4.9, HF etching) has SEM micrograph as shown in Fig. 88. The SEM micrograph pictures two separate areas of highly populated white (ceramic) particles on the left and mostly grey area (Ni matrix) on the right. It was confirmed that spectrum 1 (Fig. 88a) had lower Ni content indicating high ceramic co-deposition compared to spectrum 2 (Fig. 88b). At high magnification, the high populated ceramic area (agglomeration) is shown in Fig. 89.

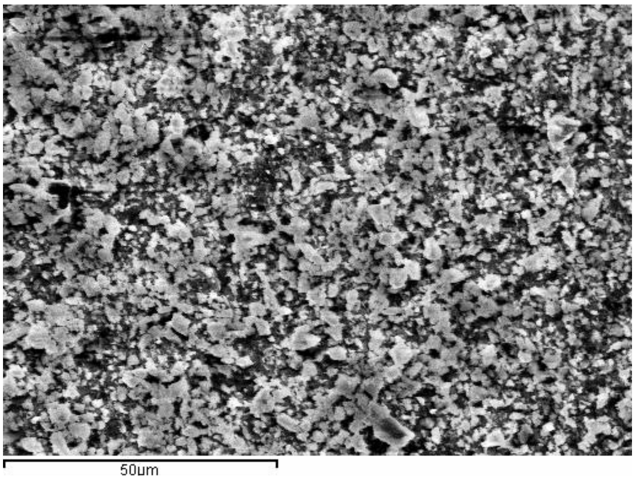

Fig. 87: Typical SEM micrograph for DoE sample of 50.21wt.%Ni

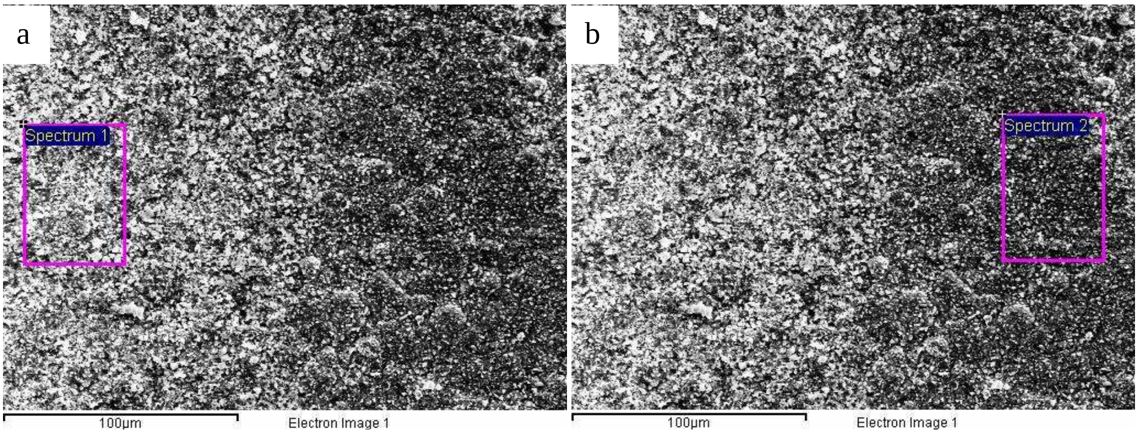

Fig. 88: SEM micrograph (a) spectrum 1 of 62.69 wt.% Ni (b) spectrum 2 of 70.45 wt.% Ni

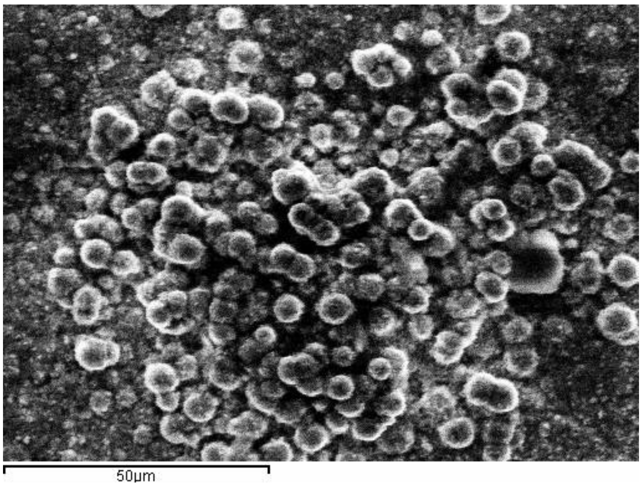

Fig. 89: High magnification of agglomeration area

4.2.2 Porosity Content

Porosity content up to 40% in SOFC anode is one of the requirements to be fulfilled. The porosity content requirement for SOFC anode is 30-40% (Koide et al. 2000). Average porosity contents for the 16 runs were in the ranges of 17-67%. The DoE approach was conducted to evaluate 4 parameters at high and low levels in order to get the optimum condition for highest porosity content. Theoretically, it is predicted parameters C and D will have greater influence in increasing the porosity content. The porosity response of all the 80 samples is listed in Table 31. The means and standard deviation for the 16 runs are given in the last two columns.

Table 31: Porosity response of the 80 samples

Std Order	A	B	C	D	Porosity Content/ %					$\bar{y}$	s^2
					R1	R2	R3	R4	R5		
1	-1	-1	-1	-1	30.96	16.36	11.11	11.58	16.44	17.29	7.20
2	+1	-1	-1	-1	36.62	43.57	13.33	28.48	14.03	27.21	12.03
3	-1	+1	-1	-1	8.24	51.63	52.59	65.00	29.41	41.37	20.15
4	+1	+1	-1	-1	22.58	28.42	15.29	50.16	39.61	31.21	12.37
5	-1	-1	+1	-1	20.00	30.57	18.62	22.50	30.91	24.52	5.23
6	+1	-1	+1	-1	6.67	13.98	29.60	16.28	27.02	18.71	8.50
7	-1	+1	+1	-1	49.87	20.00	56.92	50.00	35.38	42.43	13.23
8	+1	+1	+1	-1	47.25	22.22	44.62	20.00	50.48	36.91	13.06
9	-1	-1	-1	+1	48.24	20.00	32.31	41.28	31.43	34.65	9.58
10	+1	-1	-1	+1	67.79	52.73	20.00	25.42	31.85	39.56	17.96

11	−1	+1	−1	+1	62.03	54.43	60.00	77.39	79.13	66.60	9.86
12	+1	+1	−1	+1	35.56	75.17	26.67	46.09	38.00	44.30	16.63
13	−1	−1	+1	+1	47.50	44.92	78.46	54.78	37.39	52.61	14.07
14	+1	−1	+1	+1	57.00	26.45	13.68	4.91	26.93	25.79	17.65
15	−1	+1	+1	+1	71.00	43.33	55.38	76.36	50.48	59.31	12.46
16	+1	+1	+1	+1	6.67	25.00	63.33	9.33	22.00	25.27	20.29

The porosity response has high variation among all five replicates and thus the standard deviation is expected to have high values. The standard deviation values of the 16 runs vary between 5 and 20. The distribution of data appears normal as shown in the residual plots (Fig. 90). The normal probability plot shows most residuals are close to the blue straight line, which represents a normal distribution data. The histogram also shows the residuals are distributed in a normal manner with a balanced bell-curve shape.

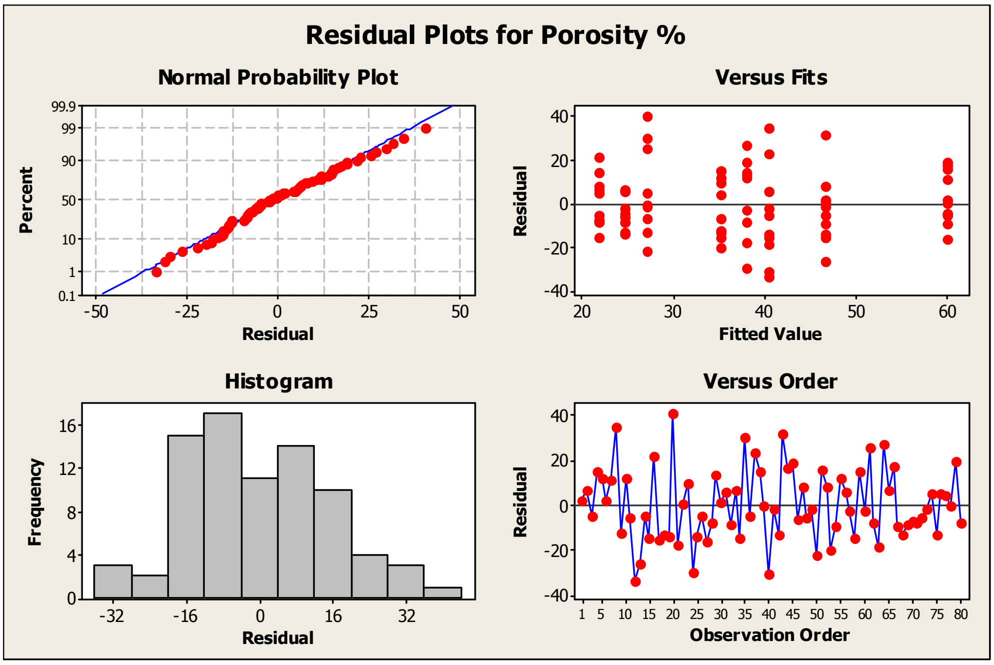

Fig. 90: Residual plots of the reduce model for porosity response

In both versus fits and versus order, the data are balanced within the constant band. Versus fits in general is normal as it does not show an outward-opening funnel shape – it does satisfy the constant variance assumption. Versus order indicates no drift in the process as the observation orders were balanced and randomly distributed around zero. Overall, the data is normal and show no cause for concern.

The details of estimated effects and coefficients for all main parameters and their interactions are given in Table 32. The main parameters A, B and D are having P-values less than 0.05 and indicate that they are significant together with the 2-way interactions of AD. Out of these four significant effects, the effect ranking is the main parameter D followed by B, then A and lastly 2-way interaction AD. The high level of both parameters D and B; and low level parameter A resulted in high porosity % response based on the effect sign.

Table 32: Estimated effects and coefficients for porosity

Term	Effect	Coef	SE Coef	T	P
Constant		36.734	1.730	21.23	0.000
A	-11.228	-5.614	1.730	-3.24	0.002
B	13.383	6.692	1.730	3.87	0.000
C	-2.079	-1.039	1.730	-0.60	0.550
D	13.553	6.776	1.730	3.92	0.000
A*B	-6.778	-3.389	1.730	-1.96	0.055
A*C	-6.819	-3.409	1.730	-1.97	0.053
A*D	-8.334	-4.167	1.730	-2.41	0.019
B*C	-2.811	-1.405	1.730	-0.81	0.420
B*D	-2.669	-1.334	1.730	-0.77	0.443
C*D	-3.452	-1.726	1.730	-1.00	0.322
A*B*C	5.043	2.522	1.730	1.46	0.150
A*B*D	-1.830	-0.915	1.730	-0.53	0.599
A*C*D	-4.048	-2.024	1.730	-1.17	0.246
B*C*D	-4.818	-2.409	1.730	-1.39	0.169
A*C*B*D	-0.049	-0.024	1.730	-0.01	0.989
S = 15.4761	PRESS = 23950.9				
R-Sq = 49.47%	R-Sq (pred) = 21.05%		R-Sq (adj) = 37.63%		

Filtering out the insignificant effects, ANOVA reduces the full model which includes three main effects of A, B and D and a 2-way interaction of AD. The ANOVA table of the reduced model is shown in Table 33 below. The main effects reduce model with P-values of 0.000 showed a perfect fit. This indicates the main effects of parameter A, B and D are 95% confidence to influent the process giving to high porosity content. Similarly to the 2-way interactions, the P-value is now reduced to 0.022 implying it is a significant effect. The interaction is analysed using the interaction plot tool.

Table 33: ANOVA table of the reduce model for porosity

Effect	Sum of Square	DF	Mean Square	F	P
Main effect	9777	3	3259.1	12.75	0.000
2-way interactions	1389	1	1389.3	5.44	0.022
Residual error	19170	75	255.6		
Total	30337	79			

4.2.2.1 Main effects

The significant main effects that influent the EN co-deposition process on percent porosity are justified by a Pareto chart in Fig. 91. The Pareto chart indicated clearly that main effects factor particle size (A), bath agitation (B) and substrate surface treatment (D) extending pass the reference line of 1.998. The most significant main effect shown is factor D with effect strength of 13.553 followed closely by factor B (13.383) and then factor A (11.228). This showed that the substrate surface treatment (D) is the main contributor to increase porosity content in the EN co-deposition. This is supported theoretically where the rougher surface caused rougher deposition and thus increases porosity within the deposition.

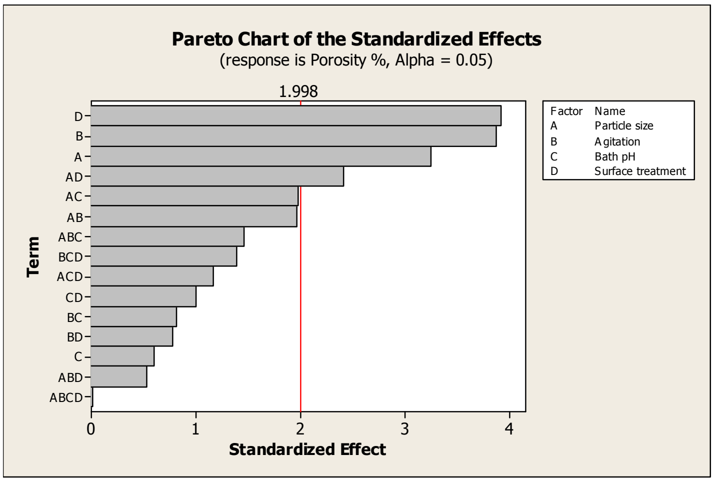

Fig. 91: Pareto chart for the porosity response

The main effect plot indicates the variation of the data mean between low and high levels for each main parameter. The main effect plot of all four parameters is given in Fig. 92. The most dominant parameter as already verified by the Pareto is the substrate surface treatment (D) with bath agitation (B) closely behind. The difference between low and high levels for both parameters D and B are the largest and difficult to differentiate. Descending rank order for the strength effect is surface treatment, bath agitation, particle size and then bath pH.

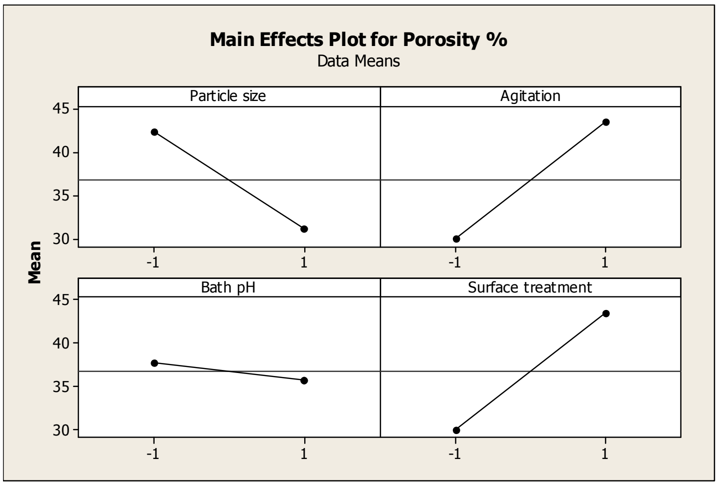

Fig. 92: Main effects plot for the porosity response

The 'higher-the-better' characteristic for porosity response described that high porosity content can be achieved at low level particle size (2 µm), high level bath agitation (mechanical stirring) and high level substrate surface treatment (mechanical blasting). Based on the main effect plots of these three main parameters, the optimum combination for high porosity % is A-1B+1D+1. The interaction between particle size and surface treatment parameters were also found to be significant and should be discussed further.

4.2.2.2 Interaction effects

The interaction plot is a powerful graphic tool which plots the mean of response of two factors. The AD interaction plot in Fig. 93 shows unparallel lines of high and low level particle size under surface treatment variation. This indicates the present of interaction between the particle size and the substrate surface treatment. The porosity content was very much affected by the substrate surface treatment. Varying substrate surface treatment from low (-1) to high (+1) level increases porosity % for both particle size at low (-1) and high (+1) levels. The effect of particle size on porosity % at low level (-1) is more pronounce than at high level (+1) as the substrate surface treatment changes from low (-1) to high (+1) level. At both particle size levels, mechanical blasting gave greater effect on porosity.

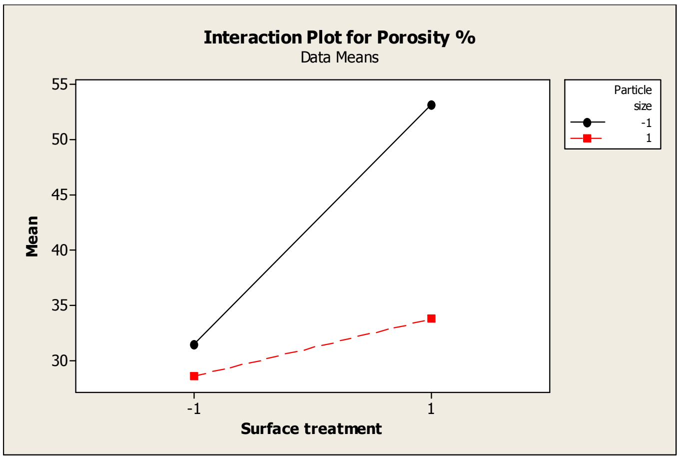

Fig. 93: Interaction (A-D) plot for porosity

Therefore, the best deposition parameter combination for the 2-way AD interaction based on this observation are low level particle size (2 µm) and high level substrate surface treatment of mechanical blasting (A-1D+1).

4.2.2.3 Optimum condition for percent porosity

The significant main effects that influence EN co-deposition process for highest porosity content are surface substrate treatment, bath agitation and particle size in descending order. The best deposition parameter combination for the desired maximum porosity content should consider both particle size and substrate surface treatment factors. These two factors were found to be related to each other.

The optimum condition can be calculated by averaging out the high and low levels combination of A, B and D as listed in Table 34. The highest porosity content was obtained at 62.96% with optimum condition of low level particle size (2 µm), high level bath agitation (mechanical stirring), low level bath pH (4.9) and high level surface treatment (mechanical blasting); A-1B+1C-1D+1.

Table 34: Porosity response values of all low and high combination for ABD

DoE Parameters			Mean Porosity Content in % for ABD
A	B	D	
+	+	+	34.79
+	+	–	34.06
+	–	+	32.68
+	–	–	10.27
–	+	+	62.96
–	+	–	41.90
–	–	+	43.63
–	–	–	20.91

Thus to achieve high porosity content, the conditions are (1) small particle size of 2 µm, (2) mechanical stirring agitation and (3) substrate surface treatment of mechanical blasting. A study by Wang et al. (2006c) has shown that fine particles introduced smaller size porosity. This indirectly indicates high porosity volume, i.e. like smaller pebbles in a jar have more quantity than the larger ones. This supported the outcome where smaller particle size gives higher porosity content than the larger particles.

The mechanical stirring bath agitation gives higher porosity as the agitation is not very aggressive compared to air bubbling thus most of the absorbed hydrogen or oxygen was not removed (Sevugan et al. 1993) and trapped inside the EN deposition introducing more porosity. Mechanical blasting resulted in a rougher substrate surface. EN deposition is very well-known to follow the substrate profile rather than filling the spaces (Taheri et al. 2001). Therefore, rougher surface caused a rougher deposition surface and thus introduced more porosity.

The porosity measurements carried out by the Archimedes buoyancy method were not very convincing. Other porosity measurements such as porosimeter or impedance spectra should be used in future research. The SEM micrograph of one of the DoE samples – sample 60 – Expt.13, Rep.3 (10 µm, bubbling, pH4.9, blasting) showing the possibility of open porosity is given in Fig. 94. Generally, the black areas are recognised to be porosity. This could be further investigated using a porosimeter in future work.

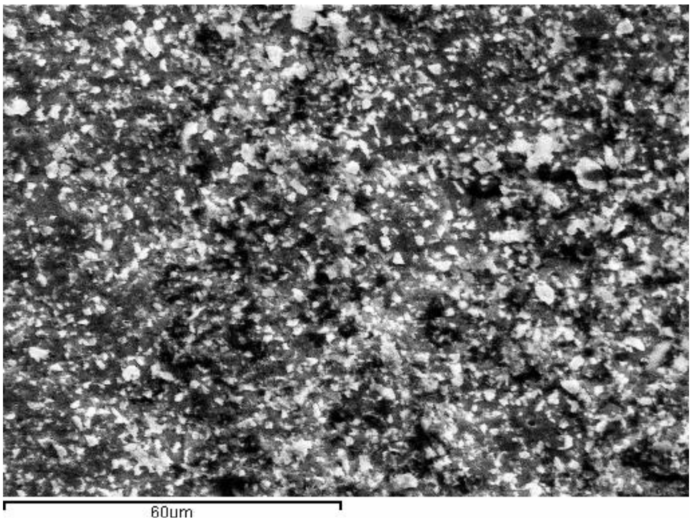

Fig. 94: SEM micrograph of DoE Sample 60

4.2.3 Model Building

A model to predict the response function can be built using a regression model. The build model can be used to illustrate the relationship between the actual data from experiment and the predicted data. Additionally, the model can be used to describe the relationship between a response and a set of process parameters that affect the response. The model can also be used to predict a response for different combinations of process parameters at their best levels. The regression coefficients of each parameter are obtained from Minitab as listed in the column labelled ‘Coef’ in Table 27 for Ni content and Table 31 for porosity %.

Based on the 80 sets of experimental data, the Ni content and Porosity % regression model were developed. Based on the analysis done by Minitab in the previous section, the reduce model which represent the optimum condition of the process was used to develop the reduce model equation. The reduce model equation with main parameters A and C and 3-way interactions of ABC is shown in [equation 4.1].

$$\hat{y} = 54.491 - 1.742A + 0.671C + 0.785ABC \quad \cdots \quad (4.1)$$

where ŷ is the response Ni content, A is particle size (µm), B is bath agitation and C is bath pH. The coefficient of determinations (R^2) was 0.72 indicating there is reasonable correlation between the actual and predicted values of Ni content as shown in Fig. 95. This means the model is reliable in predicting the response with 28% variation. Referring to the coefficient of the developed models, it was confirmed that particle size was the most prominent parameter in minimising the Ni to YSZ ratio.

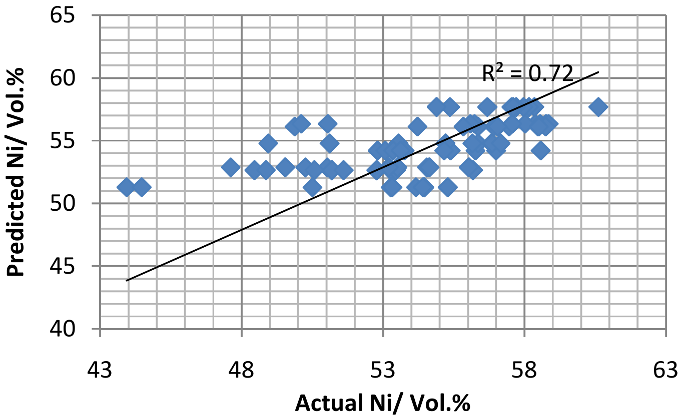

Fig. 95: Comparison of experimental and predicted values for Ni content

In Minitab analysis the optimum condition for Ni to YSZ ratio was A and B at high level and C at low level. The minimum Ni content obtained experimentally is 51.827 whereas the predicted is 51.293 as shown in the calculation below. The difference between the actual value and predicted value is 0.534. The difference between the actual and the predicted value is minimal. This shows that the model is reliable in predicting the response value at a desired parameter level.

$$\hat{y} = 54.491 - 1.742(+1) + 0.671(-1) + 0.785(+1)(+1)(-1)$$
$$= 51.293$$

Similarly for the Porosity %, the analysis done by Minitab in the previous section led to a reduced model that represents the optimum condition of the process in obtaining high porosity %. The reduced model equation contains main parameters A, B and D and 2-way interactions of AD and is shown in [equation 4.2].

$$\hat{y} = 36.734 - 5.614A + 6.692B + 6.776D - 4.167AD \quad \cdots \quad (4.2)$$

where ŷ is the response Porosity %, A is particle size (µm), B is bath agitation and D is substrate surface treatment. The coefficient of determinations (R^2) as shown in Fig. 96 is 0.47 indicating that the correlation between the actual and predicted values of Porosity % was not very good. Referring to the coefficient of the developed model, it is confirmed that the substrate surface treatment is the most prominent parameter followed by the bath pH in increasing the Porosity %.

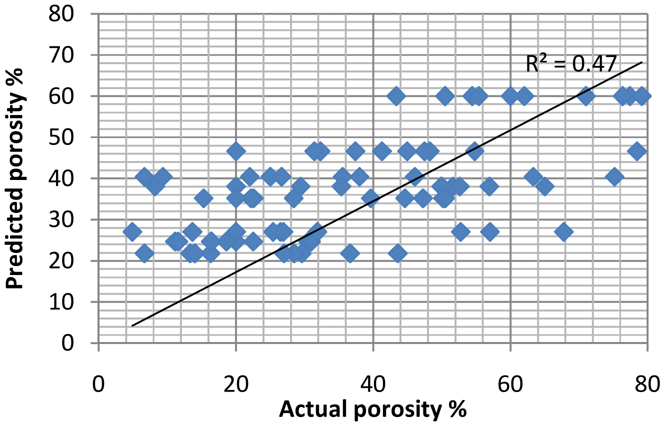

Fig. 96: Comparison of experimental and predicted values for porosity content

In the Minitab analysis, the optimum condition for Porosity % is A at low level, B and D at high level. The maximum Porosity % obtained experimentally is 62.953 whereas the predicted is 59.983 as shown in the calculation below. The difference between the actual value and predicted value is 2.970. The difference between actual and the predicted value is approximately 4.7%. This showed that the model is not very accurate in predicting the response value at a desired parameter level.

$$\hat{y} = 36.734 - 5.614(-1) + 6.692(+1) + 6.776(+1) - 4.167(-1)(+1)$$
$$= 59.983$$

The regression coefficients for numerical analysis approach model using raw data and numerical values for all four factors were determined using Minitab 15 multiple linear regression for both Ni content and percent porosity as illustrates in [equation 4.3] and [equation 4.4] respectively. The non-numerical terms, bath agitation and substrate treatment are represented by deposition rate and surface roughness respectively.

$$\widehat{y_n} = 39.7 - 0.434A + 2.82B + 3.06C + 0.072D \cdots (4.3)$$

$$\widehat{y_p} = 21.7 - 1.40A + 74.3B - 4.16C + 19.4D \cdots (4.4)$$

where y_n and y_p are Ni content and Percent porosity responses respectively; A is particle size factor (µm); B is bath agitation factor (µm/min); C is bath pH factor and D is substrate surface treatment factor (µm).

The coefficient of determinations (R^2) for both (a) Ni content and (b) percent porosity responses are as shown in Fig. 97. Both the Ni and porosity content regression models showed low correlation between the actual and predicted data with 0.321 and 0.325 coefficient of determination. This indicates that the models are not sophisticated enough to be applied in the general application terms.

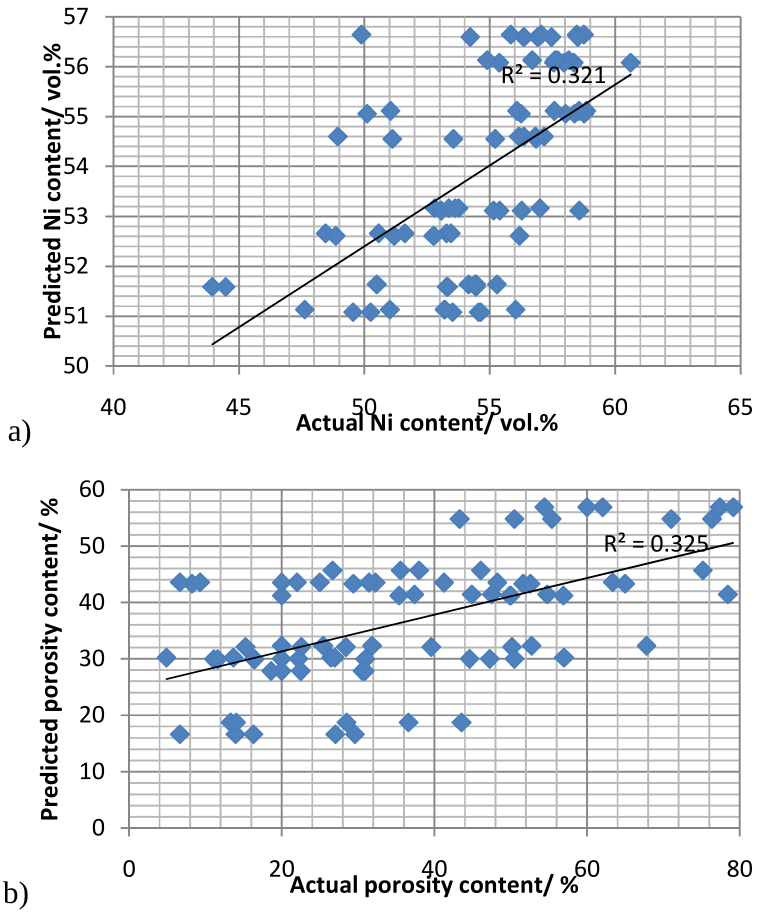

Fig. 97: Comparison of actual and predicted values of (a) Ni (Vol.%) and (b) Porosity (%) for numerical approach

As the optimum condition for Ni content is A+1B+1C-1D-1 and for porosity is A-1B+1C-1D+1, the predicted values of the optimum condition for both responses can be calculated as below. These optimum conditions were inserted into the equation to give the predicted values for Ni content and porosity % at their optimum conditions. The predicted values are 51.589 and 56.882 for Ni and porosity content respectively. Generally, both regression models by numerical approach showed low correlation between the actual and predicted data which might be due to the inaccurate substitution of numerical values for the non-numerical factors as well as unfitted models.

$$\widehat{y_n} = 39.7 - 0.434(10) + 2.82(0.42) + 3.06(4.9) + 0.072(0.7)$$

= 51.589

$$\widehat{y_p} = 21.7 - 1.40(2) + 74.3(0.42) - 4.16(4.9) + 19.4(1.4)$$

= 56.882

A study by Azmir and co-authors (2009) developed the first and second order polynomial models of their four factors Taguchi giving to a reasonably high correlation between the actual and predicted values. The coefficients of regression were determined using the same software, Minitab 15. This means this approach could be applicable in this research in order to improve the correlation coefficient of these two models. Since the polynomial models are beyond the scope of this research, they could be further investigated in future work.

In summary, two methods of analysis employing multiple linear regression were investigated. The first procedure used by assigning values +1 and -1 for all process variable coefficients (the coded approach); whilst the second procedure utilised real experiment data, so that the model could be more generally applied (the numerical approach). The model for the coded approach achieved a reasonable correlation of 0.72 for the Ni content in vol.%, whereas a lower correlation of 0.47 was found for the anode coating porosity in %. However, the numerical approach for both Ni content and Porosity % responses were less successful with coefficients of determination of 0.32 and 0.33 respectively. These differences in correlation coefficients generated by the two regression models may result from a lack of a direct relationship between (i) the form of bath agitation and the deposition rate of bath agitation and the deposition rate and (ii) the method of substrate surface treatment and the measured surface roughness. As a consequence of these limitation in the linear regression approach, non-linear regression methods involving first and second order polynomials should be considered.

4.2.4 DoE Conclusions

The effect of EN composite parameters, on Ni-YSZ composites was analysed using DoE 2^4 full factorials with respect to two responses - Ni to YSZ ratio and Porosity %. The 16 run full factorial was replicated five times investigating four parameters i.e. particle size, bath agitation, bath pH and substrate surface treatment. The DoE was analysed by ANOVA statistical tool in the Minitab software. Each response was analysed independently.

Out of four main parameters, particle size (A) at high level and bath pH (C) at low level were found to be the most significant main parameters affecting the Ni to YSZ ratio. Both of these parameters were independent from each other. The interaction between particle size-bath agitation-bath pH was found to be important as well. Particle size has highest effect followed by the 3-way interactions and lastly the bath pH. For the 3-way interaction under low level bath agitation (air bubbling), the lowest Ni to YSZ ratio was obtained at high level particle size but the bath pH changes from low to high level have no effect. On the other hand, under high level bath agitation (mechanical stirring), lowest Ni to YSZ ratio was obtained at high level particle size and low level bath pH. The optimum deposition parameter combination for minimum Ni to YSZ ratio is obtained using a larger particle size (10 µm) with mechanical stirring at lower bath pH (pH4.9). The optimum EN composite parameters combination for minimum Ni to YSZ ratio is A+1B+1C-1.

The Porosity % response shows a high influence from particle size (A) at low level, bath agitation (B) at high level and substrate surface treatment (D) at high level. The bath agitation is independent whereas particle size and substrate surface treatment has significant 2-way interactions. The substrate surface treatment has the highest effect followed closely by bath agitation then particle size and lastly 2-way interactions between particle size and bath agitation. As substrate surface treatment changes from low to high level, particle size at low level has a greater affect on porosity content. The best deposition parameter combination for maximum porosity content was obtained at low level particle size (2µm) under high level bath agitation (mechanical stirring) with high level substrate surface treatment (mechanical blasting). The optimum deposition parameters combination for maximum porosity content is A-1B+1D+1.

Based on the 80 sets of experimental data, the linear regression models were successfully developed for both Ni to YSZ ratio and Porosity % responses. The coefficients of regression were determined using Minitab 15 software. The coefficients of determinations (R^2) were found to be 0.72 and 0.47 for Ni to YSZ ratio and Porosity % responses respectively. There is a reasonable correlation between the actual values and predicted value for Ni to YSZ ratio but the correlation for Porosity % was not very good. The numerical approach models show low correlation between the actual and predicted data. The overall outcomes are summarised in Table 35.

Table 35: Overall summary on DoE analysis and regression model

Response	A	B	C	D	R^2		Actual	Predicted	
					Coded	Numerical		Coded	Numerical
Ni : YSZ	+1	+1	-1		0.72	0.32	51.827	51.293	51.589
Porosity %	-1	+1		+1	0.47	0.33	62.953	59.983	56.882

4.3 Performance Tests

4.3.1 EN Optimum condition

The DoE analysis in the previous section analysed the responses of the critical SOFC anode criteria: low Ni to YSZ ratio and adequate porosity individually. The low Ni to YSZ ratio compromises both anode electrical conductivity as well as the CTE difference between anode and electrolyte. Acceptable Ni content is within 30-50 vol.% Ni. Adequate porosity is important to ensure fuel inlet and waste gases outlet but too high porosity will weaker the anode mechanical strength. The ideal porosity content is 40%. This section analyses the combination of both responses to give the combination optimum condition using the ‘response optimiser’ in Minitab 15.

The response optimiser is able to analyse multiple responses of DoE. It suggests the most optimum condition by evaluating them concurrently and preventing sub-optimisation of one alone. The goal of each response, their limit range, weight and importance are given in Table 36. The Ni content response is aimed to obtain as close to minimum as possible as the current values ranges between 43-61 vol.% Ni. The porosity % goal is set as target at

40% porosity. Both responses are equally important thus based on these criteria, the default setting is chosen and the weight setting also remains at default.

Table 36: The response goal, limit, weight and importance

Response	Goal	Lower	Target	Upper	Weight	Importance
Ni:YSZ	Minimum	–	50	60	1	1
Porosity %	Target	5	40	80	1	1

The multiple response optimiser displays the results in the optimisation plot as shown in Fig. 98. The overall optimum composite desirability, D is 0.91318 which is close to unity indicating the ideal value. The individual desirability of each response is 0.83393 for Ni to YSZ ratio and 0.99997 for Porosity %. These values are high which indicate less constraint on both responses.

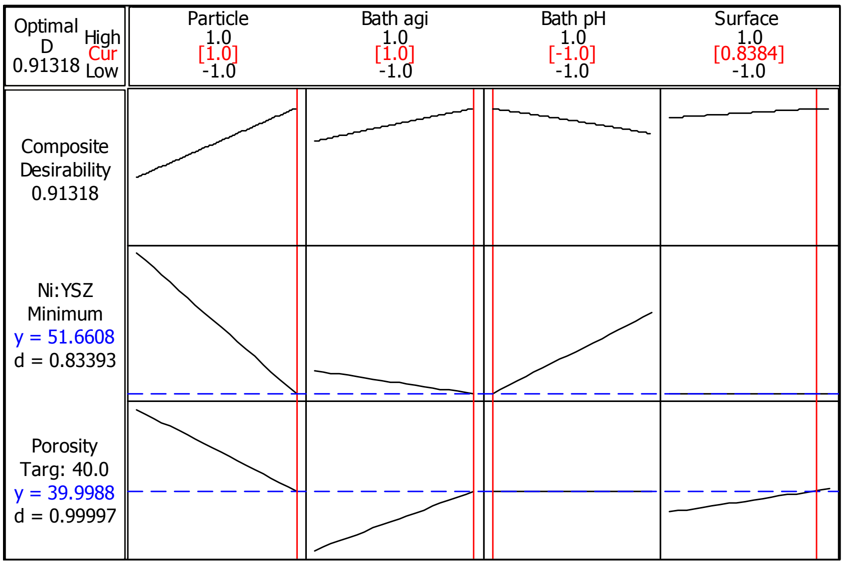

Fig. 98: Optimisation plot for both Ni to YSZ ratio and Porosity % responses

The optimum minimum Ni content is 51.6608 with the strongest effect shown by the particle size and bath pH, and the least with bath agitation. This predicted optimum minimum Ni content is close to the cube plot analysis (51.827 vol.%) and regression model (51.293 vol.%). The targeted optimum porosity % is 39.9988% with particle size, bath agitation and substrate surface treatment as the major contributing parameters. This optimum porosity content when compared to actual data of 62.953% and regression model data of 59.983% is incomparable. This observation might be due to different setting: the previous analysis was set to maximise the response but the current analysis is set to target.

The combination optimum response settings are A+1B+1C-1D[+0.8384]. This means particle size is set at high level (10 µm), bath agitation at high level (mechanical stirring), bath pH at low level (pH4.9) and substrate surface treatment at high level (mechanical blasting).

Based on the optimisation plot in Fig. 98, the two important factors are the particle size and bath agitation. This was because bath pH and substrate surface treatment were found not significant in either one of the responses. These two unimportant factors were kept on hold at its optimum setting – bath pH at low level and substrate surface treatment at high level. The Ni to YSZ ratio is limited to 30 to 52.5 and porosity % is limited to 35 to 40. The overlaid contour plot in Fig. 99 shows the white area and grey area. The white area represents the feasible region of the settings at which Ni content and porosity % were both acceptable. Thus it can be concluded that the optimum setting is when particle size is at high level and the bath agitation within the medium to high level setting. The other two parameters are on hold at low level bath pH and high level substrate surface treatment.

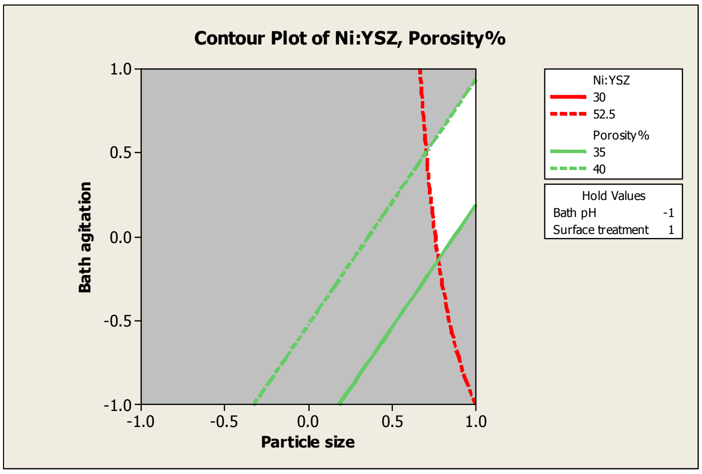

Fig. 99: Overlaid contour plot for Ni to YSZ ratio and porosity % responses

The verification of this combination of optimum conditions can be done by another set of EN co-deposition. Later, it can be further investigated by another set of fractional factorial DoE.

4.3.2 Anode performance

The Ni-YSZ co-deposition was deposited onto a ceramic substrate representing the SOFC anode. The initial sample with the thickness of 13 µm Ni-YSZ co-deposition contains 48.32 vol.% Ni. This was co-deposited with 2 µm YSZ particle size. The initial electrical conductivity tests were carried out at room temperature (25°C) and involved measurements at two different points on the surface of the anode sample. The tests were carried out at three different currents- 1mA, 50mA and 100mA. The resistance, resistivity and conductivity of the sample at the three different currents are given in Table 37.

Table 37: Initial 4-point electrical test at various current

Current	1 mA		50 mA		100 mA	
	1st Point	2nd Point	1st Point	2nd Point	1st Point	2nd Point
Resistance/ Ω	0.117	0.210	0.353	0.425	0.317	0.261
Resistivity/ 10^{-4}Ωcm	1.52	2.73	4.59	5.52	4.12	3.4
Conductivity/10^{4}Scm^{-1}	0.66	0.36	0.22	0.18	0.24	0.29

The observed values were very encouraging. The initial test was carried out at room temperature using 4-point electrical measurement. Since YSZ is non-metallic and Ni is metallic, the Ni-YSZ cermet behaves as biphasic composite system – having a conductivity percolation threshold at an adequate amount of Ni. The conductivity values of 50 vol.% Ni-YSZ is a factor of ten less than half the value of pure metallic Ni at room temperature (11.8 x10^4 (Ωcm)$^{-1}$) - Appendix C. Thus the obtained values for this initial test are still comparable.

Since the anode will be exposed to high operating temperatures (up to 1000°C), a test on the Ni-YSZ fabricated via EN deposition was carried out at temperatures increasing from 25˚C to 420˚C in air. The scatter plot of the resistivity and conductivity are given in Fig. 100. The trend of resistivity showed a linear relationship with the temperature. Resistivity increases as temperature increases. The conductivity is inversely proportional to resistivity thus it is expected to show opposite linear relationship to the resistivity. The linear decrease in conductivity with temperature is indicative of metallic conduction.

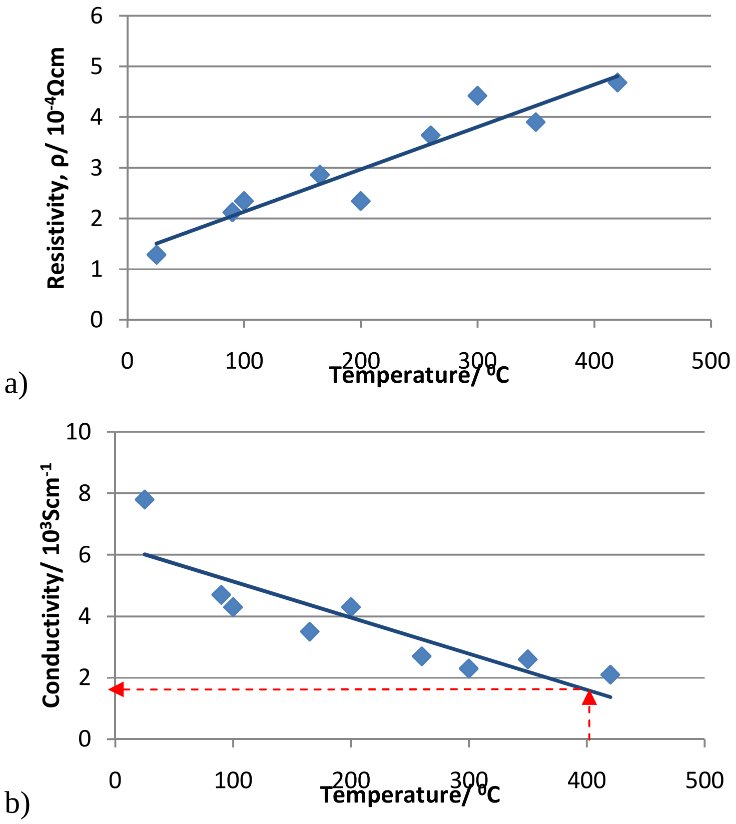

Fig. 100: Scatter plot of (a) resistivity and (b) conductivity against temperature in air

This conductivity trend was similar to the study done by Pratihar and co-author (2005) as shown in Fig. 11. The conductivity values obtained from the study at variable fabrication techniques for 40 vol.% Ni at 400^{0}C are tabulated in Table 38. Based on the best fitted linear line, at 400^{o}C, the conductivity value of 50 vol.% Ni is approximately 1500 Scm^{-1} (referring to the red dotted line in Fig. 100b). This is comparable to the conductivity obtained by the anode fabricated via EN powder coating at 40 vol.% Ni (Pratihar et al. 2005).

Table 38: Conductivity values of Ni-YSZ fabricated by various techniques at 400^{o}C

Fabrication Technique	σ/ Scm^{-1}
Solid state	450
Liquid dispersion	250
EN powder coating	1100

A study on a 50 vol.% Ni gave a conductivity of 10 Scm^{-1} and resistivity of 0.1 Ωcm (Koide et al. 2000). Comparing these values with the one obtained for Ni-YSZ anode fabricated via EN coating, the resistivity is generally lowered by one hundredth. This observation made the conductivity values for EN co-deposition higher by a factor of hundred. Another study for 50 vol.% Ni-YSZ by Aruna and co-authors (1998) stated a value of 2.5 x 10^3 Scm^{-1} at 400^oC which is comparable to the value obtained in this research.

Two series of electrical performance tests were conducted on another Ni-YSZ anode fabricated via EN co-deposition. These were carried out in two different environments – in air varying temperatures from 25^oC to 800^oC and in nitrogen varying temperatures from 25^oC to 600˚C. Both anode samples in air and nitrogen had coating deposition thickness of 10 microns. The resistivity and conductivity plots for both series are given in Fig. 101. Again, the conductivity trend decreases with temperature, an indication that it has a metallic conductivity.

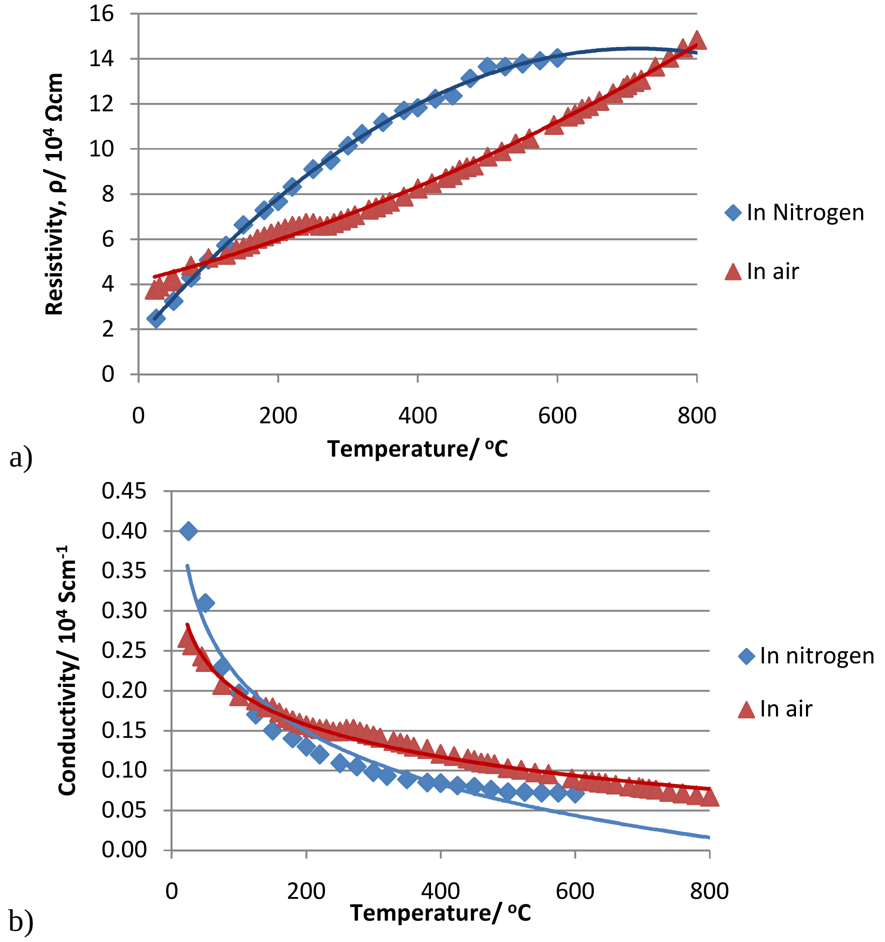

Fig. 101: Scatter plot of (a) resistivity and (b) conductivity against temperature in both nitrogen and air

The conductivity values are similar in air and nitrogen environment although the former is slightly higher. This observation might be due to the high moisture content in air compared to nitrogen. A review by Zhu and Deevi (2003 page 231) found that the Ni-YSZ anode overpotential is significantly reduced in the presence of moisture or steam. Lowering anodic overpotential enhanced the electronic conductivity.

In general, the conductivity at 600-800^{o}C of Ni-YSZ fabricated via EN deposition ranged between 700-1000 Scm^{-1} in both environments. These values are comparable with the published data from several studies as tabulated in Table 39. The role of P may be important. Parkinson stated that the electrical resistivity of EN deposited Ni increases with P content (Parkinson 1997). The Ni-P phase diagram (Fig. 30) shows the existence of Ni_3P at temperatures greater than 400^{o}C (Duncan 1996). The effect of these Ni_3P crystals for porosity as it could evaporate at higher temperature in SOFC anode application should be the subject of future work. For example, this composition might be evaporated at temperature between 1107-1517^{o}C (Viksman and Gordienko 1992).

Table 39: Published electrical conductivity of Ni-YSZ anode

Anode	T/^{o}C	Fabrication	Environment	σ/ Scm^{-1}	Ref.
40vol.% Ni-YSZ	600	Solid state coating	H_2	1500	Kim et al. (2006a)
		Solid state mixing		900	
	800	Solid state coating	H_2	1400	
		Solid state mixing		800	
45wt.% Ni-YSZ	600-800	Solid state with 2-step calcinations	H_2/Ar	500	Han et al. (2006)
		Conventional solid state mixing		430	

The anode fabricated via EN co-deposition is a possibility for in-situ fabrication of SOFC anode onto electrolyte. It is proven the anode of 50 vol.% Ni has a metallic conductivity with highest conductivity of 1500 Scm^{-1} at 400^{o}C in air (first attempt) and 700 Scm^{-1} in N_2; 1000 Scm^{-1} in air at 600^{o}C and 750 Scm^{-1} at 800^{o}C in air (second attempt).

4.4 Experimental Limitations

The majority of the experimental work involving measuring the Ni content in the anodes was carried out using a Cambridge S90 SEM fitted with only semi-quantitative EDXA software. While it was under repair, four of the samples were analysed using a FEG SEM with a fully quantitative EDX analyser. In order to determine the difference between the two analysers, five other samples were subsequently analysed on both machines and the results showed that the FEG SEM reduce Ni content by approximately 20 vol.% compared to the Cambridge SEM. Although the most important strand of the work was comparing the effects of different processing variables, the availability of a fully quantitative analyser during the research period would have been beneficial to the research but this was not possible.

The measurement of the porosity values in the anodes was carried out using Archimedes buoyancy techniques and a commercial software package – Image Pro-Plus. These techniques were not as accurate as others that were not available at the time of testing – such as mercury intrusion, IES impedance and BET analysis. Samples of the OFAAT tests were sent to a commercial company in England for more accurate porosity measurement by mercury intrusion porosimetry but these were unsuccessful due to the company being ‘unable to test two layers’ – the composite anode and the ceramic alumina substrate.

However, these experimental limitations do not impair the validity of the statistical DoE analysis regarding the significant co-deposition process parameters since the analysis interpreted the data based on the variability of distributed data from the normal.

5. CONCLUSIONS & SUMMARY

This research investigates a novel method of manufacturing solid oxide fuel cell anodes, based on the electroless co-deposition of ceramic and metal materials. Previously, these have been manufactured using processes such as tape casting and screen printing followed by high temperature sintering.

The novel part of this work involved (i) showing that electroless co-deposition of Ni–YSZ anodes could be carried out using combinations of nine different variables and (ii) the systematic testing of anodes produced by selective combinations of these variables.

The main objectives of the research were to investigate the processing parameters that would lead to favourable ceramic to metal ratios as well as sufficient porosity in the coating. The research has covered three phases namely One-Factor-At-A-Time (OFAAT), construction and implementation of Design of Experiment (DoE) and finally validating the performance of the processed anode.

The first phase consisted of nine independent OFAAT experiments to estimate the best selection of parameters in Phase 2. Out of nine independent parameters, the four most important were selected; these were particle size, bath agitation method, bath pH and substrate surface treatment. These four parameters were the basis of the DoE construction employed in Phase 2. The other parameters that remained constant were vertical orientation, YSZ as the ceramic material, 60 minutes deposition time, 50 g/l particle loading and 0.63 dm^2/l at 100 ml bath volume.

The 2^4 full factorials of 16 runs used particle sizes of 2 and 10 µm, bath agitation methods of air bubbling and mechanical stirring, bath pH of 4.9 and 5.4 and substrate surface treatment of HF etching and mechanical blasting. The DoE responses were Ni content and porosity content. The DoEs were then analysed by Minitab 15 software and it was found that the optimum condition for low Ni to YSZ ratio involved a particle size of 10 µm, bath agitation of mechanical stirring, a bath pH of 4.9 and a substrate condition of HF etching. On the other hand, the porosity response optimum condition involved a particle size of 2 µm, a bath agitation method of mechanical stirring, a bath pH of 4.9 and a substrate surface treatment of mechanical blasting.

The linear regression model was built where the regression coefficients were obtained from Minitab 15. There were two types of model built for both responses which is the coded and numerical approach models. The coded models were found to be more accurate. The experimental values were plotted against the predicted values and the coefficient of determination, R^2 of both responses were constructed. R^2 value for Ni to YSZ ratio response is 0.72 indicating a reasonable correlation between the experimental and predicted values. Porosity response model was not good enough and gave R^2 of 0.47. The numerical approach models were unrealistic as two of the factors are non-numerical and the estimated numerical values of the two agitation methods were not similar in nature.

The final phase was about verifying the optimum condition for both DoE responses that are Ni to YSZ ratio and porosity content. The Minitab 15 Response Optimiser tool was used for this purpose where the hypothesis for the responses is to minimise Ni to YSZ ratio and increase porosity content. It was found that the optimum combination condition involved a particle size of 10 µm, bath agitation of mechanical stirring, bath pH of 4.9 and substrate surface treatment of mechanical blasting. The two main parameters affecting the combination response were particle size and bath agitation.

In terms of the electrical conductivity performance, the initial electrical conductivity test carried out at room temperature showed an encouraging outcome in that the value for a 50 vol.% Ni-YSZ anode was only a factor of ten less than the equivalent loading of pure Ni. The electrical conductivity of this anode at 400^{o}C in air was comparable to published data in other studies and was superior to those recorded for anodes manufactured by traditional techniques. At temperatures up to 800^{o}C, the electrical conductivity tests were carried out in two different environments - air and nitrogen – and results were comparable to those in the public domain.

6. CONTRIBUTION TO KNOWLEDGE

The research undertaken investigates and develops a novel SOFC anode fabrication process via electroless nickel co-deposition. The incorporation of diamond (Hung at al. 2008), silicon carbide (Kalantary et al. 2006), silicon nitride (Balaraju and Rajam 2008), silicon oxide (Dong et al. 2009), boron carbide (Vaghefi et al 2003), alumina (Hazan et al. 2008a), ceria (Necula et al. 2007), yttria (McCommack et al. 2003), zirconia (Shibli et al. 2006) and iron oxide (Zeluta 2009) particles in electroless co-deposition has been investigated but none in fuel cells and none using YSZ. The application of this process in manufacturing SOFC anodes – involving the systematic investigation of selected variables on anode properties - has never been reported elsewhere. The work is a major contribution in the SOFC anode fabrication area.

The major challenges in electroless co-deposition are (i) to lower the Ni to YSZ ratio and (ii) to increase the porosity content. The DoE full factorial approach adopted in this research has led to process optimum conditions for these requirements.

The multiple linear regression models showed reasonable correlation for nickel content prediction in coded mode. Attempts have been made to improve the general applicability of the linear regression model with limited success. However, it has been identified that the use of first and second order polynomials may prove to be a better approach for predicting nickel and porosity content.

The electrical conductivity of these anodes are encouraging and worth further investigation.

7. FUTURE WORK

Future work is necessary for the continuation of the current research work. Based on the scope of the work, future work can generally focus on improving the co-deposition process to reduce the Ni to YSZ ratio as well as increasing the porosity. These can be further illustrated in the points below.

1. The YSZ deposition rate could be enhanced by inducing electrical polarity or potential in the bath (similar to electroplating after electroless deposition). The increased deposition rate might drag more ceramic particles into the coatings.
2. Consideration should be given to possible methods for reducing Ni concentration in the anode by investigating the electroless co-deposition bath chemistry.
3. One necessary improvement in the research is to measure porosity more accurately, for example by using mercury intrusion porosimetry, IES impedance, BET measurement and/or Image Pro-Plus software.
4. SOFC anodes do not only require adequate porosity but have to have open pores to allow fuel in and reactant gases out. Porosity enhancement can be achieved by several techniques as described in the literature – addition of pore former (Fergus et al. 2009) such as graphite particles, polystyrene or using a flocculant. Also, by preparing a honeycomb or 3-D pore channel network (Koh et al. 2006) to ensure open pores obtained in the fabricated anode.
5. It is clear that phosphorus exists in the EN solution used in this co-deposition. The effect of this impurity (if not burnt out for porosity) is undesirable in SOFC anodes – so using zero phosphorus solutions should be investigated.
6. The optimum combination condition for both Ni to YSZ ratio and porosity content reveals the two main parameters to be particle size and bath agitation. Regarding the other two variables investigated, bath pH is important for Ni to YSZ ratio while substrate surface treatment is important for porosity. A fractional factorial DoE is required to further investigate this effect.
7. Anode performance including its stability, durability, composition, structure, coefficient of thermal expansion and long term performance – should be investigated.
8. The non-linear regression model, possibly using first and second order polynomials should be investigated.

8. PUBLICATIONS

1. YSZ-reinforced Ni-P deposit: An effective condition for high particle incorporation and porosity level. Nor Bahiyah Baba, Alan Davidson and Tariq Muneer. Advanced Materials Research, Vol. 214, 2011, 412-417 (Scopus)

2. Effect of Electroless Coating Parameters on Ni-YSZ Composite Coating. Nor B. Baba, W. Waugh and A. Davidson. Proceedings of 2010 International Conference on Chemical Engineering and Applications (CCEA2010). ISBN 978-1-84626-023-0. Singapore. 26-28 Feb 2010 (Compendex)

3. Effect of Agitation on Ni-YSZ/CeSZ Electroless Composite Coating. Nor Bahiyah Baba, W. Waugh and A. Davidson. Proceedings of 2009 International Conference for Technical Postgraduates (TECHPOS2009). ISBN 978-983-42035-9-7. Kuala Lumpur, Malaysia. 14-15 Dec 2009

4. Ni-YSZ and Ni-CeSZ Electroless Nickel Composite Coating. Nor Bahiyah Baba, William Waugh and Alan Davidson. Proceedings of International Conference on Recent and Emerging Advanced Technologies in Engineering 2009 (iCREATE’09). Sepang, Malaysia. 23-24 Nov 2009

5. Effects of Ceramic Particle Size and Bath Conditions on Deposition Rate in Electroless Nickel/YSZ Composite Coatings. Nor Bahiyah Baba, W. Waugh and A. Davidson. Proceedings of International Conference on Advances in Materials and Processing Technologies (AMPT2009). Kuala Lumpur, Malaysia. 26-29 Oct 2009

6. Manufacture of Electroless Nickel/YSZ Composite Coating. N. Bahiyah Baba, W. Waugh and A.M. Davidson. Proceedings of WASET 2009. Volume 37. ISSN 2070-3740. Dubai UAE, 28-30 Jan 2009 (Compendex)

7. Novel Low Cost Solid Oxide Fuel Cell Anode (Poster). N. Baba and A. Davidson. Napier University FECCI Research Conference 2008.

In addition, the following events took place:

1. Attending ‘A 3-Day Course on DoE/ Taguchi Method for Process and Optimisation in Microelectronics and Packaging’ organised by Institute of Microengineering and Nanoelectronics, Universiti Kebangsaan Malaysia (UKM) on 16-18 November 2009.

2. Participation in SEBE Research Presentations - a talk on ‘Novel Low Cost Anodes for Solid Oxide Fuel Cells’ on 13 March 2008 and ‘Novel processing and modelling of solid oxide fuel cell anodes’ on Jan 2009.

3. Attending ‘Excel Advanced’ on 16th June 2008 and ‘Excel Intermediate’ on 15 May 2008 at Napier University.

4. Attending ‘Writing a literature’ on 1 May 2008, ‘Creating effective posters’ on 23 April 2008, ‘The transfer report and project planning’ on 6 March 2008, ‘Developing critical reading skills’ on 23 January 2008 and ‘Data analysis techniques’ on 13 December 2007 at Napier University.

5. Attending ‘A Hydrogen & Fuel Cell Conference’ at the James Watt Conference Centre, East Kilbride on 19 February 2008.

6. Attending ‘Risk Assessment workshop’ on 7 February 2008 at Napier University, Craighlockhart Campus.

7. Attending ‘Reference Management with Endnote’ on 6 December 2007 at Napier University.

REFERENCES

1. Abe, H., et al. (2006), 'Microstructural control of Ni–YSZ cermet anode for planer thin-film solid oxide fuel cells', *Fuel Cells Bulletin,* March 2006 (3), 12-15.
2. Agarwala, R. C. and Agarwala, V. (2003), 'Electroless alloy/ composite coatings: A review', *Sadhana,* 28 (Part 3 & 4), 475–93.
3. Ahn, J. S., et al. (2010), 'Performance of anode supported SOFC using novel ceria electrolyte', *Journal of Power Sources,* 195, 2131–35.
4. Alirezaei, Sh., et al. (2004), 'Effect of alumina content on surface morphology and hardness of Ni-P-Al_2O_3 (α) electroless composite coatings', *Surface & Coatings Technology,* 201, 2859-66.
5. AMETEK (2007), 'Talysurf CLI: 3D Surface Profiling Systems', (Leicester: Taylor Hobson Precision), Manual sheet data, 1-16.
6. An, C. M., et al. (2010), 'The effect of porosity gradient in a nickel/ yttria stabilized zirconia anode for an anode-supported planar solid oxide fuel cell', *Journal of Power Sources,* 195, 821–24.
7. Anthony, J. (2003), *Design of Experiments for Engineers and Scientist* (Butterworth-Henimen) 152, ISBN: 0750647094
8. Apachitei, I., et al. (1998), 'Particles Co-Deposition by Electroless Nickel', *Scripta Materialia,* 38 (9), 1383–89.
9. Aruna, S.T., Muthuraman, M., and Patil, K. C. (1998), 'Synthesis and properties of Ni-YSZ cermet: anode materials for solid oxide fuel cells', *Solid State Ionics,* 111, 45-51.
10. Attaoui, H. El, et al. (2007), 'Static and cyclic crack propagation in Ce-TZP ceramics with different amounts of transformation toughening', *Journal of the European Ceramic Society,* 27, 483–86.
11. Azmir, M. A. and Ahsan, A. K. (2008), 'Investigation on glass/ epoxy composite surfaces machine by abrasive water jet machining', *Journal of Materials Processing Technology,* 198, 122-28.
12. Azmir, M. A., Ahsan, A. K., and Rahmah, A. (2009), 'Effect of abrasive water jet machining parameters on aramid fibre reinforced plastics composite', *International Journal Materials Form,* 2, 37-44.
13. Badwal, S.P.S. (2001), 'Stability of solid oxide fuel cell components', *Solid State Ionics,* 143, 39-46.
14. Badwal, S. P. S. and Foger, K. (1996), 'Solid Oxide Electrolyte Fuel Cell Review', *Ceramics International,* 22, 257-65.
15. Balaraju, J.N. and Rajam, K.S. (2008), 'Preparation and characterisation of autocatalytic low phosphorus nickel coatings containing submicron nitride particles', *Journal of Alloys and Compounds,* 459 (1-2), 311–19.
16. Balaraju, J.N., Kalavati, and Rajam, K.S. (2006a), 'Influence of particle size on the microstructure, hardness and corrosion resistance of electroless Ni–P–Al_2O_3 composite coatings', *Surface & Coatings Technology,* 200, 3933 – 41.
17. Balaraju, J.N., Narayanan, T.S.N. Sankara, and Seshadri, S.K. (2006b), 'Structure and phase transformation behaviour of electroless Ni–P composite coatings', *Materials Research Bulletin,* 41, 847–60.
18. Bao, Weitao, Chang, Qibing, and Meng, Guangyao (2005), 'Effect of NiO/YSZ compositions on the co-sintering process of anode-supported fuel cell', *Journal of Membrane Science,* 259, 103-09.
19. Basu, R.N., et al. (2008), 'Processing of high-performance anode-supported planar solid oxide fuel cell', *International Journal of Hydrogen Energy,* 33, 5748-54.
20. Baudrand, D. (2006), 'Electroless Nickel Applications Involving Heat Excursions (Part II)', *Southern Metal Finishing,* 5 (10), 9.

21. Baudrand, D. (2005), 'Electroless Nickel Applications Involving Heat Excursions - Part I', *Southern Metal Finishing*, 4.

22. Baudrand, D. W. (1994), 'Electroless Nickel Plating', *ASM Handbook Volume 5*, Surface Engineering, 290-310, ISBN: 08717038X

23. Baudrand, D. W. (1978), *Metals Handbook* (8th edition).

24. Benoved, N. and Kesler, O. (2009), 'Air plasma spray processing and electrochemical characterization of Cu–SDC coatings for use in solid oxide fuel cell anodes', *Journal of Power Sources*, 193, 454–61.

25. Benyoucef, A., et al. (2009), 'Thermal stability of atmospheric plasma sprayed (Ni,Cu,Co)–YSZ and Ni–Cu–Co–YSZ anodes cermets for SOFC application', *Journal of Physics and Chemistry of Solids*, 70, 1487–95.

26. Berkel, F.P.F. van, Heuveln, F.H. van, and Huijsmans, J.P.P. (1994), 'Characterization of solid oxide fuel cell electrodes by impedance spectroscopy and I- V characteristics', *Solid State Ionics*, 72, 240-47.

27. Berkh, 0., Eskin, S., and Zahavi, J. (March 1996), 'Properties of Electrodeposited NiP-SiC Composite Coatings', *Metal Finishing*, 35-40.

28. Besra, L. and Liu, M. (2007), 'A review on fundamentals and applications of electrophoretic deposition (EPD)', *Progress in Materials Science*, 52, 1–61.

29. Besra, L., Zha, S., and Liu, M. (2006), 'Preparation of NiO-YSZ/YSZ bi-layers for solid oxide fuel cells by electrophoretic deposition', *Journal of Power Sources*, 160, 207-14.

30. Bieberle, A. and Gauckler, L. J. (2000), 'Reaction mechanism of Ni pattern anodes for solid oxide fuel cells', *Solid State Ionics*, 135, 337-45.

31. Bisgaard, S. (1998), 'A Practical Aid for Experimenters', *Preliminary Edition* (Madison: Starlight Press), 57.

32. Boder, M. and Dittmeyer, R. (2006), 'Catalytic modification of conventional SOFC anodes with a view to reducing their activity for direct internal reforming of natural gas', *Journal of Power Sources*, 155, 13-22.

33. Boer, B. de, et al. (2000), 'The effect of the presence of fine YSZ particles on the performance of porous nickel electrodes', *Solid State Ionics*, 127, 269-76.

34. Bozzini, B., Giovannelli, G., and Cavallotti, P. L. (1997), 'An investigation into microstructure and particle distribution of Ni-P/ diamond composite thin films', *Journal of Microscopy*, 185, 283-91.

35. Callister, W. D. Jr. (2006), *Materials Science and Engineering - An Introduction* (7th Edition edn.; Utah: John Wiley & Sons) 832, ISBN-13: 978-0-471-73696-7.

36. Cengel, Y. A. (2002), *Introduction to thermodynamics and heat transfer* (International Edition edn.; Singapore: McGraw Hill) 922, ISBN: 0071226605.

37. Chan, J. and Friedberg P. (2002), *Four point probe manual*, Note EECS144 Microfabrication Technology, University of California, 3, http://www-inst.eecs.berkeley.edu/~ee143/fa05/lab/four_point_probe.pdf

38. Chang, J., et al. (2003), 'A review on the energy production, consumption, and prospect of renewable energy in China', *Renewable and Sustainable Energy Reviews*, 7, 453–68.

39. Chen, K. and Chen, Y. (1997), 'A New Low-Temperature Electroless Nickel Plating Process', *Plating & Surface Finishing*, 80-82.

40. Chen, K., et al. (2007), 'Fabrication and performance of anode-supported YSZ films by slurry spin coating', *Solid State Ionics*, 177 (39-40), 3455-60.

41. Chen, Y-Y. and Wei, W-C. J. (2006), 'Processing and characterization of ultra-thin yttria-stabilized zirconia (YSZ) electrolytic films for SOFC', *Solid State Ionics*, 177, 351-57.

42. Clemmer, R.M.C. and Corbin, S.F. (2004), 'Influence of porous composite microstructure on the processing and properties of solid oxide fuel cell anodes', *Solid State Ionics*, 166, 251-59.

43. Crowe, C.T., Elger, D.F., Williams, B.C., and Roberson J.A. (2010), Engineering Fluid Mechanics (9th edition), *John Wiley & Sons*, 553, ISBN: 9780470409435.

44. Dai, J., et al. (2009), 'Preparation of Ni-coated Si_3N_4 powders via electroless plating method', *Ceramics International,* 35 (8), 3407–10.

45. Das, C.M., et al. (2007), 'Preparation and characterization of silicon nitride codeposited electroless nickel composite coatings', *Journal of Alloys and Compounds,* 436, 328-34.

46. Das, L. and Chin, D. T. (1959), 'Electrochemical Porosity Measurement of EN Coating', *Plating and Surface Finishing,* 84, 66-68.

47. Delahaye, T., et al. (2006), 'Synthesis and characterization of a $Ni/Ba_2In_{0.6}Ti_{1.4}O_{5.7}\square_{0.3}$ cermet for SOFC application', *Solid State Ionics,* 177, 2945–50.

48. Dincer, I. (2000), 'Renewable energy and sustainable development: a crucial review', *Renewable and Sustainable Energy Reviews,* 4, 157-75.

49. Dong, D., et al. (2009), 'Preparation and properties of electroless Ni-P-SiO_2 composite coatings', *Applied Surface Science,* 255, 7051-55.

50. Dongare, M. K., et al. (2002), 'Synthesis and characterization of copper-stabilized zirconia as an anode material for SOFC', *Solid State Ionics,* 152-153, 455-62.

51. Drescher, I., Lehnert, W., and Meusinger, J. (1998), 'Structural properties of SOFC anodes and reactivity', *Electrochimica Acta,* 43, 3059-68.

52. Dugasz, J. and Szasz, A. (1993), 'Factors affecting the adhesion of electroless coatings', *Surface & Coatings Technology,* 58, 57-62.

53. Duncan, R. N. (1996), 'Metallurgical Structure of EN Deposit', *Plating and Surface Finishing,* 83, 65.

54. EG&G Services, Parsons Inc., and Science Application International Corporation (2000), 'Fuel Cell Handbook', (Fifth edn., Contract No. DE-AM26-99FT40575; Morgantown, West Virginia: U.S. Department of Energy), 337.

55. Eguchi, K., et al. (2000), 'Process of solid state reaction between doped ceria and zirconia', *Solid State Ionics,* 135, 589–94.

56. Fang, X., et al. (2004), 'Synthesis and properties of Ni–SDC cermets for IT–SOFC anode by co-precipitation', *Solid State Ionics,* 168, 31–36.

57. Feldstein, N. (1990), 'Composites Electroless Plating', in G.O. Mallory and J.B. Hajdy (eds.), *Electroless Plating: Fundamentals and Applications* (Chapter 11; Orlondo, FI: AESF Publication), 269-87.

58. Fergus, J. W., et al. (2009), *Solid Oxide Fuel Cells - Materials properties and performance* (Green chemistry and chemical engineering); Florida *CRC Press Taylor & Francis Group* 295, ISBN 978-1-4200-8883-0.

59. Franceschini, G. and Macchietto, S. (2008), 'Model-based design of experiments for parameter precision: State of the art', *Chemical Engineering Science,* 63, 4846 – 72.

60. Fu, C., et al. (2010), 'Fabrication and evaluation of Ni-GDC composite anode prepared by aqueous-based tape casting method for low-temperature solid oxide fuel cell', *International Journal of Hydrogen Energy,* 35 (1), 301-07.

61. Fukui, T., et al. (2004), 'Morphology control of Ni-YSZ cermet anode for lower temperature operation of SOFCs', *Journal of Power Sources,* 125, 17-21.

62. Fukui, T., et al. (2003), 'Performance and stability of SOFC anode fabricated from NiO/YSZ composite particles', *Journal of the European Ceramic Society,* 23, 2963–67.

63. Ger, M-D. and Hwang, B. J. (2002), 'Effect of surfactants on codeposition of PTFE particles with electroless Ni-P coating', *Materials Chemistry and Physics,* 76 (1), 38-45.

64. Gonzalo-Juan, I., et al. (2010), 'Colloidal processing and sintering of porous percolative Ni-YSZ layers', *Journal of Membrane Science,* 352 (1-2), 55–62.

65. Goodenough, J. B. and Huang, Y-H. (2007), 'Alternative anode materials for solid oxide fuel cells', *Journal of Power Sources,* 173, 1–10.

66. Gorte, R.J., Kim, H., and Vohs, J.M. (2002), 'Novel SOFC anodes for the direct electrochemical oxidation of hydrocarbon', *Journal of Power Sources*, 106, 10-15.

67. Gorte, R.J., Vohs, J.M., and McIntosh, S. (2004), 'Recent developments on anodes for direct fuel utilization in SOFC', *Solid State Ionics,* 175, 1-6.

68. Gorte, R.J., et al. (2000), 'Anodes for Direct Oxidation of Dry Hydrocarbons in a Solid-Oxide Fuel Cell ', *Advanced Materials,* 12 (19), 1465-69.

69. Gould, P. (2005), 'More efficient fuel cells: Energy Generation Materials', *Materials Today June 2005*, 10.

70. Grunwald, P. (1983), *Galvanotechnik,* 74, 1286-90.

71. Guan, X., et al. (2008), 'High performance Gd^{3+} and Y^{3+} co-doped ceria-based electrolytes for intermediate temperature solid oxide fuel cells', *Materials Research Bulletin*, 43 (4), 1046–54.

72. Guo, H-X., et al. (2005), 'Synthesis of Novel Magnetic Spheres by Electroless Nickel Coating of Polymer Spheres', *Surface & Coatings Technology,* 200, 2531 – 36.

73. Haile, S. M. (2003a), 'Materials for fuel cells', *Materials Today*, 24-29.

74. Haile, S. M. (2003b), 'Fuel cell materials and components', *Acta Materialia,* 51, 5981–6000.

75. Haldane, M.A. and Etsell, T.H. (2005), 'Fabrication of composite SOFC anodes', *Materials Science and Engineering,* B121, 120-25.

76. Han, K. R., et al. (2006), 'Fabrication of NiO/YSZ anode material for SOFC via mixed NiO precursors', *Materials Letters,* 61, 1242–45.

77. Han, M-F., et al. (2008), 'Fabrication and properties of anode-supported solid oxide fuel cell', *Solid State Ionics,* 179, 1545–48.

78. Hazan, Y. de, et al. (2008a), 'Interactions and dispersion stability of aluminum oxide colloidal particles in electroless nickel solutions in the presence of comb polyelectrolytes', *Journal of Colloid and Interface Science*, 323, 293–300.

79. Hazan, Y. de, et al. (2008b), 'Homogeneous Ni-P/Al_2O_3 nanocomposite coatings from stable dispersions in electroless nickel baths', *Journal of Colloid and Interface Science,* 328, 103–09.

80. He, B., Ding, D., and Xia, C. (2010), 'Ni–LnO_x (Ln = La,Ce,Pr,Nd,Sm,Eu, and Gd) cermet anodes for intermediate-temperature solid oxide fuel cells', *Journal of Power Sources*, 195 (5), 1359–64.

81. Henry, James R. (1984), 'Electroless (Autocatalytic) Plating', (Wear cote International, Rock Island), 409-20.

82. Holtappels, P., et al. (2006), 'Preparation and electrochemical characterisation of supporting SOFC–Ni–YZT anodes', *Solid State Ionics*, 177, 2029-32.

83. Holtappels, p., Vogt, U., and Graule, T. (2005), 'Ceramic materials for advanced solid oxide fuel cells', *Advanced Engineering Materials*, 7, 292-302.

84. Honma, H. and Kanemitsu, K. (1987), 'Electroless Nickel Plating on Alumina Ceramics', *Plating and Surface Finishing*, September, 62-67.

85. Horita, T., et al. (2004), 'Design of metal/oxide interfaces for the direct introduction to hydrocarbons into SOFCs', *Journal of Power Sources*, 131, 299-303.

86. Huang, B., et al. (2007), 'Preparation and performance characterization of the Fe–Ni/ScSZ cermet anode for oxidation of ethanol fuel in SOFCs', *Journal of Power Sources*, 167, 288-94.

87. Huang, B., et al. (2006a), 'Performance of Ni/ScSZ cermet anode modified by coating with $Gd_{0.2}Ce_{0.8}O_2$ for a SOFC', *Materials Research Bulletin*, 42, 1705–14.

88. Huang, W. L., Zhu, Q., and Xie, Z. (2006b), 'Gel-cast anode substrates for solic oxide fuel cells', *Journal of Power Sources*, 162, 464-68.

89. Huang, Y. S., Zeng, X. T., and Annegren, I. (2003), 'Development of electroless Ni-P-PTFE-SiC composite coating', *Surface & Coating Technology*, 167, 207-11.

90. Hubbard, H. M., et al. (2003), 'Renewable power pathways - a review of the U.S. department of energy's renewable energy programs', (Washington D.C.: National Academy Press), 124.

91. Hung, C. C., Lin, C. C., and Shih, H. C. (2008), 'Tribological studies of electroless nickel/ diamond composite coatings on steels', *Diamond & Related Materials*, 17, 853–59.

92. IEA (2001), 'World Energy Outlook', (Paris, France: OECD/ International Energy Agency).

93. Ioselevich, A., Kornyshev, A. A., and Lehnert, W. (1999), 'Statistical geometry of reaction space in porous cermet anodes based on ion-conducting electrolytes: Patterns of degradation', *Solid State Ionics*, 124, 221-37.

94. Ivers-Tiffee, E., Weber, A., and Herbstritt, D. (2001), 'Materials and technologies for SOFC-components', *Journal of the European Ceramic Society*, 21, 1805–11.Jackson, B., Macary, R., and Shawhan, G. (1990), 'Low phosphorus electroless nickel coating technology', (Institute of Metal Finish), 75-83.

95. Jappes, J. T. W., Ramamoorthy, B., and Nair, P. K. (2005), 'A study on the influence of process parameters on efficiency and crystallinity of electroless Ni–P deposits', *Journal of Materials Processing Technology*, 169, 308-13.

96. Jia, Li, et al. (2007), 'Preparation of YSZ film by gravity-electropheretic deposition and its application in SOFC', *Ceramics International*, 33, 631–35.

97. Jia, Li, et al. (2006), 'Preparation of YSZ film by EPD and its application in SOFCs', *Journal of Alloys and Compounds*, 424, 299-303.

98. Jiang, S. P. and Badwal, S.P.S. (1999), 'An electrode kinetics study of H oxidation on Ni/Y_2O_3–ZrO_2 cermet electrode of the solid oxide fuel cell', *Solid State Ionics*, 123, 209-24.

99. Jiang, S. P., Callus, P.J., and Badwal, S.P.S. (2000), 'Fabrication and performance of Ni/3 mol% Y_2O_3-ZrO_2 cermet anodes for solid oxide fuel cells', *Solid State Ionics*, 132, 1-14.

100. Jiang, S. P., Wang, W., and Zhen, Y. D. (2005), 'Performance and electrode behaviour of nano-YSZ impregnated nickel anodes used in solid oxide fuel cells', *Journal of Power Sources*, 147, 1-7.

101. Jiang, S. P. (2006), 'A review of wet impregnation—An alternative method for the fabrication of high performance and nano-structured electrodes of solid oxide fuel cells', *Materials Science and Engineering*, A418, 199-210.

102. Jin, Y., et al. (2010), 'Improved electrochemical properties of Ni/YSZ anodes infiltrated by proton conductor SZY in solid oxide fuel cells with dry methane fuel: Dependence on amount of SZY', *Chemical Engineering Science*, 65, 597--602.

103. Jung, S., et al. (2006), 'Influence of composition and Cu impregnation method on the performance of Cu/CeO_2/YSZ SOFC anodes', *Journal of Power Sources*, 154 (1), 42-50.

104. Kalantary, M. R., Holbrook, K. A., and Wells, P. B (1993), 'Optimisation of a Bath for Electroless Plating and its use for the Production of Ni-P-SiC Coatings', *Trans. Inst. Metal Finish*, 71 (2), 55-61.

105. Kawano, M., et al. (2005), 'Synthesis and characterisations of composite particles for solid oxide fuel cell anodes by spray pyrolysis and intermediate temperature cell performance', *Journal of Power Sources*, 152, 196-99.

106. Keong, K. G., Sha, W., and Malinov, S. (2003), 'Hardness evolution of electroless nickel–phosphorus deposits with thermal processing', *Surface & Coatings Technology*, 168, 263–74.

107. Keping, H., et al. (1996), 'A Super High Speed Electroless Nickel Plating Process', *Trans Inst. Metal Finish,* 74 (3), 91-94.

108. Kharton, V. V., Marques, F.M.B., and Atkinson, A. (2004), 'Transport properties of solid oxide electrolyte ceramics: a brief review', *Solid State Ionics,* 174, 135-49.

109. Kikuchi, R., et al. (2006), 'Novel anode materials for multi-fuel applicable solid oxide fuel cells', *Journal of Alloys and Compounds,* 408-412, 622-27.

110. Kilner, J. A. and Steele, B.C.H. (1981), *Nonstoichiometric Oxides* (London: Academic Press).

111. Kim, S-D., et al. (2006a), 'Performance and durability of Ni-coated YSZ anodes for intermediate temperature solid oxide fuel cells', *Solid State Ionics,* 177, 931-38.

112. Kim, S-D., et al. (2006b), 'Nano-composite materials for high-performance and durability of solid oxide fuel cells', *Journal of Power Sources,* 163, 392–97.

113. Kim, T., et al. (2006c), 'A study of carbon formation and prevention in hydrocarbon-fueled SOFC', *Journal of Power Sources,* 155, 231-38.

114. Kingery, W. D., Bowen, H.K., and Uhlmann, D.R. (1976), Introduction to Ceramics (Second Edition); New York: *John Wiley & Sons*, 1032, ISBN: 0471478601

115. Kirubakaran, A., Jain, S., and Nema, R. K. (2009), 'A review on fuel cell technologies and power electronic interface', *Renewable and Sustainable Energy Reviews,* 13, 2430–40.

116. Kishimoto, H., et al. (2007), 'Feasibility of liquid hydrocarbon fuels for SOFC with Ni–ScSZ anode', *Journal of Power Sources*, 172, 67–71.

117. Koh, Y-H., Sun, J-J., and Kim, H-E. (2006), 'Freeze casting of porous Ni-YSZ cermets', *Materials Letters,* 61 (6), 1283–87.

118. Koide, H., et al. (2000), 'Properties of Ni/YSZ cermet as anode for SOFC', *Solid State Ionics,* 132, 253-60.

119. Kuehl, Robert O. (2000), Design of Experiments: Statistical Principles of Research Design and Analysis (Second Edition), California: *Thomson Learning*, 666, ISBN: 0534368344

120. Le, S., et al. (2010), 'Fabrication and evaluation of anode and thin Y_2O_3-stabilized ZrO_2 film by co-tape casting and co-firing technique', *Journal of Power Sources,* 195 (9), 2644–48.

121. Lee, J.-H., et al. (2002), 'The impact of anode microstructure on the power generating characteristics of SOFC', *Solid State Ionics,* 8871, 1-8.

122. Leisner, P. and Benzon, M.E. (1997), 'Porosity Measurement of Coatings', *Trans Inst, Metal Finish,* 75(2), 88-92.

123. Lessing, P.A. (2007), 'A review of sealing technologies applicable to solid oxide electrolysis cell', *Journal of Materials Science* 42, 3465-76.

124. Li, C-X., Li, C-J., and Guo, L-J. (2010), 'Effect of composition of NiO/YSZ anode on the polarization characteristics of SOFC fabricated by atmospheric plasma spraying', *International Journal of Hydrogen Energy,* 35 (7), 2964-69.

125. Li, L., An, M., and Wu, G. (2006), 'A new electroless nickel deposition technique to metallise SiC_p/Al composites', *Surface & Coatings Technology,* 200, 5102 – 12.

126. Li, L., An, M., and Wu, G. (2005a), 'Model of electroless Ni deposition on SiC_p/Al composites and study of the interfacial interaction of coatings with substrate surface', *Applied Surface Science,* 252, 959-65.

127. Li, L. B., An, M. Z., and Wu, G.H. (2005b), 'Electroless deposition of nickel on the surface of silicon carbide/aluminum composites in alkaline bath', *Materials Chemistry and Physics,* 94, 159-64.

128. Li, X. And Karimi, G. (2007), 'Fuel Cells: Intermediate and high temperature', in Barney L. Capehart (ed.), *Encyclopedia of Energy Engineering and Technology,* Vol.2; Department of Mechanical Engineering, University of Waterloo, Waterloo, Ontario, Canada: *CRC Press,* ISBN: 9780849350429.

129. Li, Y. (1997), 'Investigation of Electroless Ni-P-SiC Composite Coatings', *Plating & Surface Finishing*, November 1997, 77-81.

130. Lin, C. J., Chen, K. C., and He, J. L. (2006), 'The cavitation erosion behavior of electroless Ni–P–SiC composite coating', *Wear,* 261, 1390–96.

131. Liu, L., Kim, G-Y., and Chandra, A. (2010), 'Fabrication of solid oxide fuel cell anode electrode by spray pyrolysis', *Journal of Power Sources,* 195 (20), 7046–53.

132. Liu, W. L., et al. (2006), 'Temperature and pH dependence of the Electroless Ni-P deposition on Silicon', *Thin Solid Films,* 510, 102 – 06.

133. Liu, Y., Compson, C., and Liu, M. (2004), 'Nanostructured and functionally graded cathodes for intermediate-temperature SOFCs', *Fuel Cells Bulletin,* October 2004 (10), 12-15.

134. Lu, C., et al. (2003), 'SOFCs for direct oxidation of hydrocarbon fuels with samaria-doped ceria electrolyte', *Journal of Electrochemical Society,* 150, A354-A58.

135. Mallon, C. and Kendall, K. (2005), 'Sensitivity of nickel cermet anodes to reduction conditions', *Journal of Power Sources,* 145, 154-60.

136. Marina, O., et al. (1999), 'A solid oxide fuel cell with a gadolina-doped ceria anode: preparation and performance ', *Solid State Ionics,* 123, 199-208.

137. Marinsek, M. and Macek, K. Zupan J. (2000), 'Preparation of Ni–YSZ composite materials for solid oxide fuel cell anodes by the gel-precipitation method', *Journal of Power Sources,* 86, 383-89.

138. Martınez-Arias, A., et al. (2005), 'Cerium–terbium mixed oxides as potential materials for anodes in solid oxide fuel cells', *Journal of Power Sources,* 151, 43–51.

139. Mather, G. C., et al. (2004), 'Electrochemical behaviour of Ni-cermet anodes containing a proton-conducting ceramic phase on YSZ substrate', *Electrochimica Acta,* 49, 2601-12.

140. Matsubara, H., et al. (2007), 'Co-deposition mechanisms of nano-diamond with electrolessly plated nickel films', *Electrochimica Acta,* 52, 3047-52.

141. McCormack, A.G., Pomeroy, M.J., and Cunnane, V.J. (2003), *Journal of Electrochemical Society,* 150 (5), C356-C361.

142. Minh, N. Q. (2004), 'Solid oxide fuel cell technology—features and applications', *Solid State Ionics,* 174, 271–77.

143. Minh, N. Q. and Takahashi, T. (1995), *Science and Technology of Ceramic Fuel Cells* (Amsterdam: Elsevier Science B.V.) 366, ISBN: 044489568X

144. Minh, N. Q., et al. (1999), 'Fabrication and performance of zirconia electrolytes cells for carbon dioxide reduction for mars in-situ resource utilization applications'. <http://www.lpi.usra.edu/meetings/ISRU-III-99/pdf/8021.pdf>

145. Misono, T., et al. (2006), 'Ni-SDC cermet anode fabricated from NiO–SDC composite powder for intermediate temperature SOFC', *Journal of Power Sources*, 157, 754-57.

146. Montgomery, D. C. (2009), Design and Analysis of Experiments (Seventh Edition), International Student Version: *John Wiley & Sons Inc*. 656, ISBN: 0471661597.

147. Montgomery, D. C and Peck, E.A. (1992), Introduction to linear regression analysis (Second Edition), *John Wiley & Sons Inc*., 527, ISBN:0471533874

148. Moon, H., et al. (2008), 'Characteristics of SOFC single cells with anode active layer via tape casting and co-firing', *International Journal of Hydrogen Energy,* 33, 2826 – 33.

149. Moon, J. W., et al. (1999), 'Preparation of ZrO_2-coated NiO powder using surface-induced coating', *Materials Letters*, 38, 214-20.

150. Mori, T., et al. (2002), 'Improving the ionic conductivity of yttria-stabilised zirconia electrolyte materials', *Solid State Ionics*, 154-155, 529-33.

151. Mortimer, N.D. (2008), 'Life Cycle of the Transition to the Hydrogen Economy', *Greenhouse Issues*, 89, 1-26.

152. Mukhopadhyay, J., Banerjee, M., and Basu, R. N. (2008), 'Influence of sorption kinetics for zirconia sensitization in solid oxide fuel cell functional anode prepared by electroless technique', *Journal of Power Sources,* 175, 749–59.

153. Muller-Steinhagen, H. and Nitsch, J. (2005), 'The contribution of renewable energies to a sustainsble energy economy', *Trans IChemE,* 83(B4) (Part B), 285–97.

154. Muller, A. C., Herbstritt, D., and Ivers-Tiffee, E. (2002), 'Development of a multilayer anode for solid oxide fuel cells', *Solid State Ionics,* 152-153, 537– 42.

155. Necula, B.S., et al. (2007), 'Stability of nano-/microsized particles in deionized water and electroless nickel solutions', *Journal of Colloid and Interface Science*, 314, 514–22.

156. Ohadi, M. M. and Qi, J. (2007), 'Alternative Energy Technologies: Price Effects', in Barney L. Capehart (ed.), *Encyclopedia of Energy Engineering and Technology* (Vol.1), Department of Mechanical Engineering, University of Waterloo, Waterloo, Ontario, Canada: CRC Publisher, ISBN: 0849350395.

157. Ohara, S., et al. (2000), 'High performance electrodes for reduced temperature solid oxide fuel cells with doped lanthanum gallate electrolyte: I. Ni–SDC cermet anode', *Journal of Power Sources,* 86, 455-58.

158. Oraon, B., Majumdar, G., and Ghosh, B. (2007), 'Parametric optimization and prediction of electroless Ni–B deposition', *Materials and Design,* 28, 2138–47.

159. Orera, V. M., Merino, R. I., and Pena, F. (1994), 'Ce^{3+}-Ce^{4+} conversion in ceria-doped zirconia single crystals induced by oxide-reduction treatments', *Solid State Ionics,* 72, 224-31.

160. Parkinson, R. (1997), 'Properties and Application of Electroless Nickel', (Nickel Development Institute), 33.

161. Periene, N., Cesuniene, A., and Mtulionis, E. (1994), 'Codeposition of Mixtures of Dispersed Particles With Nickel-Phosphorus Electrodeposits', *Plating and Surface Finishing*, October 1994, 68-71.

162. Pitts, A. C. (1994), 'Building Design: Realising the Benefits of Renewable Energy Technologies', *Renewable Energy,* 5 (Part II), 959-66.

163. Pratihar, S. K., Sharma, A. D., and Maiti, H. S. (2007), 'Properties of Ni/YSZ porous cermets prepared by electroless coating technique for SOFC anode application', *Journal of Materials Science*, 42, 7220-26.

164. Pratihar, S.K., Sharma, A.D., and Maiti, H.S. (2006), 'Electrical behaviour of nickel coated YSZ cermet prepared by electroless coating technique', *Materials Chemistry and Physics,* 96, 338-95.

165. Pratihar, S. K., Sharma, A. D., and Maiti, H. S. (2005), 'Processing microstructure property correlation of porous Ni–YSZ cermets anode for SOFC application', *Materials Research Bulletin,* 40, 1936–44.

166. Pratihar, S. K., et al. (2004), 'Preparation of nickel coated YSZ powder for application as an anode for solid oxide fuel cells', *Journal of Power Sources,* 129, 138–42.

167. Primdahl, S. and Mogensen, M. (2002), 'Mixed conductor anodes: Ni as electrocatalyst for hydrogen conversion', *Solid State Ionics,* 152-153, 597-608.

168. Qiao, J., et al. (2007), 'Ni/YSZ and Ni–CeO_2/YSZ anodes prepared by impregnation for solid oxide fuel cells', *Journal of Power Sources,* 169, 253-58.

169. Radovic, M. and Lara-Curzio, E. (2004), 'Mechanical properties of tape cast nickel-based anode materials for solid oxide fuel cells before and after reduction in hydrogen', *Acta Materialia*, 52, 5747-56.

170. Rahaman, M. N. (2003), Ceramic Processing and Sintering, Materials Engineering (Second edition); New York: *Marcel Dekker, Inc*., 875.

171. Reidel, W. (1997), 'Electroless Nickel Plating', (ASN International).

172. REN21 (2009), 'Renewables Global Status Report 2009 Update', (Paris: Renewable Energy Policy Network for the 21st Century), 32.

173. Rezugina, E., et al. (2010), 'Ni-YSZ films deposited by reactive magnetron sputtering for SOFC applications', *Surface & Coatings Technology,* 204, 2376–80.

174. Ringuede, A., Fagg, D.P., and Frade, J.R. (2004), 'Electrochemical behaviour and degradation of (Ni,M)/YSZ cermet electrodes (M=Co,Cu,Fe) for high temperature applications of solid electrolytes', *Journal of the European Ceramic Society,* 24, 1355-58.

175. Rosa, Aldo V. Da (2005), *Fundamentals of Renewable Energy of Processes* (Oxford: Elsevier Academic Press) 689.

176. Rosenkrantz, Walter A. (1997), *Introduction to Probability and Statistics for Scientists and Engineers* (International Edition: McGraw-Hill) 592.

177. Rotureau, D., et al. (2005), 'Development of a planar SOFC device using screen-printing technology', *Journal of the European Ceramic Society,* 25, 2633–36.

178. Sakai, N., et al. (2006), 'Transport properties of ceria–zirconia–yttria solid solutions $(CeO_2)_x(ZrO_2)_{1-x}\}_{1-y}(YO_{1.5})_y$ (x = 0–1, y = 0.2, 0.35)', *Journal of Alloys and Compounds,* 408-412, 503-06.

179. Sakai, N., et al. (2004), 'Lanthanum chromite-based interconnects as key materials for SOFC stack development', *International Journal Application Ceramic Technology,* 1, 23-30.

180. Sammes, N. (2006), Fuel Cell Technology - Reaching Towards Commercialization, ed. Brian Derby (Fussion bonding of polymer composites, composite materials titanium corrosion and protection intelligent macromolecules for smart devices); London: *Springer-Verlog,* 298, ISBN-10: 1852339748.

181. Sammes, N. M. and Cai, Z. (1997), 'Ionic conductivity of ceria/yttria stabilized zirconia electrolyte materials', *Solid State Ionics,* 100, 39-44.

182. Sammes, N.M., et al. (1996), 64, 6.

183. Sartorius (1991), 'Manual of weighing applications Part 1: Density', 1-62.

184. Savignat, S. B., Chiron, M., and Barthet, C. (2007), 'Tape casting of new electrolyte and anode materials for SOFCs operated at intermediate temperature', *Journal of the European Ceramic Society,* 27, 673-78.

185. Schloetter (2006), 'Electroless Nickel - Solotonip 1850', *Bath 18810 - PE* (Worchestershire, England), 1-11.

186. Schneider, L.C.R et al. (2006), ‘Discrete modelling of the electrochemical performance of SOFC electrodes’, *Electrochimica Acta,* 52, 314–324

187. Senguttuvan, T. D., et al. (2006), 'Phases in copper-stabilized zirconia solid oxide fuel cells anode material', *Materials Chemistry and Physics,* 95, 197-201.

188. Sevugan, K., et al. (1993), 'Effect of Agitation in Electroless Nickel Deposition', *Plating and Surface Finishing,* (March 1993), 56-58.

189. Shackelford, J. and Alexander, W. (1992), The CRC Materials Science and Engineering Handbook, (Second Edition), London: *CRC Press Inc*., ISBN: 0849342503

190. Shade, J. and Henderson, R. (2001), 'Design of Multifactor Experiments - Foundation (Training Course)', (Good Decision Ltd.), 42.

191. Sharma, S.B., et al. (2005), 'Development of Electroless Composite Coatings by using in-situ Co-deposition followed by co-deposition process', *Sadhana,* 28, 475–93.

192. Shearer, N. W. A and Davidson, A. (2005), 'Novel methods of manufacturing solid oxide', *First World Congress of Young Scientists on Hydrogen* (Italy).

193. Sheela, G. and Pushpavanam, M. (2002), 'Diamond-dispersed electroless nickel coatings', *Metal Finishing*, January 2002, 45-47.

194. Shibli, S. M. A., Dilimon, V. S., and Deepthi, T. (2006), 'ZrO_2-reinforced Ni–P plate: An effective catalytic surface for hydrogen evolution', *Applied Surface Science,* 253, 2189–95.

195. Simwonis, D., Tietz, F., and Stover, D. (2000), 'Nickel coarsening in annealed Ni/8YSZ anode substrates for solid oxide fuel cells', *Solid State Ionics,* 132, 241-51.

196. Simwonis, D., et al. (1999), 'Properties of Ni/YSZ porous cermets for SOFC anode substrates prepared by tape casting and coat-mix process', *Journal of Materials Processing Technology,* 92-93, 107-11.

197. Singhal, S. C. (2000), 'Advances in solid oxide fuel cell technology', *Solid State Ionics,* 135, 305–13.

198. Singhal, S. C. (2002), 'Solid oxide fuel cells for stationary, mobile, and military applications', *Solid State Ionics,* 152–153, 405– 10.

199. Smil, V. (1997), 'Global Population and the Nitrogen Cycle', *Scientific American*, July, 76.

200. Song, J-H., et al. (2008), 'Fabrication characteristics of an anode-supported thin-film electrolyte fabricated by the tape casting method for IT-SOFC', *Journal of Materials Processing Technology*, 198, 414–18.

201. Staia, M.H., et al. (1997), 'Characterisation of Ni-P Electroless Deposites with Moderate Phosphorus Content', *Surface Engineering,* 13 (4), 335-38.

202. Steele, B. C. H. (2000), 'Materials for IT-SOFC stacks 35 years R&D: the inevitability of gradualness?', *Solid State Ionics*, 134, 3-20.

203. Stöver, D., et al. (2006), 'Plasma-sprayed components for SOFC applications', *Surface & Coatings Technology,* 201, 2002-05.

204. Suciu, C., et al. (2008), 'NiO/YSZ nanoparticles obtained by new sol–gel route', *Chemical Engineering Journal*, 140, 586–92.

205. Suda, S., et al. (2006), 'Preparation of SOFC anode composites by spray pyrolysis', *Journal of the European Ceramic Society,* 26, 593-97.

206. Sukuma, K. and Shimada, M. (1985), 'Strength, fracture toughness and vickers hardness of CeO_2-stabilised ZrO_2 polycrystals (Ce-TZP)', *Journal of Materials Science*, 20, 1178-84.

207. Sun, C. and Stimming, U. (2007), 'Recent anode advances in solid oxide fuel cells', *Journal of Power Sources*, 171, 247–60.

208. Suzuki, S., Uchida, H., and Watanabe, M. (2006), 'Interaction of samaria-doped ceria anode with highly dispersed Ni catalysts in a medium-temperature solid oxide fuel cell during long-term operation', *Solid State Ionics,* 177, 359-65.

209. Szczygiel, B., Turkiewicz, A., and Serafinczuk, J. (2008), 'Surface morphology and structure of Ni-P, Ni-P-ZrO_2, Ni-W-P, Ni-W-P-ZrO_2', *Surface & Coating Technology,* 202 (9), 1904-10.

210. Taheri, R., Oguocha, I. N. A., and Yannacopoulos, S. (2001), 'The tribological characteristics of electroless NiP coatings', *Wear,* 249, 389–96.

211. Taheri, R. (2002), 'Evaluation of Electroless Nickel-Phosphorus (EN) Coatings', *PhD Thesis, University of Saskatchewan, Saskaton,* 240.

212. Teixeira, L. A. C. and Santini, M. C. (2005), 'Surface Conditioning of ABS for Metallisation into the use of Chromium baths', *Journal of Materials Processing Technology,* 170, 37–41.

213. Tietz, F., Buchkremer, H-P., and Stover, D. (2002), 'Components manufacturing for solid oxide fuel cells', *Solid State Ionics*, 152-153, 373-81.

214. Tsipis, E. V., Kharton, V. V., and Frade, J. R. (2005), 'Mixed conducting components of solid oxide fuel cell anodes', *Journal of the European Ceramic Society,* 25, 2623-26.

215. Tucker, M. C., et al. (2010), 'Cu–YSZ cermet solid oxide fuel cell anode prepared by high-temperature sintering', *Journal of Power Sources,* 195, 3119–23.

216. Ukai, K., Mizutani, Y., and Kume, Y. (2001), 'Current status of SOFC development using scandia doped zirconia', *SOFC VII.*

217. Upton, G. and Cook, I. (1966), *Understanding Statistics* (Oxford: Oxford University Press) 657.

218. Vaghefi, S. M. M., Saatchi, A., and Ebrahimian-Hoseinabadi, M. (2003), 'Deposition and properties of electroless Ni-P-B_4C composite coatings', *Surface and Coatings Technology,* 168, 259-62.

219. Vaghefi, S. M. M., Saatchi, A, Hejazi, J. (1997), 'The effect of agitation on electroless nickel-phosphorus-molybdenum disulfide composite plating', *Metal Finishing*, 95 (6), 102

220. Viksman, G. Sh. and Gordienko, S.P. (1992), 'Behavior in vacuum at high temperatures and thermodynamic properties of nickel phosphide Ni_3P', *Poroshkovskaya Metallurgiya,* 12 (360), 70-72.

221. Virkar, A. V., et al. (2000), 'The role of electrode microstructure on activation and concentration polarizations in solid oxide fuel cells', *Solid State Ionics,* 131, 189-98.

222. Wahdame, B., et al. (2009), 'Design of experiment techniques for fuel cell characterisation and development', *International Journal of Hydrogen Energy,* 34, 967-80.

223. Wang, F. H., et al. (2004), 'Preparation and properties of Ni/YSZ anode by coating precipitation method', *Materials Letters,* 58, 3079-83.

224. Wang, J., Zheng, X. H., and Stevens, R. (1992), 'Fabrication and microstructure-mechanical property relationships in Ce-TZPs ', *Journal of Materials Science,* 27, 5348-56.

225. Wang, J., et al. (2006a), 'Study of slurry spin coating technique parameters for the fabrication of anode-supported YSZ Films for SOFCs', *Journal of Power Sources,* 164, 17–23.

226. Wang, W., et al. (2006b), 'GDC-impregnated Ni anodes for direct utilization of methane in solid oxide fuel cells', *Journal of Power Sources,* 159, 68-72.

227. Wang, W., et al. (2010), 'A comprehensive evaluation of a Ni–Al_2O_3 catalyst as a functional layer of solid-oxide fuel cell anode', *Journal of Power Sources,* 195, 402–11.

228. Wang, Y., et al. (2006c), 'Effects of powder sizes and reduction parameters on the strength of Ni–YSZ anodes', *Solid State Ionics,* 177, 1517-27.

229. Wei-sheng, X., et al. (2009), 'Fabrication and electrochemical performance of solid oxide fuel cell components by atmospheric and suspension plasma spray', *Transactions of Nonferrous Metals Society of China,* 19, 1539-44.

230. Weins, Ben (2010), 'The Future of Fuel Cells', *Innovating Through Synergy BenWeins Innovation Consultant* (updated 11 August 2008) <http://www.benweins.com/energy4.html>, accessed 12 Jan 2010.

231. Wen, G., Guo, Z. X., and Davies, C. K. L. (2000), 'Microstructural characteristion of electroless-nickel coatings on zirconia powder', *Scripta materialia,* 43, 307-11.

232. Williams, L. O. (1994), 'A Chemical Fuel is Required', *Applied Energy,* 47, 169-82.

233. Williams, M. C., et al. (2006), 'Solid oxide fuel cell technology development in the U.S.', *Solid State Ionics,* 177, 2039–44.

234. Wincewicz, K. C. and Cooper, J. S. (2005), 'Taxonomies of SOFC material and manufacturing alternatives', *Journal of Power Sources,* 140, 280-96.

235. Woll, R. and Burkhard, C. (2005), 'Full Factorial Design, Taguchi Design or Genetic Algorithms — Teaching Different Approaches to Design of Experiments', *Innovations in Classification, Data Science, and Information Systems* (Springer Berlin Heidelberg), 567-74.

236. Wu, Y., et al. (2006), 'The tribological behaviour of electroless Ni–P–Gr–SiC composite', *Wear,* 261, 201–07.

237. Xie, Z., et al. (2006), '$Ni_{1-x}Cu_x$ alloy-based anodes for low-temperature solid oxide fuel cells with biomass-produced gas as fuel', *Journal of Power Sources*, 161, 1056-61.

238. Xin, X., et al. (2006), 'Anode-supported solid oxide fuel cell based on dense electrolyte membrane fabricated by filter-coating', *Journal of Power Sources*, 159, 1158-61.

239. Yamamoto, O. (2000), 'Solid oxide fuel cells: fundamental aspects and prospects', *Electrochimica Acta*, 45, 2423-35.

240. Yin, Y., et al. (2006), 'Electrochemical performance of gel-cast NiO–SDC composite anodes in low-temperature SOFCs', *Electrochimica Acta*, 51, 2594-98.

241. Yoo, Y. (2006), 'Fabrication and characterisation of thin film electrolytes deposited by RF magnetron sputtering for low temperature solid oxide fuel cells', *Journal of Power Sources*, 160, 202-06.

242. Yu, J. H., et al. (2006), 'Microstructural effects on the electrical and mechanical properties of Ni–YSZ cermet for SOFC anode', *Journal of Power Sources*, 163, 926–32.

243. Zhang, C., et al. (2010), 'Improving single-chamber performance of an anode-supported SOFC by impregnating anode with active nickel catalyst', *International Journal of Hydrogen Energy*, In Press, Corrected Proof, 1-6.

244. Zhu, W. Z. and Deevi, S. C. (2003), 'A review on the status of anode materials for solid oxide fuel cells', *Materials Science and Engineering*, A362, 228-39.

245. Zuleta, A. A., et al. (2009), 'Preparation and characterization of electroless Ni–P–Fe_3O_4 composite coatings and evaluation of its high temperature oxidation behaviour', *Surface & Coatings Technology*, 203, 3569–78.

BIBLIOGRAPHY

1. Apte, P. R. (2009), 'A 3-Day Course on DOE/Taguchi Method for Process and Product Optimisation in Micro Electronics and Packaging', (Bangi: Universiti Kebangsaan Malaysia).
2. Bengisu, M. (2001), *Engineering Ceramics* (Springer) 620.
3. Brase, C. H. and Brase, C. P. (2001), *Understanding Basic Statistics* (Second edition); Boston: Houghton Mifflin Company, 588.
4. Charlie (2008), 'Design of Experiment - DOE', (updated 25 December 2002), accessed 12 March 2008.
5. Davies, P. (2006), 'BP Statistical Review of World Energy 2006 Quantifying Energy', (London: British Petroleum), 27.
6. defra (2007), 'Sustainable development indicators in your pocket 2007', in Department for Environment Food and Rural Affair (ed.), (London: National Statistic Publication), 1-132.
7. Divisek, J., et al. (1994), 'The kinetics of electrochemical reactions on high temperature fuel cell electrodes', *Journal of Power Sources,* 49, 257-70.
8. Divisek, J., Jung, R., and Vinke, I.C. (1999), 'Structure investigations of SOFC anode cermets Part II: Electrochemical and mass transport properties', *Journal of Applied Electrochemistry,* 29, 165-70.
9. Flavin, C. (1994), 'Alternative Energy Sources', *Applied Energy,* 47, 123-46.
10. Folklore, A. (1994), 'Implementation', *Applied Energy,* 47, 265-98.
11. Gardner, P., et al. (2007), 'Wind Energy - The Fact', (Brussel: The European Wind Energy Association), 1-14.
12. Harry, K. G. and Johnson, A. (2004), 'A non-destructive technique for measuring ceramic porosity using liquid nitrogen', *Journal of Archeological Science,* 34 (31), 1567-75.
13. Huijsmans, J. P. P. (2001), 'Ceramics in solid oxide fuel cells', *Current Opinion in Solid State and Materials Science,* 5, 317–23.
14. Jiang, S. P. and Chan, S. H. (2004), 'A review of anode materials development in solid oxide fuel cells', *Journal of Materials Science,* 39, 4405-39.
15. Ma, H., et al. (2010), 'A survey of China's renewable energy economy', *Renewable and Sustainable Energy Reviews,* 14, 438–45.
16. Park, S. H. (1996), *Robust Design and Analysis for Quality Engineering* (First edn.; London: Chapman & Hall) 329.

PROJECT PLANNING CHART

	Month			1	2	3	4	5	6	7	8	9	10	11	12	13	14	15	16	17	18	19	20	21	22	23	24
	Year			2006			2007												2008								
No.	Tasks			Oct	Nov	Dec	Jan	Feb	Mar	Apr	May	Jun	Jul	Aug	Sep	Oct	Nov	Dec	Jan	Feb	Mar	Apr	May	Jun	Jul	Aug	Sep
1	*Literature Background*																										
1.1	Fuel Cell	1.1.1	Type & characterisation	X	X	X																					
		1.1.2	Solid Oxide Fuel Cell (SOFC)		X	X																					
		1.1.3	SOFC Electrolyte				X	X																			
		1.1.4	SOFC Cathode					X	X																		
		1.1.5	SOFC Anode						X	X																	
		1.1.6	SOFC anode properties								X	X	X														
1.2	Processing	1.2.1	Conventional									X	X	X													
		1.2.2	Advanced Materials Processing										X	X													
		1.2.3	Electroless Nickel coating												X	X	X	X									
1.3	DOE	1.3.1	Planning																				X				
		1.3.2	Designing																				X	X			
		1.3.3	Analysing																					X	X	X	
2	*Sample/Chemical preparation*																										
2.1	Substrate	2.1.1	Cutting																X							X	
		2.1.2	Measuring dimension & thickness																	X							X
		2.1.3	Surface Treatment																					X	X		
2.2	Chemicals																		X				X			X	
3	*Tests*																										
3.1	Characterisation	3.1.1	SEM-EDXA																		X		X				
		3.1.2	Image Pro-plus																			X					
3.2	Physical	3.2.1	Archimedes density																						X	X	X
		3.2.2	Microporosimetry																								
		3.2.3	Profilometry																							X	X
4	*Experimental work*																										
4.1	OFAAT	4.1.1	Particle size																	X							
		4.1.2	Types of ceramic																		X						
		4.1.3	Bath pH																		X						
		4.1.4	Bath agitation																	X							
		4.1.5	Surface treatment																			X					
		4.1.6	Coating time																				X				
		4.1.7	Bath loading																					X			
		4.1.8	Bath volume																					X			
		4.1.9	Sample placement																		X						
4.2	DOE																									X	X
5	*Data analysis*																										
5.1	OFAAT																					X	X			X	
5.2	DOE	5.2.1	EDXA Ni:YSZ																								
		5.2.2	Image Pro-plus Ni:YSZ																								
		5.2.3	Archimedes																								
		5.2.4	Porosimetry																								
6	*Writing up*																										
6.1	Transfer Report																					X	X	X	X		
6.2	Thesis	6.2.1	Draft																								
		6.2.2	Final																								
7	*Publications*																										
7.1	Conferences																										
7.2	Journal																										

	Month			25	26	27	28	29	30	31	32	33	34	35	36	37	38	39	40	41	42	43	44	45	46	47	48
	Year			**2008**			**2009**												**2010**								
No.	**Tasks**			Oct	Nov	Dec	Jan	Feb	Mar	Apr	May	Jun	Jul	Aug	Sep	Oct	Nov	Dec	Jan	Feb	Mar	Apr	May	Jun	Jul	Aug	Sep
1	*Literature Background*																										
1.1	Fuel Cell	1.1.1	Type & characterisation												X												
		1.1.2	Solid Oxide Fuel Cell (SOFC)												X	X											
		1.1.3	SOFC Electrolyte													X	X										
		1.1.4	SOFC Cathode														X										
		1.1.5	SOFC Anode														X	X	X								
		1.1.6	SOFC anode properties															X	X	X							
1.2	Processing	1.2.1	Conventional																X								
		1.2.2	Advanced Materials Processing																X	X							
		1.2.3	Electroless Nickel coating																	X	X	X					
1.3	DOE	1.3.1	Planning																	X							
		1.3.2	Designing																		X						
		1.3.3	Analysing						X	X	X	X	X									X					
2	*Sample/ Chemical preparation*																										
2.1	Substrate	2.1.1	Cutting																								
		2.1.2	Measuring dimension & thickness	X		X																					
		2.1.3	Surface Treatment																								
2.2	Chemical				X																						
3	*Tests*																										
3.1	Characterisation	3.1.1	SEM-EDXA	X	X	X	X																				
		3.1.2	Image Pro-plus		X	X		X																			
3.2	Physical	3.2.1	Archimedes density			X																					
		3.2.2	Microporosimetry											X	X	X	X	X	X								
		3.2.3	Profilometry		X		X																				
4	*Experimental work*																										
4.1	OFAAT	4.1.1	Particle size																								
		4.1.2	Types of ceramic																								
		4.1.3	Bath pH																								
		4.1.4	Bath agitation																								
		4.1.5	Surface treatment																								
		4.1.6	Coating time																								
		4.1.7	Bath loading																								
		4.1.8	Bath volume																								
		4.1.9	Sample placement																								
4.2	DOE			X	X	X	X																				
5	*Data analysis*																										
5.1	OFAAT								X	X	X																
5.2	DOE	5.2.1	EDXA Ni:YSZ								X	X	X	X	X	X											
		5.2.2	Image Pro-plus Ni:YSZ															X	X	X	X						
		5.2.3	Archimedes													X	X	X									
		5.2.4	Porosimetry																		X	X	X				
6	*Writing up*																										
6.1	Transfer Report																										
6.2	Thesis	6.2.1	Draft																		X	X	X	X			
		6.2.2	Final																						X		
7	*Publications*																										
7.1	Conferences						X									X	X	X		X							
7.2	Journal																						X				

APPENDICES

Appendix A (Baudrand 1994)

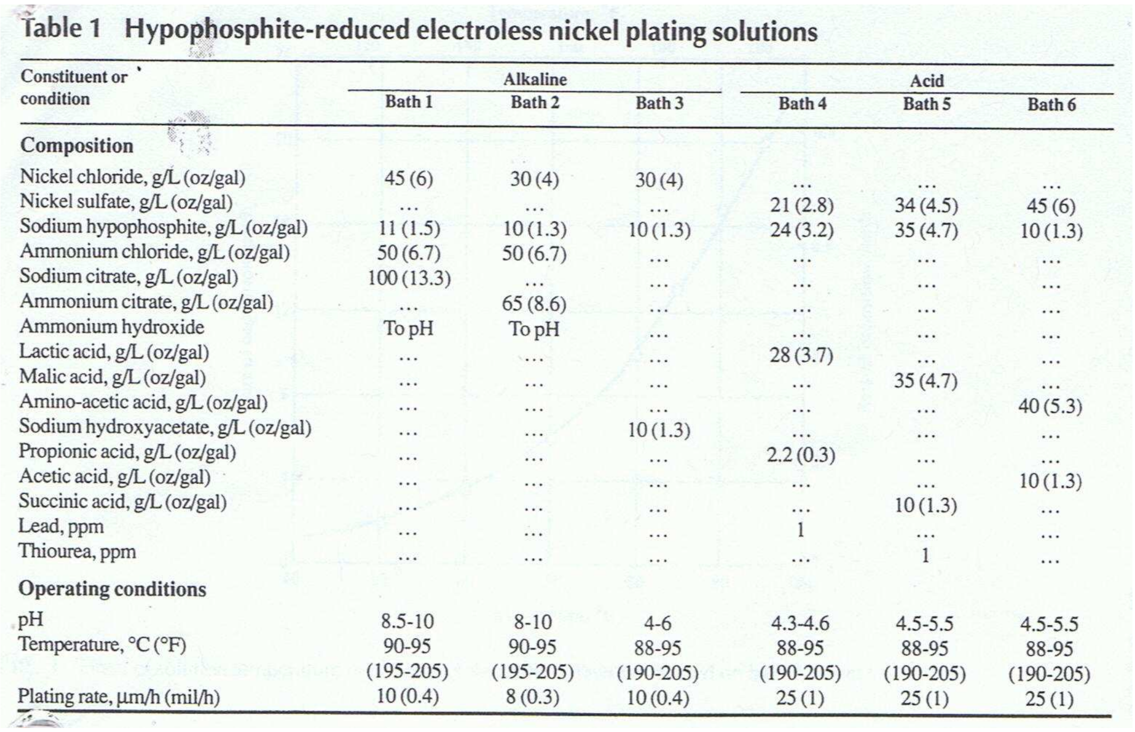

Table 1 Hypophosphite-reduced electroless nickel plating solutions

Constituent or condition	Alkaline			Acid		
	Bath 1	Bath 2	Bath 3	Bath 4	Bath 5	Bath 6
Composition						
Nickel chloride, g/L (oz/gal)	45 (6)	30 (4)	30 (4)	…	…	…
Nickel sulfate, g/L (oz/gal)	…	…	…	21 (2.8)	34 (4.5)	45 (6)
Sodium hypophosphite, g/L (oz/gal)	11 (1.5)	10 (1.3)	10 (1.3)	24 (3.2)	35 (4.7)	10 (1.3)
Ammonium chloride, g/L (oz/gal)	50 (6.7)	50 (6.7)	…	…	…	…
Sodium citrate, g/L (oz/gal)	100 (13.3)	…	…	…	…	…
Ammonium citrate, g/L (oz/gal)	…	65 (8.6)	…	…	…	…
Ammonium hydroxide	To pH	To pH	…	…	…	…
Lactic acid, g/L (oz/gal)	…	…	…	28 (3.7)	…	…
Malic acid, g/L (oz/gal)	…	…	…	…	35 (4.7)	…
Amino-acetic acid, g/L (oz/gal)	…	…	…	…	…	40 (5.3)
Sodium hydroxyacetate, g/L (oz/gal)	…	…	10 (1.3)	…	…	…
Propionic acid, g/L (oz/gal)	…	…	…	2.2 (0.3)	…	…
Acetic acid, g/L (oz/gal)	…	…	…	…	…	10 (1.3)
Succinic acid, g/L (oz/gal)	…	…	…	…	10 (1.3)	…
Lead, ppm	…	…	…	1	…	…
Thiourea, ppm	…	…	…	…	1	…
Operating conditions						
pH	8.5-10	8-10	4-6	4.3-4.6	4.5-5.5	4.5-5.5
Temperature, °C (°F)	90-95 (195-205)	90-95 (195-205)	88-95 (190-205)	88-95 (190-205)	88-95 (190-205)	88-95 (190-205)
Plating rate, µm/h (mil/h)	10 (0.4)	8 (0.3)	10 (0.4)	25 (1)	25 (1)	25 (1)

Appendix B (Baudrand 1994)

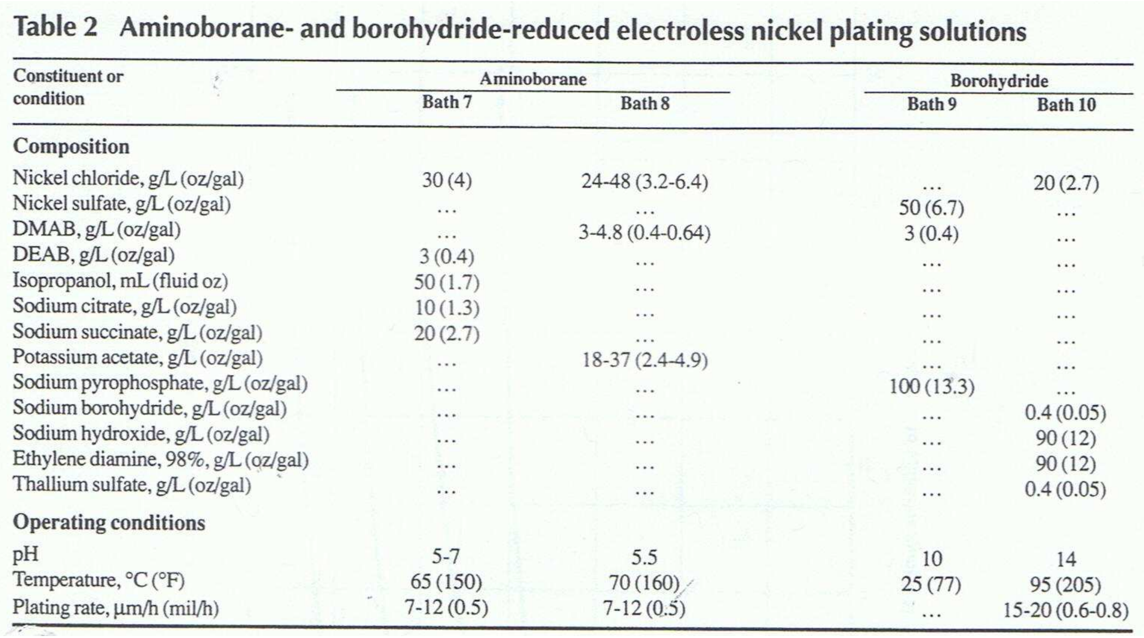

Table 2 Aminoborane- and borohydride-reduced electroless nickel plating solutions

Constituent or condition	Aminoborane		Borohydride	
	Bath 7	Bath 8	Bath 9	Bath 10
Composition				
Nickel chloride, g/L (oz/gal)	30 (4)	24-48 (3.2-6.4)	...	20 (2.7)
Nickel sulfate, g/L (oz/gal)	...	...	50 (6.7)	...
DMAB, g/L (oz/gal)	...	3-4.8 (0.4-0.64)	3 (0.4)	...
DEAB, g/L (oz/gal)	3 (0.4)	...	...	...
Isopropanol, mL (fluid oz)	50 (1.7)	...	...	...
Sodium citrate, g/L (oz/gal)	10 (1.3)	...	...	...
Sodium succinate, g/L (oz/gal)	20 (2.7)	...	...	...
Potassium acetate, g/L (oz/gal)	...	18-37 (2.4-4.9)	...	...
Sodium pyrophosphate, g/L (oz/gal)	...	...	100 (13.3)	...
Sodium borohydride, g/L (oz/gal)	...	...	...	0.4 (0.05)
Sodium hydroxide, g/L (oz/gal)	...	...	...	90 (12)
Ethylene diamine, 98%, g/L (oz/gal)	...	...	...	90 (12)
Thallium sulfate, g/L (oz/gal)	...	...	...	0.4 (0.05)
Operating conditions				
pH	5-7	5.5	10	14
Temperature, °C (°F)	65 (150)	70 (160)	25 (77)	95 (205)
Plating rate, µm/h (mil/h)	7-12 (0.5)	7-12 (0.5)	...	15-20 (0.6-0.8)

Appendix C (Callister 2006)

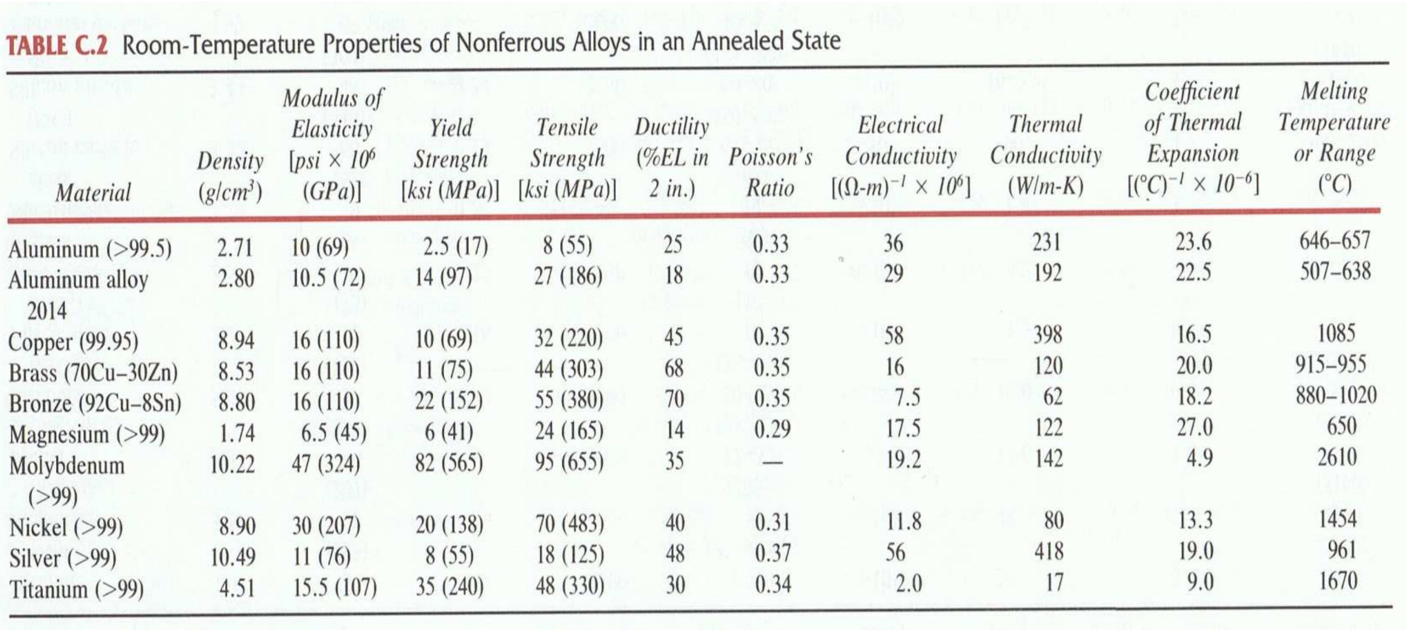

TABLE C.2 Room-Temperature Properties of Nonferrous Alloys in an Annealed State

Material	*Density* (g/cm^3)	*Modulus of Elasticity* $[psi \times 10^6$ $(GPa)]$	*Yield Strength* [*ksi (MPa)*]	*Tensile Strength* [*ksi (MPa)*]	*Ductility* (*%EL in 2 in.*)	*Poisson's Ratio*	*Electrical Conductivity* $[(\Omega\text{-}m)^{-1} \times 10^6]$	*Thermal Conductivity* (*W/m-K*)	*Coefficient of Thermal Expansion* $[(°C)^{-1} \times 10^{-6}]$	*Melting Temperature or Range* (*°C*)
Aluminum (>99.5)	2.71	10 (69)	2.5 (17)	8 (55)	25	0.33	36	231	23.6	646–657
Aluminum alloy 2014	2.80	10.5 (72)	14 (97)	27 (186)	18	0.33	29	192	22.5	507–638
Copper (99.95)	8.94	16 (110)	10 (69)	32 (220)	45	0.35	58	398	16.5	1085
Brass (70Cu–30Zn)	8.53	16 (110)	11 (75)	44 (303)	68	0.35	16	120	20.0	915–955
Bronze (92Cu–8Sn)	8.80	16 (110)	22 (152)	55 (380)	70	0.35	7.5	62	18.2	880–1020
Magnesium (>99)	1.74	6.5 (45)	6 (41)	24 (165)	14	0.29	17.5	122	27.0	650
Molybdenum (>99)	10.22	47 (324)	82 (565)	95 (655)	35	—	19.2	142	4.9	2610
Nickel (>99)	8.90	30 (207)	20 (138)	70 (483)	40	0.31	11.8	80	13.3	1454
Silver (>99)	10.49	11 (76)	8 (55)	18 (125)	48	0.37	56	418	19.0	961
Titanium (>99)	4.51	15.5 (107)	35 (240)	48 (330)	30	0.34	2.0	17	9.0	1670

Appendix D (Bisgaard 1998)

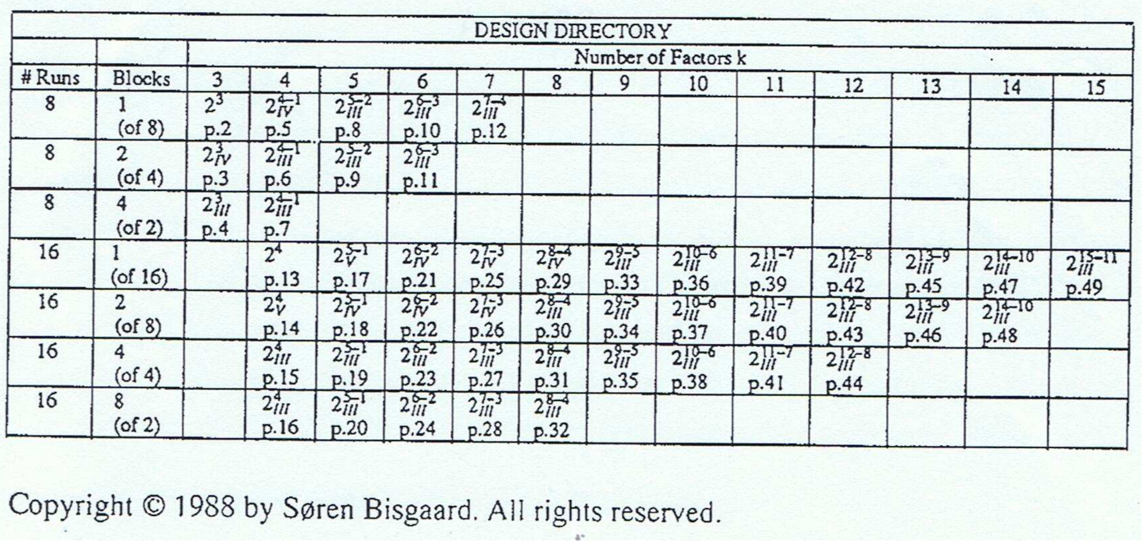

DESIGN DIRECTORY														
		Number of Factors k												
# Runs	Blocks	3	4	5	6	7	8	9	10	11	12	13	14	15
8	1 (of 8)	2^3 p.2	2^{4-1}_{IV} p.5	2^{5-2}_{III} p.8	2^{6-3}_{III} p.10	2^{7-4}_{III} p.12								
8	2 (of 4)	2^3_{IV} p.3	2^{4-1}_{III} p.6	2^{5-2}_{III} p.9	2^{6-3}_{III} p.11									
8	4 (of 2)	2^3_{III} p.4	2^{4-1}_{III} p.7											
16	1 (of 16)		2^4 p.13	2^{5-1}_{V} p.17	2^{6-2}_{IV} p.21	2^{7-3}_{IV} p.25	2^{8-4}_{IV} p.29	2^{9-5}_{III} p.33	2^{10-6}_{III} p.36	2^{11-7}_{III} p.39	2^{12-8}_{III} p.42	2^{13-9}_{III} p.45	2^{14-10}_{III} p.47	2^{15-11}_{III} p.49
16	2 (of 8)		2^4_{V} p.14	2^{5-1}_{IV} p.18	2^{6-2}_{IV} p.22	2^{7-3}_{IV} p.26	2^{8-4}_{III} p.30	2^{9-5}_{III} p.34	2^{10-6}_{III} p.37	2^{11-7}_{III} p.40	2^{12-8}_{III} p.43	2^{13-9}_{III} p.46	2^{14-10}_{III} p.48	
16	4 (of 4)		2^4_{III} p.15	2^{5-1}_{III} p.19	2^{6-2}_{III} p.23	2^{7-3}_{III} p.27	2^{8-4}_{III} p.31	2^{9-5}_{III} p.35	2^{10-6}_{III} p.38	2^{11-7}_{III} p.41	2^{12-8}_{III} p.44			
16	8 (of 2)		2^4_{III} p.16	2^{5-1}_{III} p.20	2^{6-2}_{III} p.24	2^{7-3}_{III} p.28	2^{8-4}_{III} p.32							

Appendix E

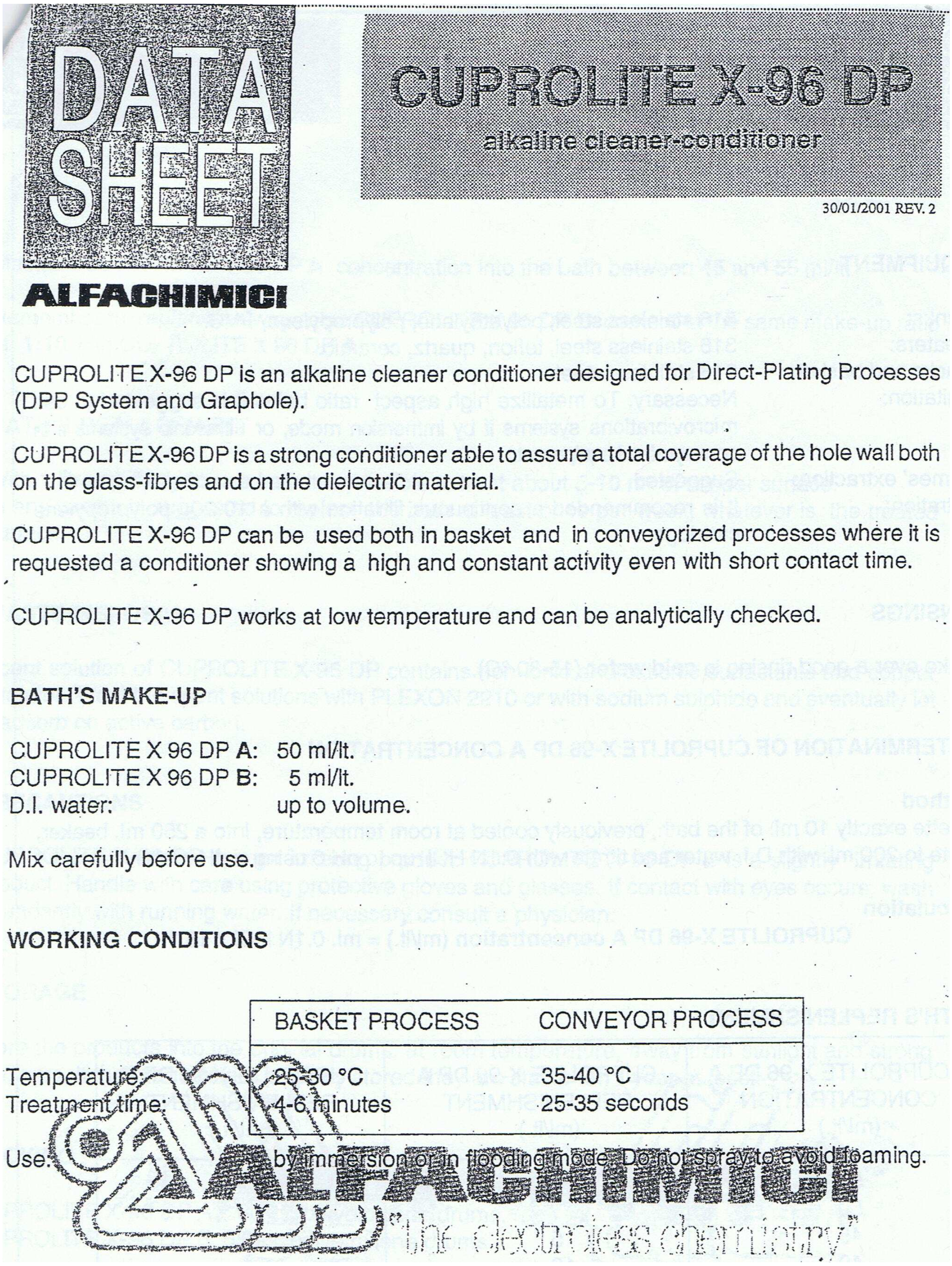

DATA SHEET

CUPROLITE X-96 DP

alkaline cleaner-conditioner

30/01/2001 REV. 2

ALFACHIMICI

CUPROLITE X-96 DP is an alkaline cleaner conditioner designed for Direct-Plating Processes (DPP System and Graphole).

CUPROLITE X-96 DP is a strong conditioner able to assure a total coverage of the hole wall both on the glass-fibres and on the dielectric material.

CUPROLITE X-96 DP can be used both in basket and in conveyorized processes where it is requested a conditioner showing a high and constant activity even with short contact time.

CUPROLITE X-96 DP works at low temperature and can be analytically checked.

BATH'S MAKE-UP

CUPROLITE X 96 DP A:	50 ml/lt.
CUPROLITE X 96 DP B:	5 ml/lt.
D.I. water:	up to volume.

Mix carefully before use.

WORKING CONDITIONS

	BASKET PROCESS	CONVEYOR PROCESS
Temperature:	25-30 °C	35-40 °C
Treatment time:	4-6 minutes	25-35 seconds

Use: by immersion or in flooding mode. Do not spray to avoid foaming.

ALFACHIMICI "the electroless chemistry"

Appendix F

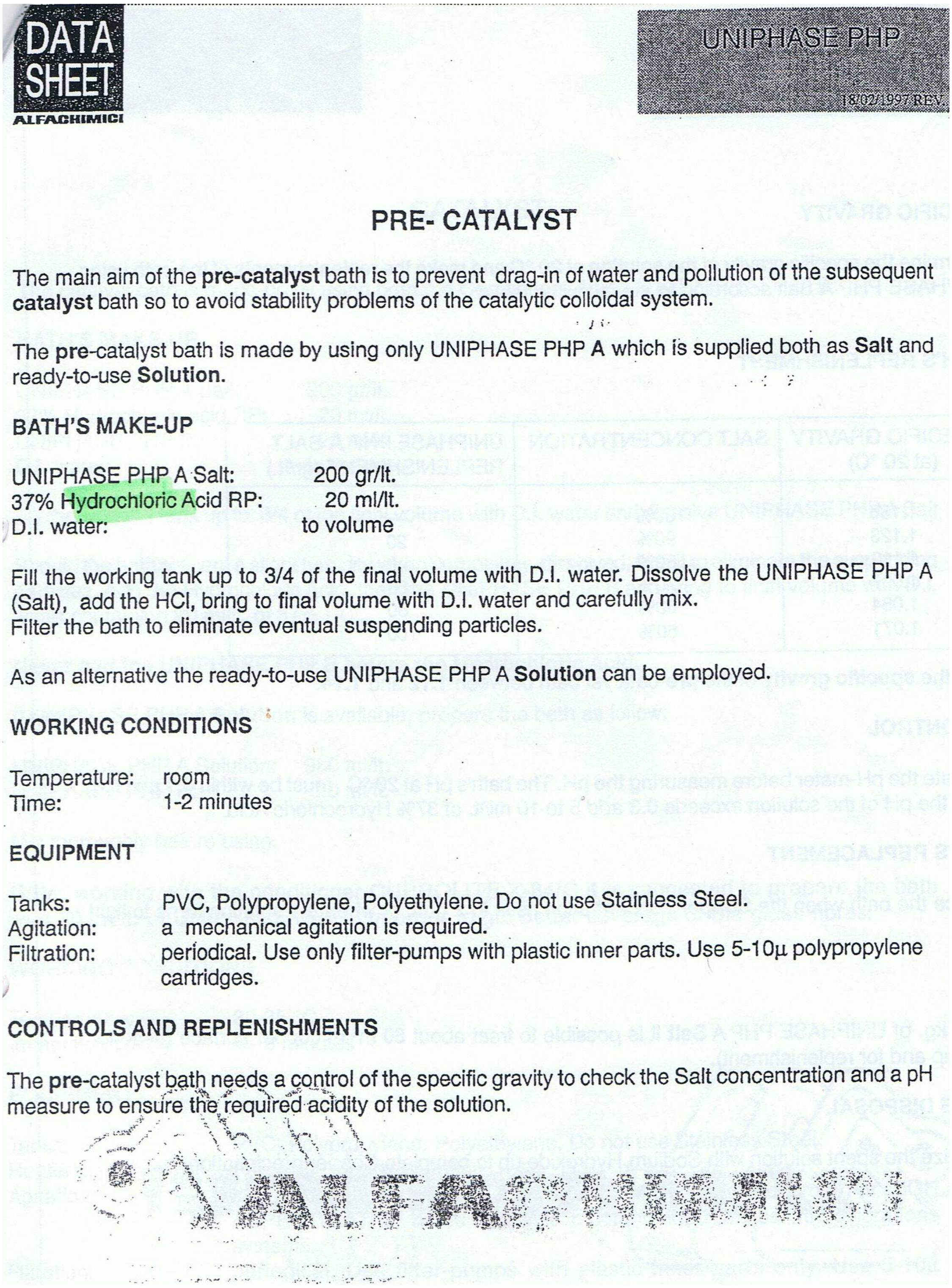

DATA SHEET
ALFACHIMICI

UNIPHASE PHP
18/02/1997 REV.

PRE- CATALYST

The main aim of the **pre-catalyst** bath is to prevent drag-in of water and pollution of the subsequent **catalyst** bath so to avoid stability problems of the catalytic colloidal system.

The **pre**-catalyst bath is made by using only UNIPHASE PHP A which is supplied both as **Salt** and ready-to-use **Solution**.

BATH'S MAKE-UP

UNIPHASE PHP A Salt:	200 gr/lt.
37% Hydrochloric Acid RP:	20 ml/lt.
D.I. water:	to volume

Fill the working tank up to 3/4 of the final volume with D.I. water. Dissolve the UNIPHASE PHP A (Salt), add the HCl, bring to final volume with D.I. water and carefully mix.
Filter the bath to eliminate eventual suspending particles.

As an alternative the ready-to-use UNIPHASE PHP A **Solution** can be employed.

WORKING CONDITIONS

Temperature:	room
Time:	1-2 minutes

EQUIPMENT

Tanks:	PVC, Polypropylene, Polyethylene. Do not use Stainless Steel.
Agitation:	a mechanical agitation is required.
Filtration:	periodical. Use only filter-pumps with plastic inner parts. Use 5-10µ polypropylene cartridges.

CONTROLS AND REPLENISHMENTS

The **pre**-catalyst bath needs a control of the specific gravity to check the Salt concentration and a pH measure to ensure the required acidity of the solution.

ALFACHIMICI

Appendix G

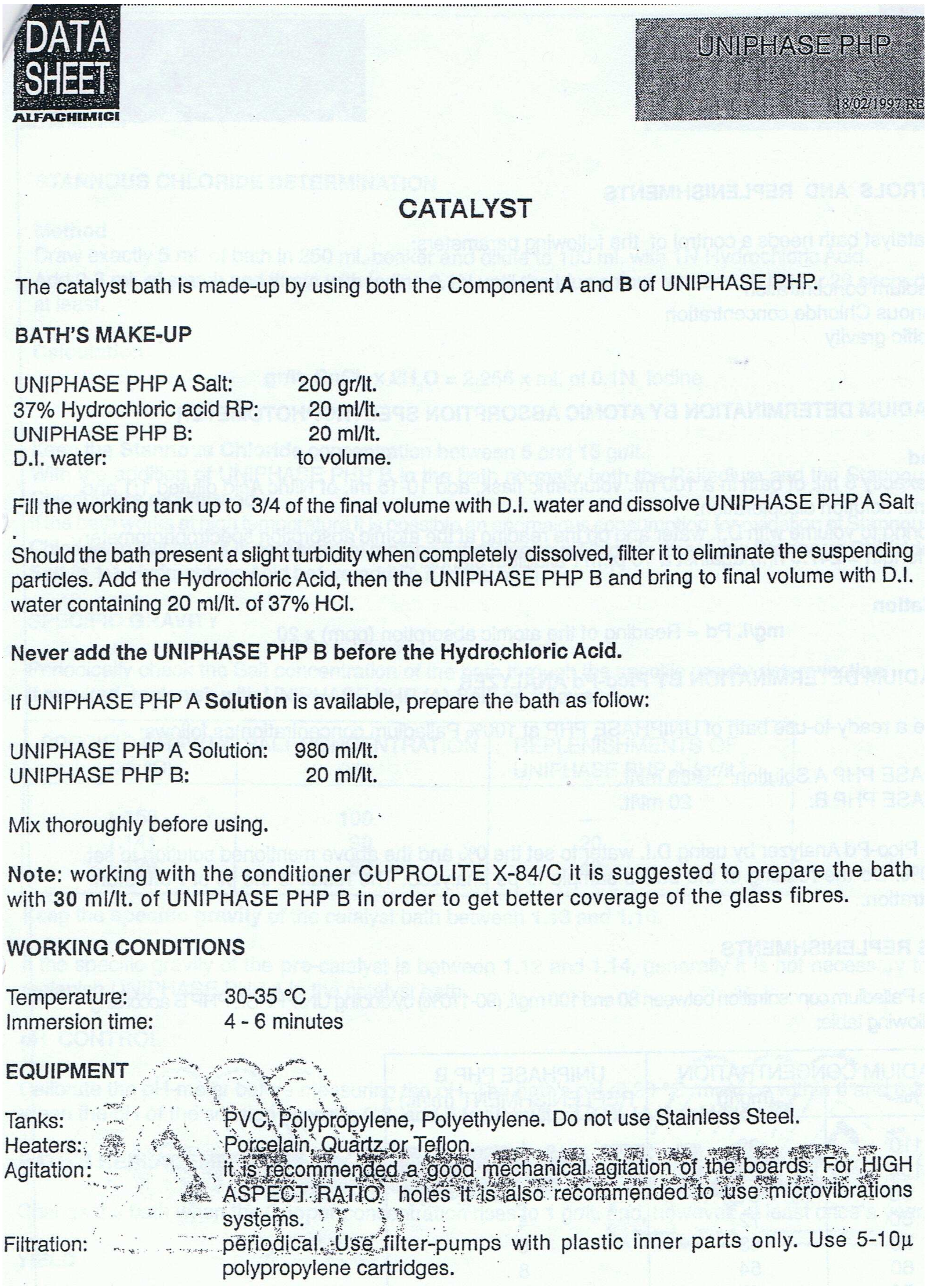

DATA SHEET
ALFACHIMICI

UNIPHASE PHP
18/02/1997 RE

CATALYST

The catalyst bath is made-up by using both the Component **A** and **B** of UNIPHASE PHP.

BATH'S MAKE-UP

UNIPHASE PHP A Salt:	200 gr/lt.
37% Hydrochloric acid RP:	20 ml/lt.
UNIPHASE PHP B:	20 ml/lt.
D.I. water:	to volume.

Fill the working tank up to 3/4 of the final volume with D.I. water and dissolve UNIPHASE PHP A Salt.

Should the bath present a slight turbidity when completely dissolved, filter it to eliminate the suspending particles. Add the Hydrochloric Acid, then the UNIPHASE PHP B and bring to final volume with D.I. water containing 20 ml/lt. of 37% HCl.

Never add the UNIPHASE PHP B before the Hydrochloric Acid.

If UNIPHASE PHP A **Solution** is available, prepare the bath as follow:

UNIPHASE PHP A Solution:	980 ml/lt.
UNIPHASE PHP B:	20 ml/lt.

Mix thoroughly before using.

Note: working with the conditioner CUPROLITE X-84/C it is suggested to prepare the bath with **30** ml/lt. of UNIPHASE PHP B in order to get better coverage of the glass fibres.

WORKING CONDITIONS

Temperature:	30-35 °C
Immersion time:	4 - 6 minutes

EQUIPMENT

Tanks:	PVC, Polypropylene, Polyethylene. Do not use Stainless Steel.
Heaters:	Porcelain, Quartz or Teflon.
Agitation:	it is recommended a good mechanical agitation of the boards. For HIGH ASPECT RATIO holes it is also recommended to use microvibrations systems.
Filtration:	periodical. Use filter-pumps with plastic inner parts only. Use 5-10µ polypropylene cartridges.

Appendix H

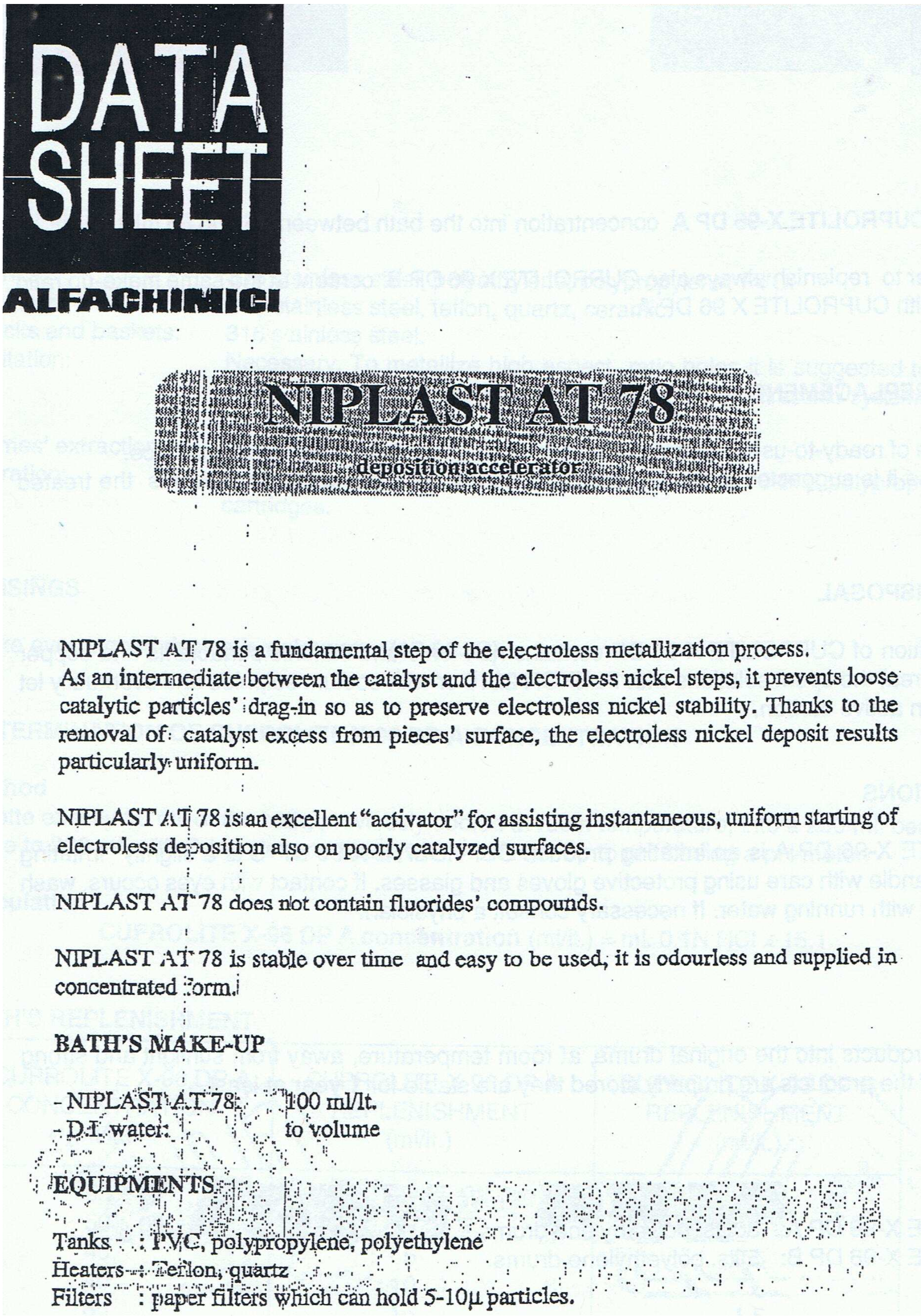

DATA SHEET

ALFACHIMICI

NIPLAST AT 78

deposition accelerator

NIPLAST AT 78 is a fundamental step of the electroless metallization process. As an intermediate between the catalyst and the electroless nickel steps, it prevents loose catalytic particles' drag-in so as to preserve electroless nickel stability. Thanks to the removal of catalyst excess from pieces' surface, the electroless nickel deposit results particularly uniform.

NIPLAST AT 78 is an excellent "activator" for assisting instantaneous, uniform starting of electroless deposition also on poorly catalyzed surfaces.

NIPLAST AT 78 does not contain fluorides' compounds.

NIPLAST AT 78 is stable over time and easy to be used, it is odourless and supplied in concentrated form.

BATH'S MAKE-UP

- NIPLAST AT 78: 100 ml/lt.
- D.I. water: to volume

EQUIPMENTS

Tanks : PVC, polypropylene, polyethylene
Heaters : Teflon, quartz
Filters : paper filters which can hold 5-10μ particles.

Appendix I

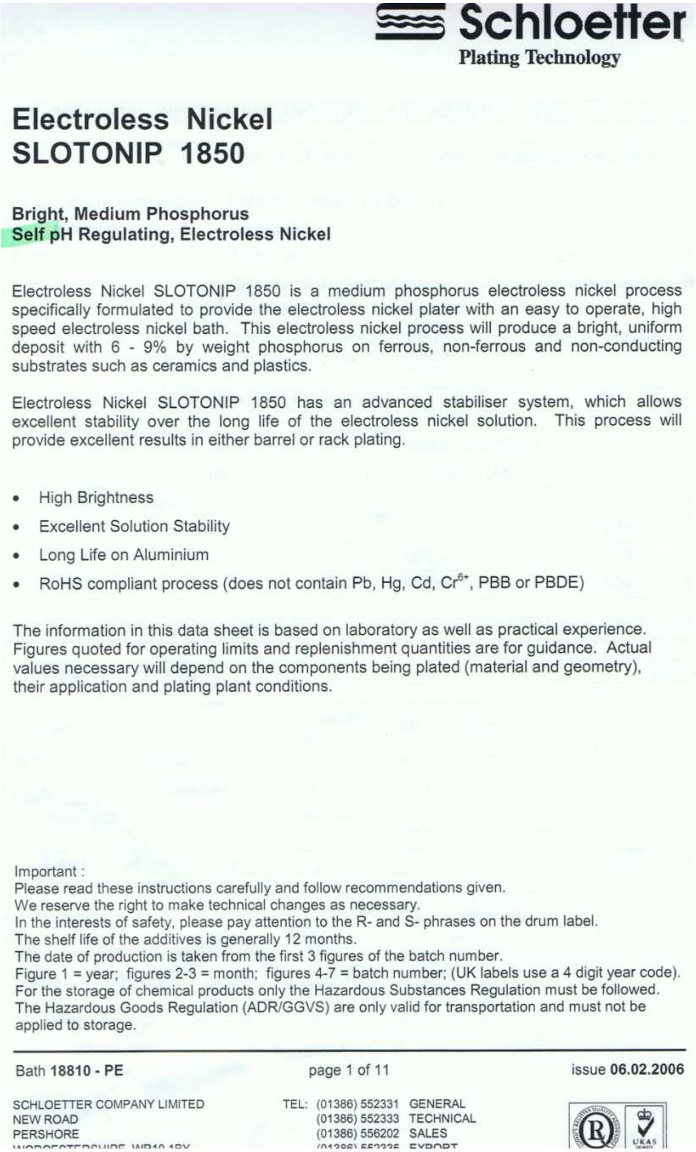

Schloetter
Plating Technology

Electroless Nickel
SLOTONIP 1850

Bright, Medium Phosphorus
Self pH Regulating, Electroless Nickel

Electroless Nickel SLOTONIP 1850 is a medium phosphorus electroless nickel process specifically formulated to provide the electroless nickel plater with an easy to operate, high speed electroless nickel bath. This electroless nickel process will produce a bright, uniform deposit with 6 - 9% by weight phosphorus on ferrous, non-ferrous and non-conducting substrates such as ceramics and plastics.

Electroless Nickel SLOTONIP 1850 has an advanced stabiliser system, which allows excellent stability over the long life of the electroless nickel solution. This process will provide excellent results in either barrel or rack plating.

- High Brightness
- Excellent Solution Stability
- Long Life on Aluminium
- RoHS compliant process (does not contain Pb, Hg, Cd, Cr^{6+}, PBB or PBDE)

The information in this data sheet is based on laboratory as well as practical experience. Figures quoted for operating limits and replenishment quantities are for guidance. Actual values necessary will depend on the components being plated (material and geometry), their application and plating plant conditions.

Important :
Please read these instructions carefully and follow recommendations given.
We reserve the right to make technical changes as necessary.
In the interests of safety, please pay attention to the R- and S- phrases on the drum label.
The shelf life of the additives is generally 12 months.
The date of production is taken from the first 3 figures of the batch number.
Figure 1 = year; figures 2-3 = month; figures 4-7 = batch number; (UK labels use a 4 digit year code).
For the storage of chemical products only the Hazardous Substances Regulation must be followed.
The Hazardous Goods Regulation (ADR/GGVS) are only valid for transportation and must not be applied to storage.

SCHLOETTER COMPANY LIMITED
NEW ROAD
PERSHORE

TEL: (01386) 552331 GENERAL
(01386) 552333 TECHNICAL
(01386) 556202 SALES

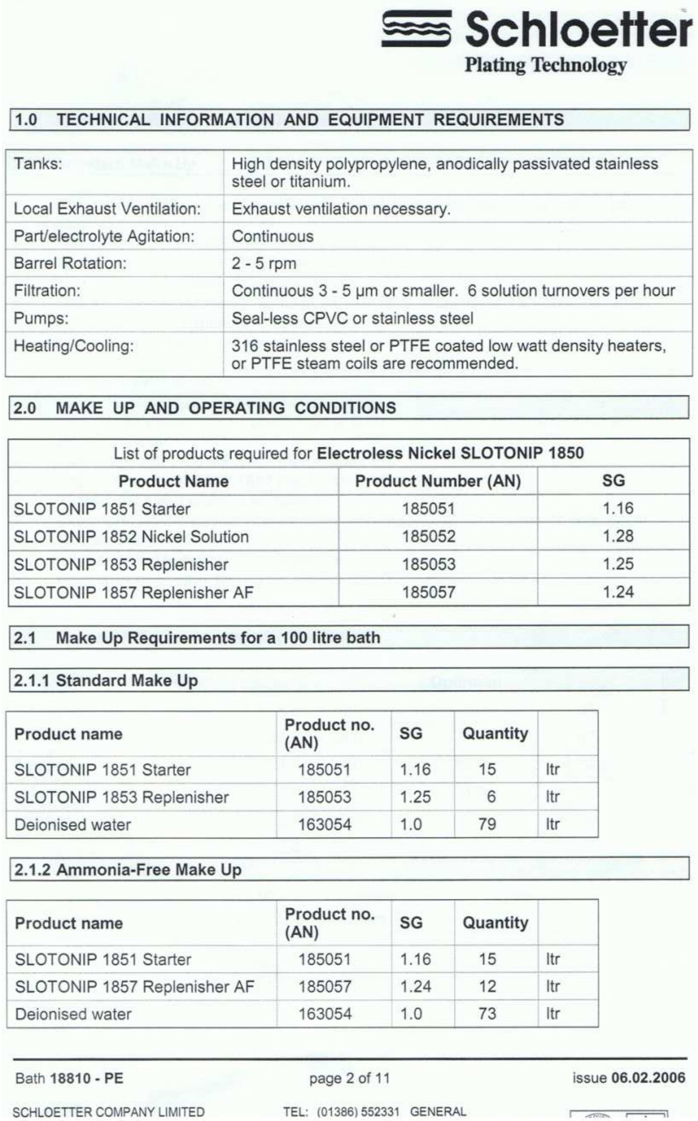

Schloetter
Plating Technology

1.0 TECHNICAL INFORMATION AND EQUIPMENT REQUIREMENTS

Tanks:	High density polypropylene, anodically passivated stainless steel or titanium.
Local Exhaust Ventilation:	Exhaust ventilation necessary.
Part/electrolyte Agitation:	Continuous
Barrel Rotation:	2 - 5 rpm
Filtration:	Continuous 3 - 5 µm or smaller. 6 solution turnovers per hour
Pumps:	Seal-less CPVC or stainless steel
Heating/Cooling:	316 stainless steel or PTFE coated low watt density heaters, or PTFE steam coils are recommended.

2.0 MAKE UP AND OPERATING CONDITIONS

List of products required for **Electroless Nickel SLOTONIP 1850**

Product Name	Product Number (AN)	SG
SLOTONIP 1851 Starter	185051	1.16
SLOTONIP 1852 Nickel Solution	185052	1.28
SLOTONIP 1853 Replenisher	185053	1.25
SLOTONIP 1857 Replenisher AF	185057	1.24

2.1 Make Up Requirements for a 100 litre bath

2.1.1 Standard Make Up

Product name	Product no. (AN)	SG	Quantity	
SLOTONIP 1851 Starter	185051	1.16	15	ltr
SLOTONIP 1853 Replenisher	185053	1.25	6	ltr
Deionised water	163054	1.0	79	ltr

2.1.2 Ammonia-Free Make Up

Product name	Product no. (AN)	SG	Quantity	
SLOTONIP 1851 Starter	185051	1.16	15	ltr
SLOTONIP 1857 Replenisher AF	185057	1.24	12	ltr
Deionised water	163054	1.0	73	ltr

SCHLOETTER COMPANY LIMITED TEL: (01386) 552331 GENERAL

Appendix J

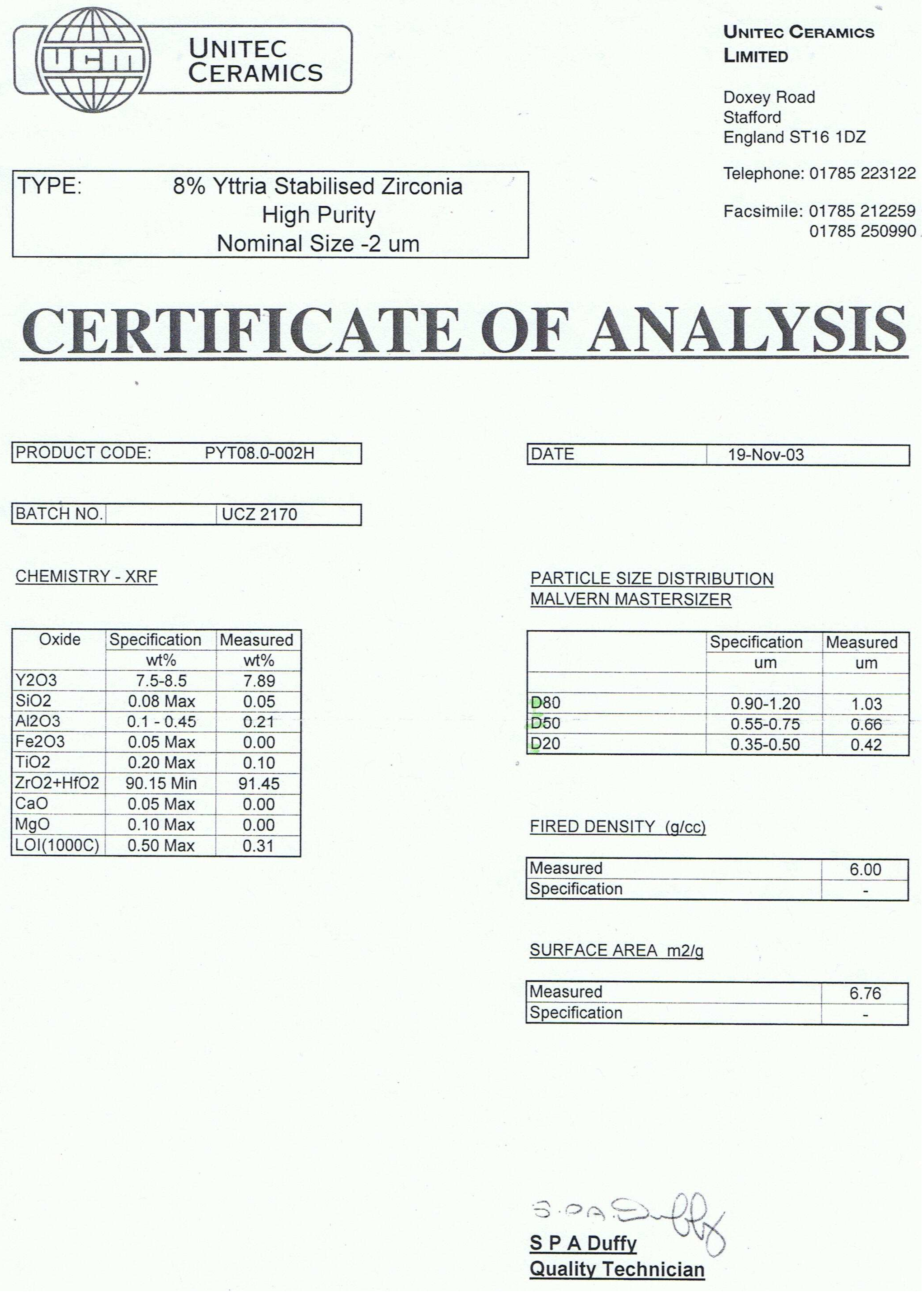

UNITEC CERAMICS

UNITEC CERAMICS LIMITED

Doxey Road
Stafford
England ST16 1DZ

Telephone: 01785 223122

Facsimile: 01785 212259
01785 250990

TYPE:	8% Yttria Stabilised Zirconia High Purity Nominal Size -2 um

CERTIFICATE OF ANALYSIS

PRODUCT CODE:	PYT08.0-002H

DATE	19-Nov-03

BATCH NO.	UCZ 2170

CHEMISTRY - XRF

Oxide	Specification wt%	Measured wt%
Y2O3	7.5-8.5	7.89
SiO2	0.08 Max	0.05
Al2O3	0.1 - 0.45	0.21
Fe2O3	0.05 Max	0.00
TiO2	0.20 Max	0.10
ZrO2+HfO2	90.15 Min	91.45
CaO	0.05 Max	0.00
MgO	0.10 Max	0.00
LOI(1000C)	0.50 Max	0.31

PARTICLE SIZE DISTRIBUTION
MALVERN MASTERSIZER

	Specification um	Measured um
D80	0.90-1.20	1.03
D50	0.55-0.75	0.66
D20	0.35-0.50	0.42

FIRED DENSITY (g/cc)

Measured	6.00
Specification	-

SURFACE AREA m2/g

Measured	6.76
Specification	-

S.P.A. Duffy

S P A Duffy
Quality Technician

Appendix K

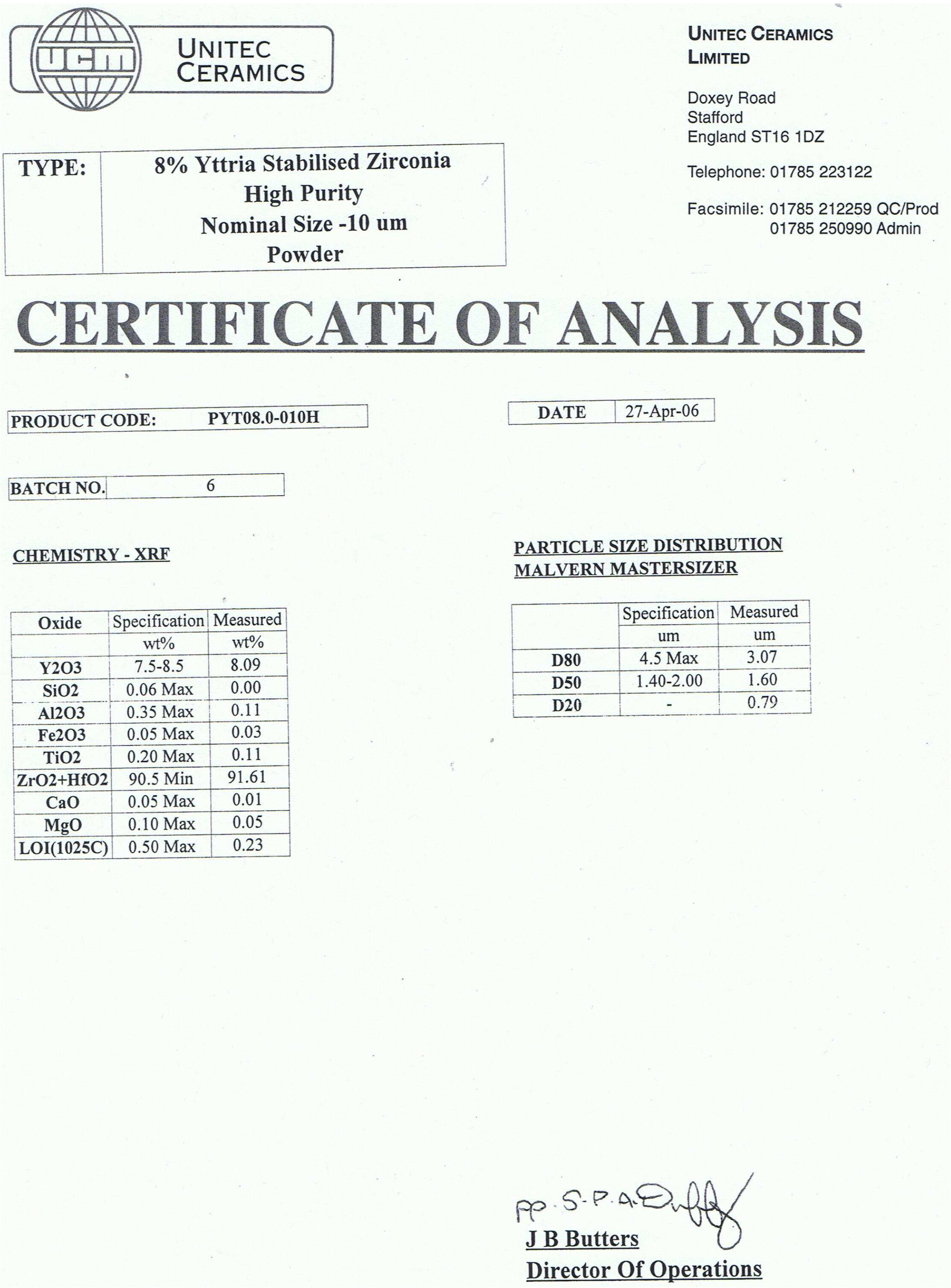

UNITEC CERAMICS

UNITEC CERAMICS
LIMITED

Doxey Road
Stafford
England ST16 1DZ

Telephone: 01785 223122

Facsimile: 01785 212259 QC/Prod
01785 250990 Admin

TYPE:	**8% Yttria Stabilised Zirconia** **High Purity** **Nominal Size -10 um** **Powder**

CERTIFICATE OF ANALYSIS

PRODUCT CODE: **PYT08.0-010H**

DATE 27-Apr-06

BATCH NO. 6

CHEMISTRY - XRF

Oxide	Specification	Measured
	wt%	wt%
Y_2O_3	7.5-8.5	8.09
SiO_2	0.06 Max	0.00
Al_2O_3	0.35 Max	0.11
Fe_2O_3	0.05 Max	0.03
TiO_2	0.20 Max	0.11
ZrO_2+HfO_2	90.5 Min	91.61
CaO	0.05 Max	0.01
MgO	0.10 Max	0.05
LOI(1025C)	0.50 Max	0.23

PARTICLE SIZE DISTRIBUTION
MALVERN MASTERSIZER

	Specification	Measured
	um	um
D80	4.5 Max	3.07
D50	1.40-2.00	1.60
D20	-	0.79

pp. S.P.A. Duffy

J B Butters
Director Of Operations

Appendix L

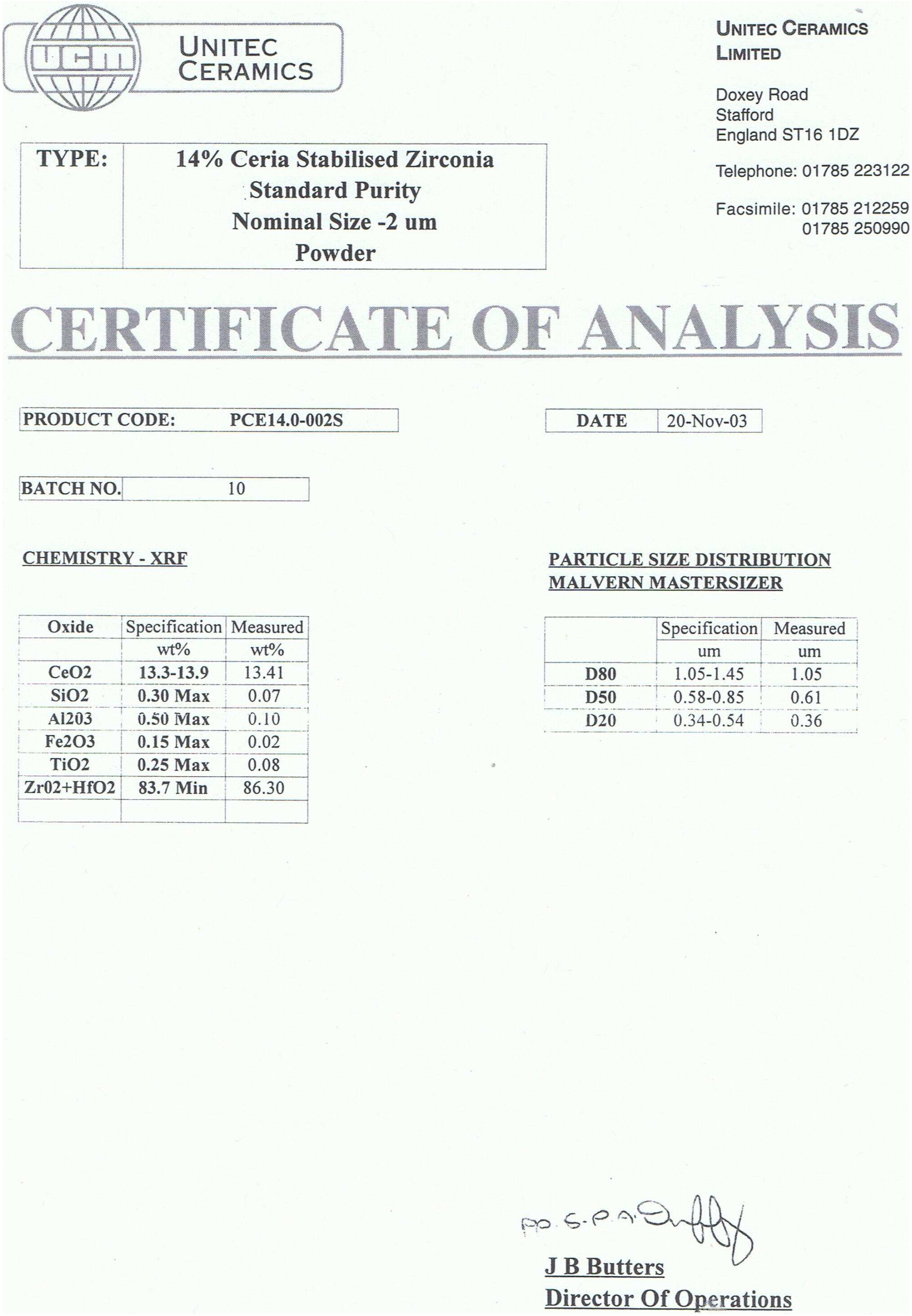

UNITEC CERAMICS

UNITEC CERAMICS LIMITED

Doxey Road
Stafford
England ST16 1DZ

Telephone: 01785 223122

Facsimile: 01785 212259
01785 250990

TYPE:	**14% Ceria Stabilised Zirconia Standard Purity Nominal Size -2 um Powder**

CERTIFICATE OF ANALYSIS

PRODUCT CODE:	**PCE14.0-002S**	**DATE**	20-Nov-03

BATCH NO.	10

CHEMISTRY - XRF

Oxide	Specification	Measured
	wt%	wt%
CeO2	**13.3-13.9**	13.41
SiO2	**0.30 Max**	0.07
Al203	**0.50 Max**	0.10
Fe2O3	**0.15 Max**	0.02
TiO2	**0.25 Max**	0.08
Zr02+HfO2	**83.7 Min**	86.30

PARTICLE SIZE DISTRIBUTION
MALVERN MASTERSIZER

	Specification	Measured
	um	um
D80	1.05-1.45	1.05
D50	0.58-0.85	0.61
D20	0.34-0.54	0.36

PP. S.P.A.

J B Butters
Director Of Operations

Appendix M (Bisgaard 1998)

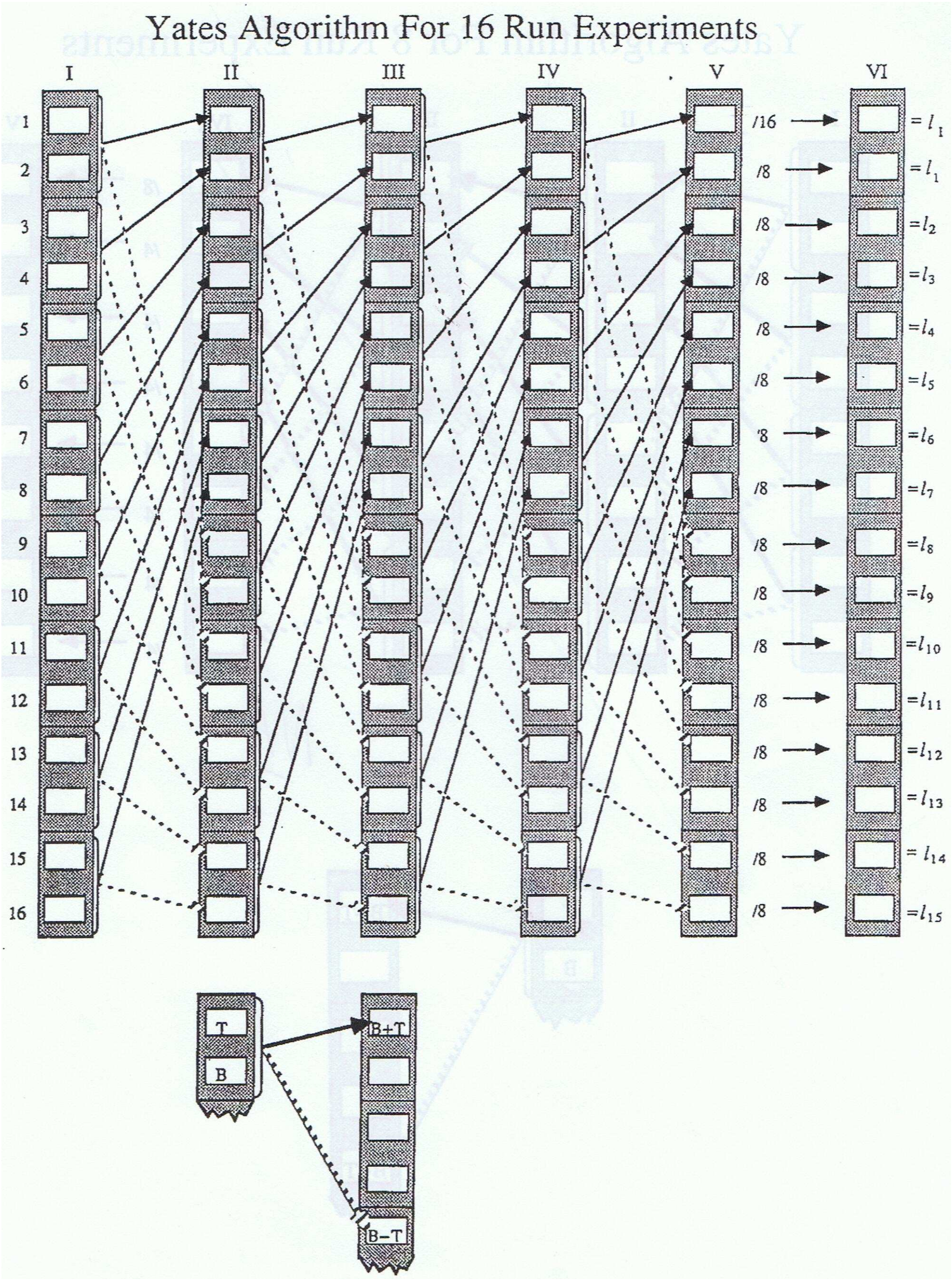

Appendix N (Shackelford and Alexander 1992)

Element	Symbol	Atomic Mass	Solid/ Gas Density (Mg/m^3)	Crystal Structure	MeltingPoint (^oC)
Oxygen	O	16.00	1.43	-	-218.4
Phosphorus	P	30.97	1.82	ortho.	44.1
Nickel	Ni	58.71	8.91	fcc	1453
Yttrium	Y	88.91	4.48	hcp	1523
Zirconium	Zr	91.22	6.51	hcp	1852